THE UNIVERSITY
of EDINBURGH

Cellular and molecular mechanisms of liver regeneration

Stephen Nicholas Greenhalgh

PhD

The University of Edinburgh

2017

Abstract

Improved understanding of how the liver regenerates would be of great value, particularly given the dearth of therapies for end-stage liver disease. Currently, the only effective treatment for total liver failure is transplantation. Such an invasive, costly and specialised intervention is unable to address the enormous global impact from diseases of the liver. Ironically, the liver has the greatest regenerative potential of any organ in the mammalian body. However, this capacity for repair is overwhelmed in the face of massive or repeated injury. Understanding the key factors driving or inhibiting successful liver regeneration offers the potential for novel, targeted therapies to promote regeneration of a patient's own liver.

Animal models are widely used when studying complex, dynamic, multicellular processes such as liver injury and regeneration. Continued progress in transgenic modification of mice, combined with ongoing advances in microscopy techniques, means that the opportunity now exists to observe labelled cells, and subcellular structures, in real time and in vivo, with previously unobtainable resolution and fidelity. Not only does this afford the opportunity for novel insights into both normal physiology and the response to injury or disease, it can vastly expand the amount of biologically relevant information that can be obtained from each experimental animal. Hence, it is possible to advance scientific knowledge and reduce experimental animal use simultaneously.

This thesis examines the role of αv integrins in liver regeneration. Integrins are expressed on the surface of cells and can perform a range of functions, including signalling and extracellular matrix adhesion. The most well-characterised role for αv integrins is activation of transforming growth factor beta, a molecule which has been shown to inhibit hepatocyte proliferation and liver regeneration. Partial hepatectomy was used as an experimental model of liver injury and regeneration. It was performed in mice, in which one or more αv integrins had been genetically depleted from specific cell types in the liver, namely hepatocytes, hepatic stellate cells or liver sinusoidal endothelial cells. These investigations revealed that depletion of integrin αvβ8 from hepatocytes led to increased hepatocyte proliferation and accelerated liver regeneration. The possible mechanisms through which hepatocyte integrin αvβ8 may exert its braking effect on liver regeneration following injury were also explored.

In parallel, a novel experimental system to permit intravital multiphoton microscopy of the regenerating liver following partial hepatectomy in mice was developed and validated. Intravital imaging of mouse liver was performed with a range of cellular labels, combined

with a fluorescent cell cycle reporter and label-free imaging modalities. This demonstrated the enormous potential of the system to study the dynamics of hepatocytes and non-parenchymal cells in the regenerative niche, reconstruct the sinusoidal vascular network in three dimensions during angiogenesis, and measure sinusoidal blood flow and parenchymal lipid deposition. Advances in experimental animal models such as this drive forward our understanding of the cellular and molecular mechanisms of liver regeneration whilst refining and reducing experimental animal use. Novel insights into the process of liver regeneration will permit the development of innovative therapeutic strategies to allow this remarkable organ to heal itself even in the face of massive or sustained insult.

Lay Summary

This thesis describes experiments that examine how a group of cell-surface molecules (αv integrins) affect liver regeneration after injury. The experiments revealed that if one particular αv integrin (αvβ8) is absent from the surface of hepatocytes, the main cell in the liver, then the liver regenerates more quickly after injury. This may be because integrin αvβ8 can activate a molecule called transforming growth factor beta, which has previously been shown to slow the rate at which hepatocytes divide during liver regeneration. Therefore, interfering with integrin αvβ8 releases this natural brake on liver regeneration.

This work also showed that integrin αvβ8 is present on human hepatocytes, in samples from both healthy and diseased liver. As such, designing a drug to block the effects of integrin αvβ8 may help injured livers to regenerate, reducing the need for liver transplants and helping more patients to survive.

As well as studying αv integrins, this thesis describes a new method to study liver regeneration in mice. Currently, one of the commonest ways to study liver regeneration in mice involves performing a surgical procedure to remove some of the liver tissue. The remaining liver then regenerates, returning to its original size within a week. The procedure is quick to perform, and modern anaesthetics and painkillers are used to minimise any suffering. However, to study how the liver is regenerating, it is then necessary to sacrifice mice to obtain liver tissue. The liver tissue is studied only once it has been removed from the mouse, which can limit the information that can be obtained. Also, each sample provides only a snapshot of what was happening at the time the mouse was killed.

The new procedure implants a titanium 'window' onto the liver surface at the same time as liver tissue is removed to trigger the process of regeneration. This means that, instead of sacrificing mice, a microscope can be used to examine the regenerating liver while mice are anaesthetised. Fewer mice are used because each mouse can be imaged more than once. Also, the liver is studied in its native environment, so new information about blood flow and moving cells can be obtained.

Declaration

I declare that this thesis has been composed solely by myself and that it has not been submitted, in whole or in part, in any previous application for a degree. Except where stated otherwise, by reference or acknowledgment, the work presented is entirely my own.

Stephen N. Greenhalgh

Acknowledgements

Scientific research in the 21st Century, by nature of the wide range of advanced techniques practised on a daily basis in modern laboratories, is rarely possible without the advice and technical expertise of a great many people. I shall apologise in advance for any errors or omissions and then attempt to express my gratitude, without being nauseatingly saccharine, to all those who have assisted and guided me during the course of my doctoral research. Eschewing tradition, it feels most appropriate to start by thanking my family. It is by dint of their love and support, so often unacknowledged, that I have been able to pursue my career, maintain my sanity, and laugh so much. Ambra has been ever-present, ever-patient, and ever-wonderful. Sofia has tolerated my absences from the role of swing-pusher for two and a half years with merely a "Papà, perché devi andare al lavoro?". The arrival of Beatrix in the last two months has added an extra frisson to my attempts to submit on time, but also some welcome perspective. Mum, Dad, and Laura are always ready to assist in any way they can, be that leaving sunnier climes to fly to Edinburgh and lend a hand, or trawling through pages of text looking for abbreviations. The Italian side of the family is, predictably, too numerous to mention, but I am indebted to them all for bringing sunshine, both literal and metaphorical, into my life.

I owe huge thanks to Neil, my supervisor, for all his support, positivity, and tolerance. If he ever regretted assisting my relocation to Edinburgh, and even welcoming me into his family home, he never let on! My co-supervisors, John Iredale and Ken Simpson, have always been extremely generous with their time and supportive of my career.

Within the Henderson group, Kylie Conroy and Alex Thompson were great companions as we helped one another with surgical procedures and endless hours of intravital imaging. Ross Dobie and Jamie Smith were sources of intellectual, practical, and emotional support on many occasions, and far more than just friends with whom to share lunch and a sense of humour. The newer members of the Henderson group – Beth Henderson, Dyana Markose, John Wilson-Kanamori, Jordan Henderson, Richard Taylor – and the wider members of the liver lab at the Centre for Inflammation Research, including Allison Mackinnon, Lara Campana, Cathy Duff, Prakash Ramachandran, and Elena Dora, have always been extremely kind, helpful, and fun to spend time with. Iain Murray and Zaniah Gonzalez also kept us company from time to time. The group has welcomed a number of visitors or affiliates, including Cecilia Boz, Mhairi Donnelly, John Connelly, Madeleine Asklöf, and Greg Swan,

who variously assisted on occasion with immunohistochemistry and image acquisition. Henry McSorley provided the cells and tips for the MFB-F11 TGFβ assay – if only it had worked! Antonella Pellicoro provided proper coffee and pettegolezzi. Rebecca Aucott, the lab manager, without doubt runs the tidiest ship in the University, and still finds time to share an appreciation of Formula One and Daniel Kitson. I would also like to acknowledge the contributions of Alison O'Meara, Pam Kane, Pat Swan and Steven McLean, for helping daily life in the CIR to run as smoothly as possible. And if it had not been for the training of Lindsay Murray, I would not have been able to stay late and alone on so many occasions.

From the wider university community, multiphoton microscopy simply would not have been possible without the expertise of Martin Lee. I am also grateful to Alan Serrels for his role in building such an impressive piece of kit. Similarly, the QMRI Flow Cytometry and Cell Sorting Facility, particularly Will Ramsey and Shonna Johnston, and the SuRF Histology team, including Mel McMillan, provided expert assistance in their respective fields. Bertrand Vernay's teaching in the wonders of ImageJ made my macro writing possible.

Caring for the mice requires a large number of people. At Little France, I am grateful to Duncan, Keith, and Laraine. At the WGH, the assistance of Simon and Michelle was invaluable. The support and oversight of the Veterinary Scientific Services team, particularly Lesley, Nacho, Montse, Caroline, Karen, and Ellen was always appreciated. Most importantly of all, I must pay tribute to Jon, our mouse technician. It is impossible to overstate his skill and dedication in caring for his animals. When it comes to recognising the contribution made by the experimental animals that we use in our research, it is difficult to find the right words. However, as a veterinarian first and foremost, I do wish to acknowledge them. We consider ourselves the superior species, yet we rely on their sacrifice to find out more about ourselves and the world.

The original abdominal imaging windows were provided by Jacco van Rheenen, of the Hubrecht Institute. Richard Collins at the Edinburgh College of Art kindly 3D-printed our prototype imaging windows, before the final versions were manufactured by ZME Fijnmechanisch Atelier B.V., with the assistance of Nikki van der Zouw.

Across the pond, I would like to acknowledge the support of all those at the University of California, San Francisco. In particular, Koy Saeteurn, who assisted with early integrin experiments, Amha Atakilit, who provided the β8 integrin subunit blocking antibody, Chris Her, for his advice on hepatocyte isolation, and Dean Sheppard, for his intellectual support.

Finally, I am extremely grateful for the financial support of the Wellcome Trust, whose funding enabled me to enter the world of research and academia. I shall do my best to repay them.

List of Abbreviations

AIW	abdominal imaging window
ALT	alanine transaminase
ALP	alkaline phosphatase
ANOVA	analysis of variance
ATP	adenosine triphosphate
BAC	bacterial artificial chromosome
BrdU	5-Bromo-2′-deoxyuridine
CARS	coherent anti-Stokes Raman scattering
CI	confidence interval
Cre	cyclization recombinase
DAB	3,3'-diaminobenzidine
DAPI	4′,6-diamidino-2-phenylindole, dihydrochloride
dH_2O	distilled water
DMEM	Dulbecco's modified eagle medium
DNA	deoxyribonucleic acid
DNase	deoxyribonuclease
EDTA	ethylenediaminetetraacetic acid
(e)GFP	(enhanced) green fluorescent protein
ELISA	enzyme-linked immunosorbent assay
FACS	fluorescence activated cell sorting
FAD	flavin adenine dinucleotide
FLIM	fluorescence lifetime imaging
Fucci	fluorescent ubiquitination-based cell cycle indicator
GR1	granulocyte receptor 1
HBSS	Hank's balanced salt solution
HGF	hepatocyte growth factor
HO-1	heme oxygenase 1
HSC	hepatic stellate cell
LAP	latency associated peptide
LLC	large latent complex
LRP1	low-density lipoprotein receptor-related protein

LSEC	liver sinusoidal endothelial cell
LTBP	latent TGFβ binding protein
MAPK	mitogen-activated protein kinase
MLEC	mink lung epithelial cell
(m)RNA	(messenger) ribonucleic acid
MT1-MMP	membrane type 1-matrix metalloproteinase, also known as MMP14
NAD(H)	(reduced) nicotinamide adenine dinucleotide
NADP(H)	(reduced) nicotinamide adenine dinucleotide phosphate
NAPQI	N-acetyl-p-benzoquinone imine
PAI-1	plasminogen activator inhibitor-1
PBAG	*Pdgfrb*-BAC-eGFP transgenic mouse
PBS	phosphate-buffered saline
PDGFRβ	platelet-derived growth factor receptor beta
pSMAD3	phospho-SMAD3
qPCR	quantitative, real-time polymerase chain reaction
RAP	LRP1-associated protein
RGD	arginine-glycine-aspartate
rhTGFβ	recombinant human TGFβ-1
RNase	ribonuclease
SEM	standard error of the mean
SLC	small latent complex
SHG	second harmonic generation
SSC-A	side scatter-area
TGFβ	transforming growth factor beta
tPA	tissue plasminogen activator
TPEF	two photon excitatory fluorescence
uPA	urokinase plasminogen activator
uPAR	uPA receptor

Table of Contents

List of Figures

List of Tables

Chapter 1 - Introduction

Outline

Effective therapies other than transplantation for both acute and end-stage liver failure do not exist. It has not yet been possible to harness the exceptional regenerative capacity of the liver, which fails in the face of massive or persistent insult. This thesis examines the role that αv integrins, specifically integrin αvβ8, play in the regulation of hepatocyte proliferation. Experimental evidence is presented that shows integrin αvβ8 on the surface of hepatocytes acts as a regulator of hepatocyte proliferation following injury. Depletion of hepatocyte integrin αvβ8 in mice results in increased hepatocyte proliferation and accelerated liver regeneration. Examination of possible mechanisms by which this regulation of hepatocyte proliferation might occur suggests that inhibition of hepatocyte integrin αvβ8 alters the expression of transforming growth factor beta (TGFβ)-responsive genes. This fits with the well-known role for integrin αvβ8 in activating TGFβ. Targeting hepatocyte integrin αvβ8 could represent a promising therapeutic strategy to promote regeneration of a patient's own liver.

Accompanying the investigations into the role of αv integrins in liver regeneration, this thesis also describes the development and validation of a new model in which the process of liver regeneration can be studied, at a cellular level, in the living animal. The widely-used mouse model of liver regeneration, two-thirds partial hepatectomy, was modified and combined with the implantation of an abdominal imaging window (AIW) onto the surface of the liver. This permits multiphoton microscopy to be performed, intra-vitally, throughout the time course of liver regeneration. The new procedure is most informative when performed in mice expressing fluorescent reporter proteins, allowing multiple cell types and sub-cellular structures to be labelled fluorescently. This facilitates the study of dynamic processes, such as sinusoidal blood flow, and of hepatocyte proliferation itself, paving the way for novel insights into the process of liver regeneration.

Background

The global burden of liver disease

The spectre of liver disease casts a long shadow worldwide. Despite a range of aetiologies, diseases of the liver can broadly be categorised as acute or chronic. Of the two, chronic liver disease places by far the greater burden on healthcare systems around the world. All chronic liver diseases invariably share a common progression: inflammation leads to fibrosis, which progresses to cirrhosis, accompanied by loss of function.[1] Once a liver has reached an end-stage, only transplantation can prevent death ensuing. The Global Burden of Disease 2015 study estimated that, between them, cirrhosis and liver cancer (90% of the latter occur in patients with the former[2]) accounted for almost 4% of the 55.8 million deaths in that year – this equates to 1 in 25 deaths worldwide.[3] Notwithstanding the advances in healthcare in many countries, overall death rates from liver disease have remained static since 1990.[3] The principal causes of chronic liver disease are viruses (Hepatitis B and C), alcohol, and obesity (leading to non-alcoholic steatohepatitis).[4] Unfortunately, the progress made in preventing and treating viral hepatitis is currently being undermined by a voracious societal trend to eat, and drink alcohol, in ever-increasing amounts.

It is for these lifestyle reasons that the situation closer to home gives even greater cause for concern. Liver disease is the third leading cause of premature death in the UK, after ischaemic heart disease and self-harm.[5] The figures calculated for years of working life lost are staggering (Box 1). Worse still, deaths from liver disease are rising year by year: the standardised mortality rate for liver disease in the under-65s has increased five-fold since 1970 (Figure 1 - 1).[5] Although the vast majority of cases of chronic liver disease may be preventable,[6] several factors combine to mean that most patients present with their disease at an advanced stage.[5] Hence, whilst prevention is the ultimate goal, effective treatments to reverse fibrosis and promote restoration of functional liver mass are urgently required. Liver transplant in every case of end-stage liver disease is neither feasible nor desirable.

Although acute liver disease pales in comparison to the behemoth that is its chronic counterpart, acute liver failure still has a huge personal and financial cost, with a frequently devastating outcome. All cases require intensive care and, in the absence of a sufficient regenerative response (as is the case in the majority of these patients), a liver transplant is the only curative treatment.[4] Despite being an active field of research, there is currently no equivalent to dialysis for the liver. As such, these patients would usually be categorised as

'super-urgent' and are reliant on a suitable donor organ becoming available in a short time frame. 'Enhancing liver regeneration in acute liver failure' is listed as a future goal in the HEPAMAP research roadmap published by the European Association for the Study of the Liver.[4]

Box 1: Liver Disease – Facts and Figures

Liver disease is the **3rd commonest cause of premature death** in the UK[5]

- **62,000 years** of working life are lost each year
- **500%** increase in mortality from liver disease in under 65s since 1970 (Figure 1 - 1)[5]
- **80%** of liver deaths are alcohol-related[6]

Obesity is also a major risk factor[6]

- 80-90% of obese individuals have non-alcoholic fatty liver disease
- 10-15% of these will develop fibrosis / cirrhosis
- on current predictions, **39 million adults** in the UK will be obese by 2030

In England and Wales (2012):[5]

- 600,000 people with liver disease
- 60,000 hospital admissions
- 11,000 deaths
- 695 liver transplants[7,8]

29 million people in the EU have chronic liver disease[9]

- 170,000 cirrhosis deaths per year

30 million people in the USA have chronic liver disease[10]

Global Burden of Disease, 2015:[3]

- 2.32% of all deaths were due to cirrhosis
- 1.45% of all deaths were due to liver cancer

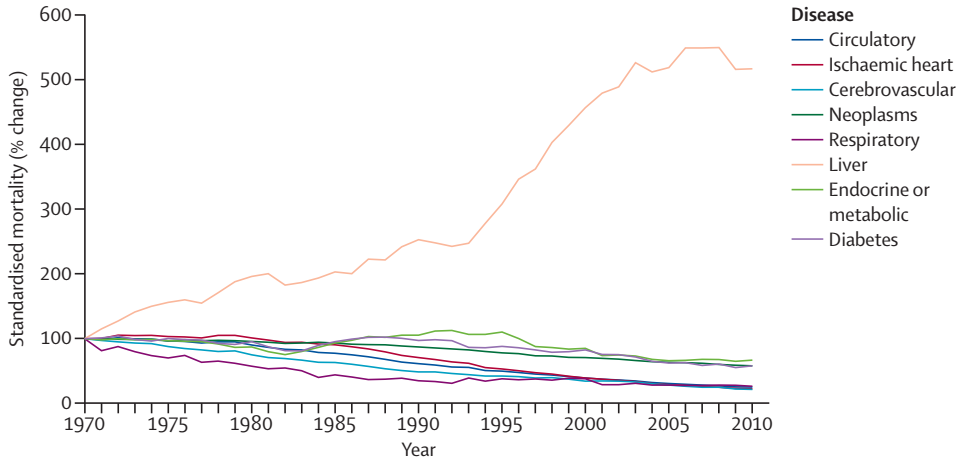

Figure 1 - 1 Standardised UK under-65 mortality rates (1970-2010).
Data normalised to 1970 (100%). Reprinted from The Lancet,[5] ©2014, with permission from Elsevier.

Promoting liver regeneration

When healthy, the liver has extraordinary regenerative potential. This may well be the result of evolutionary pressure provided by ingested toxins, whose first port of call is the liver following absorption from the gastrointestinal tract. When two-thirds partial hepatectomy is performed in the mouse, the liver returns to its pre-injury mass within eight days.[11] In humans, the rate of regeneration of healthy liver is similarly impressive. Living donors in whom right lobectomy was performed showed a return to starting liver mass at 60 days post surgery.[12] Opinions vary on the best way to encourage an injured liver to regenerate. One of the strategies currently being pursued to drive liver regeneration aims to promote the expansion of hepatic progenitor cells, thought to reside within the Canal of Hering,[13] which links the bile canaliculi with the biliary tree.[14] In the context of global hepatocyte senescence, transplanted hepatic progenitor cells have been demonstrated to repopulate the injured liver, giving rise to both hepatocytes and ductular cells.[15] However, there is good evidence to suggest that, in most mouse models of liver injury, liver regeneration occurs primarily through duplication of the adult hepatocyte population.[16,17] Hence, this body of work focuses on the terminally differentiated hepatocyte population and examines whether it is possible to promote hepatocyte proliferation through targeting of αv integrins.

αv integrins

Integrins are often described simply as cell-cell adhesion molecules, but this belies the wide range of functions that they have been shown to perform.[18] In addition to cell adhesion, integrins can interact with the cytoskeleton, act as viral and bacterial receptors, and both activate and respond to intracellular signalling. Their wide-ranging effects on cell behaviour mean that integrins have important roles in development, angiogenesis, haemostasis, inflammation, immune cell behaviour, and cancer. The eponymous 'αv' integrins are a subset of the 24 mammalian integrins, comprising five members (Box 2). In addition to the common alpha subunit, αv integrins share a key structural feature – an arginine-glycine-aspartate (RGD) binding domain (Box 2). This feature allows αv integrins to bind and activate latent TGFβ.[19-24] The ability to activate TGFβ, a major pro-fibrotic cytokine with complex, yet crucial, roles in cancer development and metastasis, has contributed to αv integrins being explored as potential therapeutic targets for the treatment of fibrosis and several different cancers.[25-27]

Box 2: Integrins and RGD binding

Integrins are a family of trans-membranous heterodimers, comprised of an alpha and beta subunit (Figure 1 - 2). In mammals, there are 18 alpha and 8 beta subunits, between them forming 24 different integrins.[18] The integrin family may be sub-classified according to form and function (Figure 1 - 3). As well as cell adhesion, integrins may engage in bi-directional signalling: inside-out and outside-in. Both external ligand binding and changes to the cytoplasmic domains can alter activation state and integrin conformation (Figure 1 - 2).

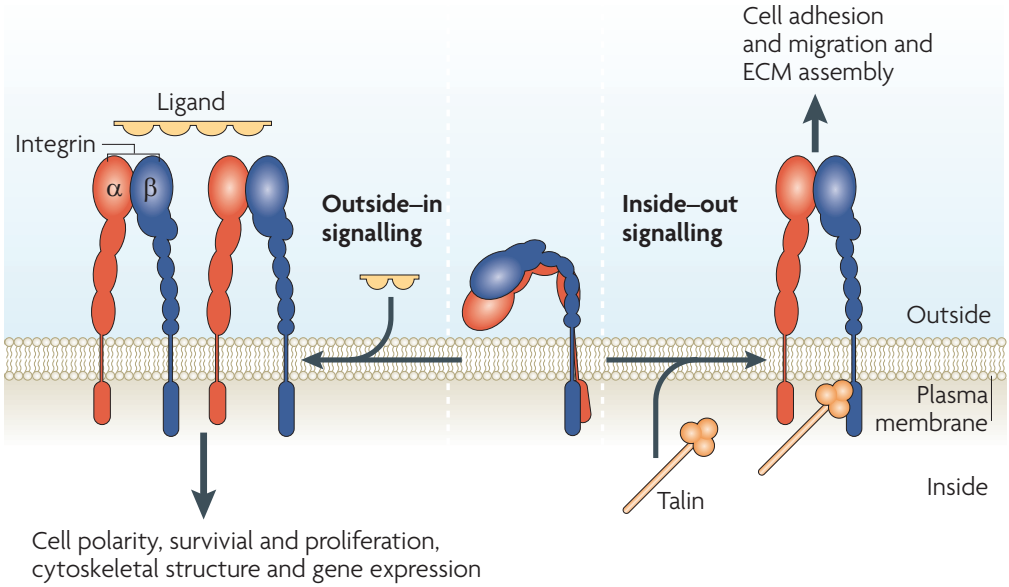

Figure 1 - 2 Integrin structure and signalling.
The integrin heterodimer consists of alpha (red) and beta (blue) subunits. The bent form (centre) is inactive. Binding of either an extracellular ligand (left) or an intracellular activator (such as the cytoskeletal protein Talin, right) leads to conformational changes in both intracellular and extracellular integrin domains, i.e. integrin activation. Reprinted from Nature Reviews Molecular Cell Biology,[28] ©2010, with permission from Macmillan Publishers Ltd.

In the context of liver fibrosis, targeting αv integrins has been shown to be anti-fibrotic, through reduced activation of TGFβ.[29] This effect was seen when αv integrins were depleted from hepatic stellate cells (HSCs), or when a novel small molecule inhibitor of αv integrins was administered parenterally.

Whereas HSCs have been demonstrated to express all but one (αvβ6) of the αv integrins,[29] the expression of αv integrins by hepatocytes, biliary epithelium and the remaining non-parenchymal cells of the liver is less well-characterised.

Box 2 Continued:

The αv integrins are distinguished by their arginine-glycine-aspartate (RGD) binding domain. There are five αv integrin subtypes (Figure 1 - 3) and all can bind the RGD domain on the latency associated peptide (LAP) that maintains the TGFβ homodimer in an inactive state. Binding of αv integrins to the LAP drives TGFβ activation.[20-24]

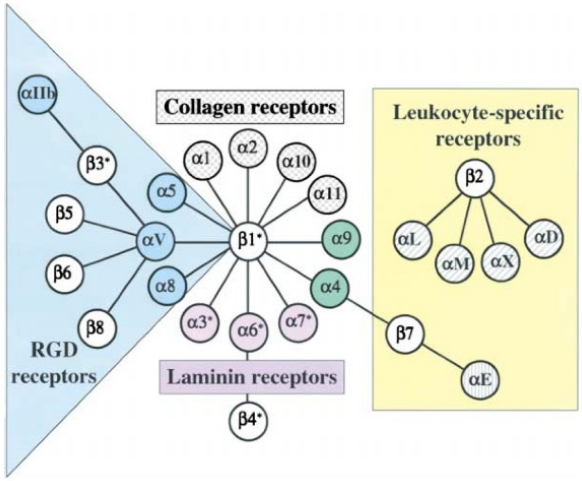

Figure 1 - 3 Mammalian integrins.
There are 24 integrin heterodimers, formed from 18 possible alpha subunits and eight possible beta subunits. Integrins may be grouped into subfamilies based on their form and function. Reprinted from Cell,[18] ©2002, with permission from Elsevier.

Three other integrins also contain an RGD binding domain, but none have been shown to activate latent TGFβ:[30]

αIIbβ3 – the principal platelet integrin, not present on the resident liver cells;[31] an RGD peptidomimetic small molecule, which binds all αv integrins, does not bind integrin αIIbβ3;[29]

α5β1 – is a major hepatocyte integrin and also present on HSCs;[29,32]

α8β1 – is present on HSCs;[33] can bind the LAP but does not activate TGFβ.[34]

Hepatocytes principally express integrins α1β1, α5β1 and α9β1.[32,35] Biliary epithelium is reported to express α2, α3, α5 and α6 integrins when uninjured.[36] Following injury, integrin αvβ6 is expressed on cholangiocytes, and also activated hepatic progenitor cells, and has been shown to have an important role in the progression of fibrosis.[37-39] Myeloid cells, and specifically macrophages, express αv integrins.[40,41] Precisely which αv integrins are expressed is less clear, although it seems that macrophages might express integrin αvβ3, but little or no integrin αvβ8.[42,43] Kupffer cells, the liver-resident macrophage, express integrin αvβ5.[44]

There is evidence that endothelial cells express αv integrins.[45,46] However, the liver sinusoidal endothelial cell (LSEC) is a specialised endothelial cell with a different expression

profile.[47] In endothelium, αvβ3 has been the most studied of the αv integrins. Initially, it appeared not to be expressed by LSECs.[48,49] However, later studies have contradicted this and also showed LSEC expression of integrin αvβ5.[50-53]

Whilst αv integrin inhibition in the liver has been demonstrated to be anti-fibrotic, and end-stage liver fibrosis is accompanied by a failure of adequate regeneration, whether any of the αv integrins have a direct role in regulating liver regeneration has not been explored. Integrin αvβ8 in particular has been shown to inhibit growth in vitro in cancer cells and airway epithelium.[54,55] There is also a large body of literature supporting an important role for αv integrins in general, and again integrin αvβ8 in particular, in the activation of TGFβ in multiple cell types, organs, and disease contexts.[24,29,37,38,40,43,55-63] Hence, it is possible that any effect that αv integrins might have on the regulation of liver regeneration may be mediated via TGFβ.

Transforming Growth Factor Beta

TGFβ is produced as an inactive complex, the active 25 kDa homodimer held within a latency associated peptide (LAP) (Box 3). This inactive 'small latent complex' is predominantly stored anchored to the extracellular matrix through covalent linkage to the latent TGFβ binding protein (LTBP). Thus, although the regulation of TGFβ may occur at a number of levels,[64] activation of latent TGFβ is a critical regulatory checkpoint.[56] The LAP contains an RGD domain, conferring the ability to bind to αv integrins. Crucially, mutation of this domain alone in mice, thus preventing αv integrin binding, recapitulates the phenotype of complete TGFβ-1 knockout.[58] Advances in the understanding of the structure of both latent TGFβ and αv integrins have demonstrated how integrin-LAP binding at the RGD domain, and the subsequent generation of mechanical force between the cell and the extracellular matrix, can lead to opening of the LAP and release of active TGFβ into the local environment.[65-68] Of note, the specifics of αv integrin-mediated TGFβ activation may vary between the different αv integrins. For example, it has been shown that MT1-MMP (membrane type 1-matrix metalloproteinase, also known as MMP14) is a necessary co-factor for the activation of TGFβ by integrin αvβ8.[21] TGFβ activation by integrin αvβ6 depends on cytoskeletal contraction and force transfer to integrin αvβ6 mediated by RhoA and Rho kinase.[69,70]

Box 3: Transforming Growth Factor Beta

The TGFβ superfamily contains TGFβ itself, as well as bone morphogenic proteins, activins and several other related peptides.[71] Active ('mature') TGFβ is a 25 kDa homodimer, but it is secreted as a larger latent complex (Figure 1 - 4).

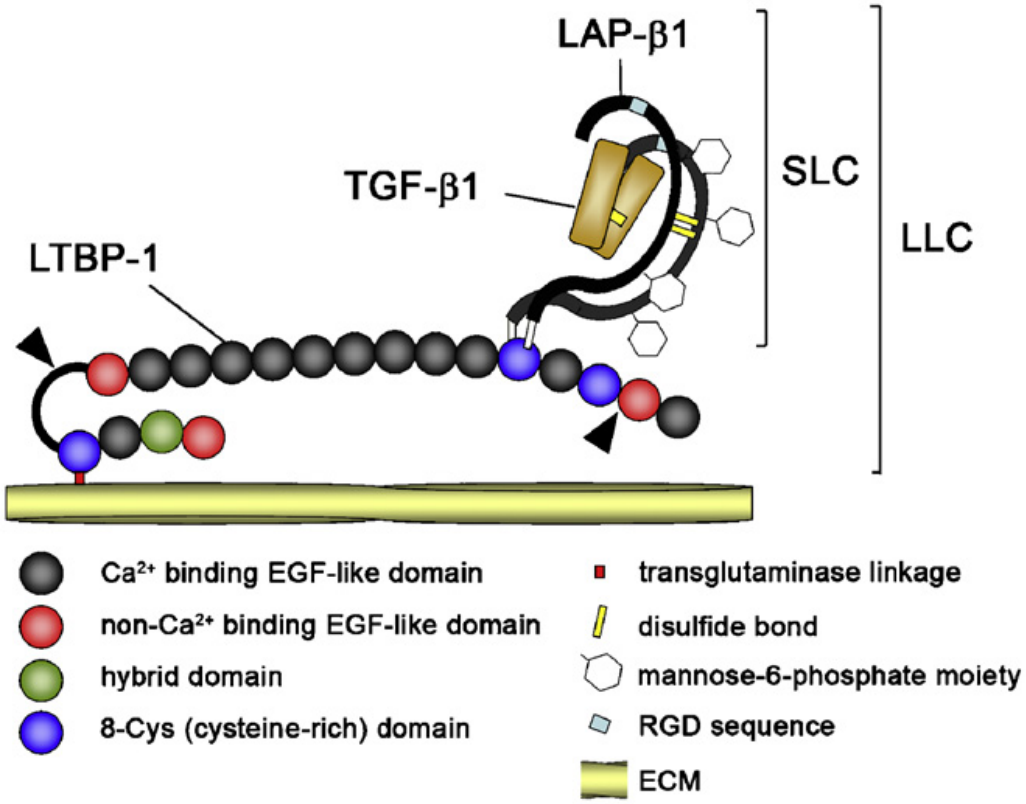

Figure 1 - 4 The latent TGFβ complex.
Active TGFβ homodimer is held non-covalently within the LAP, and this small latent complex (SLC) is anchored to the extracellular matrix by the latent TGFβ binding protein (LTBP), forming the large latent complex (LLC). Reprinted from the European Journal of Cell Biology,[72] ©2008, with permission from Elsevier.

There are three mammalian isoforms of TGFβ, all with the ability to signal via the same receptors.[73] TGFβ-1 is the isoform that has been the subject of most research. The three isoforms appear to have similar, but not entirely overlapping functions.[74] This is demonstrated by the different knockout phenotypes in development.[75-79] Only the LAPs of TGFβ-1 and TGFβ-3 have RGD domains, capable of binding to αv integrins.[80]

Box 3 Continued:

Active TGFβ can be freed from the LAP following integrin binding by mechanical or proteolytic mechanisms.[21,65-70,81,82] Mechanical release occurs following αv integrin binding to the RGD domain of the LAP. Cellular contractile force, braced against the extracellular matrix, results in a conformational change to the LAP, releasing the active TGFβ homodimer (Figure 1 - 5A). Alternatively, integrin αvβ8 appears to stabilise the SLC to permit proteolytic cleavage of the LAP, for example by MT1-MMP (Figure 1 - 5B). Other proteases, such as plasmin, thrombin and metalloproteinases, are able to activate TGFβ independent of integrins.[81] However, the biological significance of these routes is still debated, especially since mutation of just the LAP RGD domain, to prevent integrin binding, recapitulates the phenotype of TGFβ-1-null mice.[58]

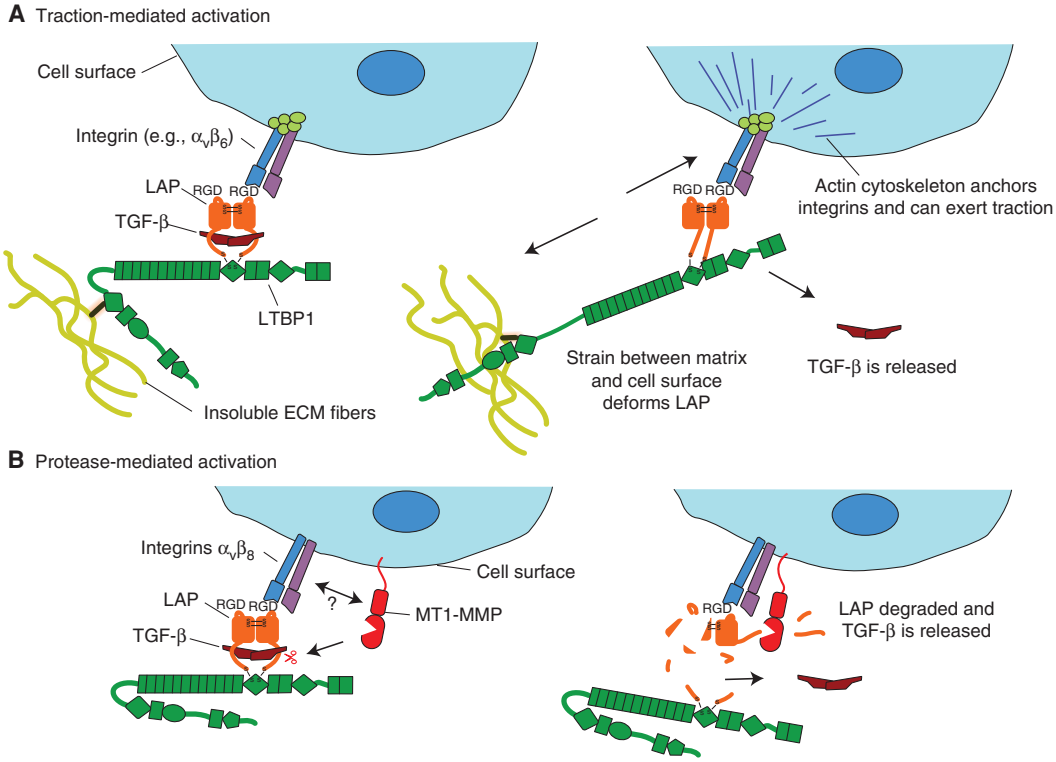

Figure 1 - 5 Integrin-mediated TGFβ activation mechanisms.
A) Traction-mediated activation: αv integrin binding to the RGD domain of the LAP facilitates transduction of cellular force; this induces a conformational change in the LAP, resulting in release of active TGFβ. B) Protease-mediated activation: integrin αvβ8 stabilises the SLC at the cell surface, facilitating proteolytic cleavage of the LAP and release of active TGFβ. Reprinted from CSH Perspectives in Biology,[82] ©2016, with permission from Cold Spring Harbor Laboratory Press.

TGFβ signalling and functions

Classically, TGFβ signalling proceeds through the binding of the active homodimer to the TGFβ receptor type II, which complexes with TGFβ receptor type I at the cell membrane (Box 4).[71,73,83,84] This receptor complex facilitates sequential phosphorylation and complexing of cytosolic SMAD proteins. These phosphorylated complexes, such as phospho-SMAD2/3/4, then enter the nucleus and bind to the regulatory elements of genes, thereby modulating transcription. It has also been known for some time that the canonical TGFβ signalling pathway is by no means the only route through which TGFβ is able to exert its effects. TGFβ is able to modulate, and signal via, several other well-known signalling pathways, including mitogen-activated protein kinases, small GTPases, and NFκB.[85]

Box 4: TGFβ signalling pathways

All three mammalian isoforms of TGFβ are able to bind the TGFβ type II receptor. This results in phosphorylation and the formation of a tetramer with the TGFβ type I receptor (Figure 1 - 6). Canonically, signalling then proceeds by SMAD phosphorylation and nuclear translocation. In the nucleus, the SMAD complex, transcription factors and co-factors, combine to drive gene expression. Multiple non-canonical TGFβ signalling pathways also exist, including via Erk, p38 and JNK mitogen-activated protein kinases, Rho GTPases, and the PI3K-AKT pathway.[85]

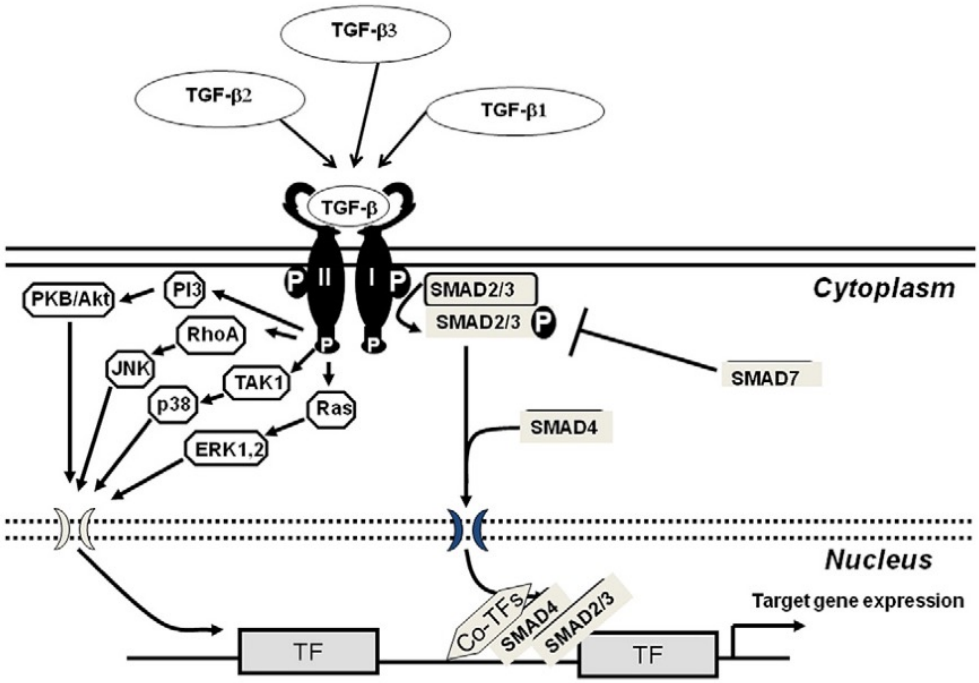

Figure 1 - 6 TGFβ signalling pathways.
TF, transcription factor. Reprinted from Biochimica et Biophysica Acta,[86] ©2011, with permission from Elsevier.

TGFβ – the duplicitous molecule

Such diverse signalling mechanisms go some way to explaining the pleiotropic functions of TGFβ. The cellular effects of TGFβ signalling are also highly context-dependent, with profound effects in such varied biological processes as development, inflammation and cancer development, as well as in maintaining cellular homeostasis.[83] The outcome of TGFβ signalling can vary markedly depending on the precise timing of signalling and the local environment in which it occurs. Such challenges to achieving a complete understanding of the multiple roles of TGFβ are exemplified by the apparently paradoxical roles in cancer.

Initially, TGFβ was shown to be inhibitory to the growth of transformed cells, thus appearing to have a predominantly tumour-suppressive action.[87] This was supported by animal models that demonstrated an increase in tumour development following disruption of the TGFβ signalling pathway.[88,89] However, TGFβ has also been shown to enhance tumour metastasis and the development of tumour vasculature.[86,90] In hepatocarcinogenesis, the role of TGFβ is further complicated by its function as a key driver of fibrosis, itself a major independent risk factor for the development of liver cancer.[2,86,91]

TGFβ and liver regeneration

In the context of liver regeneration, TGFβ is a potent inhibitor of hepatocyte proliferation. Following the identification of TGFβ in the early 1980s,[92] a glut of publications demonstrated a dose-dependent inhibition of proliferation when TGFβ was provided to hepatocytes in vitro.[93-97] Subsequently, it was confirmed that hepatocyte DNA synthesis could be inhibited in vivo, albeit transiently, by exogenous TGFβ injected at, or shortly after, partial hepatectomy in rats.[98] An increase in hepatic TGFβ transcription, peaking at 72 hours after partial hepatectomy, was postulated to serve as an intrinsic homeostatic mechanism, through which hepatocyte proliferation could be suppressed as the hepatectomised liver returns to its pre-injury state.[99] A similar finding was reported following injury with carbon tetrachloride.[100] Evidence was presented for both paracrine and autocrine sources.[99-101]

Targeting the TGFβ pathway, either by injection of an anti-TGFβ antibody or through genetic depletion of hepatocyte TGFβ type II receptor, both have the expected effect of increasing DNA synthesis and hepatocyte proliferation following partial hepatectomy.[102,103] Increased hepatocyte proliferation was also observed to accompany reduced fibrosis when TGFβ signalling was inhibited in a rat model of chronic fibrosis.[104] Furthermore, TGFβ appears to play a homeostatic role, restricting hepatocyte proliferation even in uninjured liver. When

an adenoviral delivery strategy was employed to achieve hepatic expression of a TGFβ type II dummy receptor, hepatocyte proliferation increased even in the absence of an injurious stimulus.[105] Importantly, targeting TGFβ activation, rather than TGFβ signalling directly, has also been shown to promote hepatocyte proliferation. Thrombospondin-1 has been shown to activate TGFβ in vivo.[81,106] Following partial hepatectomy, thrombospondin-1 knockout mice demonstrated increased hepatocyte proliferation and accelerated liver regeneration compared to controls.[107]

As with the inhibitory effect observed following the administration of exogenous TGFβ, the described effects on the promotion of hepatocyte proliferation were transient, suggesting that regulation of hepatocyte proliferation and liver regeneration relies on more than one factor or pathway. It is not surprising that such a key biological process has an element of redundancy, and this does not detract from the broad concept that targeting the TGFβ pathway to promote liver regeneration is an avenue worthy of ongoing exploration.

Designing targeted anti-TGFβ therapies

The importance and evident potency of TGFβ have resulted in it being widely studied as a potential therapeutic target in a range of cancers and fibrotic conditions.[108] However, in developing effective therapies directed against the action of TGFβ, it is essential to remain mindful of the pleiotropic nature of this molecule and its myriad functions in homeostasis as well as in multiple disease processes. Blunt, 'sledgehammer' approaches, blocking TGFβ signalling globally, risk causing unacceptable side effects, such as significant autoimmunity or cancer development.[76,88,89,108] For this reason, if TGFβ signalling is to be targeted successfully, nuanced approaches are required. These aim to limit excessive and harmful TGFβ activity whilst not completely abolishing the low levels of TGFβ signalling necessary for the success of core homeostatic processes.

The importance of the activation of latent TGFβ has already been highlighted as a key regulatory checkpoint. Modulating TGFβ activation in the appropriate cellular niche therefore has the potential to limit the harmful effects resulting from localised, excess TGFβ activity. Several mechanisms by which TGFβ can be released from the LAP have been identified. Activation may be mediated by plasmin, thrombospondin and, as previously described, one or more αv integrins. The αv integrins are attractive in this respect because of their proven ability to activate TGFβ in vivo. Indeed, in some contexts, αv integrins appear to be the principle mediators of TGFβ activation.[57]

Hypothesis

Consolidating the previous experimental evidence that αv integrins play a role in the progression of (fibrotic) liver disease and can activate TGFβ, which itself can inhibit hepatocyte proliferation, led to the following broad hypothesis, which is investigated through the body of work presented in subsequent chapters:

Inhibition of αv integrin-mediated TGFβ activation results in increased hepatocyte proliferation and accelerated liver regeneration

---

Aims and Goals

Incorporating the hypothesis described above, the aims and goals of the investigations reported in this thesis were as follows:

- To investigate whether αv integrins play a role in the regulation of liver regeneration
- To examine whether any role for αv integrins in regulating liver regeneration is mediated via TGFβ
- To develop a novel model to study liver regeneration in mice, combining partial hepatectomy with intravital multiphoton microscopy
- To demonstrate how intravital multiphoton microscopy can be used to study dynamic processes occurring during liver regeneration, at a cellular level, in the living animal

Tools to study liver regeneration

Models of liver regeneration

Liver regeneration is a co-ordinated, multi-cellular process, which makes it a challenge to study in vitro. This is despite recent advances in organoid technology and tissue slice culture systems.[109,110] It is also a highly dynamic process, necessitating study at multiple time points as regeneration progresses. This feature, combined with the many practical and logistical challenges, limits the study that can be performed in human subjects. Therefore, rodent models still form the mainstay of research into liver regeneration. The regenerative process can be initiated at a defined point in time, in multiple, genetically identical subjects. The injury models are refined so as to produce a consistent, reproducible time course over which liver

regeneration occurs. The entire regenerative process is then complete in a relatively short time frame, within one week in the case of the mouse.[11]

Although a number of liver injury models exist in rodents, two in particular are frequently used to study the regenerative response and are employed in the work that is described in the following chapters. Partial hepatectomy has been employed for the study of liver regeneration in mice for over 60 years.[11] It is generally considered as the purest model of liver regeneration, since it does not trigger a marked inflammatory response. The most commonly performed procedure is described variously as a 'two-thirds' or '70%' partial hepatectomy (Box 5). This degree of hepatectomy results in minimal morbidity and mortality, whilst driving significant hepatocyte proliferation and liver regeneration.[111] Removing a lesser amount of liver tissue results in a response defined primarily by cellular hypertrophy rather than true regeneration.[112] Conversely, although excision of up to 90% of the mass of the liver has been reported,[113] often referred to as 'massive' hepatectomy, this leads to (unacceptably) high mortality rates without offering significant benefits with regards to the study of liver regeneration.

The second model of liver injury and regeneration employed in this body of work is that of acetaminophen (paracetamol) overdose (Box 5).[114] The liver is able to metabolise a certain amount of acetaminophen without toxic effects. However, overdose results in accumulation of the (toxic) metabolite NAPQI, in excess of that which can be safely processed by the glutathione pathway. This results in generation of reactive oxygen species, accompanied by hepatocyte necrosis in a centrilobular distribution. In mice, this initial injury phase is complete by 24 hours and the regenerative phase dominates from this point on.[115] Experimentally, the dose of acetaminophen administered is titrated to achieve significant injury whilst minimising the incidence of total liver failure and death from multiple organ dysfunction.[114]

Box 5: Mouse models of liver regeneration

The rodent partial hepatectomy model of liver regeneration was initially described in rats.[116,117] The first large study in mice was reported in the 1950s,[11] and the model continues to be a mainstay of the study of liver regeneration to the present day, with only minor technical refinements.[111]

The multi-lobar structure of the liver makes it possible to vary the degree of partial hepatectomy.[118] However, the standard procedure comprises removal of the median and left lobes (Figure 1 - 7).

There is a repeatable, coordinated response to partial hepatectomy. Hepatocytes are the first liver cells to proliferate, with DNA synthesis peaking at 36-48 hours.[111,119,120] The majority of hepatocytes undergo one or two rounds of replication.[121] Hepatocyte proliferation is followed by proliferation of HSCs and LSECs, with regeneration essentially complete by seven days.[122]

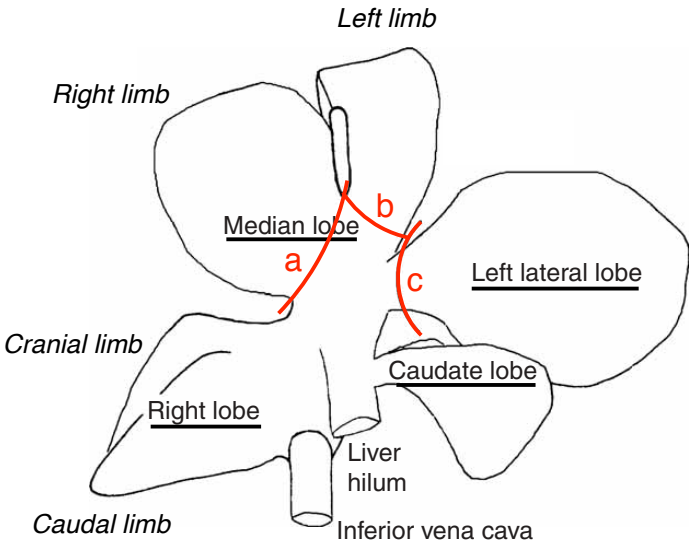

Figure 1 - 7 Mouse liver lobe anatomy and partial hepatectomy.
The multi-lobar mouse liver permits excision of lobes singly or in combination. In the standard 'two-thirds' partial hepatectomy, the left lateral and median lobes are excised. Labelled lines indicate ligating suture location for excision of the right median (a), left median (b), and left lateral (c) lobes. Adapted from Nature Protocols,[111] ©2008, with permission from Macmillan Publishers Ltd.

Box 5 Continued:

Acetaminophen-induced liver injury is a translatable model of injury and repair, as acetaminophen overdose is a major cause of acute liver failure in human patients.[123] Whereas partial hepatectomy is 'pure' model of liver regeneration, with minimal inflammation, acetaminophen evokes a strong inflammatory response whilst also driving liver regeneration.[114,115]

At low doses, the majority of acetaminophen is safely metabolised by glucuronidation and sulphation in the liver, before excretion in urine (Figure 1 - 8).[114] However, a percentage is converted to the highly toxic metabolite NAPQI (N-acetyl-p-benzoquinone imine) by the cytochrome P450 system. Even NAPQI can be processed by the liver without injury, through conjugation to glutathione. But once glutathione stores are depleted, NAPQI results in mitochondrial damage and massive hepatocyte necrosis.

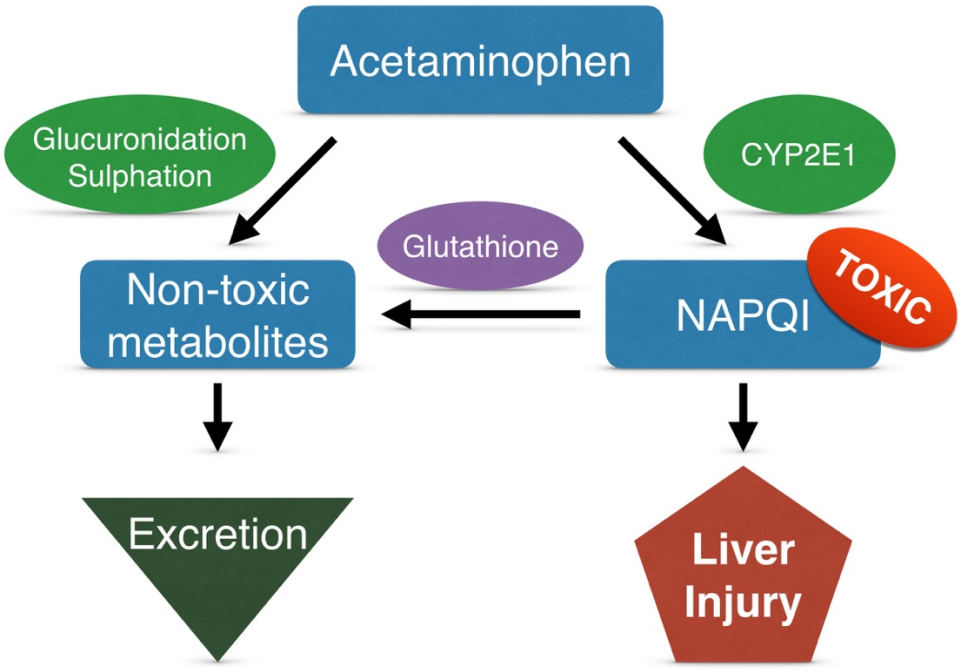

Figure 1 - 8 Routes of acetaminophen metabolism.
At low doses, acetaminophen may be safely metabolised via glucuronidation, sulphation, or conjugation with glutathione. However, in excess, the toxic metabolite NAPQI accumulates and leads to hepatotoxicity.

Transgenic mice

A further, huge advantage gained from using mice to study the process of liver regeneration derives from the major advances that have occurred in transgenic technology in this species over the preceding three decades. The advent of the Cre-lox system now permits cell-specific targeting of gene depletion and reporter protein expression.[124-126] This has greatly enhanced the precision with which gene and cell function can be interrogated. In particular, the opportunities provided by Cre-lox enable the study of certain gene products, including the β8 integrin subunit, for which global or constitutive knockout would be lethal.[127] The resource is now so great that it can essentially be considered as a transgenic targeting 'toolkit'.[128]

The bacteriophage-derived enzyme Cre recombinase essentially functions as a pair of molecular scissors, targeted to cut genomic DNA by the insertion of 'loxP' sites at precise locations (Box 6).[129] Preceding the *Cre* construct with a cell-specific promoter restricts expression to the cell type of interest, and its activity can then be temporally restricted by further transgenic modifications. Hundreds of Cre-expressing mouse lines have already been generated and the number continues to grow.[128] Individual Cre lines can then be interbred with any one of numerous 'floxed' lines to achieve the desired genetic modification, be that inactivation of a gene of interest or switching on expression of a reporter protein (Box 6).

In the liver, cell-specific expression of Cre recombinase is achievable in all of the principal cell types.[129] Depletion of all αv integrins can be achieved by interbreeding the Cre line of choice with a line in which a section of the *Itgav* gene (encoding the αv integrin subunit) has been floxed.[41] Similarly, a floxed *Itgb8* allele (encoding the β8 integrin subunit) allows Cre-mediation depletion of integrin αvβ8.[130]

Box 6: The Cre-lox system

The Cre-lox system facilitates spatial and temporal control of gene expression in mice (Figure 1 - 9).[129] Cre (cyclization recombinase) catalyses DNA recombination. The site and nature of recombination is determined by the location and orientation of two loxP sites. Spatial control of gene expression results from combining the *Cre* construct with cell-specific promoter sequences, to restrict its expression to the cell type(s) of interest. Cre expression may be constitutive in the cell type of interest, although, once recombination has occurred in a cell, the genome modification is heritable and irreversible. Temporal control of recombination may be achieved through various means. These include driving *Cre* expression via the 'Tet system', or linking *Cre* to a modified oestrogen receptor (ER^{T2}). This latter strategy retains Cre outside of the nucleus until tamoxifen (an ER ligand) is administered (Figure 1 - 9B).

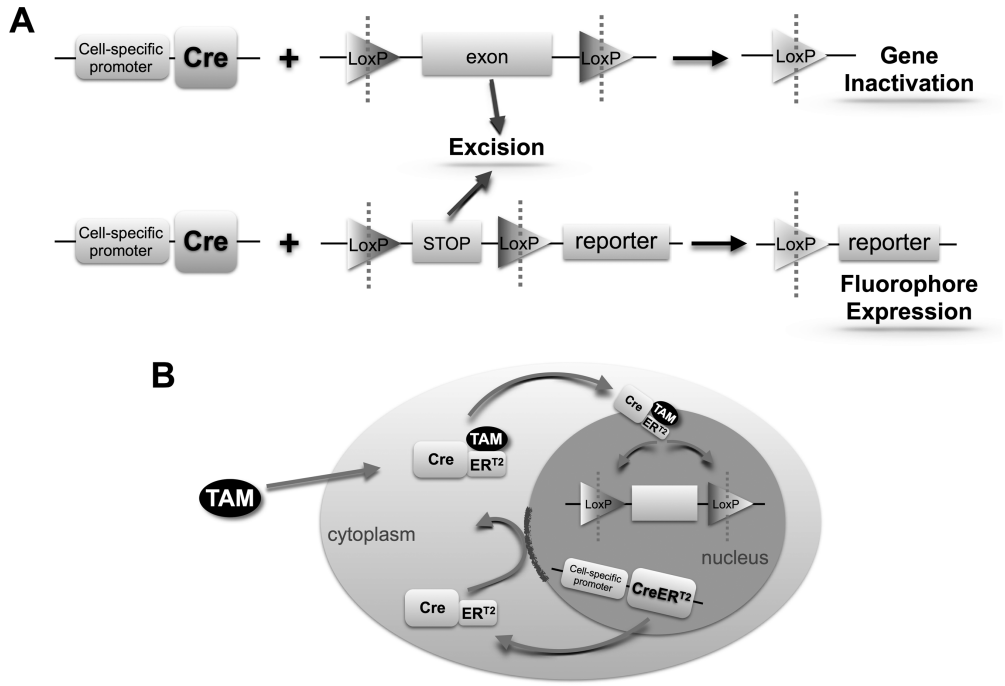

Figure 1 - 9 The Cre-lox system.
Cell-specific expression of Cre, with subsequent recombination, may be used to produce gene inactivation or activation (A). Temporal control of Cre activity may be achieved using a modified version of Cre – $CreER^{T2}$, which is unable to access the nucleus and drive recombination until tamoxifen (TAM) is administered (B). Reproduced from Hepatology,[129] under CC BY 4.0.

Box 6 Continued:

The Cre-lox system can be utilised in a number of ways; for example:

Gene inactivation: loxP sites are inserted to flank ('flox') an exon of the gene of interest; Cre-mediated recombination results in exon excision and prevents transcription of a functional gene product (Figure 1 - 9A, upper).

Gene activation: most commonly applied to switch on (fluorescent) reporter gene expression; a floxed STOP codon before the gene of interest prevents transcription except in cells (and/or until such time as) Cre-mediated excision occurs and permits gene expression (Figure 1 - 9B, lower).

Since insertion of *Cre* and the loxP sites requires two separate transgenic modifications, in theory any Cre line can be interbred with any line with a floxed allele. One copy of any *Cre* or floxed reporter allele is generally sufficient for recombination and reporter protein expression, respectively. However, for maximal gene depletion, mice must be homozygous for the floxed allele.

Assessing TGFβ activity

As stated above, TGFβ is produced in an inactive form and secreted into the extracellular matrix. In liver homogenate, at least 90% of TGFβ is inactive.[131] As such, demonstrating a role for TGFβ in a given biological process cannot be achieved merely by examining TGFβ gene or protein expression. Rather, it is necessary to assess the level of active TGFβ present at the biological site of interest, or alternatively examine downstream effects on TGFβ signalling pathways and transcription.

A number of methods to measure active TGFβ have been reported.[132] Of these, the mink lung epithelial cell (MLEC) system is frequently used to measure levels of active TGFβ.[20-24,29,55,68,70] Its principles are described in further detail in Chapter Four. Briefly, MLECs were modified to express firefly luciferase in response to active TGFβ.[133] As well as being able to measure the amount of active TGFβ in a culture medium or cell supernatant, co-culture with MLECs allows the ability of a cell type of interest to activate latent TGFβ to be assessed. More recently, an alternative system, in which mouse fibroblasts secrete alkaline phosphatase in response to active TGFβ has been reported.[134] The broad principles of both cell-based assays for active TGFβ are similar, although the newer assay claims a degree of increased sensitivity and specificity.

Demonstrating TGFβ activity in tissue remains challenging.[131] Whilst an ELISA approach has been utilised to measure both total and active TGFβ,[29,38,74] its ability to detect low levels of

active TGFβ reliably is questionable.[131] Therefore, an indirect assessment of TGFβ activity is often employed, such as detection of phosphorylated SMAD proteins or quantification of TGFβ-responsive gene expression.[24,29,62,70,91,135,136] In addition to individual genes, such as *Serpine1*, that are known to be highly responsive to TGFβ, a hepatocyte TGFβ 'signature' has been published.[137] This was defined by using microarray to identify 314 genes whose expression was significantly altered, positively or negatively, by the addition of recombinant TGFβ in vitro.

Challenges to studying liver regeneration

Although studying liver regeneration in mouse models offers several advantages in comparison to both in vitro systems and human subjects, there are still limitations. As well as the perennial question of translational relevance to human disease, experimental rodents have generally been considered to be 'single use only'. Animals are humanely killed at relevant time points to allow tissue harvest. Not only does this drastically limit the amount of information that can be gleaned from each individual experimental animal, but only a snapshot of any disease or physiological process is ever obtainable. The temporal dimension of the process under study must therefore be reconstructed by averaging multiple snapshots at each time point before combining them in sequence. It is the scientific equivalent of producing a flick book by merging four (or more) artists' illustrations on every page and always asking different artists to draw the next image in the sequence. Further challenges to biological relevance result from the fact that harvested tissue is, by definition, no longer part of a living organism. Dynamic processes such as blood flow and cell migration cannot be studied in this way. Fixation and other processing steps prior to analysis can also introduce artefacts or mask true biology. In summary, although harvesting tissue from rodent models has facilitated huge advances in our understanding of many biological processes, it can also be seen as costly, scientifically limiting, and restrictive to efforts to reduce experimental animal use.

Intravital imaging

It is for these reasons that, in recent years, rapid advances have been made with regard to imaging tissues or cells of interest in the living subject, be these patients or experimental animals. All such techniques fall broadly under the heading of intravital imaging. The key benefits of intravital imaging are the potential for the tissue of interest to be imaged on more

than one occasion, in situ, with limited or no disruption to cellular processes. External tissues and organs, such as the skin or eye, are readily accessible for imaging. Similarly, techniques such as radiography, ultrasound and magnetic resonance, have permitted intravital imaging of internally-located tissues for many years. However, intravital imaging of internal tissues at a cellular, or even subcellular, level does present a number of challenges. Primarily, light microscopy relies on there being minimal interference to the passage of the beam of light, with only a small distance (of the order of micrometres) between the cells of interest and the objective lens.

To perform intravital microscopy of the liver, several investigators have surmounted these challenges by exteriorising the organ in the anaesthetised animal.[138-143] Whilst this does at least allow dynamic processes to be studied, with the organ more or less in situ, it restricts the period over which imaging in the individual animal can be performed to a few hours at most, since such a procedure must always be performed under terminal anaesthesia. Therefore, repeated imaging in the same subject cannot be performed over a number of days.

Repeat microscopy of internal tissues requires that the tissue of interest is made available for microscopy within a closed, sterile system that also allows the experimental animal to exhibit normal behaviour as far as possible between imaging sessions. Surgical implantation of an imaging 'window' facilitates this by removing the physical barriers to light provided by skin, muscle and bone, whilst maintaining the integrity of the body cavity in question. Typically, such implants consist of a medical-grade metal or alloy with a central aperture over which a glass coverslip is placed. Imaging windows have been used to image the brain, lung (in a non-recovery setting), and various abdominal organs.[144-146] More than one type of window for intravital microscopy of the liver has been reported, illustrating the continuing evolution of such techniques.[146,147]

Intravital microscopy presents its own set of challenges to investigators, as they strive to obtain repeatable, high-quality data at subcellular resolution. Unwanted movement, including respiratory excursion of the anaesthetised animal, is probably the single greatest barrier to obtaining the perfect image. A number of modifications to window implantation technique,[146] immobilisation during imaging,[147] acquisition protocols,[148] and post-acquisition image processing[149,150] can all assist in reducing movement artefact. The tissue of interest must also maintain close apposition to the coverslip. This can be achieved using synthetic adhesive, retaining implants, or simply gravity. The presence of dead space between coverslip and tissue not only directly hampers image quality and depth, but may also promote the

accumulation of biofilms and cellular infiltrates. Furthermore, glass is a biologically reactive material, so coating the coverslip in an inert polymer has been recommended.[146]

Multiphoton microscopy

Concurrent with the technical advances to provide the appropriate conditions in which intravital microscopy of internal tissues may be performed in experimental animals, there have been continuing developments in microscopic techniques. Repeated innovations have improved image resolution and depth, provided new modalities through which biological structures can be visualised, and permitted simultaneous detection and discrimination of multiple (sub-)cellular labels. Epifluorescence and confocal microscopy have both been utilised in intravital imaging.[143,151] However, the greatest technological advance in the context of intravital microscopy came with the advent and application of multiphoton microscopy (Box 7).

The advantages of two photon excitatory fluorescence (TPEF) microscopy, compared to using a single excitatory photon of half the wavelength, include increased depth penetration, reduced light scattering, and lower phototoxicity. Multiphoton microscopy also offers the opportunity of label-free imaging, using second harmonic generation (SHG) and coherent anti-Stokes Raman scattering (CARS). This information can be acquired contemporaneously with detection of more traditional fluorescent antibody labels or dyes, usually administered intravenously. In addition, transgenic technology can be co-opted to drive fluorescent protein expression in cells or structures of interest. This may be achieved through a number of techniques, including knock-in reporter genes and Cre-lox driven reporter expression, with subsequent inter-breeding allowing expression of multiple fluorophores in a single animal. In fact, the vast array of possible labels, combined with the huge amounts of data that can be generated following the intravital imaging of just a single experimental animal, have elevated this field into the world of 'big data', alongside the complementary spheres of whole-genome and RNA sequencing.

Box 7: Multiphoton microscopy

Multiphoton microscopy is not actually a single technique. Rather, it offers several different modalities by which an image can be obtained from a biological specimen. The common feature is the use of multiple excitatory photons in combination (Figure 1 - 10).

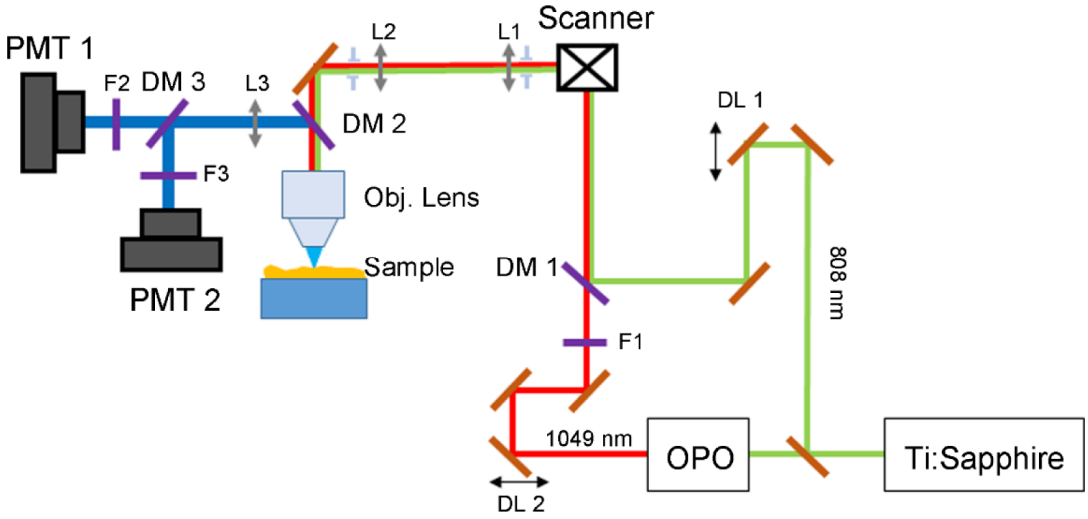

Figure 1 - 10 Example multiphoton microscope setup.
The titanium-doped sapphire laser and optical parametric oscillator (OPO) allow production of two parallel laser beams for TPEF, SHG and CARS microscopy. DL, delay line; DM, dichroic mirror; L, lens; F, bandpass filter; PMT, photomultiplier tube. Reprinted from Biomedical Optics Express,[152] ©2017, Optical Society of America.

TPEF – two photon excitatory fluorescence microscopy was first described in 1990.[153] Conventional fluorescence microscopy relies on the excitation of a molecule by a single, higher energy, shorter wavelength photon, in order to achieve emission of a lower energy, longer wavelength photon for detection. TPEF generates the same emission signal from the simultaneous (within 10^{-18}s) arrival at the focal point of two photons, themselves of lower energy and longer wavelength than the single emission photon they produce (Figure 1 - 11).

SHG – second harmonic generation is a technique that allows label-free imaging of highly ordered structures, such as collagen. Essentially, two identical photons interact with the material, resulting in the generation of a single photon of half the wavelength (Figure 1 - 11).

CARS – Coherent anti-Stokes Raman scattering is another label-free technique which exploits the differential vibrational properties of molecules within a sample. One light beam is used to provide 'pump' and 'probe' photons, in combination with a second Stokes beam. As the molecules relax from the virtual state to which they are excited, returning to the ground energy state, a detectable signal is produced (Figure 1 - 11). CARS can be used to provide an image of general cellular morphology (similar to that of standard brightfield microscopy), but is also well-suited to imaging lipid molecules within a sample.

Box 7 Continued:

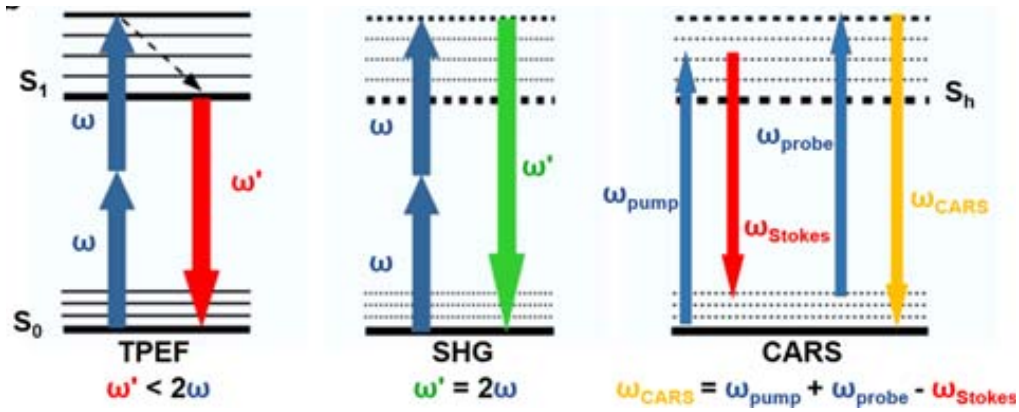

Figure 1 - 11 Multiple photons can be utilised to produce detectable emission signals from biological specimens.
S_0, ground energy state; S_1, excited state; S_h, higher virtual state; ω, frequency. Reprinted from Journal of Biophotonics,[154] ©2016, with permission from John Wiley & Sons Inc., and from Journal of Hepatology,[155] ©2010, with permission from Elsevier.

Multiphoton microscopy is well-suited to intra-vital imaging for a number of reasons: the image is generated from emitted rather than transmitted light; longer wavelength excitatory photons have increased depth penetration and result in decreased phototoxicity to live cells.[154] Further, all three techniques described above can be performed simultaneously, maximising data acquisition relative to imaging time. In liver, TPEF permits simultaneous imaging of multiple fluorescent reporter proteins, exogenously administered fluorescent labels, and intrinsic autofluorescence (such as vitamin A in HSCs). SHG can be used to image the liver capsule and collagen deposition during fibrosis. CARS can be employed to assess hepatocyte lipid dynamics in health and disease.

Although intravital multiphoton microscopy of the liver has been described, it has either been performed as a terminal procedure with the liver exteriorised, or has been applied to the study of biliary excretion or cancer.[147,156] Liver regeneration has not previously been studied with this approach. In some respects, this is surprising. Liver regeneration is a coordinated, dynamic, multicellular process, which takes place, at least in mice, over a time frame short enough to be imaged regularly from start to finish, but enduring long enough that it is unable to be encapsulated by a single, non-recovery imaging session.

The under-representation of liver regeneration within the intravital microscopy literature may be, in part, because of the challenges posed by combining the liver injury necessary to trigger regeneration with the implantation of an imaging window. Understandably, concerns might exist about the potential welfare impact of combining surgical implantation of an

imaging window, induction of liver injury, and repeated imaging sessions under general anaesthesia. Practically, the two-thirds partial hepatectomy model of liver regeneration excises all of the easily accessible liver lobes over which any imaging window might be implanted.

Subsequent chapters describe how the combination of partial hepatectomy and implantation of an imaging window is technically feasible, without increasing the experimental severity limits in place under the terms of the project licence issued by the Home Office. The novel procedure is validated by comparison with the standard model of two-thirds partial hepatectomy. Intravital microscopy of liver regeneration in transgenic, fluorescent reporter mice allows visualisation of the hepatic regenerative niche in situ, three-dimensional imaging of individual cell morphology and movement, and measurement of sinusoidal blood flow and vasculature structure, throughout the entire time course of liver regeneration.

Summary

There is a pressing need to improve our understanding of how the liver is able to regenerate, not least because of the dearth of effective treatments available when this life-sustaining organ fails. This knowledge will facilitate the discovery of novel therapeutic targets which can then be pursued as a means to promote regeneration of a patient's own liver following acute or chronic injury. The αv integrins have been shown to play a role in the progression of liver fibrosis, through their ability to activate latent TGFβ. Given that TGFβ is also a potent inhibitor of hepatocyte proliferation, the experiments described in the following chapters examine whether αv integrins may regulate hepatocyte proliferation and liver regeneration through the activation of TGFβ. In conjunction with the experiments exploring αv integrin-mediated regulation of liver regeneration, a novel experimental model is presented that allows intravital multiphoton microscopy to be performed repeatedly throughout the time course of liver regeneration. This will reduce and refine experimental animal use, maximising both the amount and physiological relevance of the data that can be obtained from each experimental animal. Equally important are the opportunities it provides to reveal previously invisible cellular and molecular mechanisms underpinning the remarkable process of liver regeneration.

Chapter 2 – Materials and Methods

Experimental animal details

Mice

Alb-Cre mice[157] were originally obtained from the Jackson Laboratory. *Pdgfrb-Cre*[158] and *Cdh5-PAC-Cre*^{ERT2} (*Cdh5-Cre*)[159] mice were obtained from R. Adams. *Itgb8*$^{flox/flox}$ mice[130] were obtained from L. Reichardt. *Itgav*$^{flox/flox}$ mice were obtained from A. Lacy-Hulbert.[41] Ai14 (Rosa-CAG-LSL-tdTomato-WPRE), mTmG (TdTomato-eGFP), and Confetti (R26R-Confetti) reporter mouse lines were obtained from the Jackson Laboratory.[160-162] PBAG (*Pdgfrb*-BAC-eGFP) reporter mice were obtained from the Mutant Mouse Regional Resource Center, USA. MacGreen mice were obtained from D. Hume.[163] Fucci (R26Fucci2aR) and *CAG-Cre* mice were obtained from R. Mort.[164] Wild-type C57BL/6J mice were obtained from Charles River Laboratories. All mice were maintained on a C57BL/6J background and housed in specific pathogen-free conditions in the animal facilities at the University of Edinburgh. All procedures were carried out under licence from, and in accordance with, UK Home Office regulations.

Age- and sex-matched littermate controls were used for all experiments. Experimental order was decided at random, with blinding to genotype or treatment group maintained until the time of data analysis. Minimum group sizes for each experiment were decided based on sample size calculations using data previously reported or generated within the group to provide estimates of mean and standard deviation, and to detect a previously agreed effect size with error thresholds for α and β of 0.05 and 0.2 respectively. Groups were then expanded by 1-2 mice per group to ensure that each experiment remained adequately powered, even in the event of surgical or post-surgical complications necessitating the early humane killing of an individual mouse or the exclusion of its data from analysis.

Genotyping of transgenic mice

For 'in-house' genotyping, ear notches were obtained and DNA extracted through addition of 75µL of 1X NaOH-EDTA solution, heating at 95ºC for 30 minutes, cooling on ice for 5 minutes, followed by addition of 75µL of 1X Tris-HCl solution and vortexing. A 50X NaOH-EDTA stock solution (1.25M NaOH, 10mM EDTA, pH 12) was prepared by dissolving 2.5g NaOH (Sigma-Aldrich, S5881) in 40mL distilled water (dH_2O), adding 1mL 0.5M EDTA (pH 8, Sigma-Aldrich, E5134), and making up to 50mL with dH_2O. A 50X Tris-HCl stock solution (2M Tris,

pH 5) was prepared by dissolving 12.114g Trizma base (Sigma-Aldrich, T6066) in 35mL dH_2O, adjusted to pH 5 by the addition of HCl (Sigma-Aldrich, 435570) and made up to 50mL with dH_2O.

A PCR mastermix was prepared in the proportions shown in Table 2 - 1 using reagents from the Taq PCR Core Kit (Qiagen, 201225). Allele-specific primers (Integrated DNA Technologies, Table 2 - 2) were prepared as 100μM stock solutions in DNase-free/RNase-free dH_2O (Thermo Fisher Scientific, 10977-035). Working solution concentration and volume added to individual mastermixes are shown in Table 2 - 2. For each reaction, 11.5μL of mastermix was used, with the addition of 1μL of extracted DNA. Amplification was performed using a T100 Thermal Cycler (Bio-Rad) and optimised cycle protocols (Table 2 - 3). PCR products were detected by DNA electrophoresis using the QIAxcel Advanced System (Qiagen) and QIAxcel DNA Fast Analysis Kit (Qiagen, 929008) according to the manufacturer's instructions. The expected size of the amplified product for each allele is shown in Table 2 - 4. The Fucci allele was genotyped by Transnetyx using real time PCR with specific probes for monomeric red fluorescent protein (mRFP) and the wild-type ROSA allele.

Table 2 - 1 Standard genotyping mastermix

Mastermix Component	Volume per sample (μL)
5X Q-solution	2.5
10X PCR Buffer	1.25
dNTP Mix	0.25
Taq DNA Polymerase	0.1
Primers	variable
H_2O	variable
Final Volume	11.5

Table 2 - 2 Primer sequences for genotyping

Allele	Primer name	Working solution (μM)	Volume per sample (μL)	Primer sequence
Ai14	wild-type for	25	0.2	AAG GGA GCT GCA GTG GAG TA
	wild-type rev			GGC ATT AAA GCA GCG TAT CC
	mutant for			CTG TTC CTG TAC GGC ATG G
	mutant rev			CCG AAA ATC TGT GGG AAG TC
Confetti*	wild-type for	25	0.5	CTC CTG GCT TCT GAG GAC C
	confetti for			GAA TTA ATT CCG GTA TAA CTT CG
	common rev			CCA GAT GAC TAC CTA TCC TC
Cre	cre for	25	0.5	GCG GTC TGG CAG TAA AAA CTA TC
	cre rev			GTG AAA CAG CAT TGC TGT CAC TT
	control for			CTA GGC CAC AGA ATT GAA AGA TCT
	control rev			GTA GGT GGA AAT TCT AGC ATC ATC C
Itgav	for	25	0.2	TTC AGG ACG GCA CAA AGA CCG
	rev			CAC AAA TCA AGG ATG ACC AAA
Itgb8	for	25	0.2	GAGATGCAAGAGTGTTTACC
	rev			CACTTTAGTATGCTAATGATGG
MacGreen	eGFP for	10	0.3	GCA CGA CTT CTT CAA GTC CGC CAT GCC
	eGFP rev			GCG GAT CTT GAA GTT CAC CTT GAT GCC
	fabpi for			CCT CCG GAG AGC AGC GAT TAA AAG TGT CAG
	fabpi rev			TAG AGC TTT GCC ACA TCA CAG GTC ATT CAG
mTmG	common for	20	0.6	CTC TGC TGC CTC CTG GCT TCT
	wild-type rev		0.4	CGA GGC GGA TCA CAA GCA ATA
	mutant rev		0.8	TCA ATG GGC GGG GGT CGT T
PBAG	eGFP for	25	0.2	CCT ACG GCG TGC AGT GCT TCA GC
	eGFP rev		0.2	CGG CGA GCT GCA CGC TGC GTC CTC
	actin for		0.4	GAT GAC GAT ATC GCT GCG CTG GTC G
	actin rev		0.4	GCC TGT GGT ACG ACC AGA GGC ATA CAG

All primers are presented as 5' – 3'. For, forward; rev, reverse. *wild-type and mutant primers run separately.

Table 2 - 3 Thermal cycler settings

Allele:	Ai14		Confetti		Cre		Itgav	
Temp (ºC) / time (min:sec):								
1. Initial denaturation	94	3:00	95	3:00	94	5:00	95	2:00
2. Denaturation	94	0:20	95	0:30	94	0:30	94	0:30
3. Annealing	61	0:30	58	0:30	57	0:45	64	0:45
4. Extension	72	0:30	72	0:30	72	2:00	72	1:00
5. Final extension	72	2:00	72	5:00	72	10:00	72	10:00
Repeats of steps 2-4	35		35		29		35	

Allele:	Itgb8		MacGreen		mTmG		PBAG	
Temp (ºC) / time (min:sec):								
1. Initial denaturation	94	5:00	94	3:30	94	3:00	94	3:00
2. Denaturation	94	0:30	94	0:30	94	0:30	94	0:30
3. Annealing	57	0:30	65	0:30	61	1:00	58	0:45
4. Extension	72	0:45	72	1:00	72	1:00	72	0:45
5. Final extension	72	10:00	72	7:00	72	2:00	72	10:00
Repeats of steps 2-4	39		34		34		30	

Table 2 - 4 Expected size of qPCR product

Allele	Product	Expected size (base pairs)
Ai14	mutant	196
	wild type	297
Confetti	mutant	300
	wild type	270
Cre	control	324
	cre	100
Itgav	floxed	400
	wild type	250
Itgb8	floxed	350
	wild type	300
MacGreen	eGFP	280
	fabpi	500
mTmG	mutant	250
	wild type	330
PBAG	eGFP	360
	actin	1000

Surgical procedures

Standard partial hepatectomy

Two-thirds partial hepatectomy was performed as previously described[111,165] with minor modifications, including performing the procedure via a 'mini-laparotomy' incision, through which the median and left liver lobes were exteriorised in preparation for excision. The two segments of the median lobe were ligated individually, either side of the gall bladder, prior to

excision. Lobe ligation was performed with 1.5M braided silk (SMI, 8015); closure of the linea alba was performed using a simple continuous suture of 1.5M polyglactin 910 (Ethicon, Vicryl, W9067). Skin closure was achieved with surgical clips (Biochrom, 9mm Autoclips, 52-3748).

Mice were anaesthetised with isoflurane (Abbott) in 100% oxygen and kept on a heated mat during anaesthesia and recovery. Eye lubricant was applied (Viscotears® Liquid Gel, Alcon Laboratories (UK) Ltd). Warmed, sterile 0.9% saline (25mL/kg, Braun, Sodium Chloride 0.9% w/v Intravenous Infusion BP) was administered subcutaneously at time of surgery. Analgesia was provided with local instillation of 2-4 drops of bupivacaine (Marcain 0.25%, AstraZeneca) at the midline at time of surgery, and buprenorphine (0.1mg/kg, Ceva, Vetergesic), diluted to 0.03mg/mL in sterile water for injection and administered subcutaneously pre-operatively and 8-12 hours post-operatively. Mice were assessed twice daily until the end of the experiment. Additional, 'rescue' analgesia (0.05-0.1mg/kg buprenorphine subcutaneously) was available for administration, but was not required.

Mice were humanely killed by cervical dislocation (or exposure to a rising concentration of CO_2 where blood sampling was required) at pre-specified time points for liver harvest. Mice were weighed at time of surgery and harvest. The weights of excised and harvested liver were also recorded; harvested liver was weighed intact prior to fixation.

Standard Abdominal Imaging Window insertion

Implantation of the abdominal imaging window (AIW) onto the uninjured liver was performed as described, with minor modifications.[146] Mice were anaesthetised and provided with local and systemic analgesia as for standard partial hepatectomy above. Following clipping, additional hair removal was performed by application of depilatory cream (Veet® Hair Removal Cream – Legs & Body – Sensitive Skin, Reckitt Benckiser) for 1-2 minutes, followed by removal with a standard swab. The surgical site was then prepared in a routine manner with chlorhexidine.

A small midline laparotomy incision was made, large enough to allow the left lateral lobe of the liver to be expressed. The falciform and hepatophrenic ligaments were carefully incised to the level of the vena cava using Castroviejo microsurgical scissors. A purse string suture was laid, through the skin and abdominal muscle layers to encompass the incision, using Mersilk 4-0 suture (Ethicon, W501). The free ends were left at the caudal end of the incision. The left lateral lobe was then expressed and positioned for application of the AIW.

The AIW (and accompanying inlay) design is shown in Chapter Five. Cyanoacrylate (Loctite Powerflex Gel, Henkel) was applied to the underside rim of the AIW (8mm internal

aperture version) before it was gently pressed onto the lobe surface and allowed to adhere undisturbed for three minutes. The lobe was then returned to the abdominal cavity and the purse string suture was tightened to draw the body wall into the central groove of the AIW, and then tied to hold the AIW in place and contiguous with the body wall. The exposed liver in the centre of the AIW aperture was moistened with saline before the inlay and coverslip assembly were screwed into place. Gentle pressure was applied laterally and dorsally to the abdominal cavity to assist the liver in contacting the coverslip. The mouse was then allowed to recover and observed closely for signs of AIW displacement.

Coverslip preparation

The AIW coverslips were prepared in a similar manner to that previously described.[146] Circular coverslips (12mm diameter, 1.5H, CellPath, SAN-5012-03A) were adhered to the external surface of the AIW inlay with cyanoacrylate (Loctite Powerflex Gel, Henkel) and allowed to dry for a minimum of two hours. The assembly was then disinfected by immersion in 70% ethanol for a minimum of 30 minutes. In a sterile flow cabinet, the coverslips were allowed to dry prior to application of a poly(L-lysine)-graft-poly(ethylene glycol) (PLL[20]-g[3.5]-PEG[2], SuSoS) solution to the underside. This was left in situ for one hour, before washing off with PBS and allowing to dry. A 1mg/mL stock solution of PLL-g-PEG was prepared by dissolving (by rolling) in 10mM HEPES buffer (pH 7.4, Sigma-Aldrich, H3375) and then filter sterilising. Shortly before use, this was diluted to the working concentration of 0.1mg/mL, again using 10mM HEPES.

Pilot experiment to compare standard partial hepatectomy with a reduced partial hepatectomy

Standard partial hepatectomy was performed in C57BL/6J mice using the anaesthesia protocol and surgical approach described above. For reduced partial hepatectomy, mice had only the right median and left lobes excised; the left median lobe was not excised. 5-Bromo-2'-deoxyuridine (BrdU) was administered as described below. At 48 hours post partial hepatectomy, mice were humanely killed by cervical dislocation. Mice were weighed at time of surgery and harvest. The weights of excised and harvested liver were recorded.

Combining partial hepatectomy with AIW insertion

The development of this technique is described in Chapter Five. Mice were anaesthetised and prepared for surgery as described above. A small (~10mm) midline laparotomy incision was made, starting from the tip of the xiphisternum. The xiphisternum itself was clamped with

haemostat forceps and then excised. The falciform and hepatophrenic ligaments were incised as described above. The median and left lateral lobes were exteriorised by moderate abdominal pressure. The right median and left lateral lobes were excised as for standard partial hepatectomy. Care was taken to avoid trauma to the left median lobe, and it was kept moist through intermittent application of sterile saline. Following excision of the first two hepatic lobes, the left median lobe was replaced within the abdominal cavity.

The midline incision was then extended caudally by another 10-15mm. Miniature Gelpi retractors (InterFocus Ltd, 17017-10) were placed to hold open the abdominal incision. A duodenal manoeuvre was performed and the intestines exteriorised onto, and covered by, a moistened swab to the left-hand side of the mouse. This facilitated visualisation of, and access to, the caudal right lobe of the liver, which was then excised in a standard manner. Excision was assisted by incision of the serous membrane linking this lobe to the caudal body wall.

Upon completion of the modified partial hepatectomy, a purse string suture was placed in an identical manner to that of the standard AIW insertion. Additional simple interrupted sutures were pre-placed in the abdominal muscle layer to allow subsequent closure of the caudal portion of the midline incision not included within the purse string. The left median lobe was drawn gently caudally and midline to permit AIW placement. The AIW (5.2mm internal aperture version) was placed onto the lobe as described above and secure within the body wall by the purse string suture. The pre-placed sutures in the abdominal wall were then tightened to complete closure of the abdominal cavity. Simple interrupted sutures were then placed caudally to the AIW to complete skin closure. The inlay (with attached coverslip) was placed as described above.

Validation of the modified partial hepatectomy with AIW insertion procedure

Wild-type mice were randomly allocated to receive one of three procedures: standard partial hepatectomy, modified partial hepatectomy (excising right median, left, and caudal right lobes) or modified partial hepatectomy with AIW insertion. All procedures were performed as described above. In the first series, livers were harvested at 48 hours, following BrdU administration as described below. Serum was also obtained. In the second series, livers were harvested at seven days. Mice were weighed at time of surgery and harvest. The weights of excised and harvested liver were recorded, accounting for the weight of the AIW where applicable.

Non-surgical procedures

Tamoxifen administration

To induce recombination in *Cdh5-Cre* lines, tamoxifen (Sigma-Aldrich, T5648) was dissolved (37ºC, overnight, protected from light, with rolling) at 20mg/mL in corn oil (Sigma-Aldrich, C8267), sterile-filtered (Millex-GP 0.22µm filter unit, Merck Millipore, SLGP033RS, unless otherwise stated), and administered intra-peritoneally at 100mg/kg. The standard dosing schedule was once daily for five consecutive days.

Acetaminophen-induced liver injury

Acetaminophen (Sigma-Aldrich, A7085) was dissolved (37ºC, 30 mins, with shaking) in 0.9% sterile saline (Baxter, UKF7124) and sterile-filtered. For routine experiments, mice were fasted for 12 hours prior to intra-peritoneal administration of 300mg/kg acetaminophen (10mg/mL solution). For intravital imaging experiments, mice were fasted for 16 hours and a 20mg/mL acetaminophen solution administered at 350mg/kg.

5-Bromo-2'-deoxyuridine administration

5-Bromo-2'-deoxyuridine powder (BrdU, Sigma-Aldrich (Roche), 10280879001) was dissolved (55ºC, 30 mins) in sterile PBS (Thermo Fisher Scientific, 14190-094) at 20mg/mL, 1mL aliquots were prepared and stored at -20ºC. To label proliferating cells, warmed, re-suspended BrdU was injected intra-peritoneally at 100mg/kg, two hours prior to humane killing.

In vivo administration of β8 integrin subunit blocking antibody

The β8 integrin subunit blocking antibody[60] and an isotope-matched, non-binding control antibody were diluted to a working concentration of 0.5mg/mL in sterile PBS. Wild-type mice received 3mg/kg of either control or blocking antibody via intra-peritoneal injection, immediately prior to two-thirds partial hepatectomy.

Injection of fluorescently-labelled red blood cells

Donor mice were humanely killed and whole blood obtained through cardiac puncture. Blood was anti-coagulated by placing immediately into collection tubes containing sodium citrate (Greiner, 9NC, 459075) and inverting gently. Following centrifugation (500g, 4ºC, 10 minutes) and removal of plasma, the red blood cells were re-suspended and centrifuged three times with PBS (Thermo Fisher Scientific, 14190-094) to wash, before re-suspending in PBS at 100 times the cellular volume in preparation for labelling. Vybrant DiO cell-labelling solution (Thermo Fisher Scientific, V22886) was added at 5µL/mL for 20 minutes at room temperature,

before centrifugation and re-suspending in an equal volume of PBS. Mice were injected with 200μL of labelled red blood cells via the tail vein.

Intravital imaging

Mice with a pre-implanted AIW were examined prior to anaesthesia for intravital imaging in order to ensure their fitness for the procedure. General anaesthesia was induced and maintained using isoflurane in 100% oxygen. Immediately following induction of anaesthesia, eye lubricant was applied and saline administered subcutaneously as described above. Mice were then placed in dorsal recumbency on a heated mat to allow examination of the AIW, coverslip and visible liver within the imaging aperture. In order to maximise the quality of the subsequent intravital images, it was usually necessary to remove and flush (with saline) or replace the coverslip and inlay assembly. This was performed in an aseptic manner, following preparation of the external surface of the AIW and surrounding skin with chlorhexidine. Accumulated biofilm on the surface of the liver was also removed with great care using sterile cotton buds or forceps. In terminal imaging experiments in which nuclear labelling was performed, Hoechst 33342 (Thermo Fisher Scientific, H1399) was prepared according to the manufacturer's instructions and applied topically to the surface of the liver at a working concentration of 5μg/mL.

Once prepared, the mouse was placed in sternal recumbency within the bespoke, heated imaging box. Anaesthesia was maintained through the provision of isoflurane (typically 0.8-1.0%) in 100% oxygen (~0.5L/min) and depth of anaesthesia was carefully titrated to maintain the mouse in the lightest possible plane. The external rim of the AIW was seated precisely within the baseplate to minimise motion artefact during imaging. Total duration of anaesthesia was restricted to two hours for recovery procedures or six hours for terminal procedures.

AIW and imaging baseplate design

Original AIWs were obtained from J. van Rheenen. The design was modified, as described in Chapter Five, using Autodesk AutoCAD 2016, (version M.49.0.0). Prototypes were printed in Vero White using an Objet Connex 260 3D printer, before being manufactured in titanium by ZME Fijnmechanisch Atelier B.V. The imaging baseplate into which the new AIW was inserted during intravital microscopy was designed as above and produced in aluminium by Computer Numerical Control machining (Proto Labs Inc.).

Sample collection and processing

Liver lobe weight measurements

Five surplus C57BL/6J mice were humanely killed by cervical dislocation, weighed, and then the liver was excised whole and weighed. Livers were then dissected and the weight of each lobe measured. Separately, five surplus C57BL/6J mice were humanely killed and surgical excision of individual lobes was performed via laparotomy, as described above. Excised liver tissue was weighed, as was the remnant liver.

Serum biochemistry

Whole blood was collected immediately post mortem by cardiac puncture, allowed to clot, and serum obtained by centrifugation (9391g, 5 minutes, twice). Samples were frozen at -20ºC pending analysis. Serum albumin, total bilirubin, alanine transaminase (ALT), and alkaline phosphatase (ALP) measurements were determined using commercial kits (Alpha Laboratories Ltd [albumin, bilirubin, ALT]; Randox Laboratories [ALP]) adapted for use on a Cobas Fara centrifugal analyser (Roche Diagnostics).

Primary hepatocyte isolation

Mice were humanely killed and livers perfused in situ, via cannulation of the thoracic vena cava, for 4 minutes with Liver Perfusion Medium (Thermo Fisher Scientific, 17701-038) followed by Liver Digest Medium (Thermo Fisher Scientific, 17703-034, pre-filtered using a Millipore Stericup-GP, SCGPU05RE) for 7-8 minutes, before a further 2 minutes of Liver Perfusion Medium. Flow rate was maintained at 5 mL/min using a peristaltic pump (Minipuls 2, Gilson) and media were maintained at 37ºC. The liver was then excised and placed in Hepatic Perfusion Medium (HPM) consisting of Dulbecco's Modified Eagle Medium (Thermo Fisher Scientific, 21969-035), 5% heat-inactivated foetal bovine serum (Thermo Fisher Scientific, 10500-064), 2% L-Glutamine 200mM (Thermo Fisher Scientific, 25030-024), 1% Penicillin-Streptomycin 10,000U/mL (Thermo Fisher Scientific, 15140-122).

The digested liver was minced and passed through a 100µm cell sieve (EASYstrainer, Greiner Bio-One, 542000), before pelleting (90g, 2 minutes, Heraeus Multifuge 1S-R, Thermo Fisher Scientific) and resuspending twice with HPM to wash. Hepatocytes were then purified by centrifugation (200g, 15 minutes) through 50% equilibrated Percoll. Equilibrated Percoll was prepared by combining Percoll (GE Healthcare, 17-0891-01) with sterile-filtered 10X Dulbecco's Modified Eagle Medium (DMEM) in a 9:1 ratio. The 10X DMEM solution was prepared from DMEM powder (Thermo Fisher Scientific, 12800-082) and 0.037g/mL $NaHCO_3$

(Sigma-Aldrich, S6297). The equilibrated Percoll was subsequently diluted 1:1 with HPM to produce 50% equilibrated Percoll solution. The purified hepatocyte pellet was then resuspended in HPM, before pelleting (90g, 2 minutes) and resuspending twice to wash out the Percoll. Total cell count and viability were calculated using a NucleoCounter NC-100 (ChemoMetec) according to the manufacturer's instructions.

Primary liver sinusoidal endothelial cell isolation

Mice were humanely killed and livers perfused in situ with ice-cold PBS (Thermo Fisher Scientific, 14190-094) via the right ventricle of the heart. Samples and reagents were kept at 4ºC unless indicated. Liver was minced prior to digestion with Collagenase Type I (Thermo Fisher Scientific, 17100-017) and DNase I (Roche, 10104159001) in HBSS (with $CaCl_2$/$MgCl_2$, Thermo Fisher Scientific, 14025-050), shaking for 20 minutes at 37ºC. Samples were passed through a 70μm cell sieve EASYstrainer, Greiner Bio-One, 542070) and diluted in PEB buffer, containing PBS (Thermo Fisher Scientific, 14190-094), 2% Foetal Bovine Serum (Thermo Fisher Scientific, 10500-064), and 2mM EDTA (Sigma-Aldrich, E5134), before pelleting (400g for 7 minutes at 4ºC, Heraeus Megafuge 40R, Thermo Fisher Scientific). Samples were resuspended in Red Cell Lysis buffer (BioLegend, 420301) for 5 minutes before washing, pelleting, resuspending, and filtering through a 35μm nylon mesh (Corning, 352235).

Samples were pelleted and blocked with 1% CD16/32 (BioLegend, 101302) and 10% mouse serum (Sigma-Aldrich, M5905) for 10 minutes. Fluorescent conjugated antibodies (Table 2 - 7), either CD31-APC and CD45-PE/Cy7, or CD31-PE/Cy7 and CD45-PerCP/Cy5.5, were then applied and samples incubated for 15 minutes before washing, pelleting and re-suspending.

Flow cytometry and fluorescence-activated cell sorting

For flow cytometry or fluorescence-activated cell sorting (FACS), cells were isolated and stained with antibody as described above. Lasers and bandpass filters for each fluorophore are shown in Table 2 - 5. Controls for compensation and gating included an unlabelled sample, beads (UltraComp eBeads, Thermo Fisher Scientific, 01-2222-42) stained with single antibodies, and 'fluorescence-minus-one' samples. A live/dead stain (DAPI, Invitrogen, D3571) was added immediately prior to cytometry or sorting. Compensation for the eGFP and tdTomato intrinsic fluorescent reporters was assessed using GFP beads (Clontech Laboratories, Inc., 632594) and cells isolated from a mouse expressing only tdTomato.

LSECs were analysed by flow cytometry using an LSRFortessa (BD Biosciences) and FlowJo 10.0.8r1, with the following gating strategy. The cell population was gated on forward (FSC-A) vs side (SSC-A) scatter, with single cells gated on FSC-A vs FSC-H. Live cells were selected based on negative DAPI staining. Endothelial cells were identified as $CD31^+$, $CD45^-$. Efficiency and specificity of recombination in the *Cdh5-Cre;*mTmG reporter mouse (following tamoxifen administration) was assessed by assessing the percentage of cells in the endothelial cell population that were GFP^+ and the percentage of GFP^+ cells that were $CD31^+$, $CD45^-$.

LSECs were isolated by FACS using a FACSAria II (BD Biosciences) to sort single, live, $CD31^+$, $CD45^-$ cells.

Table 2 - 5 Laser and filter setup for flow cytometry and FACS

Label	Laser (wavelength, nm)	Longpass filter	Bandpass filter
APC	Red (640)		670/14
DAPI	UV (355)		450/50
GFP	Blue (488)	505	525/50
PE/Cy7	Yellow-Green (561)	750	780/60
PerCP/Cy5.5	Blue (488)	685	710/50
tdTomato	Yellow-Green (561)		582/15

In vitro cell adhesion assay

To confirm optimal plating density, the utility of poly-L-lysine as a positive adhesion control, and time to adhesion, primary hepatocytes were isolated from a single wild-type mouse, as described above. Hepatocytes were plated, in triplicate, at densities of 25,000, 50,000, and 75,000 live cells per well onto tissue culture plastic (untreated), collagen-coated wells, or poly-L-lysine-coated wells of a 96-well, flat-bottomed, tissue-culture plate (Costar, 3595). Collagen-coating was achieved by preparing a sterile-filtered 50μg/mL solution of Type I Collagen (Millipore, 08-115) in 0.01N acetic acid (Sigma-Aldrich, A6283). The collagen-coated wells were coated with 64μL of the collagen solution, to achieve a coating of 10μg collagen per cm. Poly-L-lysine 0.01% (Sigma-Aldrich, P4832) was applied to relevant wells at 50μL/well. Collagen and poly-L-lysine solutions were left for two hours before washing twice with HBSS (Thermo Fisher Scientific, 14175-053). Wells were then allowed to dry for a further two hours prior to introduction of cells and medium. Cells were incubated at 37ºC in 5% CO_2. Wells were then observed at 50X magnification (Axiovert 200, Zeiss) immediately post-plating and then every 30 minutes up to two hours. Images were obtained of wells pre and post washing with HBSS at 30 minutes and 120 minutes post plating.

To perform the in vitro adhesion assay, primary hepatocytes were isolated as paired samples from one *Itgav*$^{flox/flox}$*;Alb-Cre* mice and a littermate control as described above. Order was decided at random and samples were blinded during hepatocyte isolation. An ECM Cell Adhesion Array Kit (Millipore, ECM540) was prepared and utilised according to the manufacturer's instructions. Hepatocytes were plated in triplicate at 50,000 viable cells per well, and incubated for two hours at 37ºC in 5% CO_2. Following washing, staining, and repeat washing to remove unbound stain, the cell-bound stain was solubilised and absorbance at 570nm was determined by plate reader (Synergy HT, Biotek). In addition to absolute absorbance, relative absorbance to the Bovine Serum Albumin negative control was calculated to account for any background absorbance. Similarly, relative absorbance to that of Collagen Type I was calculated to account for any small differences in viable cell number between replicates and samples.

In vitro TGFβ activation assays

Cell line culture

Cryopreserved Huh7, HepG2, and LX-2[166] (obtained from S.L. Friedman) cell lines were resuscitated and cultured in 75cm^2 culture flasks (Corning, 430641U) to 70% confluence using standard medium (DMEM, 10% foetal bovine serum, 1% penicillin and streptomycin, 1% L-glutamine). Single-cell suspensions were prepared by removing culture medium, washing with PBS, adding 1.5mL trypsin (Thermo Fisher Scientific, 25300-054), incubating at 37ºC for 5-10 minutes, inactivating trypsin with 4mL culture medium, then pelleting (300g, 5 minutes), and re-suspending in culture medium.

Transgenic mink lung cell co-culture assay

Transgenic mink lung cells (TMLCs, obtained from D. Rifkin) were cultured in standard medium (DMEM, 10% foetal bovine serum, 1% penicillin, 1% L-glutamine) with the addition of 0.25mg/mL Geneticin (G418 sulfate, Thermo Fisher Scientific, 10131035). Co-culture was performed as previously described,[132,133] in an opaque, 96-well, tissue culture-treated plate (Corning, 3917). Cells were also cultured on a standard, tissue culture-treated plate to allow microscopy examination during the incubation period. TMLCs were seeded at a density of 15,000 per well. For co-culture with cell lines, the test cells of interest were added immediately after. For co-culture with primary hepatocytes, TMLCs were allowed to attach for six hours at 37ºC in 5% CO_2, prior to addition of test cells. Primary hepatocytes were isolated as described above. Test cells were added at 25,000 per well, 50,000 per well, 75,000 per well, 100,000 per

well (not every density was used in every experiment). Control wells included: medium only, TMLCs only, test cells only, TMLCs with recombinant human TGFβ-1 (rhTGFβ), TMLCs with rhTGFβ and TGFβ antibody, TMLCs with test cells and TGFβ antibody. Test wells (TMLCs with test cells) were plated in triplicate. The final volume for each well was adjusted to 200μL. In the Huh7 co-culture experiment only, standard medium was replaced with serum-free medium after two hours. Plates were incubated for 16-20 hours at 37ºC in 5% CO_2. Following incubation, cells were washed twice with PBS. Luciferase activity was assessed using the Luciferase Assay System (Promega, E1500) according to the manufacturer's instructions. Following cell lysis and substrate addition, luminescence was immediately assessed by plate reader (Synergy HT, Biotek). Recombinant human TGFβ-1 (R&D, 240-B) was reconstituted to a stock concentration of 2μg/mL with 1mg/mL Bovine Serum Albumin (Sigma-Aldrich, A7906) in 4mM HCl (Sigma-Aldrich, 435570) and used at a working concentration of 2ng/mL. It was supplemented at 0.1ng/mL (4pM) unless otherwise stated. TGFβ antibody (R&D, MAB1835) was reconstituted at 0.5mg/mL in sterile PBS and supplemented at 0.05mg/mL.

MFB-F11 co-culture assay

MFB-F11 reporter cells were obtained from H. McSorley and cultured in standard medium with the addition of 15μg/mL Hygromycin B (Thermo Fisher Scientific, 10687-010). On reaching 90% confluence, a single-cell suspension was prepared as described above, with re-suspension in a low-serum (2.5% foetal bovine serum) medium. Cells were seeded at a density of 40,000 per well in a 96-well flat-bottom plate (Corning, 3595) and allowed to attach (3-4 hours, 37ºC, 5% CO_2). Primary hepatocytes were isolated as described above and added to the test wells at either 50,000 or 100,000 per well. rhTGFβ and TGFβ antibody were used as controls, as described above. In addition, recombinant human latent TGFβ-1 (latent TGFβ, R&D, 299-LT-005) was added at 50 or 100 ng/mL. After 36 hours, 20μL of culture supernatant was added to 180μL of p-Nitrophenyl phosphate solution (pNPP, Sigma-Aldrich, N2770) in a new 96-well plate and incubated at room temperature, protected from light, for 24 hours. Absorbance at 405nm was measured using a plate reader (Synergy HT, Biotek).

Primary hepatocyte culture with β8 integrin subunit blocking antibody

Primary hepatocytes were isolated as described above, resuspended in low-serum medium (DMEM (Thermo Fisher Scientific, 11960-044), 2.5% heat-inactivated Foetal Bovine Serum (Thermo Fisher Scientific, 10500-064), 2% L-Glutamine (Thermo Fisher Scientific, 25030-024), 1% Penicillin Streptomycin (Thermo Fisher Scientific, 15140-122)) and plated onto collagen-

coated wells (Collagen Type I, Millipore) in a 6-well plate at a density of 5 x 10^5 cells/well. Either β8 integrin subunit blocking antibody[60] or control antibody were added at 20μg/mL and samples were incubated for 24 hours at 37ºC in 5% CO_2. Wells were then washed with PBS and cells lysed as described below.

Gene expression analysis

RNA was isolated from whole mouse liver, primary hepatocytes or LSECs using an RNeasy Mini Kit (whole liver, hepatocytes) or RNeasy Plus Micro Kit (LSECs) (Qiagen, 74034/74104) according to the manufacturer's instructions. Cells were lysed with RLT buffer from the aforementioned kits, with the addition of 10μL/mL β-mercaptoethanol (Sigma-Aldrich, M7522). Homogenisation was performed using QIAShredder columns (Qiagen, 79656) and centrifugation (20238g, 2 minutes). RNA quantity and purity was assessed using the Nanodrop 1000 Spectrophotometer (Thermo Fisher Scientific).

Reverse transcription to cDNA was performed using the QuantiTect Reverse Transcription Kit (Qiagen, 205311) according to the manufacturer's instructions. Control samples with no template or with no reverse transcriptase were also prepared.

Real-time quantitative PCR was performed using the QuantiTect SYBR Green PCR Kit (Qiagen, 204143) according to the manufacturer's instructions. Reactions were set up in triplicate in a MicroAmp 96-well 0.1mL Reaction Plate (Applied Biosystems, 4346907), sealed with MicroAmp Optical Adhesive Film (Applied Biosystems, 4311971). Primers are listed in Appendix 1 and cycling conditions in Table 2 - 6. A 'no-template control' was run for each gene. Samples were amplified on an ABI 7900HT thermocycler (Applied Biosystems) and normalised to mean *Actb* and/or *Gapdh* expression. A dissociation curve was run for all analyses to assess reaction specificity and the presence of primer-dimers.

Table 2 - 6 qPCR thermal cycler settings

	Temp (ºC)	Time (min:sec)
1. Initial denaturation	95	15:00
2. Denaturation	94	0:15
3. Annealing	55	0:30
4. Extension	72	0:30
Repeats of steps 2-4	45	

TGFβ signalling qPCR array

To assess TGFβ signalling, a custom RT2 Profiler PCR array (Qiagen, 330171) was designed containing the genes shown in Appendix 2. RNA was isolated following primary hepatocyte culture with β8 integrin subunit blocking, as described above, and reverse transcribed using the RT2 First Strand Kit (Qiagen, 330401). qPCR was performed using RT2 SYBR Green ROX qPCR Mastermix (Qiagen, 330522) on an ABI 7900HT thermocycler; gene expression was normalised to mean *Actb* and *Gapdh* expression. Standardisation and expression analysis is described below.

Tissue fixation and preparation

Mouse liver tissue

Liver samples for DAB (3,3'-diaminobenzidine) immunohistochemistry were fixed overnight at room temperature in either methacarn (60% methanol, 30% chloroform, 10% acetic acid), for BrdU immunohistochemistry, or 10% neutral buffered formalin. Samples were then paraffin-embedded prior to sectioning. Standard section thickness was 4μm.

Fixed-frozen tissue preparation was performed by placing in 4% paraformaldehyde at 4ºC overnight, before washing with PBS and dehydrating through serial sucrose gradients (10% then 20% for 1 hour each at room temperature, followed by 30% overnight at 4ºC). Tissue was then placed in OCT embedding matrix (Thermo Fisher Scientific, 12678646) and frozen on dry ice. Samples were stored at -80ºC until sectioning at 10μm using a cryostat microtome (Bright Instruments, 5040).

Human liver tissue

De-identified sections of formalin-fixed, paraffin-embedded, uninjured and fibrotic human liver tissue were provided by the Lothian NRS Bioresource with approval from Tissue Governance. Samples of acetaminophen-injured human liver tissue were obtained as part of

the Pathophysiology of Acute Liver Injury Study. This study was approved by the Scotland A Research Ethics Committee and NHS Lothian Research and Development.

Immunohistochemistry and histology

Immunohistochemistry was performed on formalin-fixed, paraffin-embedded tissue unless otherwise stated. At the start of each protocol, samples were de-waxed in xylene (2 x 5 minutes) and rehydrated through decreasing alcohol concentrations (100%, 75%, 65%, 2 minutes each). The wash buffer was PBS unless otherwise stated. Primary and secondary antibodies (Table 2 - 7) were diluted in blocking solution unless ready-to-use solutions or part of a kit.

BrdU

This protocol was performed on methacarn-fixed tissue. Endogenous peroxidases were quenched with 0.3% H_2O_2 (Sigma-Aldrich, H1009) in methanol (10 minutes), followed by consecutive 10-minute incubation steps with 0.1% trypsin (Sigma-Aldrich, T7168), warm 1.8M HCl and 0.1M sodium tetraborate decahydrate (Sigma-Aldrich, S9640). Blocking (1 hour) and subsequent incubation steps utilised the Mouse on Mouse Elite Peroxidase Kit (Vector Laboratories, PK2200). Primary antibody was applied for 30 minutes. A control section to which no primary antibody was applied was stained in parallel. Secondary antibody was Mouse on Mouse Biotinylated Anti-mouse IgG Reagent, applied for 10 minutes. Detection was performed using the Elite Vectastain ABC kit (Vector, PK7100) and DAB (Dako, K3648) before counterstaining with haematoxylin, dehydration and mounting. For each sample, twenty sequential fields were acquired at x20 magnification, excluding tissue edges, staining artefact, and large deficits. Approximately 3,000 hepatocytes were counted to calculate the percentage of proliferating hepatocytes.

F4/80 / GR1 / PDGFRβ

Antigen retrieval was performed with Tris-EDTA (PDGFRβ only, 1.21g Trizma base, Sigma-Aldrich, T6066, 0.37g EDTA, Sigma-Aldrich, E5134 in 1L dH_2O, pH9, microwave 800W for 15 minutes), endogenous peroxidases were quenched with 3% H_2O_2 (Sigma-Aldrich, H1009, 10 minutes), Avidin / Biotin block (Vector, SP-2001) was applied, before blocking with 20% normal goat serum (Vector, S-1000) (PDGFRβ, GR1) or 20% normal rabbit serum (Vector, S-5000) (F4/80) for 30 minutes. Primary antibodies were applied for 2 hours at room temperature (PDGFRβ) or overnight at 4ºC (F4/80, GR1). Control sections to which no primary antibody

was applied were stained in parallel. Secondary antibody (PDGFRβ – biotinylated goat anti-rabbit; GR1 – biotinylated goat anti-rat; F4/80 – biotinylated rabbit anti-rat) was applied for 30 minutes at room temperature. Detection was performed using the Elite Vectastain ABC kit (Vector, PK7100) and DAB (Dako, K3468) before counterstaining with haematoxylin, dehydration and mounting. For each sample, ten sequential fields were acquired at x20 magnification (excluding tissue edges, staining artefact, and large deficits) and percentage positive staining calculated using FIJI (Appendix 3).[167]

For F4/80 immunofluorescence of fixed-frozen tissue, slides were air-dried for at least 60 minutes, blocked with 20% normal goat serum (30 minutes) and primary antibody was applied for 2 hours. Secondary antibody was applied for 30 minutes. Slides were mounted with Vectashield HardSet Antifade Mounting Medium with DAPI (Vector, H-1500).

Integrin β8

Antigen retrieval was performed with Tris-EDTA (microwave 800W for 15 minutes), endogenous peroxidases were quenched with 3% H_2O_2 (Sigma-Aldrich, H1009, 10 minutes), before blocking with 20% normal horse serum (Vector, S-2000, 30 minutes). Primary antibody was applied overnight at 4ºC. Control sections, to which either no primary antibody or an isotype control were applied, were stained in parallel. Detection was performed using the ImmPRESS Polymerized Reporter Enzyme Staining System (Vector, MP7401) and DAB (Dako, K3468), before counterstaining with haematoxylin, dehydration and mounting.

Desmin-Red Fluorescent Protein dual immunostaining

Antigen retrieval was performed with Tris-EDTA (microwave 800W for 15 minutes), endogenous peroxidases were quenched with 3% H_2O_2 (10 minutes), before blocking with 10% normal goat serum (30 minutes). Primary antibody against desmin was applied for 2 hours, followed by goat anti-rabbit peroxidase for 30 minutes. TSA Plus Fluorescein (Perkin Elner, NEL741001KT – 1:50) was applied for 5 minutes. Slides were returned to Tris-EDTA (microwave 800W for 3 minutes, 400W for 4 minutes), followed by repeat blocking as above. Primary antibody against red fluorescent protein was applied for 2 hours, followed by repeat peroxidase as above. TSA Plus Cyanine 3 (Perkin Elner, NEL744001KT – 1:50) was applied for 5 minutes. Nuclear counterstain was achieved with 6mM DAPI (Sigma-Aldrich, D9542) for 10 minutes, before mounting (ProLong Gold, Thermo Fisher Scientific, P36930).

Phospho-SMAD3

For DAB immunostaining, endogenous peroxidases were quenched with 3% H_2O_2 (10 minutes). Permeabilisation was performed with 0.5% Triton X-100 (Sigma-Aldrich, T8787, 10 minutes). Antigen retrieval was performed with Tris-EDTA (800W microwave, 20 minutes). Avidin / Biotin block was applied, before blocking with 20% normal goat serum (30 minutes). Primary antibody was applied overnight at 4ºC. A control section to which no primary antibody was applied was stained in parallel. Secondary antibody was biotinylated goat anti-rabbit, applied for 30 minutes. Detection was performed using the Elite Vectastain ABC kit and DAB, before counterstaining with haematoxylin, dehydration and mounting.

For immunofluorescence, TBS-tween was used as the wash buffer. A 10X stock solution was prepared (0.5M Trizma base (Sigma-Aldrich, T6066), 9% NaCl (Sigma-Aldrich, 13423), 0.5% Tween 20 (Sigma-Aldrich, P1379), pH 8.4) and then diluted 1:10 in dH_2O prior to use. Serum blocking was performed with 20% normal horse serum (30 minutes). Detection was performed using the ImmPRESS Polymerized Reporter Enzyme Staining System, followed by TSA Plus Cyanine 3 (1:100 for 5 minutes). Nuclear counterstain was achieved with 1mM DAPI for 10 minutes, before mounting.

Haematoxylin and eosin staining

This was performed within the Histology, Immunodetection and Aquila-HistoPlex section of the Shared University Research Facilities within the Queen's Medical Research Institute, according to a standard protocol. Briefly, sections were baked overnight at 55ºC overnight, before de-waxing and rehydration. Slides were then placed in Harris Haematoxylin (Thermo Fisher Scientific) for five minutes. After washing, slides were placed in 1% acid alcohol for five seconds, followed by Scott's tap water substitute for two minutes. Slides were then transferred to Eosin Y solution (Thermo Fisher Scientific) for two minutes, followed by washing, dehydration, and mounting.

Table 2 - 7 List of antibodies

Description	Application	Manufacturer	Catalogue Number	Dilution/ Working Conc^{n}
Alexa Fluor 488 Goat Anti-Rat IgG	IF (2º)	Thermo Fisher Scientific	A-11006	1:200
Anti-BrdU	IHC (1º)	Dako	M0744	1:40
Anti-CD16/32	FC	BioLegend	101302	1:100
Anti-CD31-APC	FC	BioLegend	102410	1:100
Anti-CD31-PE/Cy7	FC	BioLegend	102417	1:100
Anti-CD45-PE/Cy7	FC	BioLegend	103114	1:100
Anti-CD45-PerCP/Cy5.5	FC	BD Biosciences	550994	1:100
Anti-Desmin	IF (1º)	Abcam	ab8592	1:500
Anti-F4/80	IHC (1º)	Abcam	ab6640	1:200
Anti-F4/80	IF (1º)	Abcam	ab6640	1:100
Anti-GR1	IHC (1º)	R&D	MAB1037	1:750
Anti-Itgb8	IHC (1º)	Abcam	ab80673	1:500
Anti-Itgb8, isotype control	IHC (1º)	Abcam	ab27472	1:1
Anti-PDGFRβ	IHC (1º)	Abcam	ab32570	1:500
Anti-Red fluorescent protein	IF (1º)	Rockland	600-401-379	1:1000
Anti-Smad3 (phospho S423 + S425)	IHC/IF (1º)	Abcam	ab52903	1:100
Anti-TGFβ	In vitro assay	R&D	MAB1835	0.05mg/mL
β8 integrin subunit blocking antibody	In vivo admin^{n}	Sheppard Group, UCSF	N/A	0.5mg/mL
β8 integrin subunit blocking antibody	In vitro assay	Sheppard Group, UCSF	N/A	0.02mg/mL
β8 integrin subunit blocking antibody, isotype control	In vivo admin^{n}	Sheppard Group, UCSF	N/A	0.5mg/mL
β8 integrin subunit blocking antibody, isotype control	In vitro assay	Sheppard Group, UCSF	N/A	0.02mg/mL
Biotinylated goat anti-rabbit	IHC (2º)	Vector	BA-1000	1:1000
Biotinylated goat anti-rat	IHC (2º)	Vector	BA-9401	1:1000
Biotinylated rabbit anti-rat	IHC (2º)	Vector	BA-4001	1:200
Goat anti-rabbit peroxidase	IF (2º)	Vector	P1-1000	1:800
Mouse on Mouse Biotinylated Anti-mouse IgG Reagent	IHC (2º)	Vector	PK-2200	1:250

1º, primary; 2º, secondary; admin^{n}, administration; conc^{n}, concentration; FC, flow cytometry; IF, immunofluorescence; IHC, immunohistochemistry

Image capture

Brightfield and epifluorescence microscopy

Routine brightfield microscopy was performed on an Axiovert 200 microscope (Zeiss). Images were acquired using the Axiocam MRc Rev 3 (Zeiss) and AxioVision software (Release 4.6.3). White balance and exposure were optimised for each experiment then kept constant for all sections within an experiment. Images were saved as TIFF files. For epifluorescence, an HBO 100 (Osram) mercury lamp was used with the same microscope setup and Zeiss filter sets 02 (DAPI), 10 (for Fluorescein / Alexa Fluor 488) and 20 (red fluorescent protein).

Confocal microscopy

Confocal microscopy was performed using an LSM780 microscope system with 405/458/488/514/561/633nm laser lines and Zen 2011 SP3 (black edition, version 8.1.0.484) software (Zeiss). Laser attenuation, pixel dwell time, gain and pinhole diameter were all optimised for each fluorophore within each experiment, then kept constant for all slides. Images were saved as CZI files.

Multiphoton microscopy

Multiphoton microscopy, encompassing TPEF, SHG and CARS, was performed using the following, previously described,[168] custom-built setup. The tunable pump laser (720-990nm, 7ps, 80MHz repetition rate) and spatially and temporally overlapped Stokes laser (1064nm, 5-6ps, 80MHz repetition rate) were generated by a picoEmerald laser (APE). Output beams were channelled into an Olympus FV1000MPE inverted microscope, incorporating an NA 1.05 objective (Olympus, XLPL25XWMP). Backscattered emission signals from TPEF and CARS were separated from backscattered excitation light by means of a short-pass 690nm dichroic mirror and IR cut filter (Olympus). Emission signals were detected by 4 photo-multiplier tubes, having been deconvolved by a series of filters and dichroic mirrors. Images were recorded using FV10-ASW software (Olympus). Standard image size was 512x512 pixels. Pixel size was 0.99μm^2 for standard resolution and 0.497μm^2 for high resolution images. Z-depth was 2μm for standard resolution and 1μm for high resolution. Tiled images (3x3 or 4x4) at 30μm depth were obtained for all mice, followed by one or more z-stacks from the liver surface to the limit of detectable signal. Repeated z-stacks of the same area were acquired every 10-15 minutes for imaging of cycling hepatocytes. Continuous scanning was performed for blood flow imaging, with scan orientation matched to the direction of flow and pixel dwell time adjusted until streaks of (labelled) red blood cells were observed (~4μs).

Image processing and analysis

Processing and analysis was performed using FIJI (ImageJ, version 2.0.0-re-59/1.51n)[167] or Imaris 8.4.1 (Bitplane). Percentage positive DAB staining was calculated as described above. Quantification of phospho-SMAD3 nuclear staining was performed as follows on five high-power images per sample. Nuclei were manually defined as regions of interest and mean grey value in the Cyanine 3 channel was calculated for those areas. Three-dimensional vascular analysis using Imaris was performed in *Cdh5-Cre;*Ai14 mice as follows. For each time point and mouse, a 30μm z-stack (z-depth 2μm) from immediately beneath the liver capsule was reconstructed in Imaris. A vascular surface was created from the Ai14 channel; total area and volume were calculated. For two-dimensional vascular analysis using Angiotool,[169] the three central slices of the Ai14 channel from the previously assembled z-stack were used to produce a maximal intensity projection with FIJI. A red lookup table was applied and the images were saved as RGB TIFF files. Analysis was performed using optimised parameters, unchanged between images (threshold 15-255; vessel diameter 5-8, removing small particles (100) and filling holes (150)). Intracellular lipid analysis following partial hepatectomy was performed as follows. For each time point and mouse, a 30μm z-stack (z-depth 2μm) from immediately beneath the liver capsule was reconstructed in Imaris. In mice (*Cdh5-Cre;*Ai14) in which intrinsic endothelial labelling was present, a vascular surface was created from the Ai14 channel, as described above, to enable this to be masked from the CARS channel. A lipid surface was created in the masked CARS channel to enable the total volume of lipid to be calculated. Algorithms for lipid surface creation are shown in Appendix 4.

Calculation of sinusoidal red blood cell velocity was performed in a similar manner to that previously described.[170] First, labelled red blood cell smear length was measured. Then the starting and finishing coordinates of the smear were used to calculated the total number of pixels scanned by the detector between the smear endpoints. This was multiplied by the pixel dwell time to give the elapsed time between the start and end of the smear. Distanced travelled divided by time taken provided velocity.

No additional processing was performed prior to quantitative analysis of microscopy images. All images within an experiment were processed identically. Images presented in figures were contrast-enhanced by adjusting intensity minima and maxima. Noise was removed by use of background subtraction (using the pre-suggested filter width), baseline subtraction, and/or a median filter (either 3x3x3 or 3x3x1 as appropriate).

Statistics

Data were analysed using Microsoft Excel for Mac (version 15.33) and GraphPad Prism 7 for Mac OS X (version 7.0c). Data are presented as individual values with mean where feasible, otherwise as mean with standard error of the mean. Data were assessed visually for normality. The statistical significance of differences between two groups was calculated with a 2-tailed, unpaired Student's t test (for independent groups with equal variance) or Mann Whitney test (for independent groups with unequal variance). A paired t test was performed on hepatocyte adhesion data. For comparisons between more than two groups, an ordinary one-way ANOVA was performed, followed by Tukey's multiple comparisons test. Multiplicity-adjusted P values were calculated for each comparison. Differences with a P value of less than 0.05 were considered statistically significant. To examine the relationship between excised liver weight or serum ALT and hepatocyte proliferation index, linear regression was performed. ALT values were $\log_{10}$-transformed prior to analysis. PCR array data were standardised as previously reported,[171] to identify genes in test samples with a 95% confidence interval for standardised relative fold change that did not overlap 1 (the value assigned to the fold change for the same gene in control samples).

Chapter 3 – Cell-specific depletion of αv integrins in liver regeneration

Introduction

The αv integrins have been shown to have a key role in the progression of liver fibrosis, through activation of latent TGFβ.[29] Because TGFβ is stored as a latent complex, its activation, through release from the LAP, is a key regulatory step. The role of αv integrins in liver regeneration has not previously been explored, despite evidence that, as well as being a major inflammatory cytokine, active TGFβ is a potent inhibitor of hepatocyte proliferation.[93,98,105,172] Thus it is possible that depletion of one or more αv integrins within the liver might promote hepatocyte proliferation and accelerate liver regeneration following liver injury. This is the hypothesis explored in this chapter.

Although all five αv integrins have been shown to activate latent TGFβ,[20-24] combined global knockout of integrins αvβ6 and αvβ8 alone is sufficient to recapitulate the developmental effects of loss of TGFβ-1 and -3.[57] This suggests that these two αv integrins in particular play a major role in TGFβ activation. Expression of integrin αvβ6 in the liver appears to be relatively restricted, but has been shown in activated cholangiocytes, transitional hepatocytes, and oval cells during biliary and portal fibrosis.[39,173] Expression of integrin αvβ8 within the liver has not been well-characterised, but this integrin has been shown to play an important role in TGFβ activation in many other cells and tissues, including the respiratory, nervous and immune systems.[43,59-63] Specifically, integrin αvβ8 inhibits proliferation of lung epithelium through TGFβ activation.[55] Therefore, as well as exploring the role in liver regeneration of cell-specific depletion of αv integrins in general, the expression and cell-specific depletion of integrin αvβ8 alone were also examined.

This chapter presents data to show that depletion of hepatocyte integrin αvβ8 leads to increased hepatocyte proliferation and accelerated liver regeneration. Hepatocytes and integrin αvβ8 appear to be the key liver cell and integrin, respectively, since depletion of integrin αvβ8 or all αv integrins from HSCs or LSECs did not produce a pro-regenerative phenotype. Expression of integrin αvβ8 by hepatocytes in samples of human liver tissue was confirmed immunohistochemically. Taken together, the findings reported in this chapter

suggest that targeting hepatocyte integrin αvβ8 may represent a promising therapeutic strategy to promote regeneration of a patient's own liver.

Results

Depletion of αv integrins from hepatic stellate cells does not affect hepatocyte proliferation following partial hepatectomy

Given the previously confirmed role for HSC αv integrins in hepatic fibrosis,[29] the effect on hepatocyte proliferation of αv integrin depletion from HSCs was examined in a mouse model of liver regeneration. The same transgenic approach as that used to demonstrate the role of HSC αv integrins in liver fibrosis was employed (Figure 3 - 1a). Depletion of αv integrins was targeted to HSCs through utilisation of double transgenic mice, homozygous for a floxed *Itgav* allele and heterozygous for *Pdgfrb-Cre*. As described in Chapter I, this strategy targets Cre recombination and subsequent gene inactivation in a cell-specific manner. HSCs are targeted in a highly efficient manner by *Pdgfrb-Cre*.[29]

Partial hepatectomy was performed in $Itgav^{flox/flox}$;*Pdgfrb-Cre* mice and littermate controls (Figure 3 - 1b). The thymidine analogue BrdU was injected two hours prior to liver harvest in order to label proliferating cells. Livers were harvested at the time of peak hepatocyte regeneration in this model, 48 hours following partial hepatectomy, and BrdU immunostaining was performed. No difference in hepatocyte proliferation or liver-to-body-weight ratio could be detected between $Itgav^{flox/flox}$;*Pdgfrb-Cre* mice and controls (Figure 3 - 1c,d). This suggests that although HSC αv integrins play a key role in driving liver fibrosis in chronic injury, they do not play such an important role in the immediate regenerative response following acute liver injury.

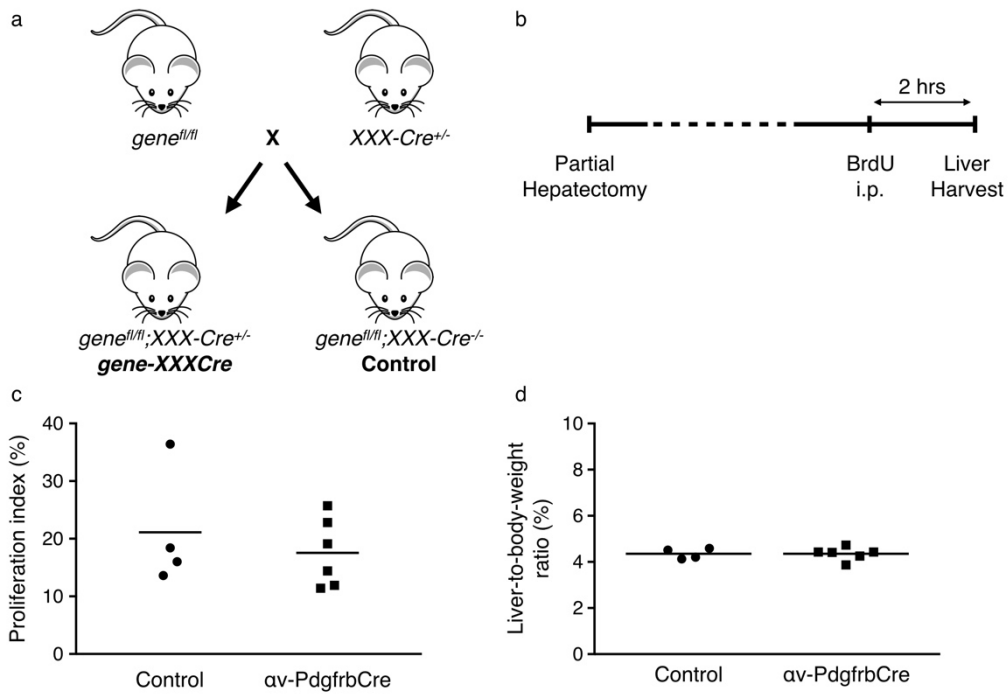

Figure 3 - 1 Depletion of αv integrins from HSCs does not promote liver regeneration following partial hepatectomy.
a) Creation of double transgenic 'Cre-lox' mice to facilitate cell-specific depletion of a target gene. This strategy also yields *Cre*-negative littermate controls. b) Schematic of partial hepatectomy model of liver regeneration; i.p., intra-peritoneal. Quantitation of $BrdU^+$ hepatocyte nuclei (c) and liver-to-body-weight ratio (d) in control and *Itgav*$^{flox/flox}$;*Pdgfrb-Cre* (αv-PdgfrbCre) mice at 48 hours post partial hepatectomy; line indicates mean.

Depletion of hepatocyte integrin αvβ8 promotes hepatocyte proliferation and liver regeneration

Whilst HSCs play a crucial role in coordinating the inflammatory response following chronic liver injury, it would be reasonable to consider hepatocytes as the dominant cell type in the hepatic regenerative response. Fate-mapping studies have provided strong evidence that, in the majority of murine models of liver injury, hepatic regeneration occurs through self-duplication of the pre-existing hepatocyte population.[16,17] Although the αv integrin subunit has five possible β subunit binding partners, individual αv integrins may be more important than others within the context of specific organs, cell types or biological processes. Integrin αvβ8 has been shown to have a key role in development, is expressed on epithelial cells in the lung, and has a growth inhibitory effect when transfected into tumour cells subsequently injected into mice.[54,57]

Hepatocytes were isolated from wild-type mice and qPCR demonstrated expression of integrin αvβ8, albeit at a low level (Figure 3 - 2a). The same technique also showed that

integrin αvβ8 is depleted from hepatocytes in *Itgb8*$^{flox/flox}$*;Alb-Cre* mice (Figure 3 - 2a). Following partial hepatectomy, hepatocyte proliferation is significantly increased at 36, 48 and 72 hours in *Itgb8*$^{flox/flox}$*;Alb-Cre* mice compared to controls (Figure 3 - 2b,d). Concomitantly, liver-to-body-weight ratio in *Itgb8*$^{flox/flox}$*;Alb-Cre* mice was also increased at 72 and 96 hours following partial hepatectomy (Figure 3 - 2c), supporting the conclusion that the observed increase in hepatocyte proliferation drives restoration of liver mass following injury.

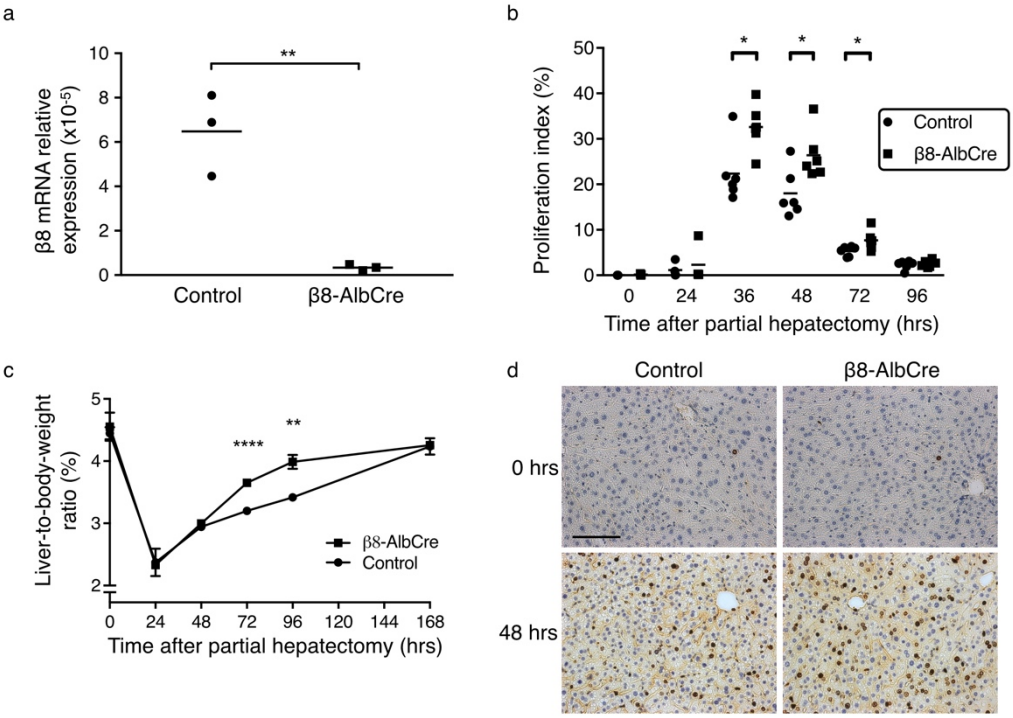

Figure 3 - 2 Depletion of hepatocyte integrin αvβ8 promotes hepatocyte proliferation and liver regeneration following partial hepatectomy.
a) qPCR of *Itgb8* expression in hepatocytes isolated from control and *Itgb8*$^{flox/flox}$*;Alb-Cre* (β8-AlbCre) mice. Quantitation of BrdU^{+} hepatocyte nuclei (b) and liver-to-body-weight ratio (c) in control and β8-AlbCre mice after partial hepatectomy (n=3-6). d) Representative images from BrdU immunostaining of liver sections from control and β8-AlbCre mice at 0 and 48 hours after partial hepatectomy. Horizontal line in (b) indicates mean; data in (c) is presented as mean, error bars show SEM. * P<0.05, ** P<0.01, **** P<0.0001. Scale bar 100μm.[*]

Depletion of hepatocyte integrin αvβ8 does not alter hepatocyte proliferation, liver architecture or liver biochemistry in the uninjured liver

Constitutive depletion of integrin αvβ8 from hepatocytes has the potential to produce a phenotype in the uninjured liver, which might explain or confound the increased hepatocyte proliferation observed following partial hepatectomy. No difference in hepatocyte proliferation or liver-to-body-weight ratio was observed in livers from *Itgb8*$^{flox/flox}$*;Alb-Cre* mice

[*] Experiments performed by N.C. Henderson and K. Saeteurn.

and controls prior to partial hepatectomy (Figure 3 - 2b,c). To examine this further, serum and liver tissue were obtained from uninjured *Itgb8$^{flox/flox}$;Alb-Cre* mice and littermate controls to assess for any obvious baseline differences in the tissue, or in circulating markers of liver injury and function. No difference in serum albumin, ALT, ALP, or total bilirubin was detected between *Itgb8$^{flox/flox}$;Alb-Cre* mice and controls (Figure 3 - 3). Quantitation of positive immunostaining for markers of Kupffer cells (F4/80), neutrophils (GR1) and HSCs (PDGFRβ) in uninjured livers revealed no differences between *Itgb8$^{flox/flox}$;Alb-Cre* mice and controls (Figure 3 - 4). Similarly, no morphological changes were observed on examination of sections stained with haematoxylin and eosin (Figure 3 - 5). These findings support the conclusion that depletion of hepatocyte integrin αvβ8 does not alter the form or function of the uninjured liver.

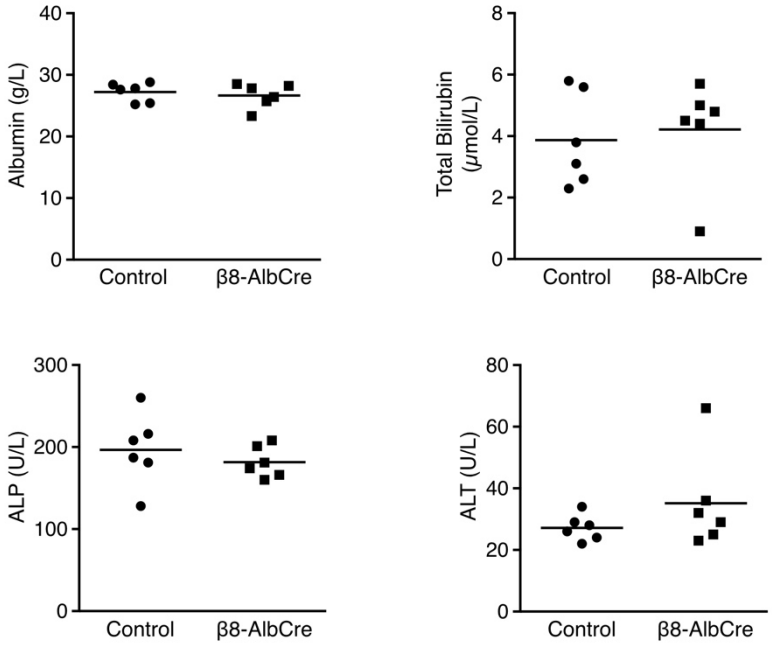

Figure 3 - 3 Depletion of hepatocyte integrin αvβ8 does not alter liver biochemistry in the uninjured mouse.
Serum biochemistry (albumin, total bilirubin, ALP, ALT) from uninjured control and *Itgb8$^{flox/flox}$;Alb-Cre* (β8-AlbCre) mice. Horizontal line indicates mean.

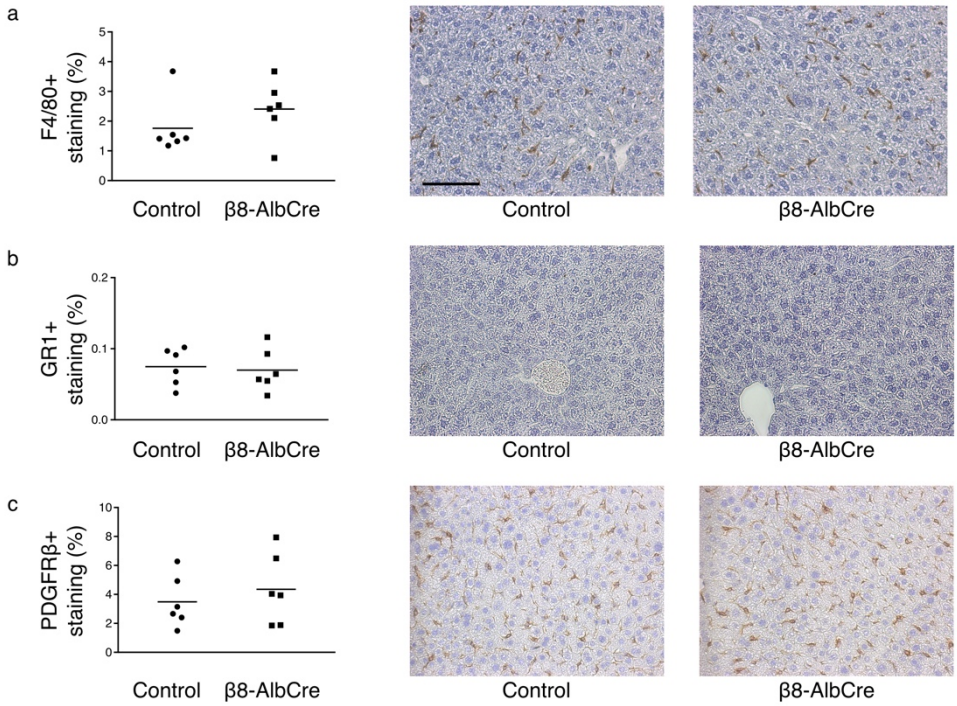

Figure 3 - 4 Depletion of hepatocyte integrin αvβ8 does not alter immunostaining for Kupffer cells, neutrophils, or HSCs in the uninjured liver.
Quantification and representative images from F4/80 (Kupffer cell, a), GR1 (neutrophil, b), and PDGFRβ (HSC, c) immunostaining of liver from uninjured control and *Itgb8*$^{flox/flox}$*;Alb-Cre* (β8-AlbCre) mice. Horizontal line indicates mean. Scale bar 100μm.

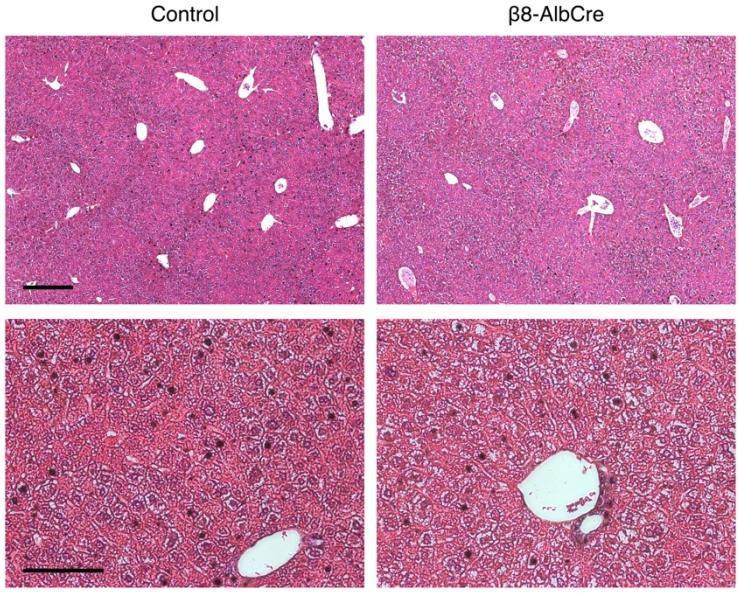

Figure 3 - 5 Depletion of hepatocyte integrin αvβ8 does not alter liver architecture.
Representative images of haematoxylin and eosin staining of liver tissue from uninjured control and *Itgb8*$^{flox/flox}$*;Alb-Cre* (β8-AlbCre) mice (n=6). Scale bars 250μm (upper) and 100μm (lower).

Depletion of hepatocyte integrin αvβ8 does not alter the degree of injury or inflammatory response following partial hepatectomy

To investigate whether depletion of hepatocyte integrin αvβ8 alters the degree of injury following partial hepatectomy, serum was obtained from *Itgb8$^{flox/flox}$;Alb-Cre* mice and controls at 48 hours following partial hepatectomy. No significant differences in serum albumin, ALT, ALP or total bilirubin were detected (Figure 3 - 6). Quantitation of positive immunostaining for markers of Kupffer cells (F4/80), neutrophils (GR1) and HSCs (PDGFRβ) in liver sections from *Itgb8$^{flox/flox}$;Alb-Cre* mice and controls at 48 hours following partial hepatectomy also did not reveal any differences between groups (Figure 3 - 7). These findings suggest that depletion of hepatocyte integrin αvβ8 does not alter the degree of injury or inflammatory responses that occurs following partial hepatectomy.

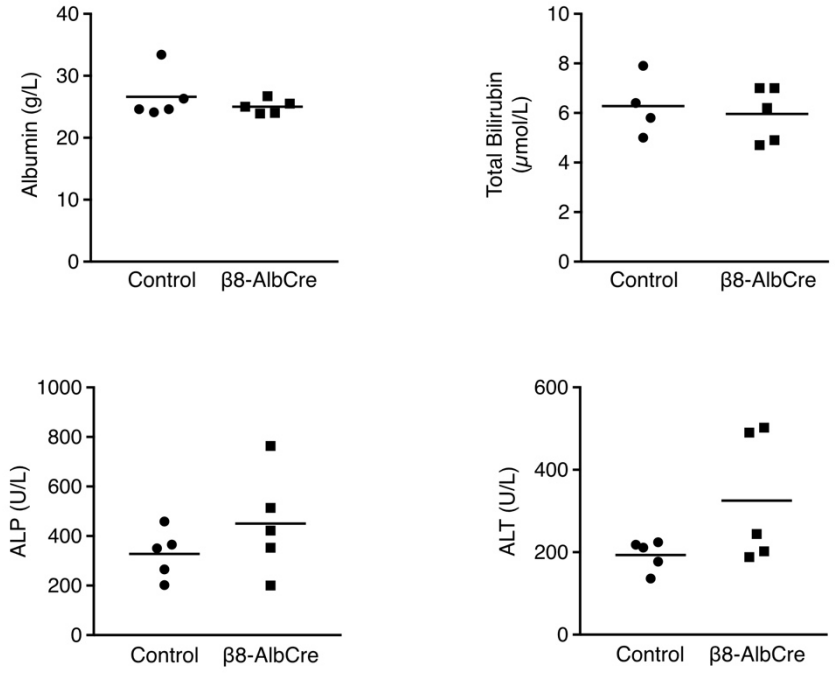

Figure 3 - 6 Depletion of hepatocyte integrin αvβ8 does not alter liver biochemistry following partial hepatectomy.
Serum biochemistry (albumin, total bilirubin, ALP, ALT) from uninjured control and *Itgb8$^{flox/flox}$;Alb-Cre* (β8-AlbCre) mice at 48 hours post partial hepatectomy. Horizontal line indicates mean.

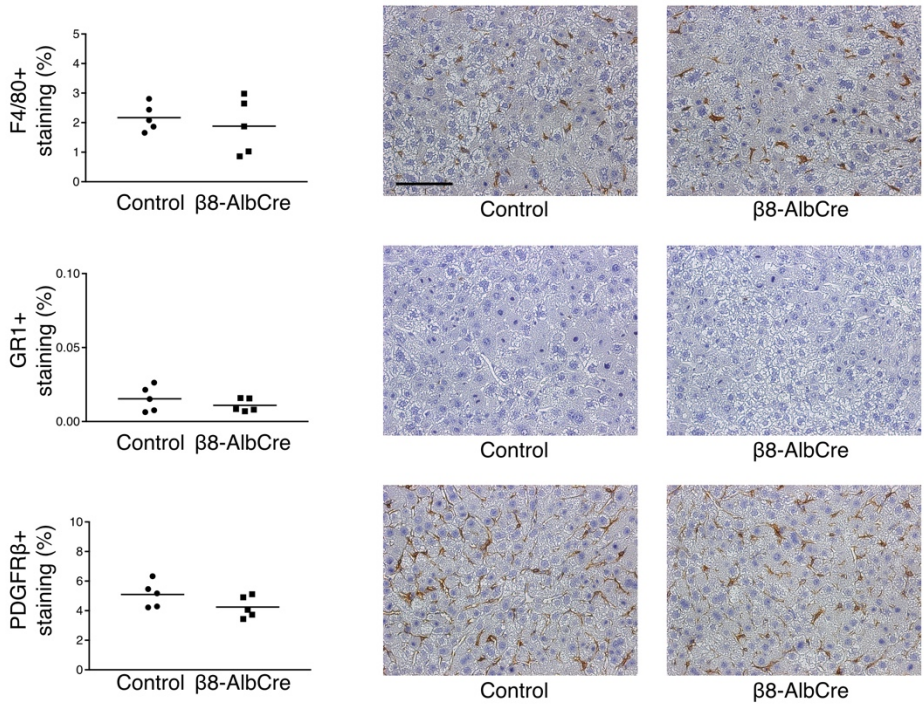

Figure 3 - 7 Depletion of hepatocyte integrin αvβ8 does not alter immunostaining for Kupffer cells, neutrophils, or HSCs following partial hepatectomy.
Quantification and representative images from F4/80 (Kupffer cell), GR1 (neutrophil) and PDGFRβ (HSC) immunostaining of liver from control and *Itgb8*$^{flox/flox}$*;Alb-Cre* (β8-AlbCre) mice at 48 hours post partial hepatectomy. Horizontal line indicates mean. Scale bar 100μm.

Depletion of hepatocyte integrin αvβ8 has no detectable effect on hepatocyte proliferation and liver regeneration in acetaminophen-induced liver injury

Given the pro-regenerative phenotype observed following depletion of hepatocyte integrin αvβ8 in the partial hepatectomy model of liver regeneration, an alternative murine model of liver injury was employed to assess whether a similar pro-regenerative phenotype could be recapitulated. Acetaminophen overdose is a clinically relevant model of liver injury that results in rapid hepatocyte injury and death, observed histologically as centrilobular necrosis.[114] The dose of acetaminophen is titrated to produce sufficient injury and subsequent regeneration, without causing death from acute hepatic failure. Experimental design is shown in Figure 3 - 8a. Interestingly, *Itgb8*$^{flox/flox}$*;Alb-Cre* mice had equivalent hepatocyte proliferation index compared to controls at 48 hours after acetaminophen administration (Figure 3 - 8b). Mean serum ALT levels were also equivalent (Figure 3 - 8c), suggesting that the degree of initial injury was consistent between the two groups. However, within both groups there was marked variation in serum ALT at 48 hours, consistent with a variable degree of hepatocyte injury (Figure 3 - 8d). Whilst not unexpected in this model of liver injury, it may well make

the detection of differences in hepatocyte proliferation more challenging. However, serum ALT at 48 hours post acetaminophen does not show any clear association with proliferation index (Figure 3 - 8d), so 'correcting' hepatocyte proliferation for the degree of injury ALT does not reduce the variability within the two groups (Figure 3 - 8e).

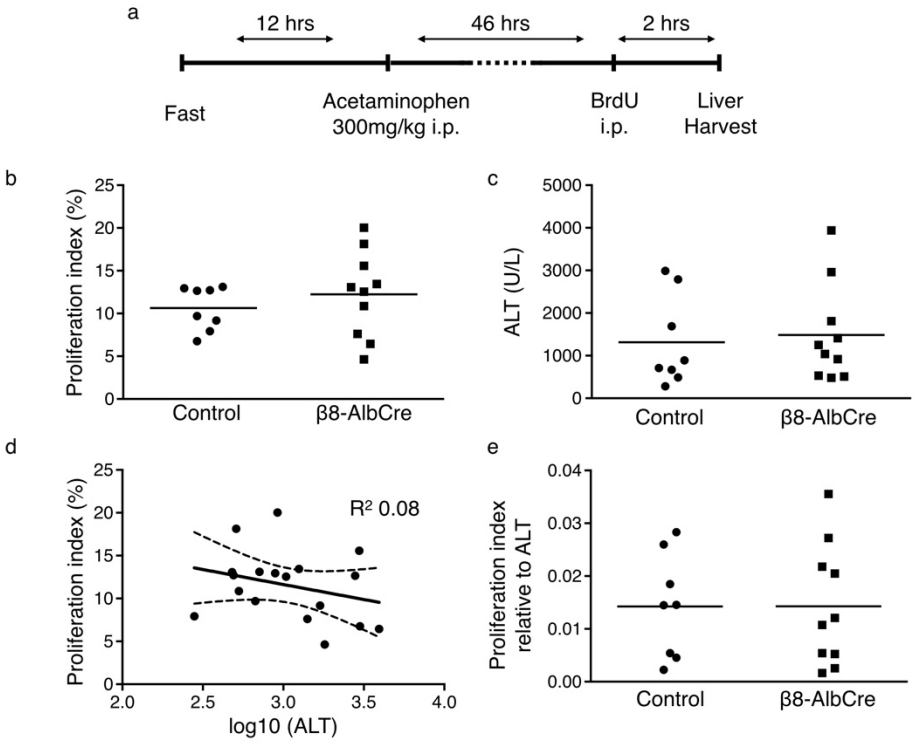

Figure 3 - 8 Depletion of hepatocyte integrin αvβ8 has no detectable effect on hepatocyte proliferation in acetaminophen-induced liver injury.
a) Schematic of experimental design; i.p., intraperitoneal. Quantitation of proliferation index (percentage of $BrdU^+$ hepatocyte nuclei) (b), serum ALT (c), linear regression of log10(ALT) and proliferation index (d), and proliferation index expressed relative to serum ALT (e) in control and *Itgb8*$^{flox/flox}$*;Alb-Cre* (β8-AlbCre) mice at 48 hours post acetaminophen administration. Solid lines indicate mean, except for (d) where solid line is line of best fit, with dotted lines indicating 95% confidence bands.

Injection of a β8 integrin subunit blocking antibody does not affect hepatocyte proliferation following partial hepatectomy

To investigate whether pharmacological blockade of hepatocyte integrin αvβ8 could recapitulate the pro-regenerative phenotype observed following genetic depletion, a β8 integrin subunit blocking antibody[60] was administered to wild-type mice undergoing partial hepatectomy. When compared to mice who received a non-binding control antibody, it was not possible to detect a difference in either hepatocyte proliferation index or liver-to-body-weight ratio at 48 hours following partial hepatectomy (Figure 3 - 9). This result suggests that a single dose of the β8 integrin subunit blocking antibody tested in this experiment is unlikely to be of therapeutic benefit in promoting liver regeneration.

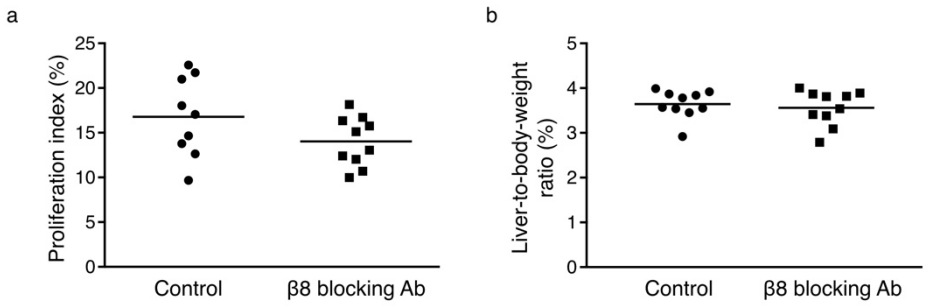

Figure 3 - 9 Administration of a β8 integrin subunit blocking antibody does not promote liver regeneration following partial hepatectomy.
Quantitation of $BrdU^+$ hepatocyte nuclei (a) and liver-to-body-weight ratio (b) at 48 hours post partial hepatectomy in mice receiving control or β8 integrin subunit blocking antibody; line indicates mean.

Depletion of integrin αvβ8 on hepatic stellate cells does not affect hepatocyte proliferation following partial hepatectomy

Hepatic stellate cells have been shown to express integrin αvβ8.[29] It is possible that the failure to observe a pro-regenerative phenotype following partial hepatectomy in mice in which all αv integrins were depleted from HSCs (as reported above) could have occurred as a result of conflicting effects from the depletion of multiple integrins. Therefore, to determine whether depletion of integrin αvβ8 alone from HSCs might result in a similar pro-regenerative phenotype to that seen following its depletion from hepatocytes, *Pdgfrb-Cre* mice were crossed with *Itgb8*$^{flox/flox}$ mice to generate an *Itgb8*$^{flox/flox}$*;Pdgfrb-Cre* line. Following partial hepatectomy, with tissue harvest at 48 hours, there was no difference in either hepatocyte proliferation index or liver-to-body-weight ratio between *Itgb8*$^{flox/flox}$*;Pdgfrb-Cre* mice and littermate controls (Figure 3 - 10). This suggests that integrin αvβ8 depletion in HSCs alone does not alter hepatocyte proliferation following liver injury.

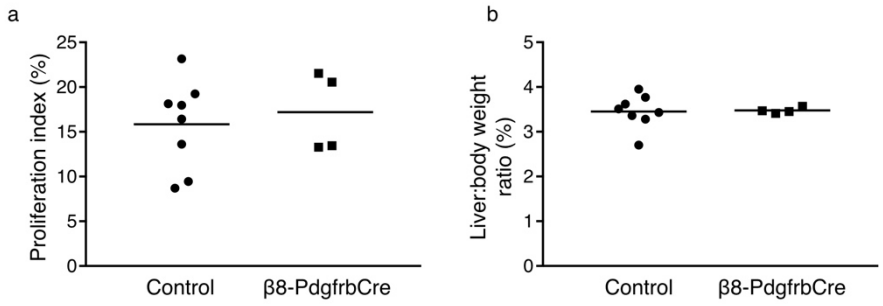

Figure 3 - 10 Depletion of HSC integrin αvβ8 does not promote liver regeneration following partial hepatectomy.
Quantitation of $BrdU^+$ hepatocyte nuclei (a) and liver-to-body-weight ratio (b) in control and *Itgb8*$^{flox/flox}$;*Pdgfrb-Cre* (β8-PdgfrbCre) mice at 48 hours post partial hepatectomy; line indicates mean.

Evaluation of a *Cdh5-Cre* to target liver sinusoidal endothelial cells

Liver sinusoidal endothelial cells have been shown to play an important role in liver regeneration.[47,174,175] Recently, a novel, inducible transgenic mouse, expressing Cre under control of the VE-Cadherin promoter, has been utilised to target LSECs.[159,175] In order to characterise recombination in this *Cdh5-PAC-Cre*^{ERT2} mouse, it was crossed separately to two reporter lines to produce *Cdh5-PAC-Cre*^{ERT2};Ai14 (*Cdh5-Cre;*Ai14) and *Cdh5-PAC-Cre*^{ERT2};mTmG (*Cdh5-Cre;*mTmG) mice. Following tamoxifen induction, multiphoton microscopy of excised whole liver and confocal microscopy of liver sections showed excellent labelling of cells lining the hepatic sinusoids, consistent with LSECs (Figure 3 - 11). No evidence of hepatocyte labelling was observed.

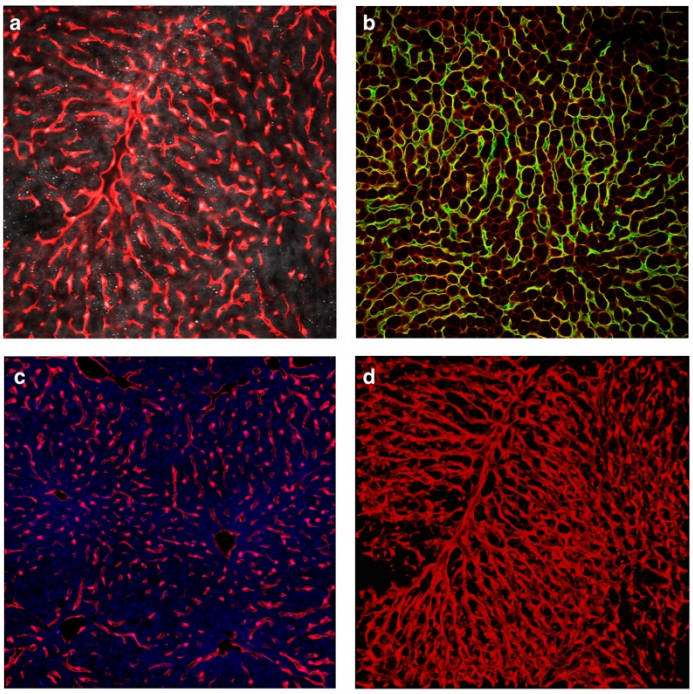

Figure 3 - 11 *Cdh5-Cre* effectively targets LSECs.
Multiphoton microscopy of excised whole liver shows labelling of sinusoids in the *Cdh5-Cre*;Ai14 mouse (a) and *Cdh5-Cre*;mTmG mouse (b, cells in which recombination has occurred express GFP). c) Confocal microscopy of fixed-frozen section of *Cdh5-Cre*;Ai14 liver shows Ai14 reporter (red) is maintained after processing; DAPI (blue). d) 3D reconstruction of z-stack from excised whole *Cdh5-Cre*;Ai14 liver (acquired using multiphoton microscopy) outlines the branching vascular tree.

Immunofluorescence was then utilised to assess the specificity of recombination and labelling in *Cdh5-Cre;*Ai14 mice. This demonstrated that *Cdh5-Cre* does not target the F4/80$^+$ Kupffer cell population within the liver (Figure 3 - 12a). Similarly, a dual immunostaining approach, to label Ai14$^+$ cells and desmin$^+$ HSCs, revealed two distinct populations, illustrating that recombination in the *Cdh5-Cre;*Ai14 mouse does not label HSCs (Figure 3 - 12b).

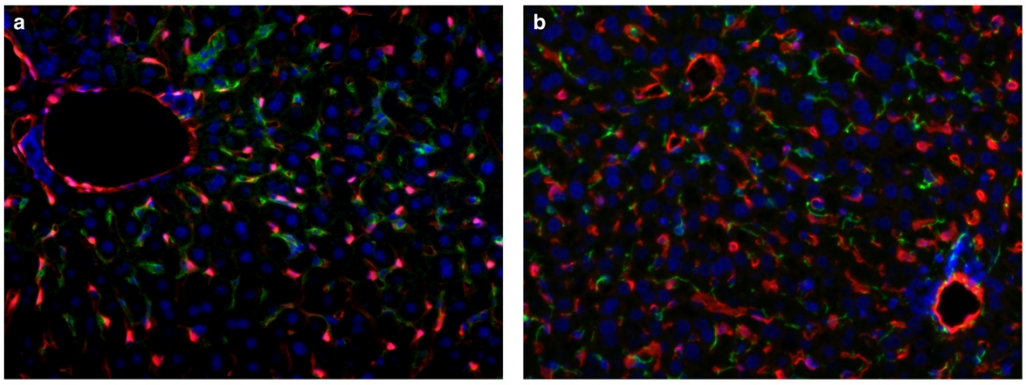

Figure 3 - 12 *Cdh5-Cre* does not target Kupffer cell or HSC populations within the liver.
a) Immunostaining of *Cdh5-Cre*;Ai14 liver for F4/80 (green); Ai14 – red; DAPI – blue. b) Immunostaining of *Cdh5-Cre*;Ai14 liver for desmin (green) and red fluorescent protein (red); DAPI – blue.

Analysis of the recombined population in *Cdh5-Cre*;mTmG mice, expressing membrane-targeted GFP, was performed using flow cytometry. From this it was determined that at least 95% of $CD31^{+}$;$CD45^{-}$ endothelial cells expressed GFP following tamoxifen induction (Figure 3 - 13a). Over 99% of GFP^{+} cells expressed CD31 (Figure 3 - 13b). Together these findings confirm that *Cdh5-Cre* targets LSECs in a highly efficient manner and with excellent specificity.

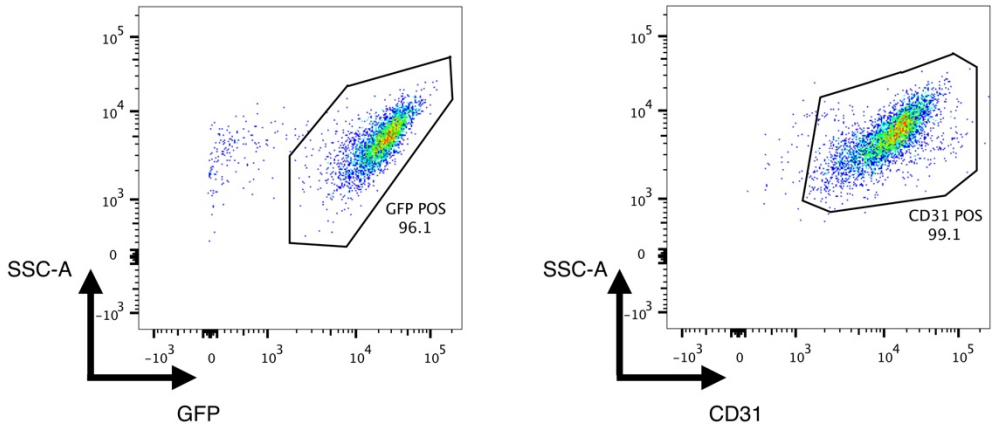

Figure 3 - 13 Flow cytometry demonstrates that *Cdh5-Cre* targets LSECs in a highly efficient manner and with excellent specificity.
Representative pseudocolour plots from flow cytometry of digested liver from *Cdh5-Cre*;mTmG mice (n=2) show >95% of singlet, live, $CD31^{+}$;$CD45^{-}$ cells are GFP^{+} (a) and >99% of singlet, live, GFP^{+} cells are $CD31^{+}$ (b). SSC-A, side scatter-area.

LSECs do not express integrin αvβ8 and depletion of all LSEC αv integrins does not affect hepatocyte proliferation following partial hepatectomy

To assess whether integrin αvβ8 depletion from LSECs might promote liver regeneration following injury, in a similar manner to that seen with integrin αvβ8 depletion from hepatocytes, it was first necessary to investigate LSEC expression of integrin αvβ8. Fluorescence activated cell sorting was utilised to obtain $CD31^{+}$;$CD45^{-}$ LSECs from the uninjured murine liver. Following cell lysis, RNA extraction and reverse transcription, it was not possible to detect expression of mRNA for the gene *Itgb8*, which encodes the β8 integrin subunit (Figure 3 - 14a). This finding suggests that LSECs do not express integrin αvβ8. LSECs have been shown to express αv integrins, namely αvβ3 and αvβ5.[29,50,52] Therefore, *Itgav*$^{flox/flox}$*;Cdh5-Cre* mice were generated through interbreeding in order to permit depletion of all αv integrins from LSECs upon tamoxifen administration. Following partial hepatectomy, there was no difference in hepatocyte proliferation index or liver-to-body-weight ratio at 48 hours between *Itgav*$^{flox/flox}$*;Cdh5-Cre* mice that received tamoxifen and Cre-negative littermate controls (to which tamoxifen was also administered) (Figure 3 - 14b,c). This suggests that depletion of αv integrins from LSECs does not promote liver regeneration following partial hepatectomy.

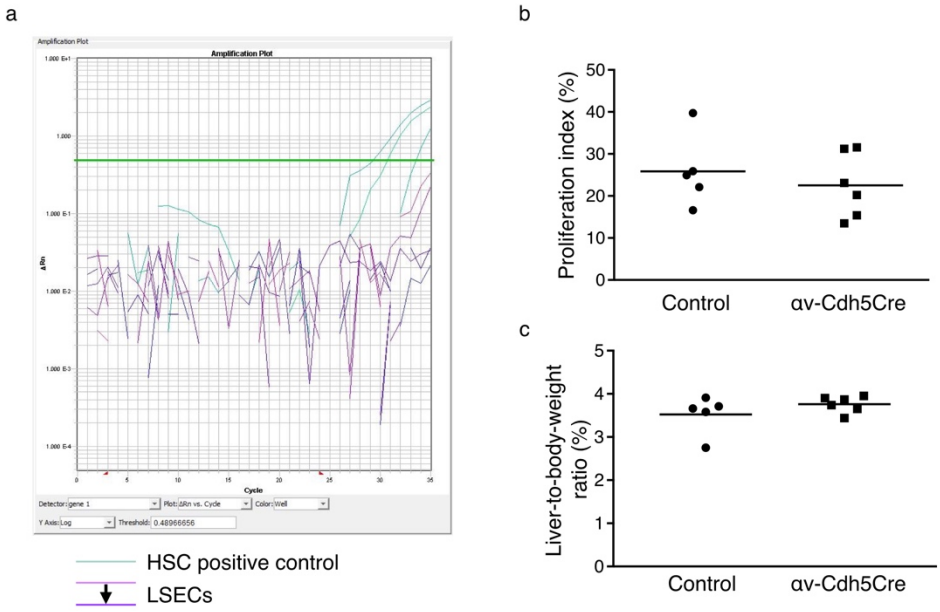

Figure 3 - 14 LSECs do not express integrin αvβ8 and depletion of LSEC αv integrins does not promote liver regeneration following partial hepatectomy.
a) qPCR failed to detect Itgb8 mRNA expression by freshly isolated LSECs (n=4); *Itgb8* mRNA was detected in an HSC positive control (green lines). Quantitation of $BrdU^{+}$ hepatocyte nuclei (b) and liver-to-body-weight ratio (c) in control and *Itgav*$^{flox/flox}$;*Cdh5-Cre* (αv-Cdh5Cre) mice at 48 hours post partial hepatectomy; line indicates mean.

Human hepatocytes express integrin αvβ8

For hepatocyte integrin αvβ8 to be a viable therapeutic target to promote liver regeneration, it must be expressed by human hepatocytes. Tissue samples were obtained from uninjured human liver, from patients with acute liver failure secondary to acetaminophen overdose, and from patients with cirrhosis. These samples were stained immunohistochemically for the β8 integrin subunit and revealed widespread expression of integrin αvβ8 by hepatocytes (Figure 3 - 15). The evidence that human hepatocytes express integrin αvβ8 in both health and disease suggests hepatocyte integrin αvβ8 may be a viable therapeutic target to promote hepatocyte proliferation and regeneration of a patient's own liver.

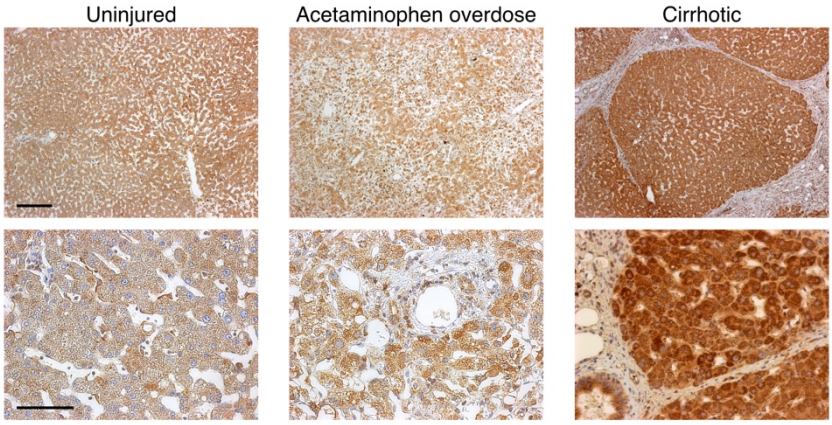

Figure 3 - 15 Human hepatocytes express integrin αvβ8.
Representative low- and high-magnification images of β8 integrin subunit immunostaining in uninjured human liver (n=5), following acetaminophen overdose (n=5), or in cirrhosis (n=6). Scale bars 250μm (upper) and 100μm (lower).

Discussion

The body of work contained within this chapter explores the role of αv integrins in liver regeneration. Whilst HSC αv integrins have been shown to have an important role in the development and progression of liver fibrosis,[29] the depletion of αv integrins, or specifically integrin αvβ8, from HSCs does not promote hepatocyte proliferation. Conversely, depletion of integrin αvβ8 from hepatocytes does promote hepatocyte proliferation and accelerate liver regeneration following partial hepatectomy. LSECs do not express integrin αvβ8, at least in the uninjured liver, neither does depletion of all αv integrins from LSECs promote hepatocyte proliferation following partial hepatectomy. Human hepatocytes express integrin αvβ8 in uninjured liver, and this expression persists in both acute liver failure following acetaminophen overdose and in cirrhosis.

Dissecting the roles of individual αv integrin subtypes

Integrin αvβ8 has previously been shown to be expressed by epithelial cells in the lung and was shown to have a growth regulatory function.[54] Although normal airway epithelial cells express integrin αvβ8, lung carcinoma cells do not. When lung and colon carcinoma cell lines were transfected to express integrin αvβ8, a reduction in proliferation was observed. The transfected lung carcinoma cells also formed fewer, smaller tumours when injected into mice. The data presented above fits with a role for integrin αvβ8 in epithelial cell growth regulation.

Whether any of the remaining four αv integrins also have a growth-inhibitory role in the liver is, as yet, unconfirmed. As previously noted, expression of integrin αvβ6 in the liver appears relatively restricted, but its expression may drive both fibrosis and hepatobiliary carcinoma.[39,173] The expression and role of other αv integrins in the liver, namely αvβ1, αvβ3, and αvβ5, is gradually being elucidated, but a complete picture is yet to emerge.

Recently, hepatocyte β1 integrin has been shown to be required for successful liver regeneration.[176] However, the β1 integrin subunit is particularly promiscuous, having the potential to bind twelve of the eighteen alpha subunits.[18] No attempt was made in the aforementioned study to determine which of the β1 integrin heterodimers was responsible for the observed phenotype, so whether integrin αvβ1 has a role in liver regeneration is uncertain. Investigating the role of integrin αvβ1 remains challenging because no specific genetic technique exists to deplete integrin αvβ1 alone, without simultaneously targeting other αv integrins or β1 subunit binding partners. A small molecule inhibitor of integrin αvβ1 has now been developed, which does not inhibit cell adhesion mediated by any of the other four αv integrins.[24] The inhibitor was then used to ameliorate mouse models of fibrosis in lung and liver.[24] If hepatocyte expression of integrin αvβ1 were confirmed, the effect of integrin αvβ1 inhibition on liver regeneration following partial hepatectomy would be interesting to examine.

Cell-specific depletion of the β3 integrin subunit through use of Cre-lox has been reported, albeit in platelets and myeloid cells.[177] It should be eminently feasible to generate a mouse in which the gene encoding the β5 integrin subunit is floxed, allowing its cell-specific depletion. Using similar transgenic approaches to those employed here, this would facilitate investigation of the individual contribution of these αv integrins to the regulation of liver regeneration. Such investigations might also serve to highlight the benefits of targeting specific αv integrins to promote liver regeneration, in contrast to the anti-fibrotic effects seen with inhibition of all αv integrins. For example, inhibition of integrin αvβ3 has been suggested to reduce hepatocyte proliferation and suppress angiogenesis following liver injury.[178,179]

Assessing hepatocyte proliferation

BrdU is a thymidine analogue and acts a marker of proliferation by its incorporation and subsequent detection in cells in S phase of the cell cycle between the time of BrdU administration and tissue harvest and fixation. Other methods to detect cell proliferation, such as Ki67 immunostaining, can also be used. However, all these methods only serve to provide

a snapshot of which cells are progressing through the cell cycle, and it is likely that not every hepatocyte entering S phase and replicating its DNA continues on to complete cytokinesis. This is why hepatocyte proliferation data is augmented by measurement of liver-to-body-weight ratio. Elevation of both above baseline, or relative to control, supports the conclusion that increased hepatocyte proliferation is occurring and leading to regeneration of functional hepatic mass.

The αv integrins and hepatic non-parenchymal cells

Depletion of HSC αv integrins, HSC integrin αvβ8 alone, or depletion of LSEC αv integrins all failed to increase hepatocyte proliferation or liver-to-body-weight ratio at 48 hours following partial hepatectomy. It is not possible to rule out a small effect, or one which occurs at a different time point following injury. The 48-hour time point was chosen for liver harvest because 36-48 hours is the time of peak hepatocyte proliferation following partial hepatectomy in the mouse.[119,120] As such, this was considered the best single time point to be able to detect an effect on hepatocyte proliferation. Once no effect was demonstrated, consideration was given to harvesting at a range of time points following partial hepatectomy. However, the likelihood of detecting a difference in hepatocyte proliferation at other time points when no effect was apparent at 48 hours following partial hepatectomy was considered low. As such, the use of additional mice to confirm this would be hard to justify.

Hepatocyte integrin αvβ8 in acetaminophen-induced liver injury

The failure to observe an effect of hepatocyte integrin αvβ8 depletion on liver regeneration following acetaminophen overdose may have occurred for a number of reasons. It is possible that a subtle effect might be masked by other factors specific to the more inflammatory milieu in which hepatocyte injury and subsequent liver regeneration occurs in this model. Hepatocyte proliferation following acetaminophen overdose is both more localised and less pronounced than that which occurs following partial hepatectomy. Both these features could make detection of differences in proliferation more challenging. The degree of injury occurring following acetaminophen administration is also quite variable from mouse to mouse. The experiment was powered based on data previously obtained by Alexandra Thompson, anticipating a proliferation index of 8% in control mice and with an 80% power to detect an increase (or decrease) in proliferation index of 4%, considered to be an appropriate effect size (estimated SD 3%, α=0.05). Despite the wide variation in liver injury that was

observed, reflected in the serum ALT, the control group mean proliferation index and standard deviation were broadly as expected (mean 10.6%, SD 2.5%). Increased variation was seen in the proliferation index of *Itgb8$^{flox/flox}$;Alb-Cre* mice (mean 12.2%, SD 5.0%), but this difference in variation was not statistically significant. The similar and overlapping 95% confidence intervals of both experimental groups (control 8.5-12.8%, *Itgb8$^{flox/flox}$;Alb-Cre* 8.7-15.8%) also support the conclusion that no large effect exists, rather than that the study failed to detect one. Thus, although mean proliferation index was marginally increased in *Itgb8$^{flox/flox}$;Alb-Cre* mice compared to control, it may well be that integrin αvβ8 plays a lesser or no role in regulating hepatocyte proliferation in this model of liver injury.

The β8 integrin subunit blocking antibody

Injection of a β8 integrin subunit blocking antibody at the time of partial hepatectomy also did not reveal a similar phenotype to genetic depletion. Whilst a detectable difference in hepatocyte proliferation between those mice administered blocking antibody and controls would have provided an elegant proof of the concept that pharmacological blockade of integrin αvβ8 could promote liver regeneration, there are many possible reasons for the failure to observe any effect. Despite being based on expert recommendation from the group who both produced and have extensive experience of using this blocking antibody, the dose, route and timing of injection may not have been optimal to achieve the desired promotion in hepatocyte proliferation following partial hepatectomy. Since the antibody was not specifically targeted to hepatocyte integrin αvβ8, it is possible that binding to integrin αvβ8 on other cell types, or off-target binding, could have resulted in poor affinity to, or incomplete blockade of, hepatocyte integrin αvβ8. Further pharmacological blockade experiments could be performed, first to confirm binding to hepatocyte integrin αvβ8, and subsequently to assess alternative dosing regimens, including increased and repeated dosing, or an intravenous rather than intraperitoneal route of administration. Therefore, although this experiment did not demonstrate an effect on hepatocyte proliferation from administration of a β8 integrin subunit blocking antibody at the time of partial hepatectomy, this does not rule out the possibility that pharmacological targeting of the αvβ8 integrin could be of therapeutic benefit through promotion of hepatocyte proliferation.

LSECs and αv integrins

Endothelial cells have been reported to express multiple αv integrins.[45] However, LSEC expression of specific αv integrins may differ from, and be lower than, that of other endothelial cells.[48,52] No expression of integrin αvβ8 by LSECs isolated from uninjured liver was detected. However, it is possible that LSECs might express *Itgb8* following injury. This could be investigated further by attempting isolation of LSECs following partial hepatectomy, although the ability to obtain adequate numbers of cells for RNA extraction, reverse transcription and qPCR by routine methods would be hampered by the small size of the remnant liver. An alternative approach would be to attempt to detect β8 integrin subunit expression in situ, with co-localisation of a suitable LSEC marker such as CD31. Again, this is hampered by the current lack of a suitable antibody against the β8 integrin subunit which works well in murine tissue. At time of writing, there is also no well-validated antibody against the β8 integrin subunit for use in flow cytometry, which would otherwise be another potential modality through which to confirm whether LSECs ever express integrin αvβ8.

Depletion of all αv integrins on LSECs did not reveal a positive or negative effect on hepatocyte proliferation following partial hepatectomy. However, it should be noted that successful depletion of αv integrins from LSECs in the *Itgav*$^{flox/flox}$*;Cdh5-Cre* mouse was not confirmed either at the transcript or protein level. Although the *Cdh5-Cre* transgene encodes an inducible form of Cre recombinase, the validation experiments performed with *Cdh5-Cre*;Ai14 and *Cdh5-Cre*;mTmG reporter mice demonstrated highly efficient recombination following tamoxifen administration, so there is no reason to suspect that LSEC αv integrin depletion would be any less efficient. Hepatocyte proliferation was only measured at 48 hours post partial hepatectomy in *Itgav*$^{flox/flox}$*;Cdh5-Cre* mice and controls. Given that LSECs have been shown to express integrins αvβ3 and αvβ5,[50,52] and, separately, inhibition of integrins αvβ3 and αvβ5, using Cilengitide, has been shown to impair angiogenesis in mouse models of chronic liver disease,[179] it would be of interest to assess both angiogenesis and hepatocyte proliferation at a later time point following partial hepatectomy. Following partial hepatectomy, the first round of hepatocyte division precedes LSEC proliferation, which principally occurs between three and six days post partial hepatectomy.[180] If integrins αvβ3 and αvβ5 are the predominant αv integrin heterodimers expressed by LSECs, their depletion might impair angiogenesis following partial hepatectomy, in a similar manner to that seen in models of chronic liver disease. Impaired angiogenesis might be expected to retard liver regeneration, either by a direct inhibitory effect on subsequent rounds of hepatocyte

proliferation, or more generally by slowing the rate at which the liver returns to its normal size.

Kupffer cells and αv integrins

Of the principal hepatic cell types, only the potential role of integrin αvβ8 expression by Kupffer cells was not explored in this body of work. Kupffer cells do express αv integrins,[29,44] but it has also been reported that macrophages express 'very low or undetectable' levels of *Itgb8*.[43] It would be relatively straightforward to confirm whether Kupffer cells express integrin αvβ8 at the transcript level, using fluorescence assisted cell sorting to isolate Kupffer cells, followed by RNA extraction, reverse transcription and qPCR for *Itgb8*, in the same manner as was performed for LSECs. However, until very recently, cell-specific targeting of Kupffer cells has not been possible, so it would be difficult to use a transgenic approach to deplete integrin αvβ8 solely in Kupffer cells. The most commonly utilised 'macrophage-specific' Cre drivers, LysM-*Cre* and *Csf1-Cre*, target the entire monocyte-derived cell population, and have also been shown to target neutrophils to a significant degree.[129] Recently, the *Clec4f* gene has been identified as a means of selectively depleting Kupffer cells.[181] A *Clec4f-Cre* mouse has been generated, but it remains to be seen whether it is able to drive efficient and specific recombination in Kupffer cells. If successful, such a strategy could be used to investigate the role of Kupffer cell expression of specific proteins, including integrin αvβ8, on liver regeneration.

Redundancy in regeneration regulation

As one would expect for the regulation of such an important, coordinated process as liver regeneration, integrin αvβ8 is clearly not the only means of slowing or stopping hepatocyte proliferation.[180,182] A diverse range of pathways, including liver metabolism, the immune response, and liver vasculature, have been shown to play important roles in liver regeneration.[175,183,184] Redundancy is commonly observed in many biological processes and often acts as a protective mechanism to prevent severe physiological derangement in circumstances where a particular regulatory pathway is disrupted. In the context of integrin αvβ8, constitutive depletion of this integrin from hepatocytes did not lead to hepatomegaly, nor to uncontrolled proliferation following injury. However, targeting hepatocyte integrin αvβ8 does appear to tip the balance towards a pro-regenerative phenotype and it may therefore be possible to use this knowledge to therapeutic advantage.

Summary

The results of the experiments described in this chapter show that depletion of hepatocyte integrin αvβ8 leads to increased hepatocyte proliferation and accelerated liver regeneration following partial hepatectomy in mice. Depletion of integrin αvβ8 from HSCs does not appear to affect hepatocyte proliferation following partial hepatectomy and LSECs do not express integrin αvβ8 in uninjured liver. Hepatocyte-specific depletion of integrin αvβ8 does not generate an obvious phenotype in uninjured liver, nor does it affect the degree of injury or inflammatory response following partial hepatectomy. The fact that human hepatocytes appear to express integrin αvβ8, in both health and disease, makes this integrin a potential therapeutic target to promote liver regeneration in patients with acute or chronic liver injury. Integrin αvβ8 has been shown to activate TGFβ in a number of other cell types and organs.[43,59-63] The following chapter will explore whether a similar mechanism underlies the apparent role for hepatocyte integrin αvβ8 as a brake on liver regeneration following partial hepatectomy.

Chapter 4 – Mechanistic studies of the role of integrin αvβ8 in liver regeneration

Introduction

Having confirmed that hepatocyte integrin αvβ8 depletion promotes hepatocyte proliferation and accelerates liver regeneration following partial hepatectomy in mice, attempts were made to dissect the mechanism underlying this phenotype. Integrin αvβ8 has been shown to have a key role in activating TGFβ in several different tissues and disease processes.[43,59-63] In development, global knockout of integrins αvβ6 and αvβ8 is sufficient to recapitulate the TGFβ-null phenotype,[57] suggesting that these two integrins in particular are critical to the process of TGFβ activation. In the partial hepatectomy model of liver regeneration, altered TGFβ activation appeared to be the most likely mechanism through which depletion of hepatocyte integrin αvβ8 could promote liver regeneration, particularly given the well-characterised ability of TGFβ to inhibit hepatocyte proliferation.[93,98,105,172] As previously introduced, TGFβ is stored within the extracellular matrix, held in an inactive state by its seclusion within the LAP, which itself is anchored to the matrix by the LTBP. For this reason, assessing TGFβ transcription and protein levels within a cell or tissue is not particularly informative, as neither necessarily correlates with the extent of local TGFβ activity. Demonstrating alterations in TGFβ activation status in vivo is extremely challenging and, most commonly, in vitro assays are employed in a surrogate capacity.[132]

An alternative approach to investigate a mechanistic role for TGFβ in a given scenario is to examine the downstream signalling pathway. Canonically, following binding of active TGFβ to the TGFβ receptor (II) and formation of the TGFβ receptor I-II complex, intracellular signalling occurs through sequential phosphorylation of SMAD proteins, ultimately leading to nuclear translocation of the SMAD2,3,4 complex and a change in transcription.[84] As with TGFβ itself, it is not simply sufficient to detect and quantify the presence of the SMAD proteins, since it is their phosphorylation state that is altered during TGFβ signalling. Furthermore, as well as the classical TGFβ signalling pathway, TGFβ is also able to signal non-canonically via several other pathways, including multiple mitogen-activated protein kinase (MAPK) pathways, the PI3K-Akt pathway, and the NF-κB pathway.[85] As such, a failure to detect a change in canonical signalling does not necessarily rule out a role for TGFβ.

The αv integrins are also known to interact with the extracellular matrix. The principal binding partner for integrin αvβ8 is vitronectin, but it has also been reported to act as a ligand for collagen IV, laminin and fibronectin.[185,186] It is therefore possible that depletion of hepatocyte integrin αvβ8 could change the interaction between hepatocytes and the surrounding extracellular matrix, in such a way as to facilitate cellular proliferation.

In this chapter the time course of integrin αvβ8 expression in the liver following partial hepatectomy is presented, which supports the postulated role for integrin αvβ8 as a regulator of hepatocyte proliferation. The effect of hepatocyte integrin αvβ8 depletion on hepatocyte adhesion is also examined. Finally, a range of techniques are employed to investigate whether depletion of hepatocyte integrin αvβ8 alters TGFβ signalling and how this might promote hepatocyte proliferation and liver regeneration.

Results

Whole liver expression of the β8 integrin subunit following partial hepatectomy

Partial hepatectomy was performed in wild-type mice and livers harvested at multiple time points following surgery for quantification of whole liver β8 integrin subunit expression by qPCR.[†] This revealed a marked downregulation of expression immediately following partial hepatectomy, which reached a nadir at 12 hours after injury (Figure 4 - 1). Thereafter, β8 integrin subunit expression increased, peaking at around 10 times baseline expression by 120 hours post partial hepatectomy. Expression then returned to baseline levels by 168 hours (seven days). This time course supports the hypothesis that integrin αvβ8 acts a brake on hepatocyte proliferation. In the normal liver, the immediate downregulation of expression following injury appears to be permissive for the initiation of hepatocyte proliferation. Once liver regeneration is nearing completion and the liver is close to its pre-injury functional mass, the observed increase in β8 integrin subunit expression is consistent with a role in suppressing ongoing hepatocyte proliferation.

[†] Experiment performed by N.C. Henderson and K. Saeteurn.

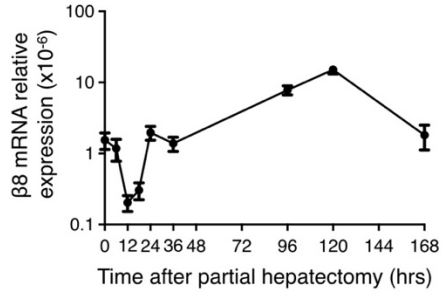

Figure 4 - 1 Whole liver expression of integrin αvβ8 following partial hepatectomy.
qPCR for *Itgb8*, n=3-6 per time point. Data presented as mean; error bars – SEM.

Depletion of integrin αvβ8 on hepatocytes does not alter adhesion to multiple matrix proteins

To examine whether depletion of integrin $\alpha v\beta 8$ on hepatocytes would alter their ability to adhere to the extracellular matrix, an in vitro extracellular matrix adhesion assay was performed. Primary hepatocytes were isolated from *Itgb8*$^{flox/flox}$*;Alb-Cre* mice and controls, and plated separately onto seven different extracellular matrix proteins or bovine serum albumin (as a negative control).‡ Following incubation and washing, a cell stain was applied to detect the degree of cellular adhesion in each well by means of a colorimetric technique.

In four independent experiments comparing adhesion between primary hepatocytes from an *Itgb8*$^{flox/flox}$*;Alb-Cre* mouse and a Cre-negative control, no difference in adhesion to any of the extracellular matrix proteins tested was detected (Figure 4 - 2). In addition to measuring absolute absorbance for each well (Figure 4 - 2a), relative absorbance was calculated to the bovine serum albumin negative control (Figure 4 - 2b) and also to collagen I, to reduce any variation arising from differences in the number of viable cells plated per column (Figure 4 - 2c).

‡ Poly-L-lysine is often used as a positive control in adhesion assays due to its highly adhesive properties. However, during assay optimisation, it was observed that hepatocyte adhesion to type I collagen was greater than adhesion to 0.01% poly-L-lysine, negating the benefit of this additional step.

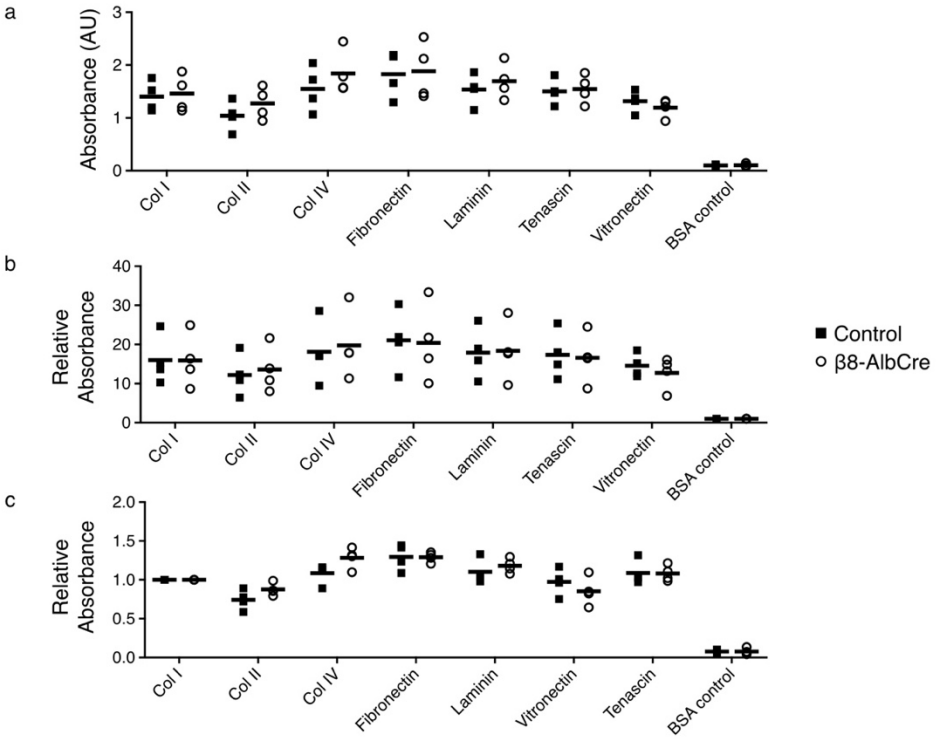

Figure 4 - 2 Depletion of hepatocyte integrin αvβ8 does not alter adhesion to extracellular matrix proteins.
Isolated hepatocytes from control and *Itgb8*$^{flox/flox}$*;Alb-Cre* (β8-AlbCre) tested in a colorimetric extracellular matrix adhesion assay. Line indicates mean; BSA, bovine serum albumin; Col, collagen.

In vitro assays to detect TGFβ activation by hepatocytes

Because of the challenges posed by detecting TGFβ activation status in vivo and in situ, a commonly used method to measure active TGFβ is an in vitro assay employing transgenic mink lung epithelial cells (MLECs).[133] These cells express firefly luciferase under control of the promoter for PAI-1 (plasminogen activator inhibitor-1), a protein whose expression is upregulated by TGFβ signalling. As such, TGFβ signalling leads to increased production of firefly luciferase, which results in an increase in luminescence when the substrates luciferin and ATP are added to the MLEC lysate. A cell's ability to activate latent TGFβ can therefore be assessed by co-culture with MLECs (Figure 4 - 3).[132]

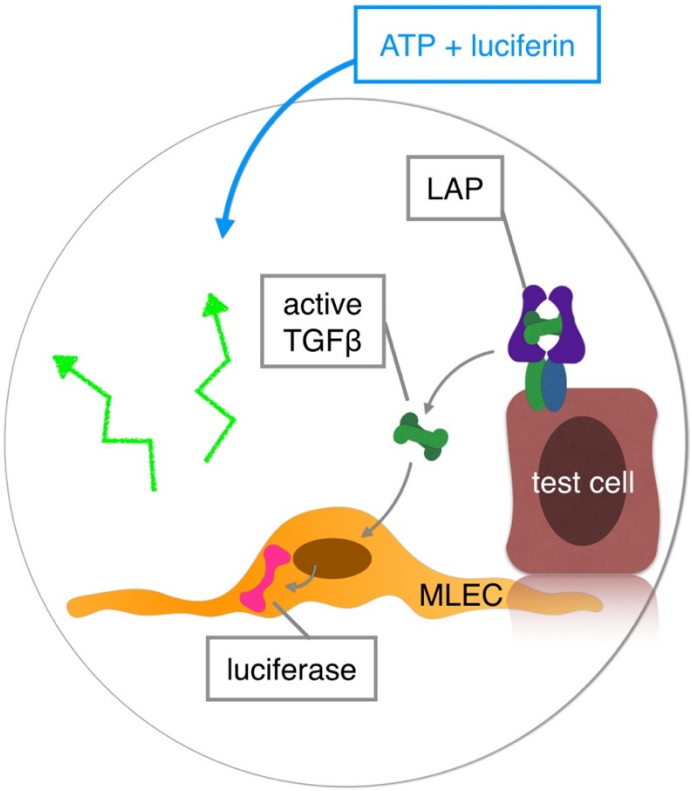

Figure 4 - 3 Schematic to illustrate the principal of the MLEC TGFβ activation assay.
Test cells are co-cultured with MLECs and facilitate release of active TGFβ from the LAP. Active TGFβ drives luciferase expression by MLECs. Following cell lysis, luciferase production is assessed by addition of the substrates ATP and luciferin, followed by measurement of light production.

An initial attempt to optimise the assay for detection of TGFβ activation by hepatocytes was made using the Huh7 hepatoma cell line. MLECs (15,000 per well) and Huh7 cells (25,000-75,000 per well) were co-cultured in serum-free medium for 16 hours. Following washing and cell lysis, the luciferase substrates luciferin and ATP were added, and luciferase activity measured with a luminometer.

The results from this experiment were unable to demonstrate activation of TGFβ by the Huh7 cell line, above the low level of background luminescence from MLECs cultured alone (Figure 4 - 4a). Indeed, the decreasing luciferase activity noted with increasing Huh7 cell number, albeit non-significant, suggests that they might even act as a sink for active TGFβ and reduce the amount of active TGFβ signalling in MLECs. The MLECs are clearly responsive to active TGFβ, as evidenced by the increasing luminescence associated with increasing concentrations of recombinant human TGFβ-1 (rhTGFβ) provided as positive control (Figure 4 - 4b). This effect is blocked by the addition of anti-TGFβ antibody.

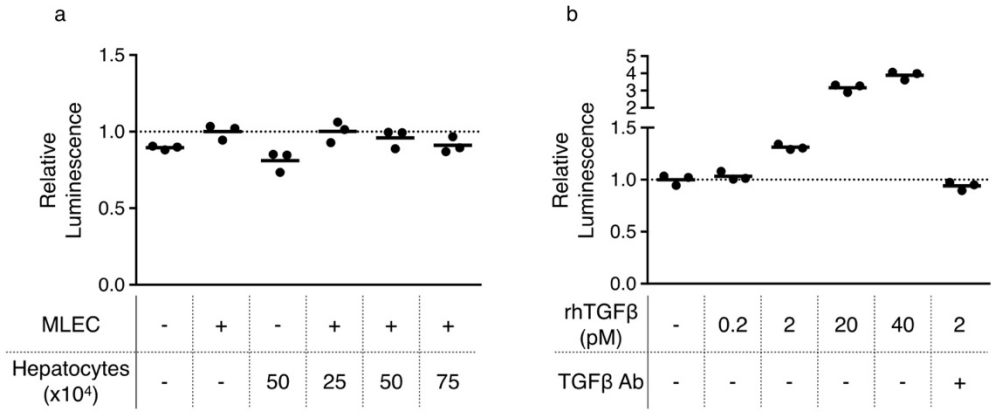

Figure 4 - 4 The MLEC TGFβ activation assay is unable to detect activation of TGFβ by the Huh7 cell line.
a) Relative luminescence following 16-hour incubation of Huh7 cells, MLECs and MLEC-Huh7 co-cultures. b) MLECs respond in a dose-dependent fashion to the addition of recombinant human TGFβ (rhTGFβ); this response is abolished by addition of TGFβ antibody (TGFβ Ab). All conditions tested in triplicate and expressed relative to mean luminescence of MLEC culture alone; solid line indicates mean.

To investigate whether the failure to detect TGFβ activation was specific to the Huh7 cell line, the co-culture experiment was repeated, this time comparing the Huh7 line with another hepatocyte cell line (HepG2), and the LX-2 hepatic stellate cell line. Two small modifications in the experimental design were also made. Firstly, the period of co-culture was extended to 20 hours, in the hope that this would result in increased, and more easily detectable, luciferase production by the MLECs in co-culture. Secondly, foetal bovine serum was added to the co-culture medium to try to ensure that a source of TGFβ was present. Once again, despite a marked response of MLEC cells to rhTGFβ, an increase in the amount of active TGFβ in the co-culture system was not demonstrated with Huh7, HepG2 or LX-2 cell lines (50,000 test cells per well) (Figure 4 - 5). Furthermore, luciferase activity was decreased from that of MLECs cultured alone when MLECs were co-cultured with Huh7, HepG2 or LX-2 cells, suggesting that these cells lines may all decrease the amount of active TGFβ signalling in MLECs.

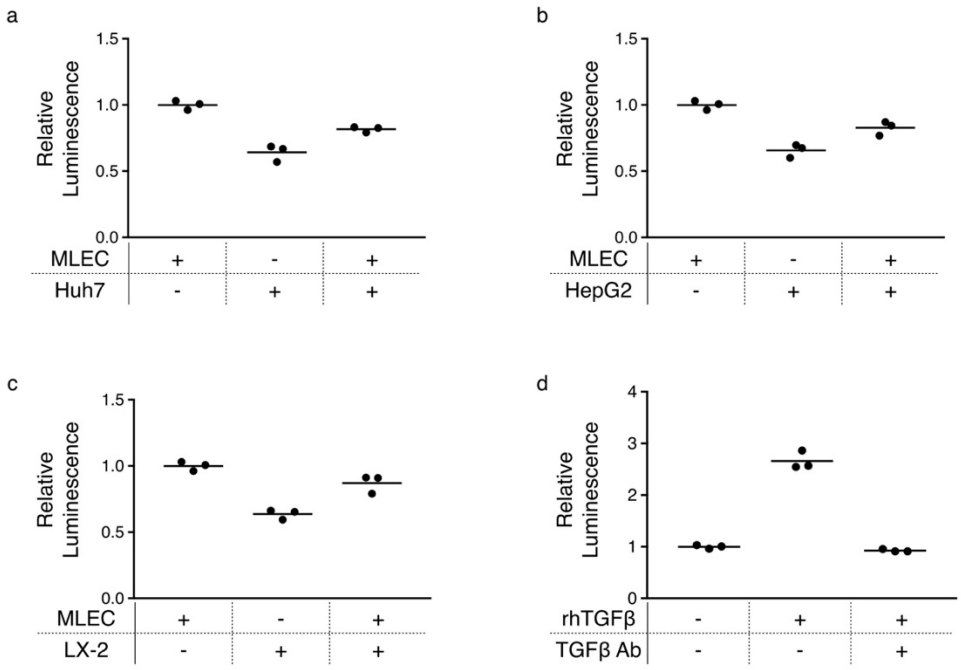

Figure 4 - 5 The MLEC TGFβ activation assay is unable to detect activation of TGFβ by the Huh7, HepG2 or LX2 cell lines.
Relative luminescence following 20-hour MLEC co-culture with a) Huh7, b) HepG2, and c) LX-2 cell lines. d) MLECs respond to the addition of rhTGFβ; this response is abolished by addition of TGFβ antibody (TGFβ Ab). All conditions tested in triplicate and expressed relative to mean luminescence of MLEC culture alone; solid line indicates mean.

Despite the possibility, raised by the above experiments, that it might not be possible to detect TGFβ activation by hepatocytes using the MLEC co-culture assay, it was decided to proceed with isolating primary hepatocytes, since these were the cells of interest. Although immortalised cell lines are frequently used for in vitro studies of cell functions, their phenotype and protein expression can vary markedly from primary cells.[187] Primary hepatocytes were isolated from control mice from the *Itgb8*$^{flox/flox}$*;Alb-Cre* line, added to wells pre-plated with 15,000 MLECs, and incubated for 20 hours. Brightfield microscopy of duplicate test wells confirmed that both MLECs and primary hepatocytes had plated down as expected and did not show evidence of marked cell death. Once again, following measurement of luminescence, it was observed that the presence of hepatocytes did not result in increased TGFβ signalling in MLECs (Figure 4 - 6). Further, it again appeared that the presence of hepatocytes in co-culture with MLECs reduced TGFβ signalling in MLECs below that of MLECs alone. The only difference from the cell line co-culture experiments was that increasing numbers of hepatocytes did not show the trend of decreased TGFβ signalling;

rather a mild increase in luminescence was observed, never exceeding that seen in MLECs alone.

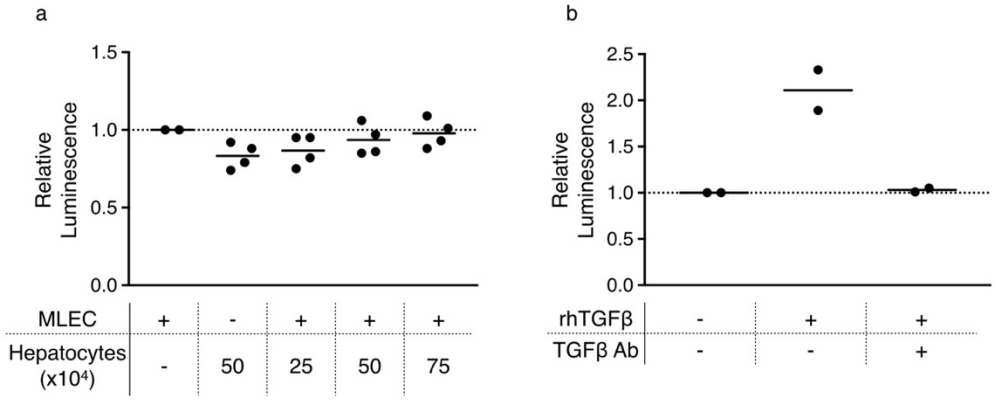

Figure 4 - 6 The MLEC TGFβ activation assay is unable to detect activation of TGFβ by primary mouse hepatocytes.
a) Relative luminescence following 20-hour MLEC co-culture with primary murine hepatocytes plated at various densities. b) MLEC response to the addition of rhTGFβ was confirmed for each MLEC sample; this response is abolished by addition of TGFβ antibody (TGFβ Ab). Each data point indicates one mouse or cell sample. Each sample tested in triplicate and expressed relative to mean luminescence of MLEC culture alone; solid line indicates mean.

An alternative in vitro TGFβ activation assay has been reported, which is able to detect as little as 1pg/mL of active TGFβ.[134] This sensitivity is somewhat improved on that reported for the MLEC co-culture assay.[133] The broad principles of the two assays are similar, but in the newer one, murine fibroblasts (MFB-F11) were transfected to express a secreted alkaline phosphatase in response to TGFβ. Reporter enzyme activity is then assessed by the addition of p-Nitrophenyl phosphate as substrate followed by measurement of absorbance at 405nm (Figure 4 - 7).

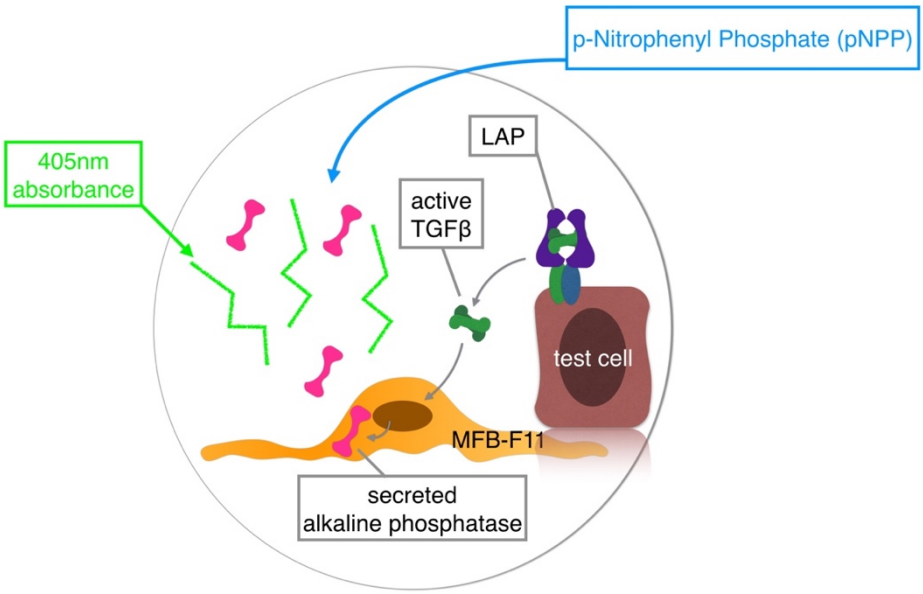

Figure 4 - 7 Schematic to illustrate the principle of the MFB-F11 TGFβ activation assay.
Test cells are co-cultured with MFB-F11 cells and facilitate release of active TGFβ from the LAP. Active TGFβ drives expression of secreted alkaline phosphatase by MLECs. Enzyme activity is assessed by incubation with the substrate p-Nitrophenyl Phosphate, followed by measurement of absorbance at 405nm.

Primary hepatocytes from control mice were obtained, as previously, and co-cultured with the pre-plated MFB-F11 cells. As additional refinements to the prior co-culture experiments, a lower serum medium containing only 2.5% foetal bovine serum was used during the co-culture, since serum itself contains some active TGFβ and therefore high concentrations can reduce the sensitivity of the assay. Also, a source of latent TGFβ was provided to some wells, through the addition of recombinant human latent TGFβ1. The assay appeared technically successful in that increased enzyme activity, above the baseline activity of MFB-F11 cells in culture medium, was observed when rhTGFβ was added to the culture medium (Figure 4 - 8a). This increase was abolished by the addition of anti-TGFβ antibody. Hepatocyte monoculture alone revealed increased absorbance above baseline (Figure 4 - 8b). As with the MLEC assay, co-culture of hepatocytes with MFB-F11 reporter cells was unable to detect TGFβ activation above the background signal present in wells containing only hepatocytes (Figure 4 - 8b). A dose-dependent response was seen when latent TGFβ was added to the co-culture, but an even greater response was seen when latent TGFβ was added to wells containing only MFB-F11 reporter cells (Figure 4 - 8c). Therefore, either MFB-F11 cells are able to activate latent TGFβ independently, or the recombinant human latent TGFβ1 product contains active TGFβ.

The results of the assay as a whole suggest that, despite being sensitive to low levels of rhTGFβ (4pM), even this reportedly more sensitive TGFβ activation assay is unable to detect any ability of hepatocytes to activate TGFβ in vitro.

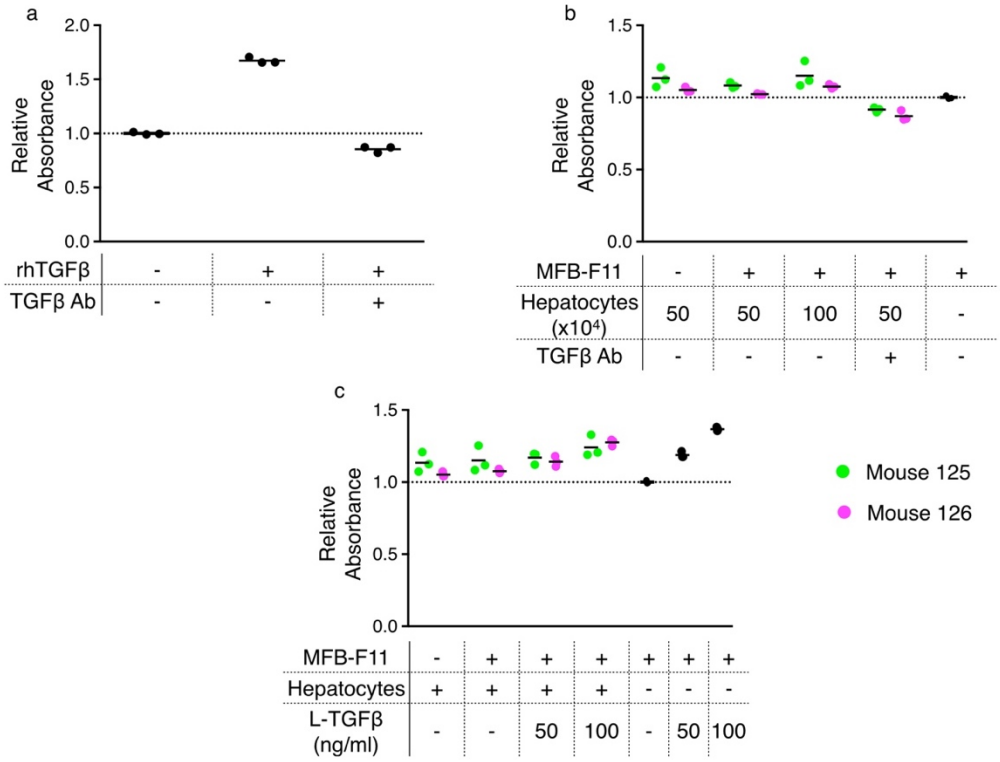

Figure 4 - 8 The MFB-F11 TGFβ activation assay is unable to detect activation of TGFβ by primary mouse hepatocytes.
a) MFB-F11 response to the addition of rhTGFβ was confirmed; this response is abolished by addition of TGFβ antibody (TGFβ Ab). b) Relative absorbance following 20-hour MFB-F11 co-culture with primary murine hepatocytes. c) Addition of latent TGFβ (L-TGFβ) to culture medium increases absorbance in both MFB-F11-hepatocyte co-culture and MFB-F11 monoculture. Each sample tested in triplicate and expressed relative to mean absorbance of MFB-F11 culture alone; solid line indicates mean.

Immunohistochemical detection of TGFβ signalling in hepatocytes following partial hepatectomy

The activation of the canonical TGFβ signalling pathway can be examined ex vivo through detection of phosphorylated SMAD proteins in the nuclei of the cells of interest. An antibody against a phosphorylated form of SMAD3, specifically detecting the amino acid phosphorylation (Serine 423 and Serine 425) that occurs as a result of TGFβ signalling, was used to assess for the presence of active TGFβ signalling following partial hepatectomy. The presence of hepatocyte nuclear pSMAD3 is detectable immunohistochemically in liver harvested from mice at 48 hours post partial hepatectomy (Figure 4 - 9a). As expected, the number of hepatocyte nuclei in which pSMAD3 is detectable, and the strength of the detected

signal, is lower than is present in liver tissue harvested seven days following bile duct ligation, a far more inflammatory liver injury (Figure 4 - 9b).

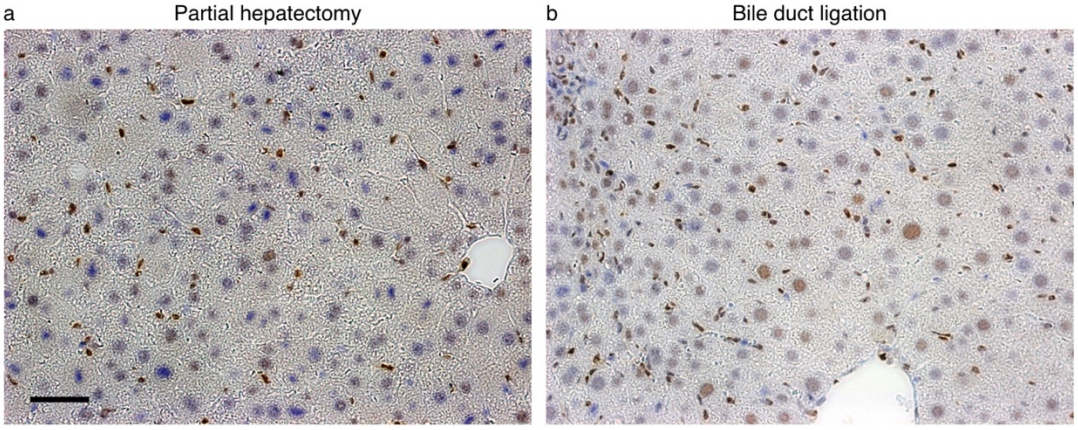

Figure 4 - 9 TGFβ signalling can be detected in hepatocyte nuclei following liver injury.
Representative images from pSMAD3 immunostaining of murine liver tissue at 48 hours post partial hepatectomy (a) and 7 days post bile duct ligation (b). Brown staining indicates pSMAD3 positivity; scale bar 50μm.

The immunohistochemistry protocol was then optimised to use a fluorescent readout of pSMAD3 immunostaining and thus permit quantification of fluorescent intensity as a measure of the amount of nuclear pSMAD3 present. Immunostaining was performed in liver sections harvested from *Itgb8*$^{flox/flox}$*;Alb-Cre* mice and controls at 48 hours post partial hepatectomy. Mean fluorescence intensity for hepatocyte nuclear pSMAD3 was not different between the two groups (Figure 4 - 10), leading to the conclusion that any reduction in canonical TGFβ signalling in hepatocytes in *Itgb8*$^{flox/flox}$*;Alb-Cre* mice, if indeed present, was not detectable using this methodology.

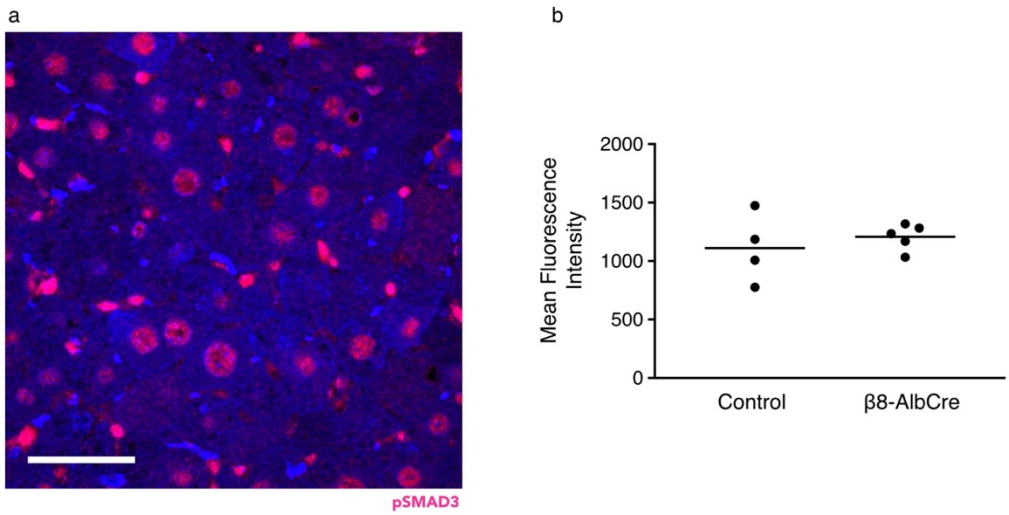

Figure 4 - 10 Quantification of pSMAD3 immunostaining in hepatocyte nuclei following partial hepatectomy.
a) Representative image of pSMAD3 immunostaining of murine liver at 48 hours post partial hepatectomy; pSMAD3 – red, DAPI – blue, scale bar 100μm. b) Mean fluorescence intensity of hepatocyte nuclei following pSMAD3 immunostaining of liver tissue from control and *Itgb8*$^{flox/flox}$*;Alb-Cre* (β8-AlbCre) mice at 48 hours post partial hepatectomy; line indicates mean.

Inhibition of integrin αvβ8 modulates TGFβ-responsive genes in hepatocytes

Because of the challenges in detecting changes in TGFβ signalling in or ex vivo, an in vitro experiment was designed to examine the effect of β8 integrin subunit blockade on hepatocyte TGFβ signalling (Figure 4 - 11a). Freshly isolated hepatocytes were plated onto collagen and treated with either β8 integrin subunit blocking antibody or non-binding control antibody. Following a 24-hour incubation, the cells were lysed and RNA extracted. A custom qPCR array was designed and performed to examine the effects of β8 integrin subunit blocking antibody on the transcription of known TGFβ-responsive genes in hepatocytes.[137] Transcription of αv and β8 integrin subunits, and of canonical TGFβ signalling pathway components, was also assessed (Appendix 2 and 5). Following standardisation, to account for the effect of biological variation between mice, 20 of 87 genes assessed (23%) had a consistent, detectable fold change in expression relative to control, comprising 8 upregulated and 12 downregulated genes (Figure 4 - 11b). Many of these changes were relatively small, but of the 12 genes in which greater than 10% up- or downregulation was detected when compared to control, 10 genes (83%) responded as predicted. Of particular note, the gene most downregulated was *Hmox1* (mean fold regulation -1.4), whilst the most upregulated gene was *Plat* (mean fold regulation 3.3).

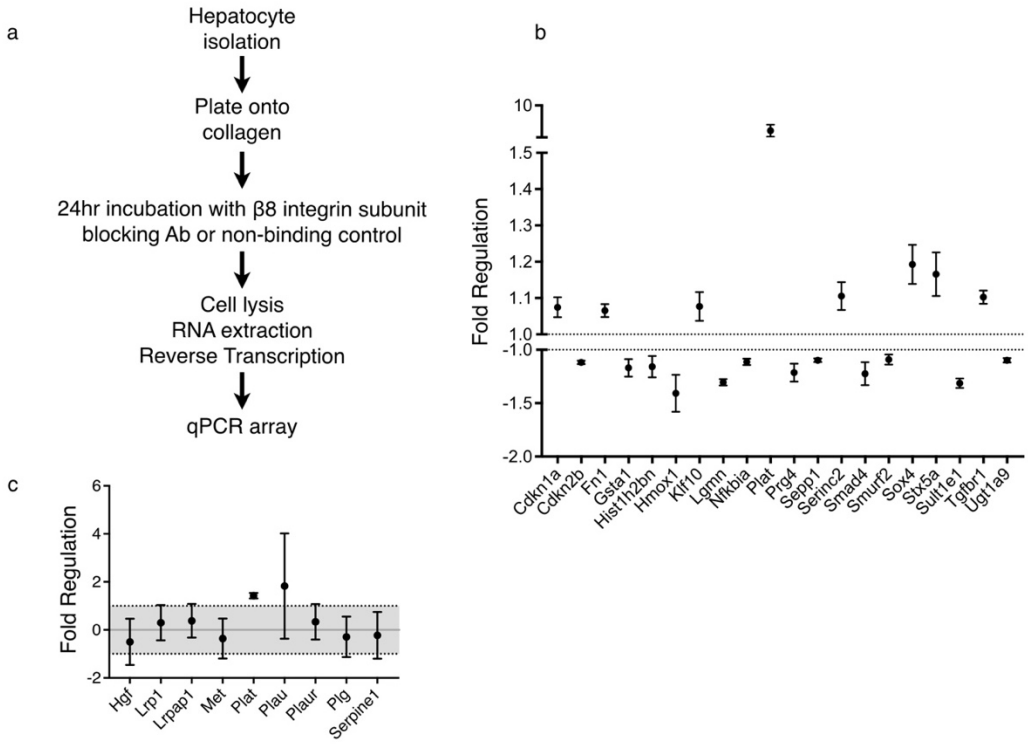

Figure 4 - 11 Inhibition of integrin αvβ8 modulates TGFβ-responsive genes in hepatocytes.
a) Schematic of experimental design to assess the effect of integrin αvβ8 inhibition on hepatocyte expression of TGFβ-responsive genes. b) Genes from the qPCR array with a detectable change in hepatocyte expression following integrin αvβ8 inhibition. Fold regulation >1 indicates upregulation, <-1 indicates downregulation relative to control. c) qPCR of plasminogen activator system genes. All data n=3, presented as mean, error bars – SEM.

Hmox1 encodes heme oxygenase 1 (HO-1), which has been shown to be induced by TGFβ in human lung epithelial cells.[188] *Plat* encodes tissue plasminogen activator (tPA), which is principally known for its role in coagulation, through conversion of plasminogen to plasmin. However, tPA has also been shown to convert inactive hepatocyte growth factor (pro-HGF) to its active form,[189] and thus an increase in tPA production could potentially drive liver regeneration by increasing the activation of HGF. Initial attempts to demonstrate differences in hepatocyte expression of HO-1 and tPA via an immunohistochemical approach were hampered by the large amount of apparently non-specific binding of both antibodies when compared with isotype controls (Appendix 6).

The effect of αvβ8 inhibition on the plasminogen activator system in hepatocytes

Tissue plasminogen activator has a homologue, the urokinase plasminogen activator (uPA), and both have been shown to activate HGF.[189] The regulation of tPA activity by hepatocytes has also been demonstrated. The majority of exogenously administered tPA is cleared by

hepatocytes in the rat liver,[190] following binding to the low-density lipoprotein receptor-related protein (LRP1).[191] Endocytosis can be inhibited by binding of the low-density lipoprotein receptor-related protein associated protein (RAP) to LRP1.[192] As such, the increased expression of *Plat* by hepatocytes treated with β8 integrin subunit blocking antibody was confirmed, and also expression of the genes encoding uPA, the uPA receptor (uPAR), LRP1, and RAP was examined. Since tPA and uPA convert plasminogen to plasmin (itself able to activate HGF), but are inhibited by plasminogen activator inhibitor-1 (PAI-1), expression of the genes encoding plasminogen and PAI-1 was also assessed. Finally, hepatocyte expression of the genes encoding HGF and its receptor, c-Met, was measured.

Standard qPCR for the aforementioned genes was performed on the RNA obtained from the freshly isolated hepatocytes treated with either β8 integrin subunit blocking antibody or non-binding control antibody. This confirmed the upregulation of *Plat*, but failed to show any significant changes in any of the other plasminogen activator-related genes (Figure 4 - 11c), suggesting that hepatocyte integrin αvβ8 may have a regulatory role in tPA expression, but does not act elsewhere in the plasminogen activator system.

Discussion

The goal of this body was work was to try to establish the mechanism through which depletion of integrin αvβ8 leads to increased hepatocyte proliferation and accelerated liver regeneration following partial hepatectomy in mice. The previously reported role of integrin αvβ8 as a ligand for various matrix proteins and its well-documented ability to activate latent TGFβ were both investigated. Depletion of integrin αvβ8 does not appear to have a significant effect on hepatocyte adhesion. Demonstrating the ability of hepatocyte integrin αvβ8 to activate TGFβ proved extremely challenging, but evidence did emerge that blocking this integrin can lead to upregulation of tPA expression, although whether this occurs through a decrease in TGFβ signalling remains unconfirmed. An increase in tPA expression could explain the pro-regenerative phenotype observed in mice depleted of hepatocyte integrin αvβ8, since tPA has been shown to activate HGF, a potent stimulator of hepatocyte proliferation.

Hepatic expression of β8 integrin following partial hepatectomy

A regulatory role for integrin αvβ8 in hepatocyte proliferation was supported by the β8 integrin subunit expression time course following partial hepatectomy. The initial downregulation during the first 24 hours following liver injury may be permissive for the

initiation of hepatocyte proliferation. Subsequently, the peak of expression, reaching 10 times that of baseline, occurred at five days post partial hepatectomy, as the liver is approaching its pre-injury weight, and may therefore assist in terminating the regenerative process. However, it should be noted that β8 integrin subunit expression was assessed in whole liver, due to the challenges associated with isolating hepatocytes immediately following partial hepatectomy. As such, the changes observed following partial hepatectomy could be due to altered expression in non-parenchymal cells in addition to, or instead of, transcriptional alterations in hepatocytes themselves. One way in which the contribution of hepatocytes to whole liver αvβ8 integrin expression could be investigated further would be to repeat the expression time course experiments in *Itgb8*$^{flox/flox}$;*Alb-Cre* mice. By comparing the whole liver expression results from wild-type mice and those in which integrin αvβ8 is depleted from hepatocytes, it would indirectly be possible to characterise the contribution of hepatocyte *Itgb8* expression at each time point.

Hepatocytes and TGFβ activation assays – is no result a result in itself?

The inability to detect hepatocyte activation of TGFβ in vitro, using hepatocyte cell lines or freshly isolated primary hepatocytes, may have occurred for a variety of reasons. Clearly, it is possible that hepatocytes are unable to activate significant quantities of TGFβ even in vivo and the in vitro findings were an accurate reflection of this. However, several other possible explanations may be advanced for the failure to detect experimentally a process which functions well in vivo.

The failure to detect TGFβ activation by the Huh7 or HepG2 cell lines in the early MLEC TGFβ activation assays was not overly surprising. However, the inability to detect TGFβ activation by the LX-2 line was unexpected, since HSCs have previously been shown to activate TGFβ.[29] HSCs are usually activated for five days on tissue culture plastic prior to experimental use, but in the MLEC TGFβ activation assay LX-2 cells were used shortly after resuscitation. This may have affected their ability to activate TGFβ. Furthermore, it has been shown that protein expression in immortal cell lines can differ substantially from the primary cells whose phenotype they attempt to mimic.[187] Indeed, this proteomic study by Pan et al., albeit in an alternative hepatic cell line (Hepa1-6) to those used in the experiments presented above, observed upregulation of TGFβ signalling pathways amongst other changes in the proteome. A similar change might explain the observed tendency for decreasing activation

signal with increasing Huh7 cell number, if the Huh7 cells were, in effect, sweeping up TGFβ from the co-culture medium.

Addition of even small amounts of rhTGFβ resulted in detectable signal from the MLECs, so it appears that the reporter cells were responding as expected and problems with the assay setup itself do not explain the lack of detectable TGFβ activation. Expression of αv integrins, repeatedly shown to be capable of activating latent TGFβ, was not confirmed in any of the cell lines tested. To investigate this further, αv integrin subunit, and relevant beta subunit, expression by these cell types could have been assessed, at both the mRNA and, where possible, protein level. However, this would not necessarily have contributed greatly to the overall body of work investigating the ability of murine hepatocytes to activate TGFβ, since these were all human cell lines. Consideration was also given to testing the assay with a mouse hepatocyte cell line. No such line was readily available and, in any case, a cell line's ability or otherwise to activate TGFβ would not have furthered the key question of whether depletion of integrin αvβ8 on primary mouse hepatocytes reduces their ability to activate TGFβ.

Given the previous evidence that TGFβ activation by activated HSCs can be detected in the MLEC TGFβ activation assay,[29] primary HSCs could have been isolated contemporaneously with hepatocytes from the same animal. This would have served as a cellular positive control, in addition to the pharmacological positive control provided by rhTGFβ. However, not only would this have added complexity to the isolation protocol, potentially compromising the number and viability of hepatocytes that could be obtained, but it would also have introduced certain temporal challenges which would have been difficult to surmount. Whilst HSCs are usually activated by five days of culture on plastic, primary hepatocytes are more challenging to maintain in culture and may undergo significant phenotypic changes during such periods. It was therefore desirable that the hepatocyte co-culture assay should be set up immediately following isolation. Hence the possibility of simultaneously assaying hepatocytes and HSCs from the same mouse was not pursued further.

Unfortunately, the MLEC TGFβ activation assay did not detect TGFβ activation by wild-type murine hepatocytes, which therefore precluded demonstration of any reduction in TGFβ activation following depletion or inhibition of integrin αvβ8. With no good antibody available to detect murine integrin αvβ8 through immunohistochemistry, immunocytochemistry, flow cytometry or Western blot, it was not possible to confirm that isolated murine hepatocytes continue to express integrin αvβ8 at the cell surface following isolation. Almost certainly, the

attempts to detect hepatocyte activation of TGFβ were hampered by the fact that, particularly in uninjured liver, expression of integrin αvβ8 is low, as supported by the hepatocyte *Itgb8* mRNA expression data presented in Chapter Three (Figure 3 - 2a). Consideration was given to the possibility of transfecting either primary hepatocytes or a hepatocyte cell line to cause overexpression of integrin αvβ8. However, although this would likely make confirmation of the ability of integrin αvβ8 to activate TGFβ easier, something that is already well-documented in the current literature, it would be open to the obvious criticism that such a mechanism might not be occurring in vivo.

Another method which would increase hepatocyte expression of integrin αvβ8, and also provide a more relevant setting in which to examine the hepatocyte's ability to activate TGFβ in the context of liver regeneration, would be to perform partial hepatectomy with subsequent hepatocyte isolation. However, the obvious sequela in the immediate aftermath of partial hepatectomy is a drastic reduction in the number of hepatocytes. As such, it was considered that it would be difficult to isolate sufficient numbers for in vitro experimental purposes until at least 72 hours following partial hepatectomy. Had hepatocytes been isolated post partial hepatectomy, at peak integrin αvβ8 expression, this may well have facilitated detection of their ability to activate TGFβ, and demonstrate a difference in hepatocytes depleted of integrin αvβ8. However, given that significantly increased hepatocyte proliferation was recorded earlier in the regenerative phase, any findings regarding TGFβ activation later in liver regeneration would again be open to the criticism that a different mechanism might exist to explain the earlier effects.

It is also feasible that the presence of hepatocytes in co-culture with the reporter cells impacted on the survival of the latter, or their ability to respond to the presence of active TGFβ. Although there was no evidence of this when wells containing either one or both cell types were examined microscopically, this possibility could have been examined in more detail, and potentially circumvented through prior culture of isolated hepatocytes alone, with subsequent culture of the reporter cells in the hepatocyte culture medium. However, this approach would not have prevented any autocrine TGFβ uptake by hepatocytes from occurring, nor increased the amount of active TGFβ available to bind receptors on reporter cells.

Missing links may thwart TGFβ activation

The liberation of active TGFβ from the LAP is a process for which the presence of αv integrins alone is probably not sufficient. Recent studies have demonstrated how integrin αvβ6 is able

to liberate active TGFβ through binding to the RGD domains of the LAP and inducing a conformational change in the latter which permits escape of the active TGFβ homodimer.[66,68] This mechanotransduction also requires that the small latent complex, comprising TGFβ and the LAP, is anchored by the LTBP to the extracellular matrix. Insufficient extracellular matrix in the in vitro TGFβ activation assay could have resulted in a failure to activate latent TGFβ even if binding of the LAP to hepatocyte integrin αvβ8 had occurred.

Potential modifications to the assay to optimise the provision of a suitable extracellular matrix could have included pre-plating the MLEC or MFB-F11 reporter cell lines for a longer period, prior to the addition of the test hepatocytes. However, this may have resulted in increased variability were different rates of reporter cell proliferation to occur across wells during the lengthened test period. When plated in isolation, hepatocytes are usually plated onto collagen. Pilot experiments showed that freshly isolated hepatocytes appeared to adhere well to plates containing previously plated MLECs, so additional coating of plates with collagen was not performed. However, the addition of collagen may have assisted the deposition of a suitable extracellular matrix to which stores of latent TGFβ could anchor.

In contrast to a mechanotransduction mechanism of TGFβ activation, the first study to show that integrin αvβ8 activates TGFβ concluded that the presence of MT1-MMP (also known as MMP14) was required for activation to occur.[21] This implies that an alternative, protease-mediated mechanism, rather than mechanical activation through stretching of the LAP, occurs in the case of integrin αvβ8-mediated TGFβ activation. The gene encoding MMP14 was assessed as part of the qPCR array that was performed on primary hepatocytes treated with β8 integrin subunit blocking antibody or control, and the results confirmed that hepatocytes reliably express this gene (Appendix 5). Hence, a lack of MMP14 would not appear to be the cause of the failure to detect TGFβ activation by integrin αvβ8 on hepatocytes. However, protein expression was not confirmed, so it is possible that insufficient surface expression, cleavage during the hepatocyte isolation process, or even a failure of co-localisation might have prevented successful TGFβ activation.

An alternative TGFβ activation assay

Following the inability to detect hepatocyte activation of TGFβ using the MLEC assay, an alternative in vitro co-culture TGFβ activation assay was trialled. This more recently developed assay is reported to be able to detect concentrations of active TGFβ as low as 1pg/mL, and is highly specific for TGFβ signalling because of the design of the promoter

element preceding the reporter gene, which only responds to SMAD-mediated signalling.[134] In comparison, the MLEC assay is reported to be able to detect TGFβ concentrations of 0.2pM (≡5pg/mL) or greater. Unfortunately, despite this increased sensitivity, it was still not possible to detect convincing hepatocyte activation of TGFβ. One potentially complicating factor is that the MFB-F11 assay employs a secreted alkaline phosphatase as its reporter gene. There is a long-standing acceptance that alkaline phosphatase is expressed by hepatocytes,[193] so this may have reduced the sensitivity of the assay to detect TGFβ activation, by increasing the amount of background signal. It could also explain why the detectable absorbance of hepatocytes cultured alone was similar (in fact, slightly higher) than MFB-F11 cells cultured alone, whereas one would normally not expect to be able to detect any reporter activity in the test cells themselves. Surprisingly, a more recent study has suggested that ALP is not expressed in mouse liver, so the MFB-F11 assay may indeed be suitable for use with hepatocytes or other liver cells.[194]

Is there TGFβ to activate?

A further challenge in these in vitro activation assays relates to the provision of a suitable source of latent TGFβ. Although hepatocytes can produce TGFβ, there is evidence that, particularly in uninjured liver, their expression of TGFβ is low (Appendix 5).[101] Thus, the failure to detect hepatocyte activation of TGFβ may have resulted from there being insufficient stores of latent TGFβ to activate. An attempt was made to supply a latent source of TGFβ, but its ability to stimulate MFB-F11 reporter cells directly suggests that either MFB-F11 cells are able to activate latent TGFβ independently or, more likely, the product contained an amount of active TGFβ, which blunted the sensitivity of the assay. Foetal bovine serum can also provide a source of TGFβ, but the presence of active TGFβ in this fraction of the culture medium will also reduce the sensitivity of these assays to detect small degrees of TGFβ activation. During assay optimisation, no obvious benefit was noted when either low-serum or serum-free media were used for co-culture.

Combined with the pre-existing knowledge that hepatocytes are highly responsive to TGFβ signalling,[137] it is possible that the small amount of TGFβ they may be able to activate via integrin $\alpha v\beta 8$ acts primarily in an autocrine fashion, binding TGFβ receptors on the hepatocytes themselves, rather than becoming available to signal to reporter cells in co-culture. The concept of hepatocytes as net consumers of, rather than contributors to, the

extracellular pool of active TGFβ would fit the results of the TGFβ activation assays performed on freshly isolated primary murine hepatocytes.

Assessing TGFβ signalling in hepatocytes

As well as the inability to detect hepatocyte activation of TGFβ, immunostaining for pSMAD3 failed to detect a difference in canonical TGFβ signalling between the hepatocyte nuclei of control and *Itgb8*$^{flox/flox}$*;Alb-Cre* mice at 48 hours post partial hepatectomy. As with the consideration of the findings from the in vitro TGFβ activation assays, this may well support the conclusion that canonical TGFβ signalling is not altered by loss of hepatocyte integrin αvβ8 at this time point following partial hepatectomy. However, alternative explanations for the observed findings can again be offered. For example, because of the relatively weak nuclear pSMAD3 signal in hepatocytes following partial hepatectomy, when compared with that occurring in a more florid inflammatory process such as bile duct ligation, significant signal amplification was necessary to enable fluorescent detection in post partial hepatectomy liver tissue. This may have had the unwanted consequence of masking any small differences in signal between test and control tissues. Further, the absence of detectable change at one particular time point does not preclude a role for canonical TGFβ signalling at an alternative stage in the time course of liver regeneration. The multitude of signalling pathways through which TGFβ is able to exert its effects means that a failure to detect an effect in the canonical signalling pathway also does not rule out a role for TGFβ signalling through an alternative pathway, such as MAPK, PI3K-Akt, or NF-κB.[195]

Is persisting with TGFβ detrimentally dogmatic?

The continued emphasis on attempting to demonstrate a role for TGFβ in mediating the positive effects on hepatocyte proliferation that were observed following depletion of hepatocyte integrin αvβ8 might seem misguided. However, in over twenty years since the discovery of integrin αvβ8, this is the principle mechanism through which integrin αvβ8 effects have been demonstrated to be mediated. There is an increasingly large body of literature showing that integrin αvβ8 is able to activate latent TGFβ in a wide range of cell types and tissues.[43,59-63] Although all αv integrins have been shown to be able to bind latent TGFβ, these studies demonstrate that targeting integrin αvβ8 alone is sufficient to alter a disease phenotype, through a change in TGFβ activation. Integrin αvβ8 is also able to bind to proteins in the extracellular matrix, principally vitronectin, fibronectin, laminin, and collagen

IV.[185,186] In contrast to the integrin αvβ8-mediated effects on TGFβ signalling, sufficient redundancy within the αv integrin family as a whole appears to exist such that depletion or inhibition of integrin αvβ8, or mutation of its intracellular domain, does not alter a cell's ability to bind to the extracellular matrix.[185,196] The lack of effect of integrin αvβ8 manipulation on cell adhesion is supported by the current work, which showed no difference in hepatocyte binding to vitronectin, fibronectin, laminin, or collagen IV when integrin αvβ8 was depleted. Although this lack of effect was demonstrated using hepatocytes from control and *Itgb8*$^{flox/flox}$*;Alb-Cre* mice, one would anticipate that similar findings would also have resulted had wild-type hepatocytes, with or without the addition of β8 integrin subunit blocking antibody, been used instead.

From assays to arrays

Rather than exhaustively dissect multiple possible TGFβ signalling mechanisms in sequence, and following the failure to detect any alteration in canonical signalling, it was decided to pursue a broader approach to examining potential integrin αvβ8-mediated effects on TGFβ signalling. This led to the experiments in which primary murine hepatocytes were isolated and treated with β8 integrin subunit blocking antibody, followed by RNA isolation, to examine the effects on multiple potential readouts of TGFβ signalling in hepatocytes. A blocking antibody approach was utilised instead of comparing control hepatocytes with those from *Itgb8*$^{flox/flox}$*;Alb-Cre* mice with the aim of reducing biological variation through use of paired samples from the same mouse. It was also thought that more prominent transcriptional changes would be more likely to occur in hepatocytes subjected to sudden blockade, rather than those with constitutive integrin αvβ8 depletion, in which the transcriptome has been afforded the time to adapt and return to a state of equilibrium.

Overall, consistent changes were observed in over a quarter of the downstream signalling genes surveyed. Although the majority of these were only small in magnitude, this is perhaps not surprising given that the isolated hepatocytes came from uninjured liver and were unstimulated. Twelve genes showed a fold regulation of greater than 10% when compared to controls, with ten of these responding as predicted. Furthermore, the array principally incorporated hepatocyte TGFβ 'signature' genes, shown to be significantly up- or downregulated in response to the provision of active TGFβ, rather than genes responsive to a reduction in the amount of tonic TGFβ signalling activity, hypothesised to occur when

integrin αvβ8 is blocked. The magnitude of change occurring when tonic activity is inhibited is unlikely ever to match that seen when a system is actively stimulated.

The gene most upregulated by inhibition of integrin αvβ8 on hepatocytes was *Plat*, encoding tPA. As a plasminogen activator, tPA has a well-established role in the context of coagulation. However, both tPA and its homologue uPA are also able to activate HGF.[189] tPA has been shown to have an anti-fibrotic effect in murine bile duct ligation, or following carbon tetrachloride administration, with reduced hepatocyte proliferation in tPA-null mice in the bile duct ligation model.[197-199] Liver regeneration following partial hepatectomy was shown to be transiently impaired in uPA-deficient mice.[200] Deficiency in uPA was also shown to retard liver regeneration following administration of the pro-apoptotic ligand Fas.[201] uPA and tPA were demonstrated to have a synergistic role in resolution of acute liver injury following carbon tetrachloride administration.[202] Whilst hepatocyte expression of uPA has not been confirmed, hepatocytes have been shown to express uPAR.[203] Increased uPAR expression correlates with increased uPA activity, and both were shown to occur immediately following partial hepatectomy in rats.

Interestingly, several studies have also linked plasminogen activators with αv integrins. Both uPA and uPAR have been shown to associate and interact with multiple αv integrins.[204-207] Specifically, αv integrin interaction with vitronectin has been suggested to localise uPA to focal areas on the cell surface and, in ovarian cancer cells, decreased uPA and uPAR expression.[208,209] In breast cancer cells, inhibition of αv integrins reduced p38 MAPK signalling and uPA expression.[210]

The evidence that plasminogen activators have a role in liver fibrosis, combined with tantalising glimpses of a possible role in liver regeneration, links to αv integrins, and the finding of upregulation following hepatocyte integrin αvβ8 inhibition, prompted the assessment of expression of a number plasminogen activator-associated genes in control hepatocytes and those treated with β8 integrin subunit blocking antibody. This confirmed the upregulation of *Plat* expression following inhibition of integrin αvβ8 on hepatocytes, but did not show any other transcriptional changes in the genes encoding uPA, plasmin, HGF, and their associated receptors or regulatory molecules. The upregulation of Plat is encouraging, but arises from transcriptional analysis only, so remains to be validated through the demonstration of changes in tPA protein levels or activity. Similarly, although transcriptional changes were not observed elsewhere in the plasminogen activator pathway, this does not preclude a role in integrin αvβ8-mediated regulation of liver regeneration by means of, for

example, changes in cellular location or activation state. There are a number of ways in which integrin might impact plasminogen activator pathways, either downstream or independent of TGFβ signalling, to regulate hepatocyte proliferation and liver regeneration. These are presented visually in Figure 4 - 12.

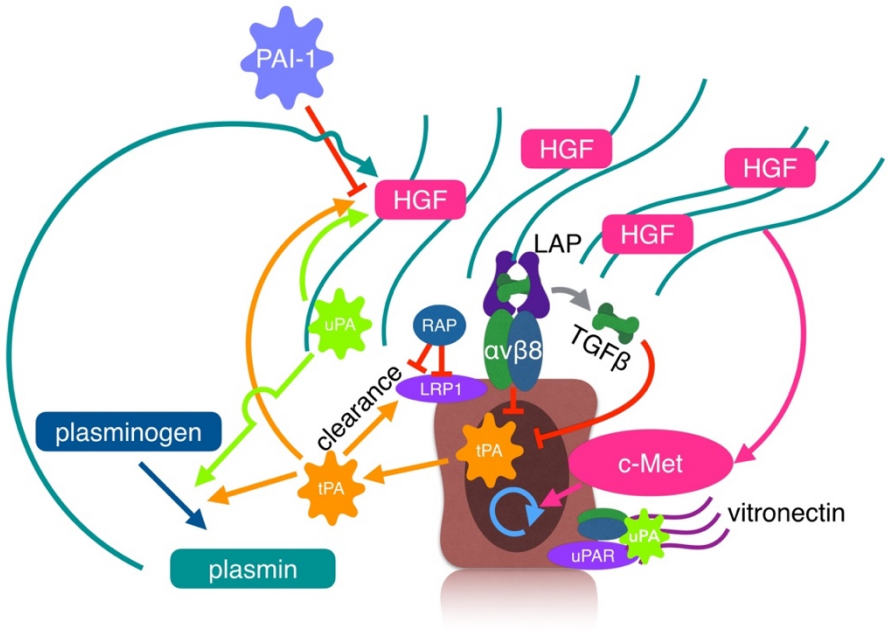

Figure 4 - 12 Plasminogen activators and hepatocyte proliferation: possible mechanisms. Hepatocyte integrin αvβ8 regulates tPA expression, either via direct intracellular signalling, or through activation of latent TGFβ. tPA and uPA can activate matrix-bound HGF, either directly or via increased plasmin production. HGF signals via the c-Met receptor to drive hepatocyte proliferation. tPA and uPA activity is inhibited by PAI-1. tPA clearance can occur through LRP1 association and endocytosis, but is inhibited by RAP. uPA may complex with uPAR and vitronectin-binding αv integrins.

Should integrin αvβ8 be confirmed to regulate hepatocyte proliferation via tPA, there would remain the question of whether the effect on tPA occurs secondary to integrin-mediated TGFβ activation. Recently, evidence has emerged that integrin αvβ8 has intracellular signalling capability, in addition to its well-characterised extracellular roles in TGFβ activation and matrix adhesion. Integrin αvβ8 was shown to associate with Rho-GDP dissociation inhibitor 1 and thereby regulate activation of Rho GTPases, that in turn promote cell motility and invasiveness in a model of glioblastoma.[211] Signalling was abolished by mutation of the cytoplasmic tail of integrin αvβ8. Thus, it is also feasible that direct intracellular signalling by integrin αvβ8, independent of TGFβ activation, might regulate tPA or alternative cell proliferation pathways.

Summary

This chapter describes the body of work performed to explore the mechanism through which depletion of hepatocyte integrin αvβ8 promotes hepatocyte proliferation and accelerates liver regeneration. The time course of β8 integrin subunit expression in the liver, following partial hepatectomy, supports a role for integrin αvβ8 as a brake on hepatocyte proliferation. This regulation does not appear to occur through anchorage to the extracellular matrix, since depletion of hepatocyte integrin αvβ8 does not alter cellular adhesion to extracellular matrix proteins.

The most frequently reported role for integrin αvβ8 is its ability to activate TGFβ, a potent suppressor of hepatocyte proliferation. However, confirming that targeting hepatocyte integrin αvβ8 was able to modulate TGFβ activation proved extremely challenging, not least because of the inability to detect activation of TGFβ by isolated primary hepatocytes from uninjured liver. Canonical TGFβ signalling does occur in hepatocytes following partial hepatectomy, as evidenced by the detection of nuclear pSMAD3. However, it was not possible to demonstrate a reduction in this signalling in *Itgb8*$^{flox/flox}$*;Alb-Cre* mice. A qPCR array to assess a number of genes shown to be modulated by TGFβ did provide evidence that inhibition of hepatocyte integrin αvβ8 leads to changes consistent with a reduction in active TGFβ and downstream signalling. Most prominently, inhibition of hepatocyte integrin αvβ8 resulted in increased expression of *Plat*, the gene encoding tPA. Further work is required to confirm this finding, and clarify its implications, but tPA is known to activate HGF. As such, it is feasible that hepatocyte integrin αvβ8 may regulate hepatocyte proliferation through TGFβ activation and a reduction in tPA expression. Targeting hepatocyte integrin αvβ8 appears to increase tPA expression, which may drive HGF activation and hence promote hepatocyte proliferation and liver regeneration following injury.

Chapter 5 – Developing intravital microscopy of liver regeneration

Introduction

Reductionist approaches, such as in vitro cell culture experiments, can be particularly helpful in investigating the effect of specific molecules on intracellular signalling pathways and cell phenotypes. However, they are unable to reflect accurately the complex, multicellular environment in mammalian tissues. Harvesting tissue for ex vivo analysis, whilst permitting examination of entire tissue, can only provide a snapshot of the physiological process of injury and healing at a single time point, particularly when tissue harvest necessitates culling of the animal in question on either practical or humane grounds. In order to understand better how tissues respond to injury, and the cellular interactions that drive regeneration and repair, it is desirable to be able to observe these processes in situ in the living organism. The challenges of actually doing so in mammals are numerous and varied, and may depend on the tissue of interest, the study species, the nature of the injury, and timeline of the tissue response to the injurious stimulus.

Many of the imaging modalities utilised in medical diagnostics, such as computed tomography, positron emission tomography, ultrasound and magnetic resonance, are of great utility in observing healthy tissue and the response to injury or disease at a macroscopic level. However, they lack the resolution necessary to observe individual cells. Traditional epifluorescence or confocal microscopy techniques provide the required resolution,[143,151] but the practical implementation of these techniques, when applied to whole tissues, results in them being of limited utility, primarily because of restricted depth penetration (<100μm). Photobleaching and phototoxicity are also negative, and potentially limiting, consequences of intravital confocal microscopy.[143] The development of multiphoton microscopy, with its enhanced depth penetration into the tissue of interest, enhances the ability to perform in vivo imaging of mammalian tissues in situ. However, a further challenge lies in accessing the tissue of interest, if one wishes to study structures that are not external like the skin or eye. One approach is simply to exteriorise the tissue of interest and this has previously been performed in the liver.[212,213] Although facilitating in vivo imaging, the principal limitation of such a technique is the restriction to a single imaging session during terminal anaesthesia of the

animal under study. An alternative approach is to implant a device that maintains the integrity of the body cavity in which the tissue of interest is located, whilst also providing an optical conduit through which imaging can be performed. Such a technique was first utilised to image the liver a decade ago.[147] Subsequently, Ritsma et al. described the implantation of an abdominal imaging window (AIW) that could be used to facilitate multiphoton microscopy of a range of abdominal organs, including liver, kidney, spleen, and the gastrointestinal tract.[146]

In principle, AIW implantation provides an excellent means by which to study the process of liver injury and regeneration with cellular resolution. It facilitates repeated, sequential imaging of the same liver throughout the time course of injury and repair, and also permits detailed study of key waypoints with continuous imaging over an extended period. In order to achieve this, current experimental models of liver injury and regeneration need to be combined with AIW implantation and validated. AIW implantation has previously been combined with acetaminophen-induced liver injury within our group, with initial validation comparing this new technique with standard acetaminophen-induced liver injury.[214] This chapter describes the development of a new model, allowing partial hepatectomy and AIW implantation, alongside ongoing refinements to both models. Through an iterative process of optimisation, of both the models themselves and subsequent multiphoton imaging, it is now possible to study the process of liver injury and regeneration following AIW implantation, using intravital multiphoton microscopy, in two separate murine models. The opportunity to study liver injury and regeneration in this way, for the first time, has the potential to offer exciting, novel insights into the processes and cellular coordination underpinning successful liver regeneration. This improved understanding will then offer refined and clinically relevant targets for intervention to drive liver regeneration in patients with liver disease.

Results

Exploring the combination of partial hepatectomy with AIW implantation

Partial hepatectomy in mice has been used to study liver regeneration for over half a century and remains widely used to this day.[11,111] The most commonly performed technique is often referred to as 'two-thirds' partial hepatectomy and involves excision of the left lateral (hereafter referred to as 'left') lobe and both limbs of the median lobe (Figure 5 - 1). This degree of hepatectomy drives a strong regenerative response, with hepatocyte proliferation in the

remnant lobes peaking at 36-48 hours,[119,120] whilst still allowing the animal to survive. A greater degree of hepatectomy is associated with increased mortality,[113] whilst excision of smaller amounts of liver tissue results in hypertrophy rather than true regeneration through hepatocyte proliferation.[112] Fortuitously, the liver lobes excised during the standard two-thirds partial hepatectomy are those most easily accessible following a midline laparotomy with the animal in dorsal recumbency.[215]

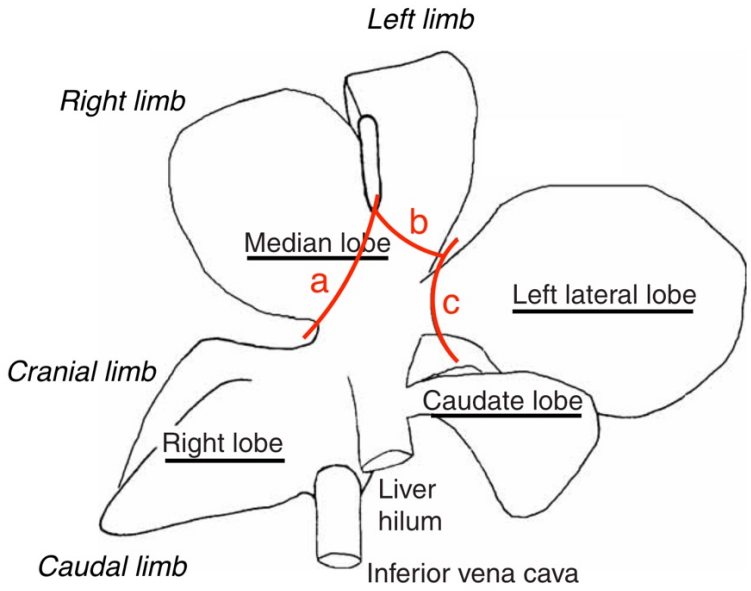

Figure 5 - 1 Mouse liver lobe anatomy as relating to partial hepatectomy.
In the standard 'two-thirds' partial hepatectomy, the left lateral and median lobes are excised. Labelled lines indicate ligating suture location for excision of the right median (a), left median (b), and left lateral (c) lobes. Adapted from Nature Protocols,[111] ©2008, with permission from Macmillan Publishers Ltd.

In desiring to combine AIW implantation with the two-thirds partial hepatectomy model of liver regeneration in mice, the greatest challenge lay in reconciling the two standalone procedures. For routine AIW implantation onto the liver surface, the implant is adhered to the largest, most superficial, left liver lobe. The option of implanting the AIW onto a lobe that does not usually have contact with the ventral body wall was immediately discounted, since this would make anchoring the AIW within the ventral body wall extremely challenging. Therefore, the standard partial hepatectomy technique needed modification to permit AIW implantation onto one of the three liver lobes normally excised in the standard procedure.

Liver lobe weights and options for partial hepatectomy

Five wild-type mice were culled, their livers removed, and the weights of individual lobes were measured (Figure 5 - 2a). This confirmed that the right median and left lobes together comprise the majority (54%) of total liver weight and, by extension, account for the majority

of the liver tissue that is excised during a standard partial hepatectomy (Figure 5 - 2b). The left median lobe, in contrast, comprised only 10% of total liver weight, and accounted for only 16% of the total weight of the three lobes that are excised during a standard partial hepatectomy. In a separate cadaveric study, in which lobes were excised in the same manner as would occur during surgical excision in the anaesthetised animal, standard partial hepatectomy was compared with two possible variants, which would spare either the left median or left lobe for subsequent AIW implantation. In addition to weighing each of the excised lobes, the remnant liver was weighed to allow calculation of percentage hepatectomy for each procedure. Comparing standard partial hepatectomy with excision of just the right median and left lobes did not reveal a significant difference in percentage partial hepatectomy (mean difference -6.5%, P = 0.11) (Figure 5 - 2c). Conversely, excising both median and both right lobes, in order to spare the large left lobe, did significantly reduce the degree of partial hepatectomy performed (mean difference -8.3%, P = 0.04).

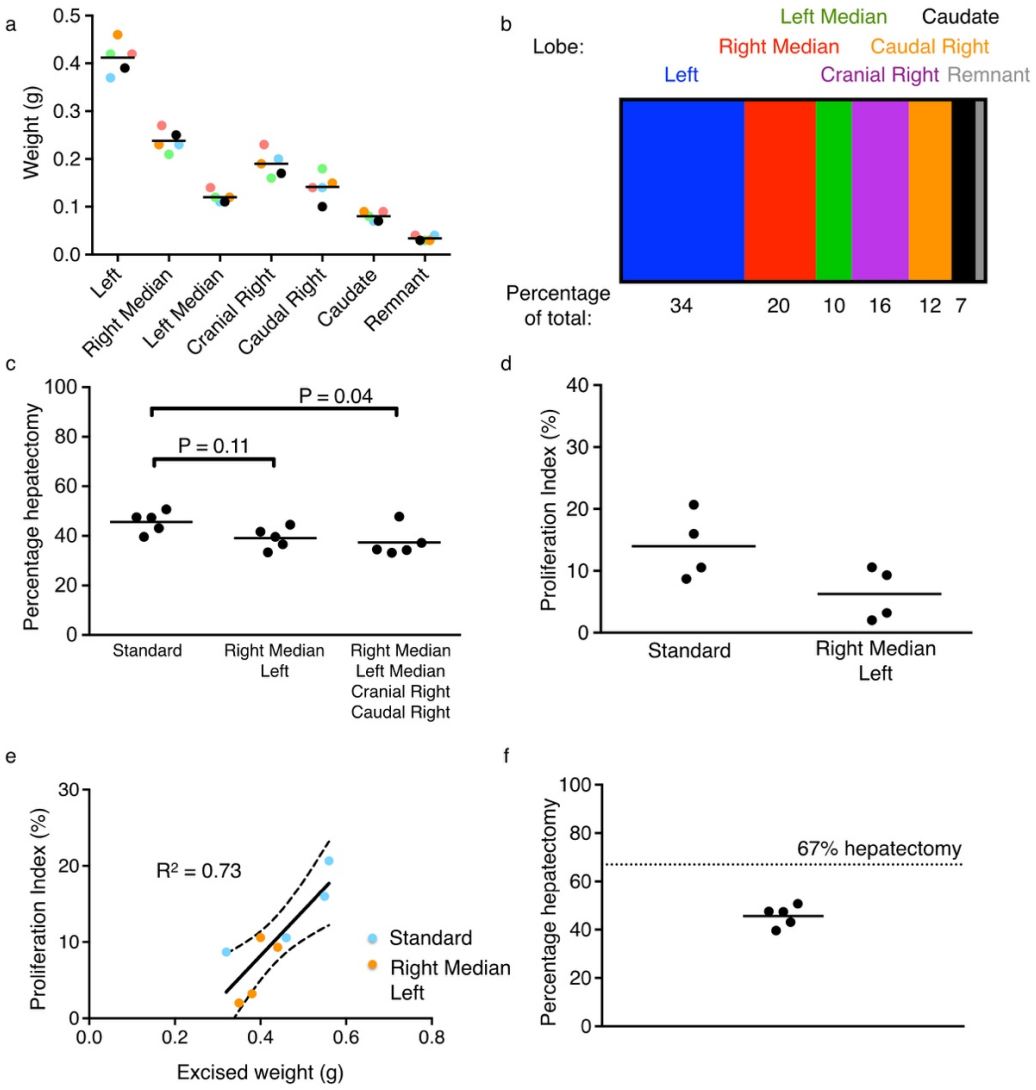

Figure 5 - 2 Mouse liver lobe weights and their contribution to partial hepatectomy.
Individual lobe weights (a) and mean percentage of total liver weight (b) for C57BL/6J mice (each colour in (a) represents one mouse). c) Comparison of percentage hepatectomy achieved in standard and two alternative partial hepatectomies, excising the listed lobes. d) Quantitation of $BrdU^+$ hepatocyte nuclei at 48 hours after standard and reduced (right median and left lobes only) partial hepatectomy. e) Linear regression of excised liver weight and proliferation index for the experiment shown in (d); solid line of best fit, dotted lines indicate 95% confidence bands. f) Percentage partial hepatectomy achieved by performing standard partial hepatectomy in C57BL/6J mouse cadavers; dotted line indicates two-thirds hepatectomy. Horizontal lines indicate mean throughout.

Reduced partial hepatectomy leads to decreased hepatocyte proliferation

Following the liver lobe weight measurements, a pilot experiment was performed to compare the standard 'two-thirds' partial hepatectomy with a partial hepatectomy procedure in which only the right median and left lobes were excised. When assessing hepatocyte proliferation index at 48 hours, a marked decrease was observed in those mice that had received the reduced hepatectomy (Figure 5 - 2d). Although the power of the study meant that this finding did not reach statistical significance (P = 0.07), it strongly suggested that combining a reduced

partial hepatectomy with AIW insertion on the left median lobe might not result in sufficient injury to drive an adequate regenerative response for subsequent study. Linear regression of excised liver weight and hepatocyte proliferation index confirmed that there is a strong association between the two ($R^2 = 0.73$) (Figure 5 - 2e). Targeting excision of >0.5g of liver (>2% body weight) is necessary to achieve the expected hepatocyte proliferation index of 15-20% at 48 hours post partial hepatectomy.

Standard partial hepatectomy does not result in two-thirds hepatectomy in the C57BL/6J mouse

A further interesting discovery from the cadaveric experiments examining liver lobe weights of C57BL/6J mice was that the long-held belief that excising the left and median lobes equates to a two-thirds partial hepatectomy may be a small, but significant, over-estimate. It appears that, at least in C57BL/6J mice, the combined weights of the entire left and median lobes comprise, at most, 63% of the total liver mass (calculated from data presented in Figure 5 - 2a). Indeed, in the cadaveric study in which lobe excision was performed as if in vivo, mean percentage hepatectomy achieved was only 46% (Figure 5 - 2f).

A modified partial hepatectomy equivalent to standard partial hepatectomy

The investigations into combining AIW implantation and partial hepatectomy had, at this point, identified the left median lobe as the most suitable accessible lobe on which to implant the AIW, due to its relatively small contribution to the total mass of excised liver in a standard partial hepatectomy. Of the other superficial lobes, the left lobe alone constitutes around one-third of the total liver mass, so retaining it for AIW insertion, in addition to the non-resectable portion of the liver hilus, would not be compatible with the goal of achieving close to two-thirds partial hepatectomy. Similarly, the option of retaining the right median lobe was discounted because this would necessitate excision of the cranial right lobe as a comparable alternative, something which would be technically demanding given its cranial and dorsal location within the abdominal cavity, close to the diaphragm and lying directly underneath the right median lobe. The pilot experiment comparing standard partial hepatectomy with a reduced partial hepatectomy, excising right median and left lobes alone, suggested a reduced hepatectomy would not drive adequate hepatocyte proliferation. As such, excision of additional liver tissue was required. The measurement of individual lobe weights identified the right caudal lobe as similar in mass to the left median lobe (Figure 5 - 2a,b), so the

combined excision of right median, left, and caudal right lobes had the potential to match the degree of partial hepatectomy achieved by the standard technique.

To confirm the feasibility of this modified partial hepatectomy, it was performed in four mice in order to obtain post partial hepatectomy liver tissue for optimisation of multiphoton imaging protocols. Despite the lack of a control group, and recognising that the cohort was relatively aged and consisted of females and males, this experiment demonstrated that the technique was technically feasible, and excision of an adequate weight of liver tissue was achieved in three of the four mice (Table 5 - 1). One mouse (ID23) had evidence of compromised hepatic blood supply (most likely resultant from stenosis of the suprahepatic vena cava) on post mortem examination, but all survived until the predetermined time of liver harvest.

Table 5 - 1 Excised liver weight following modified partial hepatectomy

Mouse ID	Sex	Age at surgery (weeks)	Surgery weight (g)	Excised liver weight (g)	Excised liver (percent body weight)	Notes
25	f	26	23.9	0.44	1.84	Harvest at 48hrs
24	f	26	25.1	0.76	3.03	Harvest at 72hrs
23	f	26	23.5	0.51	2.17	Harvest at 24hrs
16	m	28	38.8	1.22	3.14	Harvest at 72hrs

f, female; m, male

Modified partial hepatectomy with AIW implantation

A series of cadaveric surgeries were performed to explore the feasibility of combining the modified partial hepatectomy with AIW insertion (Figure 5 - 3a). The final, complete procedure is described in detail in Chapter Two. Briefly, a standard midline 'mini-laparotomy' incision was initially performed and the right median and left lobes were excised in the same manner as for a standard partial hepatectomy (Figure 5 - 3b – 1,2). The midline excision was then extended caudally to facilitate access to the caudal right lobe (Figure 5 - 3b – 3). This was further aided by placement of abdominal retractors and a duodenal manoeuvre to displace the intestines lying superficial to this lobe. The caudal right lobe was then excised in a standard manner. The AIW was adhered to the left median lobe and secured within the ventral body wall by a purse string suture (Figure 5 - 3b – 4,5,6). The remaining section of the laparotomy incision was closed in a routine manner.

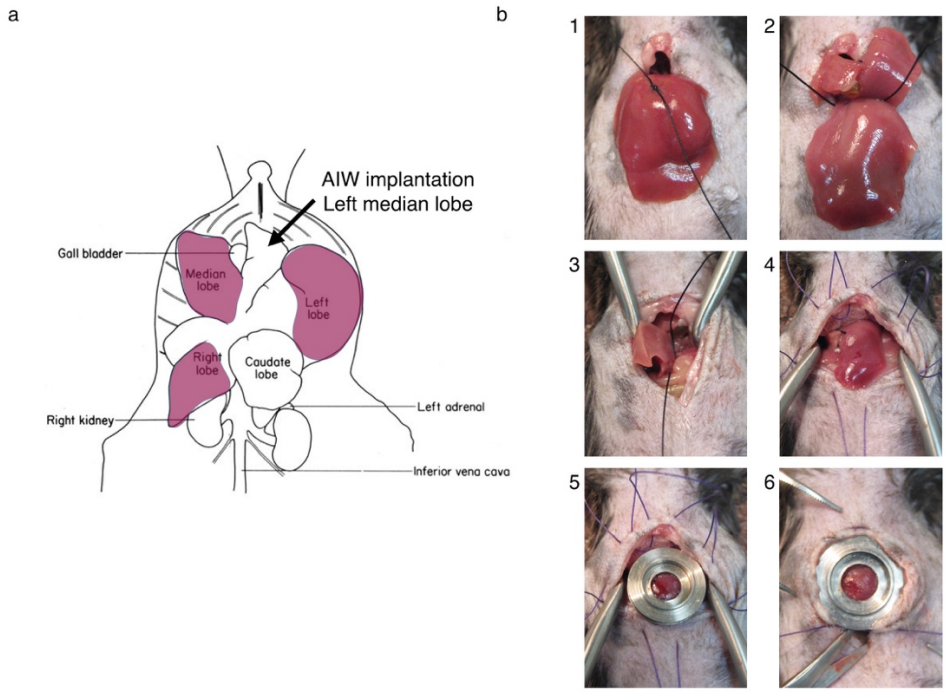

Figure 5 - 3 Modified partial hepatectomy with AIW implantation.
a) Mouse liver lobe anatomy, with lobes excised in the modified partial hepatectomy highlighted (magenta) and indicating site of AIW implantation. Annotation of an original drawing in The Anatomy of the Laboratory Mouse,[216] ©1965, reproduced by permission from Elsevier. b) Photo series illustrating modified partial hepatectomy and AIW implantation, as described in the accompanying text.

Validating modified partial hepatectomy and AIW implantation in mice as a model of liver regeneration

Having developed a novel procedure to combine partial hepatectomy with AIW insertion, it was necessary to examine whether either the modified partial hepatectomy or the presence of the AIW might significantly alter the hepatocyte proliferation and liver regeneration seen following a standard partial hepatectomy. As such, two experiments were designed to compare the standard partial hepatectomy with the modified partial hepatectomy and the modified partial hepatectomy with AIW implantation. The first experiment examined hepatocyte proliferation and liver regeneration at 48 hours post partial hepatectomy, whilst the second examined liver regeneration at one week post surgery.

Excised liver weight does not differ between standard and modified partial hepatectomy

In both experiments the weight of excised liver for each mouse was recorded as a primary measure of whether removal of a comparable mass of liver tissue was achievable in mice receiving either modified partial hepatectomy or modified partial hepatectomy and AIW

insertion, when compared to standard partial hepatectomy. No significant difference in the weight of excised liver tissue was observed between groups, and the data also showed that excision of at least 0.5g was achievable in the vast majority of cases (Figure 5 - 4a,b).

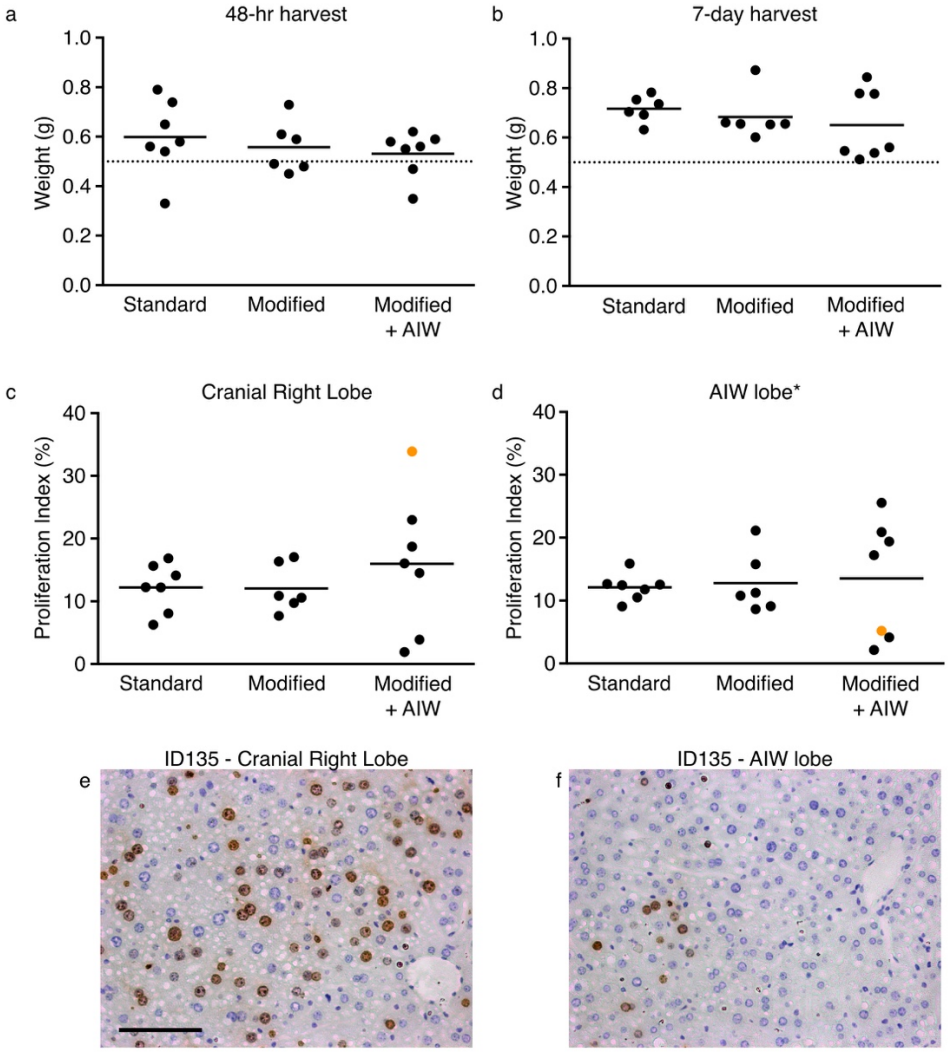

Figure 5 - 4 The effect of modified partial hepatectomy and AIW implantation on excised liver weight and 48-hour hepatocyte proliferation index.
Weight of excised liver in two experiments (48-hour harvest (a), 7-day harvest (b)) to compare standard partial hepatectomy ('Standard') with modified partial hepatectomy ('Modified') and with modified partial hepatectomy and AIW implantation ('Modified + AIW'). Quantitation of $BrdU^+$ hepatocyte nuclei at 48 hours post partial hepatectomy in the cranial right lobe (c) and left median or caudal right lobe (AIW lobe, d). *Left median lobe for Modified and Modified + AIW groups, caudal right for Standard group. Orange dot highlights mouse ID135 in (c) and (d). Representative BrdU immunostaining from cranial right (e) and AIW (f) lobes of mouse ID135; positive nuclei are brown; scale bar 100μm. Solid horizontal lines indicate mean.

The effect of modified partial hepatectomy and AIW implantation on hepatocyte proliferation

The 48-hour time point is of key importance because this is the time of peak hepatocyte proliferation following partial hepatectomy. Immunostaining for BrdU, which was

administered two hours prior to liver harvest, was performed to allow quantification of the hepatocyte proliferation index. This revealed no significant difference between the amount of hepatocyte proliferation in mice receiving standard partial hepatectomy, modified partial hepatectomy alone, or modified partial hepatectomy with AIW implantation (Figure 5 - 4c). The initial comparison was performed on the cranial right liver lobe, which was retained in all three groups. However, it was also important to assess hepatocyte proliferation in the left median lobe, to which the AIW was adhered; this lobe is excised in the standard partial hepatectomy procedure. Overall, no significant difference in hepatocyte proliferation was observed between mice receiving the modified partial hepatectomy alone, or modified partial hepatectomy with AIW implantation, nor did these values differ significantly from the hepatocyte proliferation index in the caudal right lobe in mice in which standard partial hepatectomy was performed (Figure 5 - 4d).

Although overall hepatocyte proliferation indices did not differ significantly between groups, there was an increased variation within the group receiving modified partial hepatectomy and AIW implantation. Two mice showed a failure of hepatocyte regeneration, manifested as a hepatocyte proliferation index ≤5% in both lobes in which hepatocyte proliferation was assessed. This is most likely due to a failure to excise sufficient liver mass, since these mice had less than 0.5g liver (<2% of bodyweight) excised. One other mouse (ID135) exhibited a failure of appropriate hepatocyte proliferation in the left median (AIW) lobe alone. This is likely due to surgical or AIW-related compromise of vascular flow to this lobe; post mortem examination identified a pale left median lobe even prior to immunohistochemical confirmation of drastically reduced hepatocyte proliferation (Figure 5 - 4e). Interestingly, hepatocyte proliferation index in the cranial right lobe in this mouse was double that of the mean for this group, highlighting the remarkable regenerative capacity of the murine liver (Figure 5 - 4f). Reassuringly, in the remaining mice receiving modified partial hepatectomy with AIW implantation, where sufficient liver mass was excised and lobar blood flow was not compromised, hepatocyte proliferation at 48 hours was at an expected level and in fact slightly above that seen in mice receiving standard partial hepatectomy. This confirms that this novel, combined procedure can be used to study liver regeneration in mice.

Inter-lobe comparison of hepatocyte proliferation

Analysis of hepatocyte proliferation in two lobes from each mouse enabled a side-by-side comparison to be made to examine whether differences in the calculated proliferation index are present between lobes following partial hepatectomy (Figure 5 - 5). Although small shifts

in the calculated proliferation index were observed among the paired samples, there was no consistent trend or overall statistical difference in proliferation index between lobes in any of the three experimental groups. This suggests that the presence of an AIW does not have a localised lobar effect on hepatocyte proliferation index (except in the case of the previously reported mouse in which a marked reduction in hepatocyte proliferation was observed). It also suggests that liver regeneration following partial hepatectomy occurs equally among all remnant lobes.

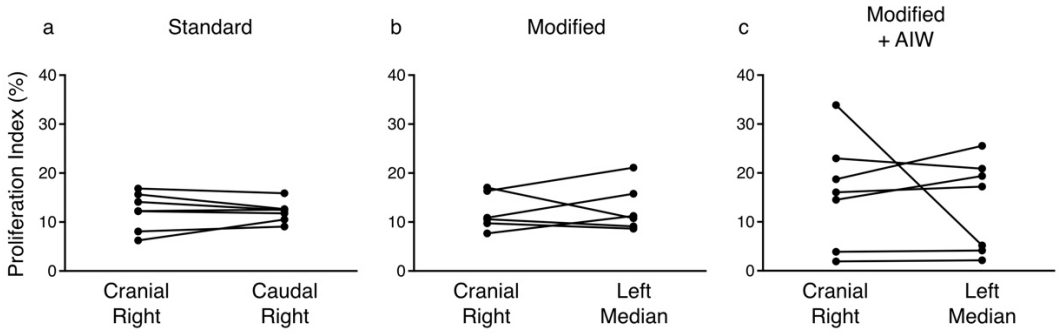

Figure 5 - 5 Inter-lobe comparison of hepatocyte proliferation following partial hepatectomy. Quantitation of $BrdU^+$ hepatocyte nuclei at 48 hours post partial hepatectomy in each of two lobes per mouse following standard (a) or modified (b) partial hepatectomy, or modified partial hepatectomy with AIW implantation (c). Solid lines connect proliferation indices from the same mouse.

The effect of modified partial hepatectomy and AIW implantation on the cellular inflammatory response

Immunostaining to label HSCs (PDGFRβ), Kupffer cells (F4/80) and neutrophils (GR1) was performed on liver tissue harvested at 48 hours post surgery. Partial hepatectomy is a model of liver regeneration that is characterised by minimal inflammatory response. However, it was reasonable to suspect that the increased manipulation required to access and excise the caudal right lobe, or the presence of an AIW might lead to an augmented inflammatory response, particularly neutrophil infiltration, which might then alter the dynamics of liver regeneration following injury.

In fact, no difference in percentage positive staining for neutrophils was noted between any of the three surgical groups (Figure 5 - 6a,b), nor between the two lobes assessed for each mouse (Figure 5 - 6d-f). Although no comparison was made with uninjured liver, negligible neutrophil staining (<0.01%) was observed in all samples. Not only does this confirm that partial hepatectomy alone does not promote neutrophil recruitment to the liver, but also that the presence of the AIW does not drive significant additional neutrophil infiltration.

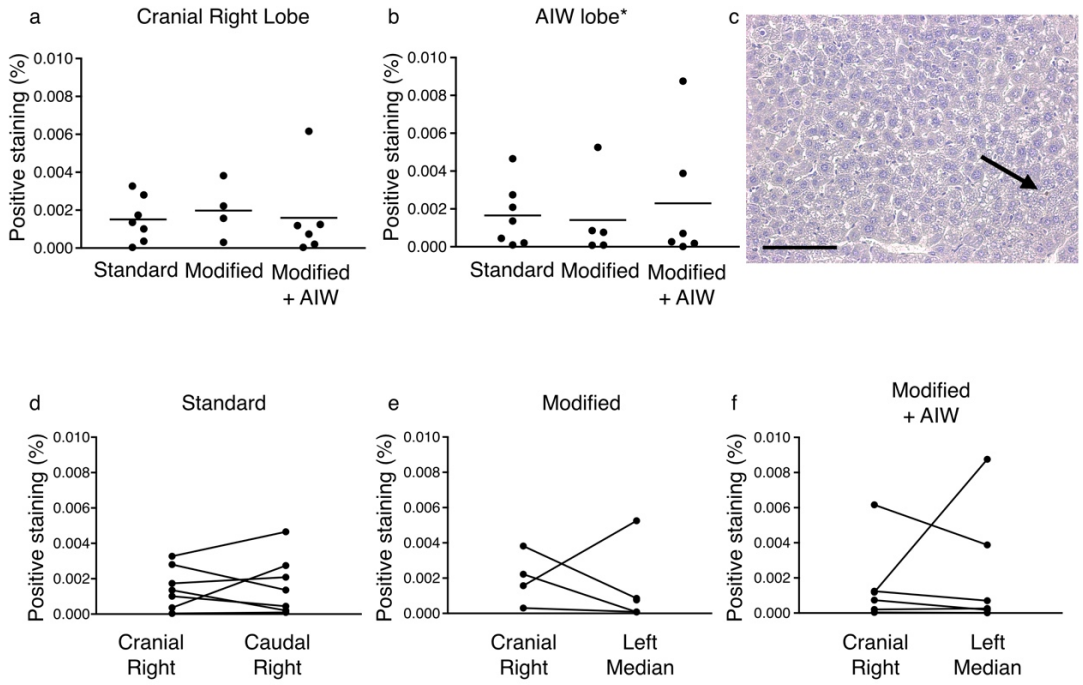

Figure 5 - 6 The effect of modified partial hepatectomy and AIW implantation on neutrophil immunostaining in the liver.
Quantitation of $GR1^+$ immunostaining at 48 hours post partial hepatectomy in the cranial right lobe (a) and left median or caudal right lobe (AIW lobe, b). *Left median lobe for Modified and Modified + AIW groups, caudal right for Standard group. c) Representative image illustrates rare $GR1^+$ neutrophils (brown) within the hepatic parenchyma (arrow); scale bar 100μm. Inter-lobe comparison of $GR1^+$ immunostaining at 48 hours post partial hepatectomy in each of two lobes per mouse following standard (d) or modified (e) partial hepatectomy, or modified partial hepatectomy with AIW implantation (f). Solid lines connect values from the same mouse.

Similarly, no significant changes were detected in percentage positive staining for HSCs, either between surgical cohorts or the lobes in individual mice (Figure 5 - 7). This suggests that the modified partial hepatectomy and AIW implantation do not drive a change in HSC size or number in the first two days following surgery.

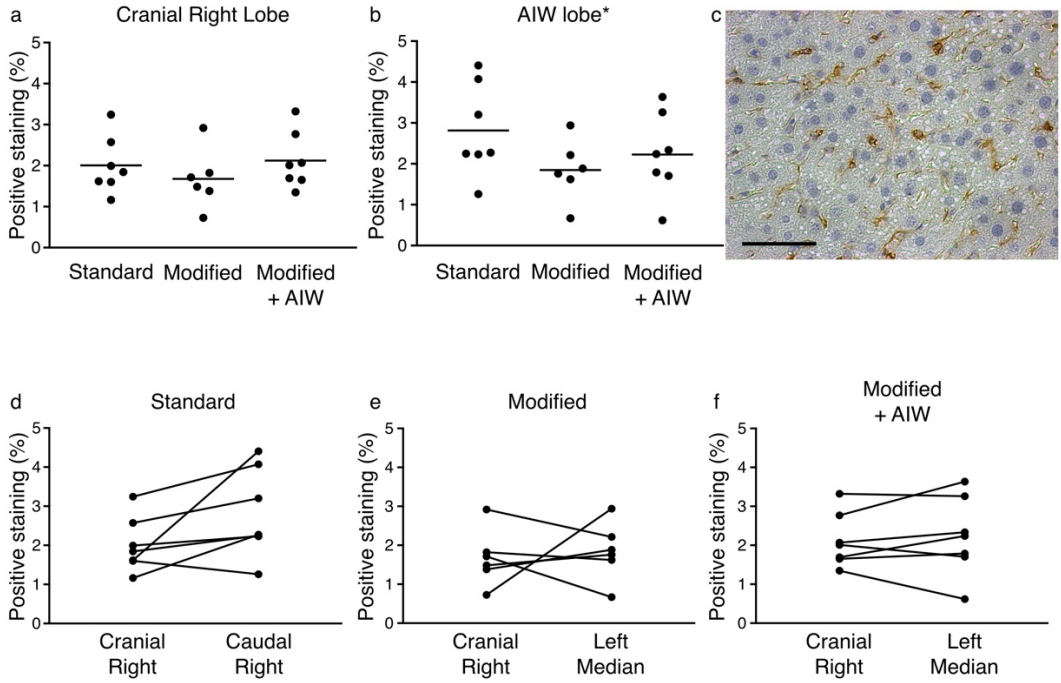

Figure 5 - 7 The effect of modified partial hepatectomy and AIW implantation on HSC immunostaining in the liver.
Quantitation of PDGFRβ$^+$ immunostaining at 48 hours post partial hepatectomy in the cranial right lobe (a) and left median or caudal right lobe (AIW lobe, b). *Left median lobe for Modified and Modified + AIW groups, caudal right for Standard group. c) Representative image of PDGFRβ$^+$ staining (brown); scale bar 100μm. Inter-lobe comparison of PDGFRβ$^+$ immunostaining at 48 hours post partial hepatectomy in each of two lobes per mouse following standard (d) or modified (e) partial hepatectomy, or modified partial hepatectomy with AIW implantation (f). Solid lines connect values from the same mouse.

Lastly, F4/80 immunostaining was performed to label Kupffer cells in the liver tissue harvested at 48 hours post surgery. Again, no significant difference was detected in percentage positive staining between groups (Figure 5 - 8a,b), although a slight upward trend was observed when comparing the caudal right lobe in standard partial hepatectomy with the left median lobe in modified partial hepatectomy, with a further slight increase when AIW implantation was performed (Figure 5 - 8b). Further, although there was no difference in staining between the two lobes examined in mice receiving either standard or modified partial hepatectomy alone (Figure 5 - 8d,e), a small but statistically significant increase in percentage positive staining for F4/80 (mean increase 0.9%, 95% CI 0.01-1.8%) was observed when the left median (AIW) lobe was compared with the cranial right lobe in mice receiving modified partial hepatectomy and AIW implantation (Figure 5 - 8f). These findings suggest that the combination of the modified partial hepatectomy procedure and the presence of the AIW may cause a small increase in Kupffer cell number or size in the lobe over which the AIW is implanted.

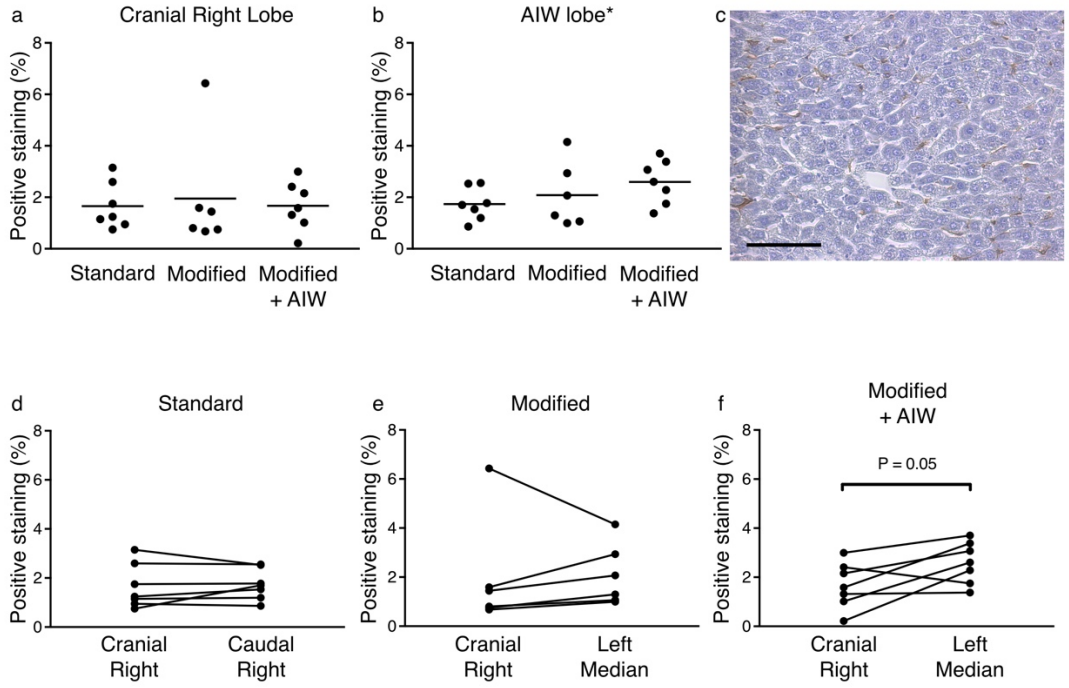

Figure 5 - 8 The effect of modified partial hepatectomy and AIW implantation on Kupffer immunostaining in the liver.
Quantitation of F4/80 immunostaining at 48 hours post partial hepatectomy in the cranial right lobe (a) and left median or caudal right lobe (AIW lobe, b). *Left median lobe for Modified and Modified + AIW groups, caudal right for Standard group. c) Representative image of F4/80 staining (brown); scale bar 100μm. Inter-lobe comparison of F4/80 immunostaining at 48 hours post partial hepatectomy in each of two lobes per mouse following standard (d) or modified (e) partial hepatectomy, or modified partial hepatectomy with AIW implantation (f). Solid lines connect values from the same mouse.

The effect of modified partial hepatectomy and AIW implantation on liver biochemistry

Serum was also obtained at the 48-hour time point to allow assessment of biochemical markers related to hepatic injury and function. This aimed to assess whether a different degree of liver injury might occur in the different surgical groups. Although there was some increased variability in the mice receiving modified partial hepatectomy (with or without AIW implantation), the mean value for each parameter did not differ significantly between surgical groups (Figure 5 - 9). This supports the conclusion that the modified partial hepatectomy technique, either alone or in combination with AIW implantation, leads to a similar degree of liver injury when compared to standard partial hepatectomy.

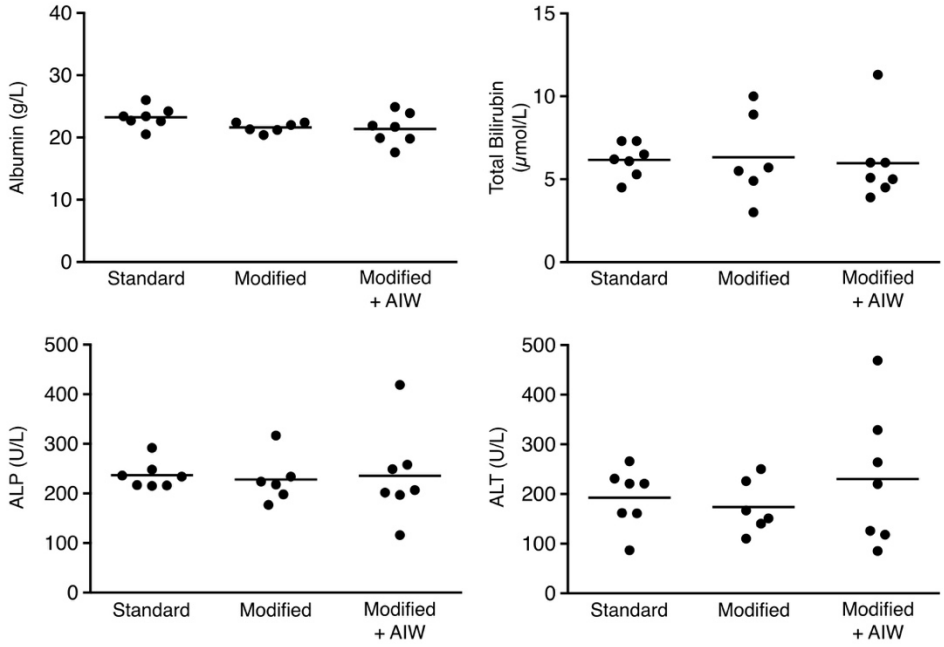

Figure 5 - 9 The effect of modified partial hepatectomy and AIW implantation on liver biochemistry.
Serum biochemistry (albumin, total bilirubin, ALP, ALT) at 48 hours following standard or modified partial hepatectomy, or modified partial hepatectomy with AIW implantation. Horizontal line indicates mean.

The effect of modified partial hepatectomy and AIW implantation on seven-day liver and body weights

In a second experiment comparing standard partial hepatectomy, modified partial hepatectomy, and modified partial hepatectomy with AIW implantation, mice were culled at seven days post surgery. This enabled calculation of liver to body weight ratio at the time point that marks the end of liver regeneration in the standard partial hepatectomy model. Although liver to body weight ratio did not differ significantly between surgical groups (Figure 5 - 10a), this 'headline' measure does not reflect certain underlying changes of interest. Seven-day liver weight was slightly, but significantly, decreased in mice receiving modified partial hepatectomy and AIW implantation in comparison to mice receiving standard partial hepatectomy (mean difference 198mg, 95% CI: 19 - 377mg) (Figure 5 - 10b). It is possible that the observed difference at seven days was due to a pre-existing difference in uninjured liver weight. However, given that mice were randomly allocated to surgical group, and neither body weight at time of surgery (Figure 5 - 10c) nor excised liver weight (Figure 5 - 4b) differed between surgical groups, there is no reason to suspect this. There was a slight decrease in seven-day liver weight in mice receiving modified partial hepatectomy compared to mice receiving standard partial hepatectomy, but this difference was non-significant (mean

difference 58mg, 95% CI: -11 - 228mg) (Figure 5 - 10b). No significant difference was observed when harvest liver weight in mice receiving modified partial hepatectomy was compared with mice receiving both modified partial hepatectomy and AIW implantation (mean difference 141mg, 95% CI: -38 - 320mg). These findings suggest that the combination of modified partial hepatectomy and AIW implantation results in a slight retardation or inhibition of liver regeneration in mice.

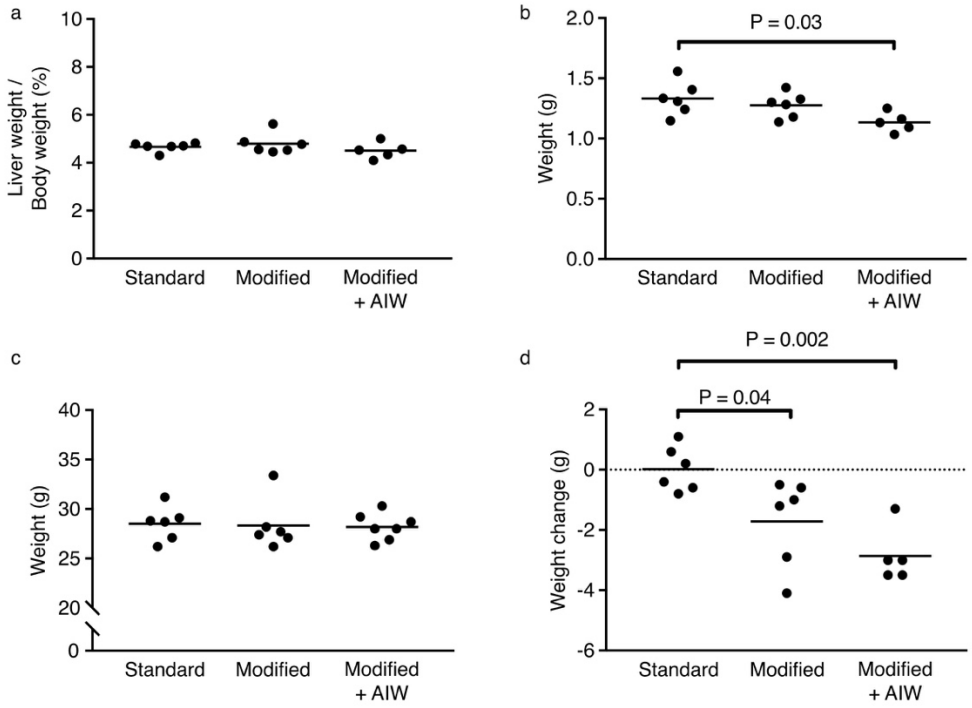

Figure 5 - 10 The effect of modified partial hepatectomy and AIW implantation on liver and body weights at seven days.
Harvest liver to body weight ratio (a), harvest liver weight (b), mouse weight at surgery (c), and seven-day weight change (d) for mice receiving standard or modified partial hepatectomy, or modified partial hepatectomy with AIW implantation. Horizontal line indicates mean.

The apparent equivalence in seven-day liver to body weight ratio among surgical groups, despite the small differences in liver harvest weight, results from the finding that body weight at harvest also differed between the groups. Both the mice receiving modified partial hepatectomy alone and those receiving modified partial hepatectomy and AIW implantation showed increased and moderate weight loss compared to mice receiving standard partial hepatectomy (Figure 5 - 10d). Mice undergoing standard partial hepatectomy showed, on average, no weight change at seven days when compared to their pre-surgery weight. Modified partial hepatectomy resulted in mean weight loss of 1.7g (95% CI: 0.2-3.2g), equivalent to a 6% mean decrease from weight at time of surgery. Modified partial hepatectomy with AIW implantation resulted in mean weight loss of 2.9g (95% CI: 1.7-4.0g)

at seven days post surgery, equivalent to a 10% mean decrease from weight at time of surgery. Whilst this degree of weight loss may not impact significantly on the process of liver regeneration, it may serve as a surrogate indicator that the modified partial hepatectomy, with or without AIW implantation, is a slightly more invasive procedure and both increased monitoring of weight and additional husbandry measures to promote food intake and post-surgical recovery may be indicated.

Anaesthetic and peri-operative considerations associated with modified partial hepatectomy and AIW implantation

As expected, the time required to perform partial hepatectomy and AIW insertion is roughly twice that needed for either procedure alone. Perhaps naively, this was not anticipated to be a significant issue, given that total surgical time would still only be around one hour, and anaesthetic and perioperative management protocols already incorporated measures to maintain body temperature, provide fluid support, and minimise the risk of hypoxia. Despite this, a number of adverse effects were seen in the first cohort of mice in which modified partial hepatectomy was performed, with or without AIW insertion. Specifically, 2/4 mice receiving modified partial hepatectomy with AIW implantation, and 1/2 mice receiving modified partial hepatectomy alone, manifested prolonged recovery from general anaesthesia, continued obtundation, and hindlimb paresis. These mice were therefore culled on welfare grounds. Post mortem examination revealed no evidence of surgical complications nor were these signs seen in mice receiving standard partial hepatectomy. Given this, and the fact that insertion of the AIW per se is minimally invasive and relatively atraumatic, it seemed likely that the adverse effects observed were most likely related to peri-operative factors, such as an issue with thermal support provided intra-operatively by the heat mat, and exacerbated by the increased surgical time and prolonged general anaesthesia. Figure 5 - 11 illustrates that surgical time, and as a result time under general anaesthesia, is slightly increased by performing the modified instead of standard partial hepatectomy; mean increase in time under anaesthesia versus standard partial hepatectomy was 9 minutes (95% CI: -2 – 21 minutes). Implantation of the AIW in addition to modified partial hepatectomy increased duration of general anaesthesia still further when compared to standard partial hepatectomy (mean increase 40 minutes, 95% CI: 28-51 minutes).

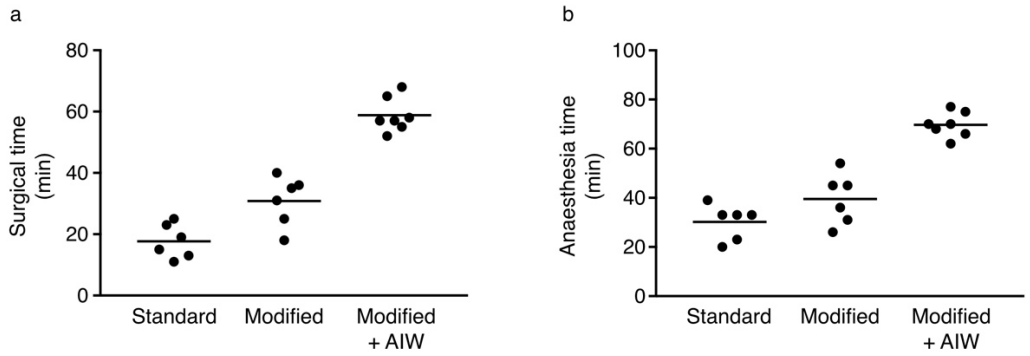

Figure 5 - 11 The effect of modified partial hepatectomy and AIW implantation on surgical and anaesthesia time.
Surgical time (a) and total time under general anaesthesia (b) for standard or modified partial hepatectomy, or modified partial hepatectomy with AIW implantation. Horizontal line indicates mean.

Thereafter, a raft of further optimisations to the anaesthetic protocol and perioperative management were introduced. This included close titration of anaesthetic depth, additional administration of subcutaneous fluids at the start and end of the procedure, tighter control of thermal support until full recovery to minimise the risk of either overheating or hypothermia, and adjustments to limb immobilisation to reduce the risk of inadvertent neurological or vascular compromise. Following the introduction of these improvements, no further perioperative adverse effects of a similar nature were observed in any subsequent experiments involving partial hepatectomy and AIW implantation.

It is important to note that the presence of the AIW itself can lead to adverse events. In the experiment in which livers were harvested seven days after partial hepatectomy, with or without AIW implantation, one mouse was culled after the AIW displaced during recovery. A second mouse was culled at 44 hours post surgery after becoming obtunded. Post mortem examination revealed that a section of jejunum had become entrapped between the liver lobe and the AIW, leading to intestinal obstruction.

Optimising AIW design and imaging setup

Previous AIW iterations

In addition to developing a novel experimental model combining partial hepatectomy with AIW insertion, it was also necessary to redevelop both the AIW implant itself and the baseplate into which it sits, in order to optimise the quality of the images acquired during multiphoton microscopy. The design of the original AIW implant used by Ritsma et al.[146] (Figure 5 - 12a) had already been updated on two occasions, once to make the glass coverslip replaceable (by using a removable circlip rather than glue to anchor it in place) (Figure 5 -

12b), and subsequently to introduce a two-part design in which the glass coverslip is adhered to a circular titanium inlay which is then screwed into the body of the AIW (Figure 5 - 12c). Whilst this latter iteration facilitates coverslip replacement, and thereby helps maximise optical resolution, the complete range of the modifications introduced by the van Rheenen group in Utrecht also posed some additional challenges to obtaining high-quality multiphoton images. Principally, the coverslip now sits on top of the inlay, which screws into the upper surface of the AIW body; in contrast, in the previous iteration the coverslip was placed within the body of the AIW, facilitating contact with the liver surface. To maximise image quality and imaging depth during multiphoton microscopy, it is essential that the liver surface makes intimate contact with the coverslip; dead space is a potent foe for the photon!

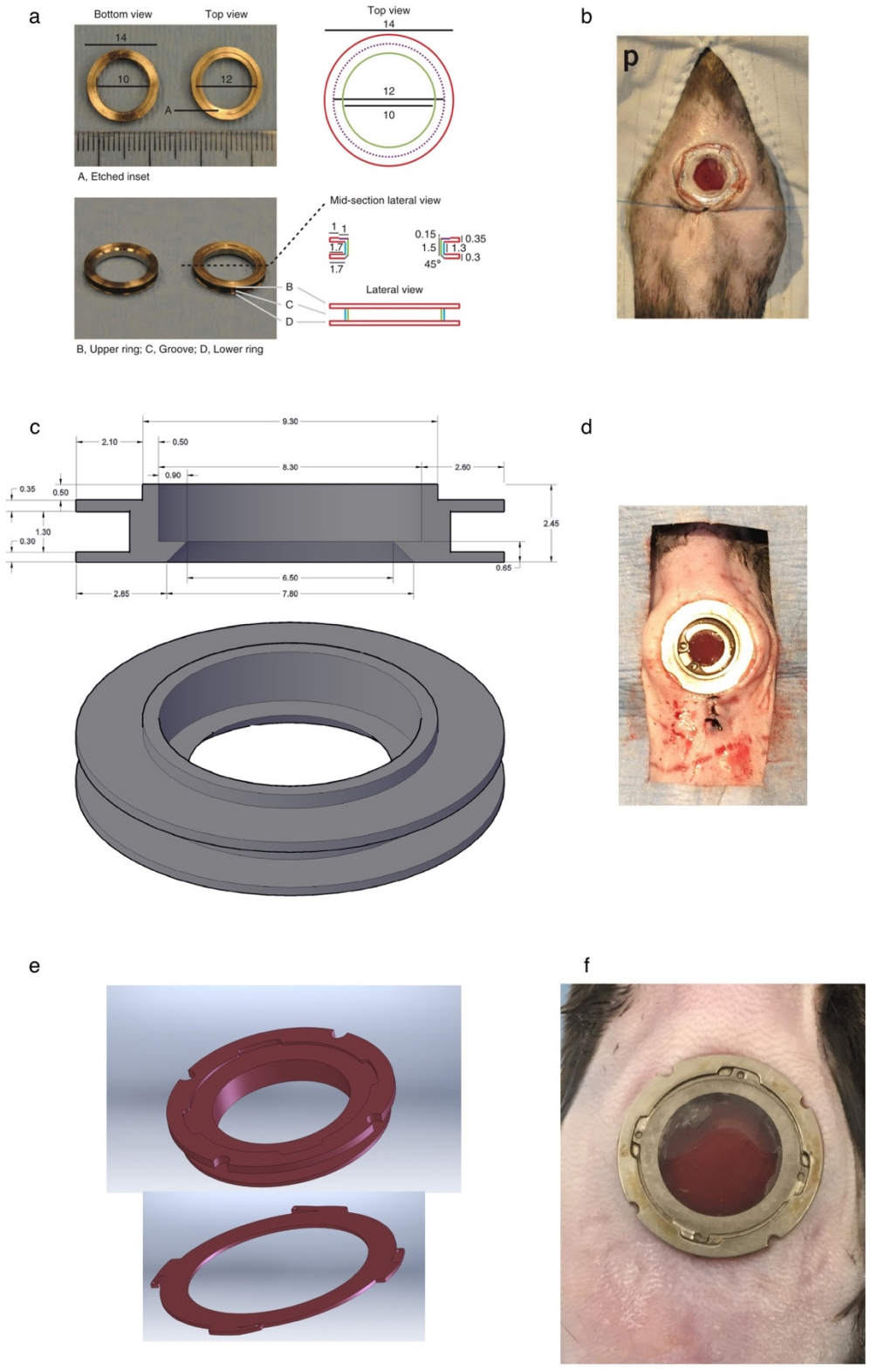

Figure 5 - 12 AIW iterations.
Design (a) and in situ photograph (b) of the original AIW. Adapted from Nature Protocols,[146] ©2013, with permission from Macmillan Publishers Ltd. Design (c) and in situ photograph (d) of the first modification in AIW, with the coverslip held in place by a circlip. Graphical representation (e) and in situ photograph (f) of the third AIW iteration, with removable inlay to which the coverslip is adhered. Images in (e) used with permission of J. van Rheenen. All measurements in mm.

Modified AIW design

Two new versions of the AIW were designed to suit better the specific requirements of intravital microscopy of the murine liver, with and without partial hepatectomy. These alterations are illustrated in the following figure and comprised three major modifications (Figure 5 - 13). The circumference of the external rim of the AIW was enlarged to enable four deeper notches (1.5mm versus 1.1mm) to be cut into the rim, improving the ability to immobilise the AIW when placed onto the imaging baseplate (Figure 5 - 13a,b blue arrows). The depth of the groove into which the purse string suture is placed was reduced from 1.3mm to 1.1mm, to reduce the overall depth of the AIW and facilitate contact between the liver and the coverslip (Figure 5 - 13a,b red rectangles). Thirdly, the inner wall of the AIW was slanted in an attempt to fit the natural contour of the liver, assisting its ability to enter into the inner aperture of the AIW and thus again bringing it closer to the coverslip (Figure 5 - 13a,b green ovals). The only difference between the two new versions was in the diameter of the internal aperture. One had a larger (8mm diameter) internal aperture to maximise the amount of liver available for imaging when the AIW was implanted, without partial hepatectomy, onto the large left lobe (Figure 5 - 13a). The second new version had a reduced (5.2mm diameter) internal aperture for use when the AIW was implanted onto the smaller left median lobe, following modified partial hepatectomy (Figure 5 - 13b). Having decided on the above modifications, prototypes were printed in plastic and suitability assessed on mouse cadavers prior to manufacture in titanium (Figure 5 - 13c).

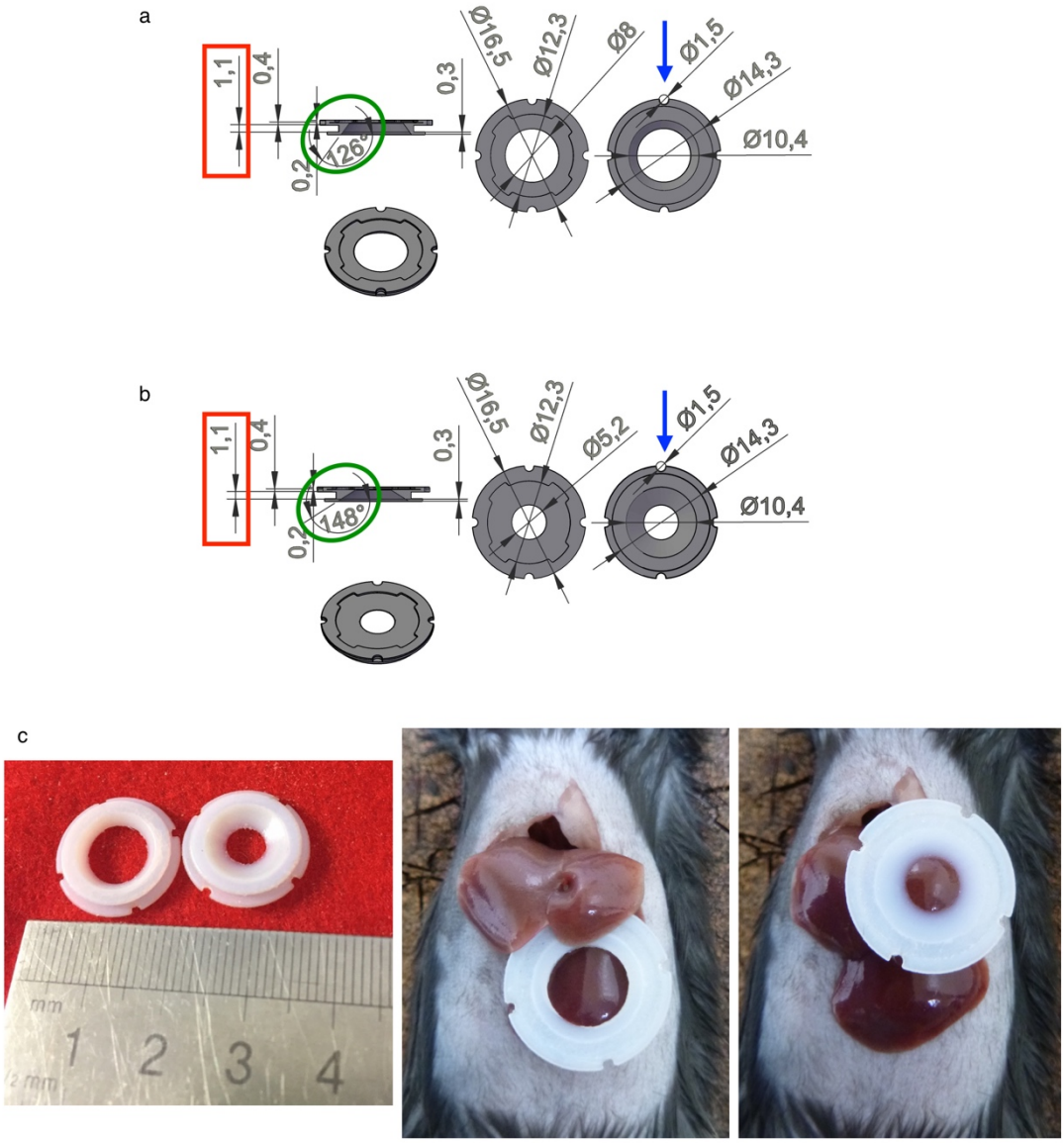

Figure 5 - 13 Modified AIW design.
Design of large aperture AIW (a) for standard implantation on left lobe and small aperture AIW (b) for implantation on left median lobe following partial hepatectomy. c) Plastic prototypes of the modified AIW design assessed in situ in a mouse cadaver. All length measurements in mm; ø, diameter.

Imaging baseplate modification

In order to accommodate the new AIW design, it was also necessary to re-design the baseplate into which the AIW sits to allow intravital microscopy to be performed. The original imaging baseplate had been manufactured to permit imaging of mammary tumours (Figure 5 - 14), so both the position of the imaging aperture and its simple, circular design were not optimised for the requirements of an AIW overlying the liver.

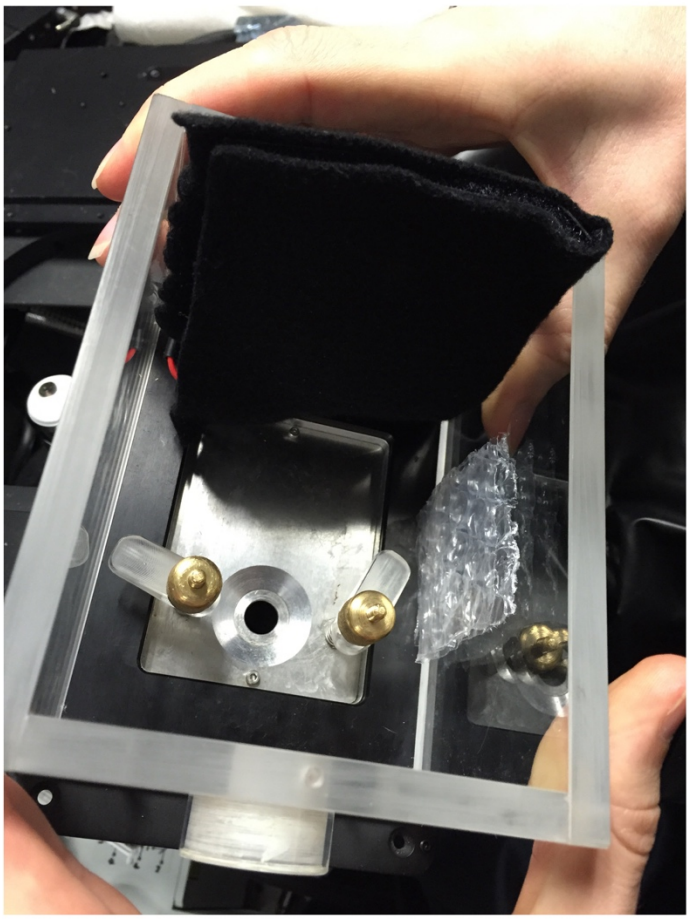

Figure 5 - 14 Imaging box including original baseplate.

The accompany figure (Figure 5 - 15) shows the new baseplate design with an enlarged, central aperture to accommodate the AIW whilst also allowing the anaesthetised mouse to lie centrally within the heated imaging box. The addition of four nubbins, which interlock with the grooves of the AIW, facilitates stabilisation of the AIW and ensures identical orientation is maintained throughout repeated imaging sessions.

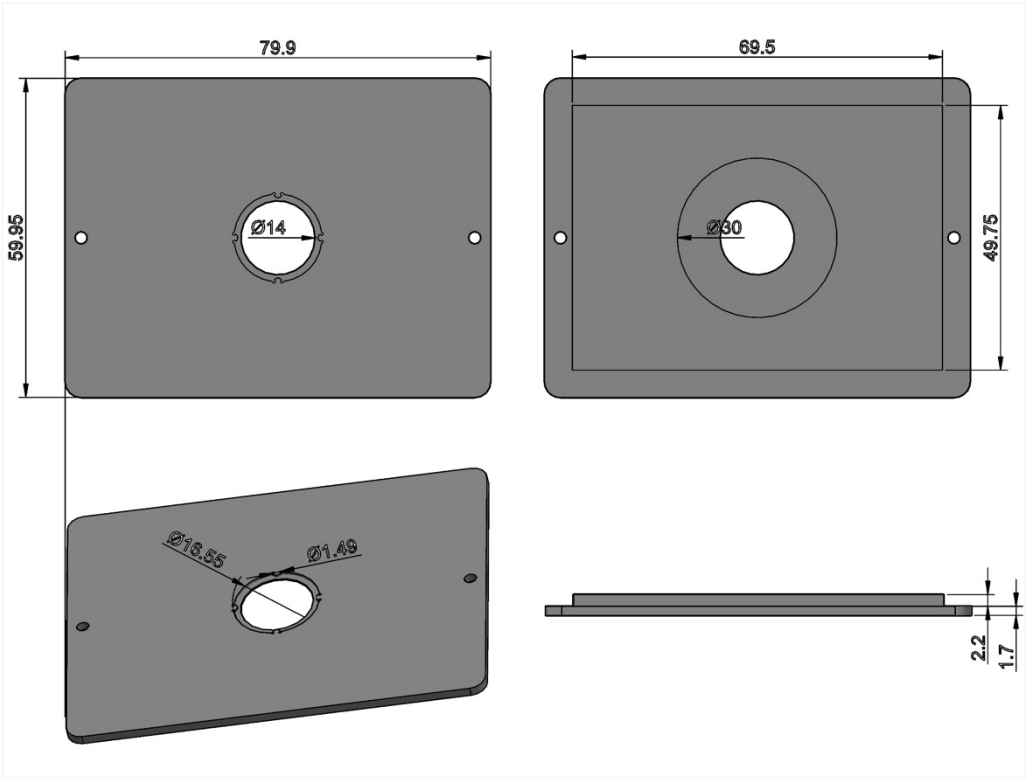

Figure 5 - 15 New imaging baseplate design.
All length measurements in mm; ø, diameter.

Further optimisations to the intravital imaging protocol

In parallel to the improvements made to the design of the AIW and imaging baseplate, changes to other aspects of the intravital imaging protocol were necessary to obtain high-quality, stable multiphoton images of the liver. Marked respiratory excursion is one reason why the liver may move during scan acquisition, even when the AIW is fitted correctly within the baseplate, and is easily recognised by its impact on the acquired image (Figure 5 - 16a). It was ascertained that this pattern of respiration was occurring due to mice being in a deep plane of anaesthesia. Previously, maintaining a deep plane of anaesthesia had been considered preferable, because it was thought that a lower respiratory rate would improve image quality. However, since there was no system for aligning image acquisition with the expiratory pause, whether a scan was completed during a period without respiratory excursion was entirely arbitrary. Conversely, during a light plane of anaesthesia, despite a relatively rapid respiratory rate (60-100 breaths per minute), the concomitant reduction in the degree of respiratory excursion meant that the liver was no longer displaced by respiration and therefore high-quality images could be acquired (Figure 5 - 16b). This required careful titration of anaesthetic depth, with isoflurane vaporiser settings routinely in the range 0.5-1%, despite the minimum alveolar anaesthetic concentration of isoflurane in the C57BL/6J reported to be

1.3%.[217] Such an example illustrates how simple, practical refinements in experimental technique can benefit both the experimental animal and the quality of the data obtained.

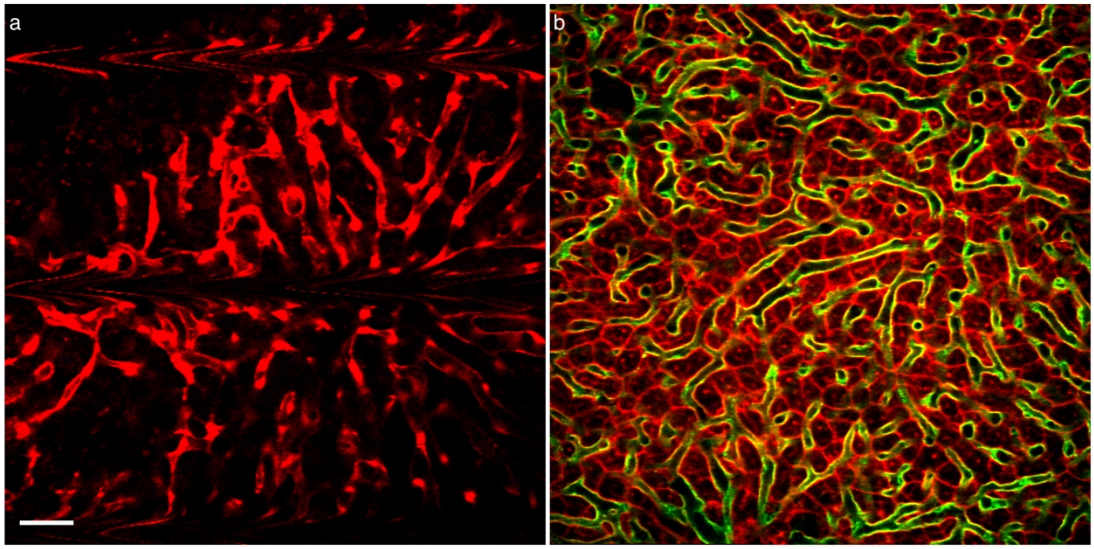

Figure 5 - 16 Respiratory movement can greatly affect image quality in intravital microscopy.
a) Marked respiratory artefact during intravital multiphoton microscopy of *Cdh5-Cre*;Ai14 mouse liver (Ai14, red, LSECs). b) In the absence of excessive respiratory movement, images from intravital multiphoton microscopy, such as this image of *Cdh5-Cre*;mTmG liver, are indistinguishable from those obtained ex vivo (eGFP, green, LSECs; tdTomato, red, all cell membranes). Scale bar 50μm.

Acetaminophen-induced liver injury in the context of intravital microscopy

The effects of anaesthesia on experimental models frequently risk being neglected, with anaesthesia often viewed as a benign means to an end, rather than an integral part of any experimental study. The effects of general anaesthesia have already been observed in this body of work in relation to the extended surgical time required to combine modified partial hepatectomy with AIW implantation, and also in the quality of images obtained during intravital microscopy. A further example in which factors relating to anaesthesia may have altered the experimental model was observed when acetaminophen-induced liver injury was combined with AIW implantation and, crucially, subsequent intravital imaging.

The standard protocol used to induce liver injury with acetaminophen (as described in Chapters II and III and recommended in the literature[114]) comprises administration of 300mg/kg acetaminophen intra-peritoneally, following a 12-hour fast to deplete liver glutathione levels. The work of Alexandra Thompson validated that prior implantation of the AIW did not alter the degree of injury (serum ALT), centrilobular necrosis, or inflammatory response (neutrophil infiltration) observed in response to acetaminophen.[214] However, when the same dose of acetaminophen was administered to mice with an implanted AIW at the end of baseline intravital imaging, which typically lasts 1-2 hours, we noted that the degree of

centrilobular injury appeared to be reduced, despite both the fast period and acetaminophen dose remaining unchanged. Measurement of serum ALT, albeit in a limited number of animals, also suggested that lower levels of injury than expected were occurring in most (Figure 5 - 17a). A number of possible explanations remained once issues with product, preparation or administration had been ruled out. Considered most likely was the possibility that pre-conditioning from the isoflurane anaesthetic, or other physiological response to prolonged anaesthesia, was causing the liver to become more resistant to the toxic effects of acetaminophen.

Teasing apart the precise reason for the observed effects, although of personal interest and scientific merit, was considered beyond the scope of the current body of work. Instead, small, empirical adjustments were made to the injury protocol: the fast was extended to 16 hours, the dose of acetaminophen administered was increased to 350mg/kg, and the saline volume in which the acetaminophen was administered was factored into the total peri-anaesthetic fluid calculations. This resulted in a consistent and expected level of liver injury, evidenced by visible and quantifiable centrilobular necrosis during intravital imaging and on histology at 24 hours post-injury (Figure 5 - 17b-e).

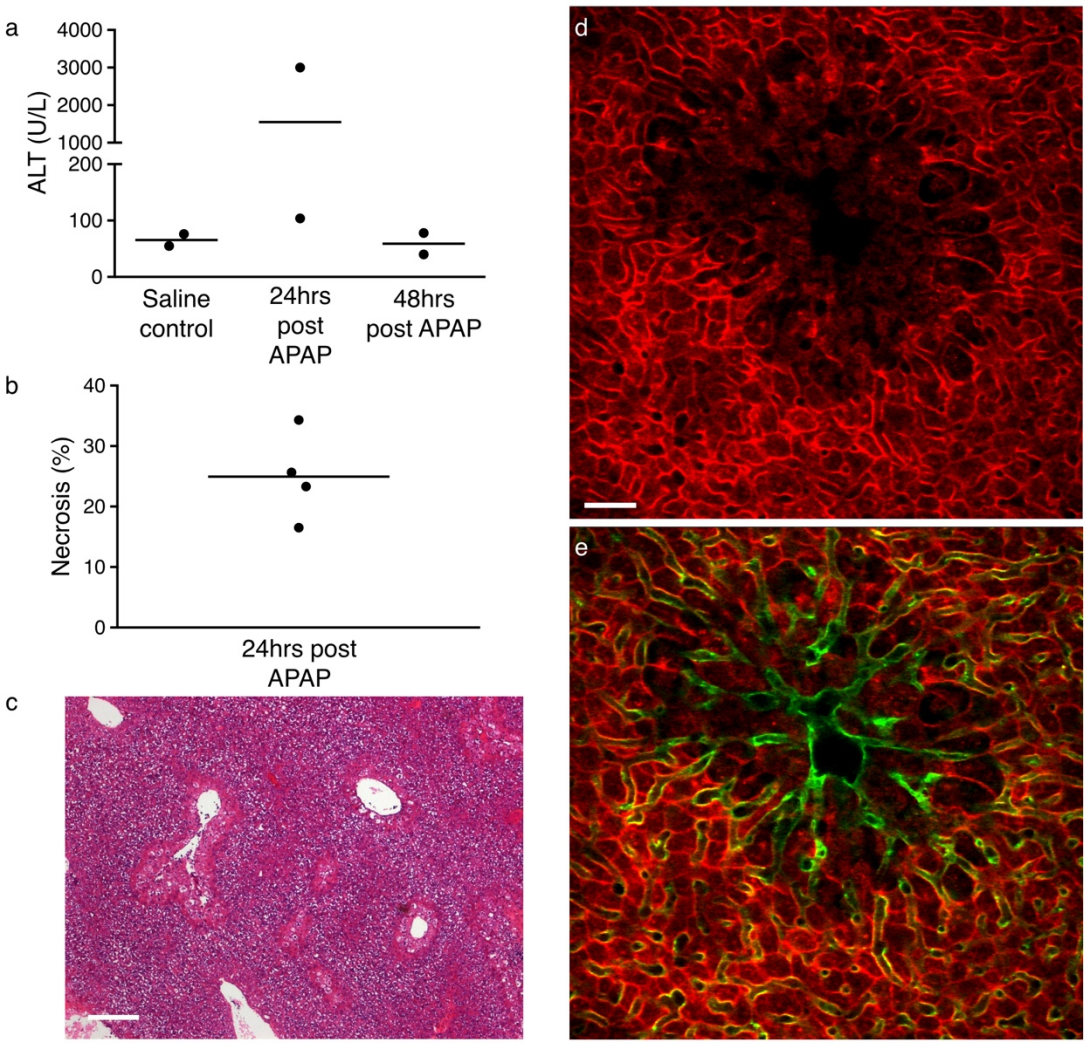

Figure 5 - 17 Intravital microscopy affects acetaminophen-induced liver injury.
a) The standard acetaminophen administration protocol (300mg/kg i.p. after 12-hour fast), leads to little or no liver injury in the majority of mice, as assessed by serum ALT. b) Administration of 350mg/kg acetaminophen after 16-hour fast leads to expected levels of hepatic necrosis in mice undergoing intravital imaging. c) Representative image, demonstrating acetaminophen-induced liver injury, following haematoxylin and eosin staining of liver harvested immediately after intravital microscopy at 24 hours post acetaminophen (higher dose). d,e) Appropriate hepatocyte injury is evident on intravital multiphoton microscopy at 24 hours after acetaminophen administration (higher dose) in *Cdh5-Cre*;mTmG mice (eGFP, green, LSECs; tdTomato, red, all cell membranes). APAP, acetaminophen. Scale bars 200μm (c), 50μm (d,e).

Discussion

The primary aim of this body of work was to develop the ability to visualise liver regeneration in vivo, at a cellular level, following partial hepatectomy in mice. The standard partial hepatectomy technique was successfully modified to facilitate AIW implantation. Not only was this combined procedure demonstrated to be technically feasible, but comparison with standard partial hepatectomy validated it as a viable model of liver regeneration. The amount of liver excised, and the degree of injury and percentage hepatocyte proliferation at 48 hours

post hepatectomy were not significantly different. Immunostaining of the HSC, Kupffer cell and neutrophil populations also did not reveal significant differences from a standard partial hepatectomy, although a small increase in Kupffer cell staining was noted when the AIW lobe was compared to a non-window lobe from the same mouse. Although liver to body weight ratio at seven days post hepatectomy was no different between groups, liver weight itself was, on average, 15% less in mice receiving modified partial hepatectomy with AIW implantation compared to standard partial hepatectomy, suggesting that the presence of the AIW may retard the return to baseline liver weight to some extent. As well as developing this new means through which to study liver regeneration in vivo, significant optimisations were made to facilitate the intravital imaging process itself. Both the AIW and imaging baseplate were redesigned to improve the quality of the multiphoton images that can be acquired. The surgical and imaging anaesthesia protocols were also improved, to the benefit of both experimental animal and data acquisition. Finally, further modifications were made to the second model of liver regeneration, acetaminophen-induced liver injury, to produce reliable injury following AIW implantation and intravital imaging. As such, two validated experimental models for the study of liver regeneration in vivo using multiphoton microscopy are now at the forefront of the toolkit available to the research community. They will enable us to further our understanding of this remarkable organ and hopefully to reveal new insights into the cellular processes and interactions that are necessary for successful liver regeneration to occur.

The partiality of hepatectomy in mice

It has previously been shown that removal of adequate liver mass is required to drive true liver regeneration, rather than merely inducing cellular hypertrophy.[112] This likely explains why a marked reduction in hepatocyte proliferation was observed following a reduced partial hepatectomy, sparing the left median lobe for AIW implantation. The data from this experiment also confirmed the strong association between weight of excised liver and subsequent hepatocyte proliferation index at 48 hours post hepatectomy. Excision of at least 0.5g of liver, or 2% of body weight, should be targeted in order to achieve a hepatocyte proliferation index of 15-20% at 48 hours. Weighing the excised liver at the time of partial hepatectomy should be mandatory, as it is both easy to do and offers an objective measure of the success of the procedure, potentially providing an explanation should insufficient regeneration subsequently be observed.

Having ruled out the option of simply sparing the left median lobe for AIW implantation, whilst excising the right median and left lobes as per a standard partial hepatectomy, the weights of each of the lobes in the C57BL/6J mouse were assessed in order to determine the most effective means of arriving at a degree of partial hepatectomy comparable to the standard procedure, whilst leaving an accessible lobe to facilitate placement of the AIW. The ideal lobe for AIW implantation is the left, for reasons of size, accessibility and distance from the motion artefact-inducing diaphragm. However, achieving an effective degree of hepatectomy without its excision is simply not feasible. Similarly, leaving the right median lobe would have challenging consequences, as it would necessitate excision of the relatively inaccessible cranial right lobe lying directly underneath it. Conversely, the caudal right lobe was confirmed to be approximately the same size as the left median lobe, enabling it to be substituted for the left median and thus become part of a modified partial hepatectomy procedure in which the right median, left and cranial right lobes are excised, leaving the left median lobe for AIW placement.

These investigations into liver lobe weights in the C57BL/6J mouse also challenged the long-held assumption that the standard partial hepatectomy procedure (removing both median lobes and the left lobe) leads to excision of two-thirds of liver mass (or even 70% as is sometimes stated). Although the measured lobe weights generally matched those recorded in other studies,[113,215] there were some small but important differences. In the study by Greene et al., the left median lobe contributed 15% of total liver weight in seven male C57BL/6J mice, in comparison to the figure of 10% reported above.[215] This allowed the authors to conclude that 68% hepatectomy could be achieved following a standard partial hepatectomy. Although from the same strain, the mice in that study were younger (7-8 weeks old) than those used here, both for assessment of liver lobe weight and for partial hepatectomy and AIW implantation (routinely males of 12-20 weeks). Hori et al. studied male mice from the C57BL/6NHsd strain.[113] In these mice, assessed at 10-20 weeks of age, the relative contributions of the median and left lobes (21% right median, 12% left median, 32% left) more closely matched those reported here (20% right median, 10% left median, 34% left). As such, in this study too, the contribution to total liver weight (65%) from the entire weights of these three lobes did not quite reach the target value of 67%.

Crucially, whilst the left lobe can, and should, be excised in its entirety by ligating at the hilus, it is not recommended to excise the two limbs of the median lobe in a similar fashion, for fear of causing stenosis of the suprahepatic vena cava.[111] In the first report of partial

hepatectomy in mice ('white mice of strain A'),[11] 65% hepatectomy was achieved through excision of the three lobes in their entirety. However, the number of adverse outcomes is not reported, and the authors did note focal necrosis and sinusoidal thrombi to be common, which suggests a degree of vascular compromise. If the recommendation of Mitchell and Willenbring is followed, the median lobe ligature(s) should be 'no closer than 2mm from the suprahepatic vena cava',[111] and therefore the maximum achievable partial hepatectomy may be no more than 55-60%. This is supported by a review of rodent models of partial hepatectomies, in which the difference between rat and mouse livers are highlighted.[118,218] Indeed, when partial hepatectomy was performed in cadavers, as described above, mean percentage hepatectomy was as low as 46%. Such a low figure is unlikely to arise purely from poor technique, given that the cadaveric nature of the surgeries meant that there were no additional challenges posed by respiratory movement, subconscious concerns about ligating lobes too proximally, or time pressure.

It could be argued that, even if the base of the lobe is not completely excised, and therefore does not contribute to the recorded weight of excised tissue, the process of ligation, with the resulting tissue trauma and localised stagnation of blood flow, renders any remnant liver tissue non-functional. However, this has not been demonstrated conclusively and, anecdotally, enlargement of liver tissue immediately proximal to the location of the ligating suture is observed, in addition to regeneration in those lobes that are not excised. The differences in lobar weights and degree of achievable hepatectomy may also derive from the manner in which liver weights are measured. Some may weigh only the lobar parenchyma after each lobe has been dissected individually, whereas in this work the entire liver weight, including hilus, was always used as the denominator for the calculations of percentage hepatectomy. This was considered to be the truest measure of total liver mass, unaffected by differences in dissection technique.

The overall goal of the 'two-thirds' partial hepatectomy model is to drive adequate liver regeneration for further study. As such, the precise amount of liver excised is of less importance than both the level of consistency within and across experiments, and the ability to drive an acceptable level of hepatocyte proliferation for further study. However, the possibility that the standard partial hepatectomy achieves less than the desired excision of two-thirds of liver mass, and the potential for variation between different strains or ages of mice, must be borne in mind, above all when attempting to compare findings when differences in surgical technique or strain are present. Recording and presenting the amount

of liver excised can act as a useful validation of any stated technique, particularly if whole liver and uninjured lobe weights from control mice are reported in conjunction.

The modified partial hepatectomy facilitates AIW implantation

Having proposed a modified technique which would be equivalent to standard partial hepatectomy, its practicality was first explored in a pilot experiment, which showed that sufficient liver (>2% body weight) could be excised in the majority of cases without obvious adverse effects. Cadaveric surgeries were then performed to confirm the exact sequence of modified partial hepatectomy with AIW implantation. Key features of this new procedure that should be emphasised are that it is easiest and quickest to excise the right median and left lobes via a mini-laparotomy excision, as for a standard partial hepatectomy, prior to extending the excision to excise the caudal right lobe. However, great care must be taken to keep the left median lobe moist and undamaged in preparation for later AIW implantation.

Excising the caudal right lobe is made much more straightforward through the use of mini-Gelpi retractors to keep the abdominal incision open, facilitating visualisation and lobe manipulation. However, care must be taken with the position of the retractor tips in the body wall, and it is also necessary to ensure that the weight of the retractor itself does not restrict respiration. Visualisation and access to the caudal right lobe is enhanced further by performing a duodenal manoeuvre and carefully exteriorising the intestines to the left-hand side of the mouse. Careful draping should be in place to maintain asepsis and the intestines should be placed onto, and covered by, a moistened swab.

Once the modified partial hepatectomy is complete, AIW implantation proceeds essentially as for a standard implantation. However, as well as paying particular attention to the placement of the purse string suture, and ensuring it is correctly seated within the groove of the AIW, it is usually necessary to close the caudal portion of the extended laparotomy incision separately. This is made easier by pre-placement of simple interrupted sutures in the muscle layer of the abdominal wall, prior to tightening of the purse string suture around the AIW.

Validating modified partial hepatectomy and AIW implantation

In the initial experiments in which the modified partial hepatectomy technique was combined with AIW implantation, several features were assessed to determine whether this novel procedure was broadly comparable to the standard partial hepatectomy model and therefore

provided an appropriate means through which to study the process of liver regeneration. Most importantly, the new technique was shown to drive appropriate levels of hepatocyte proliferation at 48 hours post surgery, as long as sufficient liver tissue is excised. More than 0.5g of liver was excised in the majority of cases (8/13) in the first validation experiment. This rose to all cases in the second experiment, suggesting that experience improves the amount of liver tissue that can be excised, which should ensure that appropriate hepatocyte proliferation occurs. Proliferation index did not change significantly between AIW and non-AIW lobes in the same mouse, except in one case in which a failure of appropriate regeneration in the AIW lobe was accompanied by compensatory proliferation in the non-window lobe. This suggests that the presence of the AIW itself has minimal, if any, effect on hepatocyte proliferation.

Immunostaining for HSCs, Kupffer cells and neutrophils suggested that no major changes in these populations occur following modified partial hepatectomy and AIW implantation. Partial hepatectomy is considered to be a relatively non-inflammatory model of liver regeneration, so it is reassuring that neither the slightly more invasive hepatectomy procedure nor the presence of the AIW triggers neutrophil infiltration. Immunostaining for Kupffer cells did reveal a slight increase in positive staining in the AIW lobe, when compared to a non-AIW lobe in the same mouse. A trend for difference between the same two lobes was also observed when modified partial hepatectomy was performed without AIW implantation. This suggests that the combination of increased handling and the presence of the AIW itself may promote a small increase (of <1% positive staining area) in number or size of Kupffer cells in the left median lobe. Such an increase is not particularly surprising, and its significance is uncertain. It could be explored further by, for example, flow cytometry phenotyping of Kupffer cells isolated from the AIW lobe compared with those isolated from a non-AIW lobe in the same mouse.

Measuring percentage positive staining provides a relatively crude assessment of cell populations, although it does permit detection of both changes in number and size of cells in the population under consideration. For example, the lack of detectable change in HSC staining does not preclude changes in activation status. Furthermore, immunostaining was only performed on tissue obtained at 48 hours after hepatectomy and AIW implantation, so the potential for more chronic changes in these populations was not assessed. Additional immunostaining at later time points and for cell-specific phenotypic markers, or flow cytometric analysis, could be employed to examine these aspects in more detail.

Serum biochemical analysis also revealed no major differences between standard and modified partial hepatectomy, with or without AIW implantation. This suggests that the degree of injury is comparable across the different procedures. Some increased variation in the assessed liver enzymes (ALP and ALT) was observed in the modified partial hepatectomy with AIW group. This likely reflects the increased tissue handling and reduced experience with this procedure. It would be expected that the degree of variation would reduce with increasing familiarity with the new technique.

The seven-day liver and body weights of mice receiving modified partial hepatectomy and AIW implantation revealed the greatest difference from standard partial hepatectomy of all the variables assessed, with both liver and body weights significantly decreased at this time point. A less pronounced effect was also observed with modified partial hepatectomy alone, suggesting that both the more invasive hepatectomy and the presence of the AIW contribute to the changes seen. The cause and relationship between these two findings is not entirely clear. It is possible that the more invasive nature of these procedures, and the longer duration of general anaesthesia, led to a catabolic state which was not sufficiently reversed in the post-operative period. As well as manifesting as weight loss, this alone could delay the return to baseline liver weight. Something as simple as post-operative ileus, secondary to increased handling of the gastrointestinal tract, could be sufficient to drive reduced food intake and resultant weight loss. Alternatively, based on the difference in harvest liver weights between the three surgical groups, one might conclude that it is the presence of the AIW that makes the greatest contribution to the observed difference, rather than the type of partial hepatectomy performed. This may be an unavoidable consequence of the AIW implant being adhered to the left median lobe, acting as a physical barrier to expansion of this lobe following partial hepatectomy. Alternatively, the presence of the implant may simply reduce mobility and therefore food intake. Because it is not possible to measure both starting liver weight and seven-day liver weight in the same mouse, it is also possible that the observed difference in seven-day harvest weight could be due to an underlying difference in starting liver weight. However, this is unlikely given that mean body weight at the time of surgery did not differ between groups. At this stage, it does appear that mice receiving modified partial hepatectomy and AIW implantation do experience a retardation in the later stage of liver regeneration, despite having similar hepatocyte proliferation at 48 hours post hepatectomy. If this occurred secondary to increased weight loss, this may well reduce, or disappear, if the

weight loss can be prevented by increased experience with the procedure and better post-operative management.

Several caveats should be applied to the results obtained from the validation experiments. Although allocation to procedure and the order in which procedures were performed were both randomised, it was not possible to blind to the surgery, or at the time of tissue harvest and weight measurement. Blinding was in place for all histological assessments. Proliferation index and immunostaining were assessed in sections cut through the entire lobe of interest. Samples were not embedded in a specific orientation, so it is possible that changes occurring only at the surface of the lobe on which the AIW was implanted were missed or masked by an assessment which included liver tissue further from the implantation site. However, the left median lobe itself is quite small, therefore there are not large amounts of tissue distant to the AIW. Other than more narrowly defined fixation, embedding and sectioning protocols, the best way to detect changes occurring at the site of AIW implantation is through intravital imaging and ex vivo multiphoton microscopy of the liver lobe surfaces. Additionally, the data presented here were collected from early attempts at the new technique, so not only was standard partial hepatectomy compared to a modified version (with or without AIW implantation), but a routinely performed technique was being compared with a novel one. In light of this alone, it would not have been surprising if greater differences had been observed between the various procedures. The increased variability sometimes observed in the groups receiving modified partial hepatectomy may not be inherent to the procedure itself, but related more to relative inexperience with the technique, in contrast to the standard partial hepatectomy procedure. Indeed, it is highly likely that, as familiarity and technical expertise improve, more consistent injury and hepatocyte proliferation will occur in mice receiving modified partial hepatectomy and AIW implantation, with a reduction in post-operative adverse effects, including weight loss. The key conclusion from the totality of the validation measurements is that liver injury and regeneration is definitely sufficient, using the modified hepatectomy technique, to permit study using intravital imaging via an AIW.

Surmounting the challenges of modified partial hepatectomy with AIW implantation

The development of a novel partial hepatectomy technique that permitted intravital injury posed a number of technical challenges, several of which have been enumerated already. Broadly, these can be considered to be peri-operative, post-operative, and related to the ability

to acquire high-quality microscopic images in an intravital setting. Many can be solved through close attention to the practicalities of the surgery and general anaesthesia.

To date, over 100 AIW implantations (with and without partial hepatectomy) have been performed. As with standard partial hepatectomy, the main adverse effects which may be observed during the modified partial hepatectomy procedure are: iatrogenic pneumothorax during dissection of the falciform and hepatophrenic ligaments, stenosis of the suprahepatic vena cava secondary to overly proximal placement of the right median lobe ligature, and haemorrhage. All are avoided by good surgical technique. In addition, trauma to the left median lobe, during excision of the underlying left lobe and subsequent AIW implantation, can lead to vascular compromise, necrosis and a failure of regeneration. Careful handling is essential. The most serious, and somewhat unpredictable, adverse effect relating to AIW implantation is displacement of the implant itself from the body wall and purse string suture. When this has occurred, it has predominantly arisen during the recovery period, allowing the rapid humane killing of the affected animal. However, this does not obviate the need to make every effort to ensure that the purse string and body wall are appropriately situated within the groove of the AIW, and the suture tightened sufficiently to reduce the risk of displacement as far as possible. Once an AIW has been implanted, experimental animals should be carefully examined at least twice daily. Any suspicion that the AIW is starting to evert or displace from the retaining suture should be immediately acted upon, since unnoticed AIW displacement will result in evisceration of the abdominal contents. Failure of the liver to adhere to the entire circumference of the AIW allows the possibility of omental or intestinal encroachment. On the few occasions that this has occurred, it has usually been benign, at most hindering ongoing imaging. However, in the case of entrapment, this can result in intestinal obstruction, so this possibility should be considered should a mouse become obtunded, inappetent or show reduced faecal output.

More minor, but more commonly noted, adverse effects associated with AIW implantation onto the liver include cavitation of the liver tissue within the aperture of the AIW, and the appearance of a biofilm on the liver surface. Neither appear to have any impact on animal welfare, but occurrence of either compromises successful intravital imaging. The cause of these superficial changes is not entirely clear, but likely relates to the presence of the AIW implant and glass coverslip. Measures aimed at minimising the incidence and degree of such changes include ensuring that the AIW is well-seated onto the liver surface, such that the liver almost protrudes up through the imaging aperture. This is facilitated by the bevelled

edges of the new AIW design. It is also recommended that the glass coverslips are coated with the biologically inert substance polyethylene glycol prior to use,[146] since glass itself is known to be relatively reactive and can promote an inflammatory response.

The longer period under general anaesthesia required to perform the modified partial hepatectomy procedure and AIW implantation initially resulted in severe adverse effects in a number of cases, necessitating humane killing of three experimental animals. However, the incidence of severe adverse effects attributable to general anaesthesia decreased to zero with the introduction of a number of small, practical changes, focused on maintaining physiological homeostasis as far as possible. Similarly, more careful titration of anaesthetic depth whilst performing intravital imaging led to a marked reduction in respiratory artefact in the acquired images, even without direct control of respiration through positive-pressure ventilation or the ability to link image acquisition to respiratory pattern. These examples illustrate how close attention to detail can make huge differences both to experimental animal welfare and, as a direct result, the data that can be acquired from such experiments. This was even the case in a setting where ideal peri-operative monitoring, including rectal temperature, oxygen saturation, heart and respiratory rate, was not available. The ability to monitor these additional parameters for the duration of anaesthesia would likely optimise consistency and animal welfare still further. Maintaining physiological homeostasis as far as possible also serves to minimise the potentially confounding effects of general anaesthesia. In the validation experiments comparing modified hepatectomy and AIW implantation with standard partial hepatectomy, the time under general anaesthesia was also significantly different between groups. Consideration was given to controlling for this by keeping the standard partial hepatectomy mice under anaesthesia and with their abdominal cavity open, to match the length of time required to perform the modified technique and AIW implantation. However, the goal of the validation experiments was to compare the novel technique with the standard procedure as it is usually performed. Adding an additional, fourth group (standard partial hepatectomy with extended anaesthesia) was considered, but deemed an unnecessary use of animals and resources.

Anaesthesia may protect the liver from acetaminophen toxicity

Repeated general anaesthesia may have resulted in a protective effect on acetaminophen-induced liver injury. It might have been expected that clinical signs and liver injury would worsen when the standard acetaminophen administration protocol was combined with an

abdominal surgery and repeated general anaesthesia for imaging. Paradoxically, although a single episode of general anaesthesia for AIW implantation did not alter the degree of injury seen following acetaminophen administration, as shown in the validation experiments performed by Alexandra Thompson,[214] the administration of acetaminophen at the end of a baseline imaging session led to reduced and inconsistent injury, as assessed by serum ALT and intravital imaging. More than one possible explanation may be posited. Reduced core body temperature, as is likely to be present at the end of 60-120 minutes of general anaesthesia, may alter the pharmacodynamics of acetaminophen absorption, delivery to the liver, and subsequent metabolism in such a way that minimises hepatocyte injury. Similarly, the provision of 100% oxygen in the period prior to acetaminophen administration might pre-condition the liver to limit acetaminophen's toxic effects.

Alternatively, the volatile anaesthetic isoflurane may itself alter metabolic pathways within the liver to protect it from acetaminophen-induced injury. A possible interaction between isoflurane and acetaminophen does not appear to have been studied directly. However, almost thirty years ago, sub-anaesthetic concentrations of isoflurane were shown to have a protective effect on liver damage in rats when co-administered with carbon tetrachloride.[219] Isoflurane has also been demonstrated to protect hepatocytes from hypoxia-reperfusion injury in isolated, perfused rat liver.[220] Acetaminophen is converted to its toxic metabolite NAPQI by the cytochrome P450 isoform CYP2E1.[114] This same isoform has been shown to be responsible for a significant proportion of isoflurane metabolism in human liver,[221] so it is possible that isoflurane competes with acetaminophen and limits the accumulation of toxic metabolites. Several studies have also shown that isoflurane induces hepatocyte expression of the hepato-protective enzyme heme oxygenase 1.[222-224] Alternatively, an explanation for the reduction in ALT and visible liver injury may be revealed by studies on the range of effects that isoflurane can have on gene expression, including expression of drug-metabolising enzymes.[225-227] Of particular note, pathway analysis of genes upregulated by isoflurane anaesthesia, detected by microarray of rat liver, suggested a link to glutathione metabolism, the precise pathway responsible for detoxification of acetaminophen metabolites.[227]

Whatever the underlying mechanism, the challenge posed by the decreased response to acetaminophen of mice receiving multiple episodes of isoflurane anaesthesia was the inability to achieve sufficient, repeatable levels of liver injury to allow subsequent study of the regenerative process. This was surmounted in the short term by increasing the length of fast

prior to acetaminophen administration and a small increase in the dose of acetaminophen administered. A similar effect has not been noted with partial hepatectomy and repeated intravital imaging, perhaps because in this model the injury occurs during the first general anaesthetic, at the time of AIW implantation. However, since the modified partial hepatectomy with AIW validation experiments were performed without subsequent imaging sessions, the possibility that these have an effect on the regenerative time course post hepatectomy should be borne in mind.

The modification to the standard acetaminophen protocol can be viewed in the same light as the changes to partial hepatectomy that were made to permit AIW implantation. The aim of both these models is to cause liver injury and stimulate regeneration which can then be studied through an intravital approach. A level of fidelity to previous animal models is desirable so that any findings can be compared and validated, but exact recapitulation of the injury models in an intravital setting is unnecessary. The original animal models themselves only broadly replicate the clinical courses they are aimed at modelling, but they must not become so far removed as to lose all translational relevance. However, further exploration of the interesting phenomenon that repeated anaesthesia appears to protect from acetaminophen-induced liver injury should be considered, given the existing body of evidence showing protective effects in other forms of liver injury, and the tantalising possibility that a previously unknown and clinically employable hepato-protective mechanism may underlie the reduced injury response observed.

Intelligent design

Re-designing the AIW and baseplate in conjunction was undertaken with the aim of improving intravital image quality and the reliability with which useable images could be obtained. The primary goals were to minimise the distance between liver and coverslip, and assist with immobilisation of the AIW, and by extension the liver, during imaging. It was also necessary to produce an AIW with a smaller aperture, to fit onto the left median lobe following partial hepatectomy.

The AIW improvements detailed above certainly assist in minimising the distance between liver and coverslip, although the narrower AIW groove and enlarged outer circumference do make seating the implant within the body wall more challenging. Also, the underlying principle of the current design, with the coverslip adherent to the upper surface of the removable inlay, whilst facilitating coverslip replacement, continues to make perfect

apposition of liver and coverslip challenging. The presence of dead space appears to encourage the formation of a biofilm, which limits the depth of imaging and can be challenging to remove. The ever-present coverslip, even when coated with polyethylene glycol, no doubt also alters the local environment of the liver lobe. No longer does it sit inside of the body wall, bathed in peritoneal fluid. Rather, it is separated from the ambient temperature of the outside world by 170μm of glass. The medium- and long-term effects on cellular health and function remain uncertain. To minimise any such adverse effects, consideration could be given to a more protected design. For example, a more insulated seal could be screwed into the implant, in place of the removable inlay, with a fresh inlay and coverslip substituted for each imaging session.

Alongside the improvements in AIW design, the imaging baseplate modifications have improved image acquisition by reducing respiratory-related movement of the AIW. The new, central location of the imaging aperture also allows the mouse to be placed in a more comfortable, neutral position. However, the present design of the AIW recess, although preventing movement in two planes, does not immobilise the AIW completely, so a degree of movement in the z plane can sometimes occur. Ideally, a baseplate would be designed to allow simple yet total immobilisation of the AIW during imaging. Others have attempted to achieve this with quite complex, interlocking designs, the downsides of which are the time and skill required to fix them in place, along with the inability to rapidly release the AIW should this be required for reasons of mouse welfare.[147] One elegant approach would be to incorporate an electromagnet into the plate design, which could allow instant immobilisation of the AIW. However, this would also require that the AIW was manufactured from a more strongly ferromagnetic metal, as opposed to the current titanium.

Summary

This chapter describes how the traditional standard partial hepatectomy technique was successfully modified to permit AIW implantation. Thus, it is now possible to image liver regeneration following partial hepatectomy with cellular resolution, in vivo, at multiple time points during the regenerative process. A number of readouts were assessed to demonstrate that this new procedure does indeed cause an appropriate level of injury and drive subsequent hepatocyte proliferation in a comparable fashion to that which occurs in the standard partial hepatectomy model. However, a retardation of the return to normal liver weight was observed

at seven days. Although this difference from the standard model may reduce as experience with the new procedure increases, it should be borne in mind when studying the later phase of liver regeneration. In addition to developing a new model of liver regeneration for compatibility with intravital imaging, multiple optimisations were made to the design of the AIW itself, the imaging baseplate, and the procedural elements relating to implantation and subsequent imaging. This led to improvements in both image quality and experimental animal welfare. The developments described in this chapter lay the groundwork for novel insights into the cellular processes underpinning liver regeneration following partial hepatectomy or acetaminophen-induced liver injury in mice. The following chapter describes how fluorescent reporter mice, exogenous labelling techniques, and label-free imaging using multiphoton microscopy, can be combined with these injury models to study liver vasculature, sinusoidal blood flow, lipid deposition, non-parenchymal cell populations, and the regenerating hepatocyte. Thus, it is possible to study the dynamic changes that occur in vivo, in the same experimental animal, during the time course of liver regeneration.

Chapter 6 – Intravital microscopy of the regenerating liver

Introduction

The combination of implantation of an AIW onto the surface of the liver with multiphoton microscopy provides a powerful tool with which to study cellular physiology in the liver, both during normal homeostasis and following injury. The previous chapter described the development and validation of a murine model to permit intravital microscopy of liver regeneration following partial hepatectomy. The implantation of the AIW at the time of injury subsequently allows multiple imaging sessions to be performed, such that the time course of regeneration can be tracked in the same experimental animal. The ability to perform partial hepatectomy and AIW implantation complements the AIW insertion and acetaminophen-induced liver injury model previously developed and validated by colleagues within the Henderson group.[214] Thus, in addition to using AIW implantation alone to study the uninjured murine liver, these two novel injury and imaging models (outlined schematically in Figure 6 - 1) provide enormous opportunity to study many aspects of the cellular and physiological response to liver injury, and improve our understanding of the hepatocyte proliferation and liver regeneration that follow.

Implantation of the AIW renders intravital multiphoton microscopy technically feasible, by bringing the liver into contact with a glass coverslip through which light can pass unhindered whilst the abdominal cavity remains sealed. However, as well as the ability to deliver photons directly into the liver tissue, consideration must be given to the readouts that can be obtained using this technique. A key benefit from performing multiphoton microscopy in the mouse is the wide range of options through which to label fluorescently those cells comprising, or entering into, the liver. As outlined in Chapter One, this can be achieved through transgenic approaches, targeting fluorophore expression to one or more cell types of interest. One common approach is to harness the Cre-lox system, to switch on expression of a fluorescent reporter protein in the cell type of interest. The flexibility of this system means that different 'Cre driver' alleles, expressing Cre recombinase under the control of a cell type-specific promoter, can be combined with any one of a range of fluorescent reporter alleles. Expression of Cre recombinase in the cell type of interest leads to a recombination event which

results in ongoing expression of the fluorescent protein in both the cells in which recombination occurs and any daughter cells.

An alternative transgenic labelling approach is to link the fluorescent reporter protein directly to a cell type-specific promoter, using a promoter sequence for a gene that is primarily or exclusively expressed in the cell of interest. Whenever this gene is expressed, the 'knock-in' fluorescent reporter gene is also transcribed. These differing transgenic labelling approaches can be combined, through use of different reporter proteins, to result in labelling of more than one cell type in the same experimental animal. Furthermore, fluorophores conjugated to antibodies, or specific dyes (such as those binding DNA), can be administered topically or systemically to label cells or structures of interest. Readouts from fluorescent labelling can also be combined with the previously introduced 'label-free' techniques, such as SHG and CARS. Importantly, it is often possible to acquire multiple readouts simultaneously or in rapid succession, which is a clear advantage in an intravital context. The transgenic toolkit currently available to our research group to permit imaging of the multiple facets of liver regeneration is summarised in Table 6 - 1.

Overall, the opportunities afforded by intravital multiphoton microscopy are vast and constantly evolving, in relation to the cells, structures and processes which can be imaged. This chapter attempts to demonstrate the breadth of opportunity this technique offers to the study of liver regeneration, with examples of the types of images that can be obtained and the quantitative analysis that may be performed.

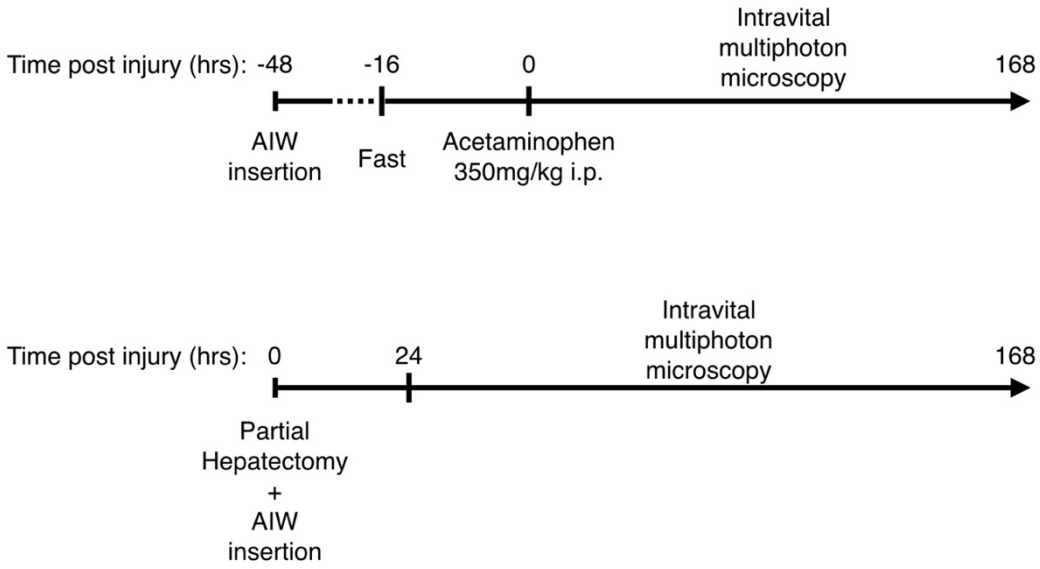

Figure 6 - 1 Experimental models for intravital imaging of liver injury and regeneration.
Model 1 (upper): the AIW is implanted two days before acetaminophen-induced liver injury. Intravital imaging is performed immediately prior to acetaminophen administration and then may be repeated, at intervals, until seven days post injury. i.p., intra-peritoneal. Model 2 (lower): Partial hepatectomy and AIW implantation are performed at the same surgery. Intravital imaging of regeneration may be performed repeatedly from 24 hours to seven days post injury.

Table 6 - 1 A transgenic toolkit for intravital multiphoton microscopy of liver injury and regeneration

Allele	Description	Use	Comments	Reference(s)
Ai14	Fluorescent reporter	Cre-mediated expression of cytosolic tdTomato		Madisen 2010[160]
Alb-Cre	Cre driver	Cell-specific expression of Cre recombinase in hepatocytes	May also target a proportion of cholangiocytes	Postic 1999[157]
CAG-Cre	Cre driver	Germline expression of Cre recombinase	Used to drive efficient recombination of the Fucci reporter allele	Sakai 1997[228]
Cdh5-Cre	Cre driver	Cell-specific expression of Cre recombinase in LSECs	Induced by tamoxifen administration	Wang 2010[159]
Confetti	Fluorescent reporter	Stochastic, Cre-mediated expression of mCerulean, green, red or yellow fluorescent protein	Can be utilised to visualise clonal expansion, or for fate-mapping when linked to an inducible Cre driver	Snippert 2010,[162] Tarlow 2014[229]
Fucci	Fluorescent reporter	Cell cycle labelling. Cre-mediated expression of nuclear mCherry (dominant in G1) and mVenus (dominant in S/M/G2)		Mort 2014[164]
MacGreen	Fluorescent reporter	Constitutive expression of eGFP in *Csf1r*-expressing cells	Originally reported as a macrophage label, but also labels neutrophils and dendritic cells	Sasmono 2003,[163] MacDonald 2005,[230] Sasmono 2007[231]
mTmG	Fluorescent reporter	Constitutive expression of membrane-targeted tdTomato, Cre-mediated expression of membrane-targeted eGFP		Muzumdar 2007[161]
PBAG	Fluorescent reporter	Constitutive expression of eGFP in *Pdgfrb*-expressing cells	Labels HSCs	Henderson 2013[29]

Results

Intravital microscopy of Fucci transgenic mice permits visualisation of the hepatic regenerative niche

The Fucci reporter mouse

Fluorescent labelling of specific cell populations is widely used to facilitate visualisation and map cell fate. However, in order to study liver regeneration, and specifically the hepatocyte proliferation that underpins it, the ability to identify cycling cells is essential. Ex vivo studies have suggested a zonal pattern to the hepatic regenerative response,[180] but the precise combination of local factors that combine to drive proliferation in any particular hepatocyte has yet to be fully elucidated. The concept of the hepatic regenerative niche, a localised region within the lobular anatomy of the liver, is an attractive one, since it might allow identification and characterisation of a subset of hepatocytes predisposed to proliferate in response to liver injury. Equally plausible is the possibility that all hepatocytes are created equal and it is changes in the cellular environment, be that from secreted factors, variations in sinusoidal blood flow, altered extracellular matrix stiffness, or interaction with non-parenchymal or inflammatory cells, that drive the hepatocyte to begin cycling.

The ability to assess cell cycle stage in hepatocytes, in vivo, would assist greatly with attempts to understand the local factors driving hepatocyte proliferation. We therefore obtained an R26Fucci2aR (Fucci) reporter mouse that was recently generated by colleagues at the University of Edinburgh.[164] Following Cre-mediated recombination, nuclear accumulation of the mCherry fluorescent reporter protein occurs whilst the cell is in the G1 stage of the cell cycle. This transitions to predomination of the mVenus fluorescent reporter protein as the cell enters S-phase, and persists through G2 and M phases, disappearing immediately prior to cytokinesis. The G1/S transition is identified by co-localisation of both proteins within the same nucleus (Figure 6 - 2a).

An initial attempt to drive reporter expression, by generating mice carrying both the hepatocyte-targeting *Alb-Cre* and R26Fucci2aR alleles, did not lead to widespread labelling of nuclei (data not shown). However, excellent nuclear labelling was seen in the liver following a breeding strategy which led to constitutive, germline expression of the *Fucci2a* construct (Figure 6 - 2b). Briefly, mice carrying the R26Fucci2aR allele were interbred with mice carrying the *CAG-Cre* allele. This germline Cre drives recombination at the zygote stage, with a permanent, heritable excision of the floxed STOP codon which would previously have

prevented reporter protein expression. As such, subsequent generations continue to express the Fucci2a proteins constitutively without the requirement for further Cre-mediated recombination.

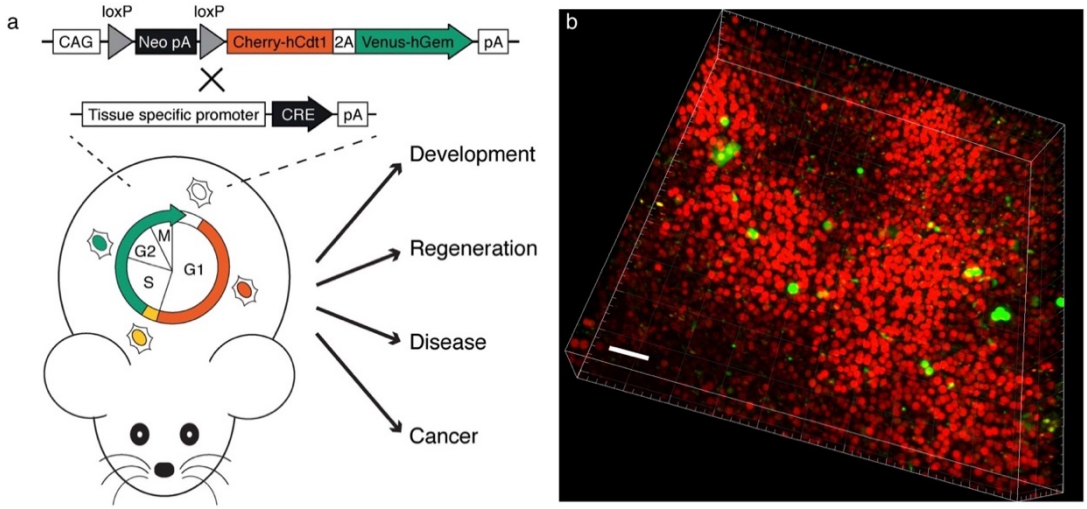

Figure 6 - 2 The Fucci reporter mouse allows fluorescent labelling of cycling hepatocytes in vivo. a) Schematic showing the R26Fucci2aR construct and how nuclear labelling changes through the cell cycle. Reprinted from Cell Cycle,[232] ©2015, with permission from Taylor & Francis. b) Constitutive expression of the Fucci2a construct results in widespread labelling of hepatocyte nuclei with mCherry (red, G1) and/or mVenus (green, S/G2/M). The image shown is a three-dimensional reconstruction of a z-stack obtained by multiphoton microscopy of freshly harvested, whole liver from a *CAG-Cre*;Fucci mouse, 48 hours after acetaminophen administration. Scale bar 50μm.

Intravital visualisation of the cell cycle following partial hepatectomy

Partial hepatectomy and AIW implantation were performed in mice carrying the recombined R26Fucci2aR allele. Intravital microscopy was performed at 24, 48 and 72 hours post partial hepatectomy, with imaging at 96 hours performed on liver in a dish immediately after culling. This revealed the expected peak in hepatocyte cycling around 48 hours, with a gradual decrease in the number of mVenus-positive nuclei thereafter (Figure 6 - 3).

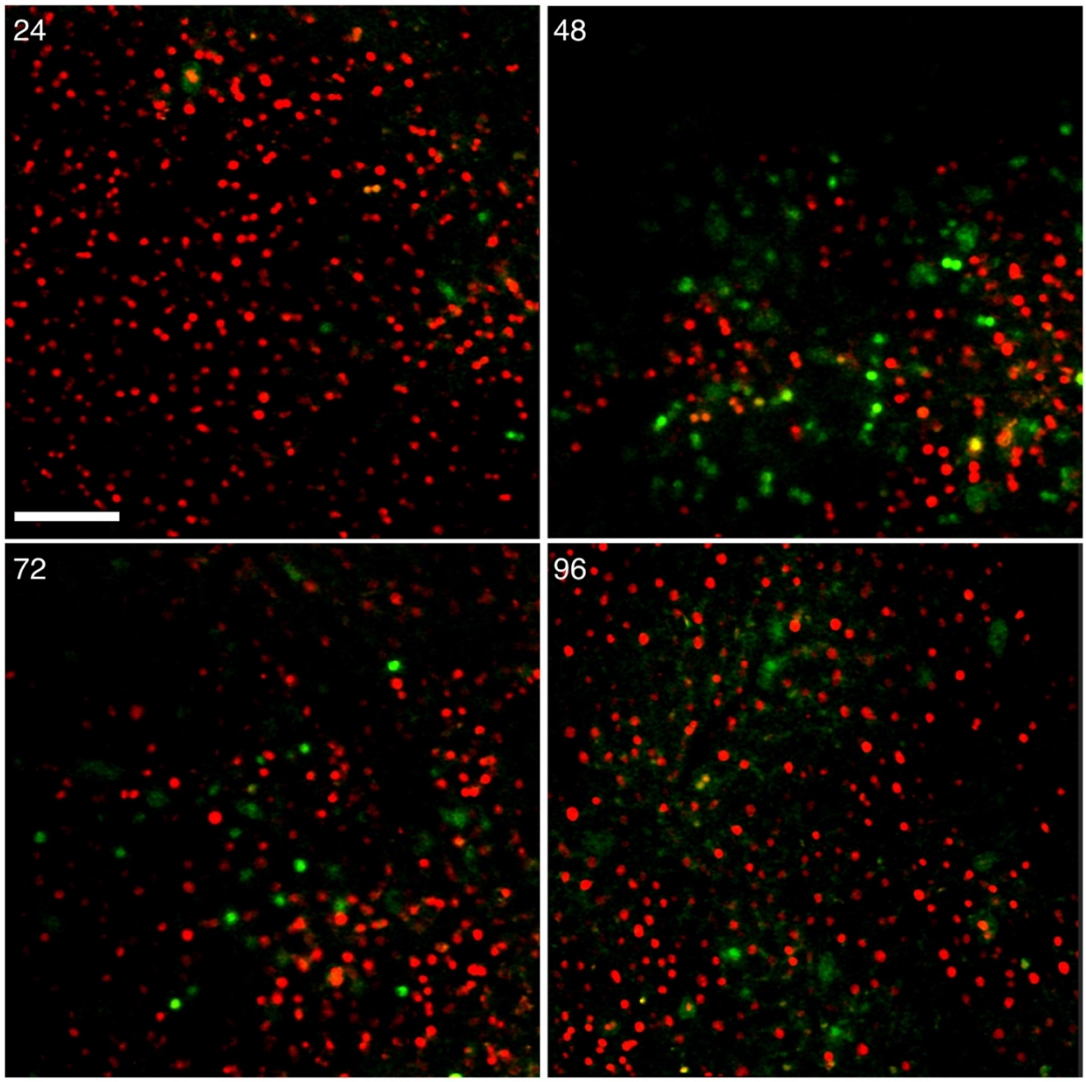

Figure 6 - 3 The Fucci reporter allele allows repeated assessment of hepatocyte cell cycle state using intravital imaging following partial hepatectomy.
Intravital multiphoton microscopy of the same *CAG-Cre*;Fucci mouse at 24, 48 and 72 hours following partial hepatectomy, and of freshly harvested, whole liver at 96 hours, demonstrates the peak in cycling hepatocytes that occurs around 48 hours after partial hepatectomy. mCherry, red (G1); mVenus, green (S/G2/M). Scale bar 100μm.

This study marked the first occasion on which hepatocytes were directly observed undergoing proliferation during liver regeneration, repeatedly, in the same mouse. Although an important step forward, the Fucci reporter alone provides limited information, since fluorescent labelling is restricted to the nucleus. Some morphological information can be gleaned through acquisition of the CARS signal (Figure 6 - 4a). However, the depth penetration for CARS is generally lower than that for detection of fluorescent reporters. Furthermore, the increase in hepatocyte lipid in the immediate aftermath of partial hepatectomy results in such a strong CARS signal that it is challenging to obtain good morphological detail as well (Figure 6 - 4b). Further, the design of the multiphoton microscope used for this work necessitated the manual

substitution of mirrors and re-tuning of the pump laser between Fucci and CARS acquisition. Therefore, Fucci reporter mice were interbred with mice carrying the *Cdh5-Cre* and mTmG alleles. This produced a triple transgenic mouse with the Fucci cell cycle label, fluorescent labelling of all cell membranes (membrane-targeted tdTomato), and the option to induce membrane-targeted eGFP labelling of LSECs through prior administration of tamoxifen (Figure 6 - 4c,d).

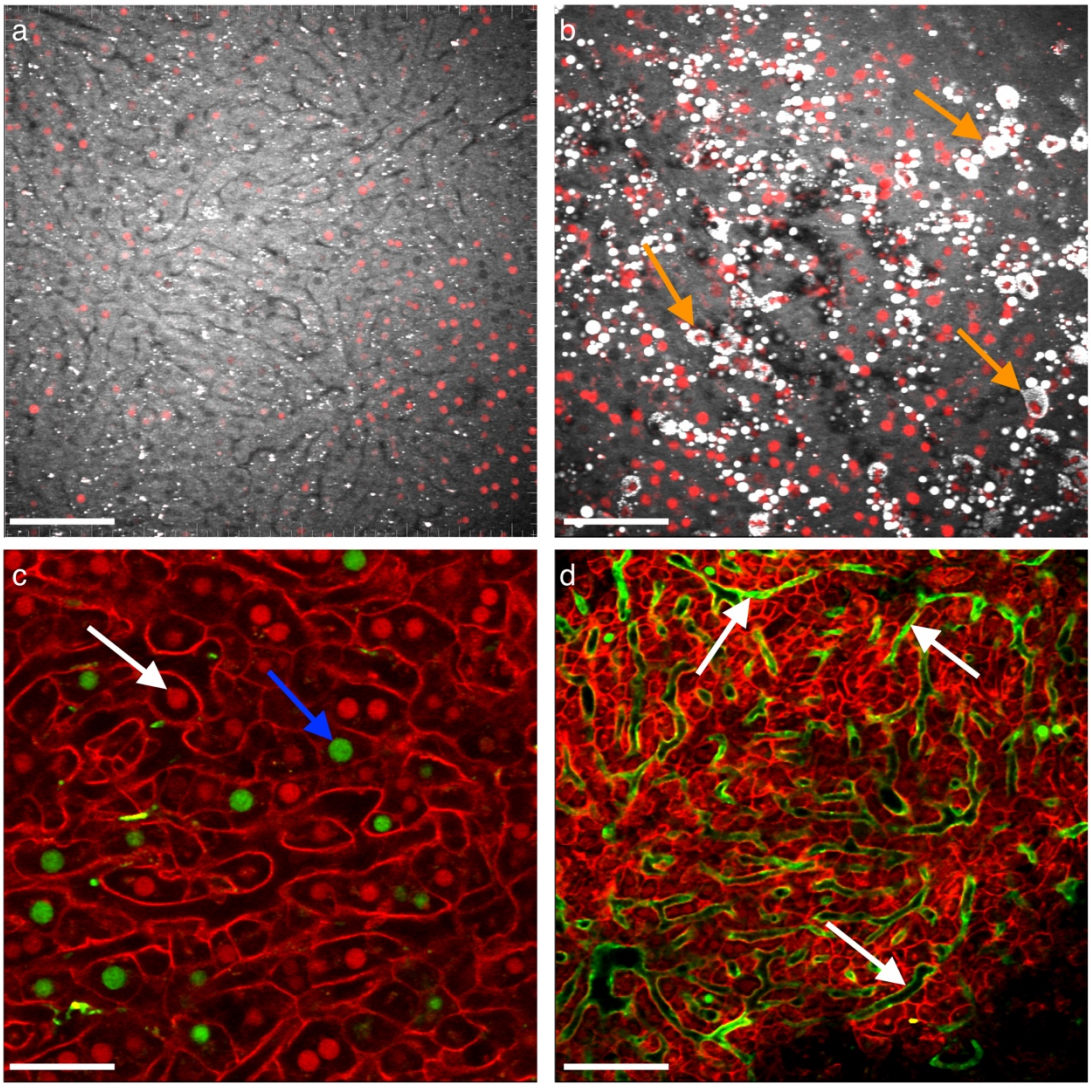

Figure 6 - 4 Combining the Fucci cell cycle label with visualisation of hepatic morphology.
a) The CARS signal allows visualisation of hepatocyte and sinusoidal morphology in combination with nuclear cell cycle label (CARS, grey; Fucci-mCherry, red). However, following partial hepatectomy (b), the CARS signal becomes dominated by the accumulation of hepatocyte lipid (orange arrows). Images obtained from freshly harvested, whole liver, either uninjured (a) or 96 hours post partial hepatectomy (b). (c) Combining Fucci and mTmG alleles allows concurrent visualisation of hepatocyte cell cycle stage (mCherry, red, G1, white arrow; mVenus, green, S/G2/M, blue arrow) and hepatocyte morphology (tdTomato, red, all cell membranes). Intravital multiphoton microscopy at 48 hours after acetaminophen. d) Tamoxifen administration in the Fucci;*Cdh5-Cre*;mTmG mouse leads to cellular and nuclear labelling as described in (c), with additional labelling of LSECs (membranous eGFP, green, white arrows). Intravital multiphoton microscopy of uninjured liver. Scale bars 100μm (a,b,d) or 50μm (c).

Intravital imaging of the hepatic regenerative niche following acetaminophen-induced liver injury

The combination of the mTmG and Fucci alleles is particularly useful for intravital microscopy following acetaminophen administration, since labelling of the hepatocyte cell membrane makes it much easier to identify areas of centrilobular injury and relate these to cycling hepatocytes (Figure 6 - 5). As predicted, and previously observed in BrdU immunohistochemistry of liver, the mVenus-positive, cycling hepatocytes appear to cluster on the periphery of the injured zone.

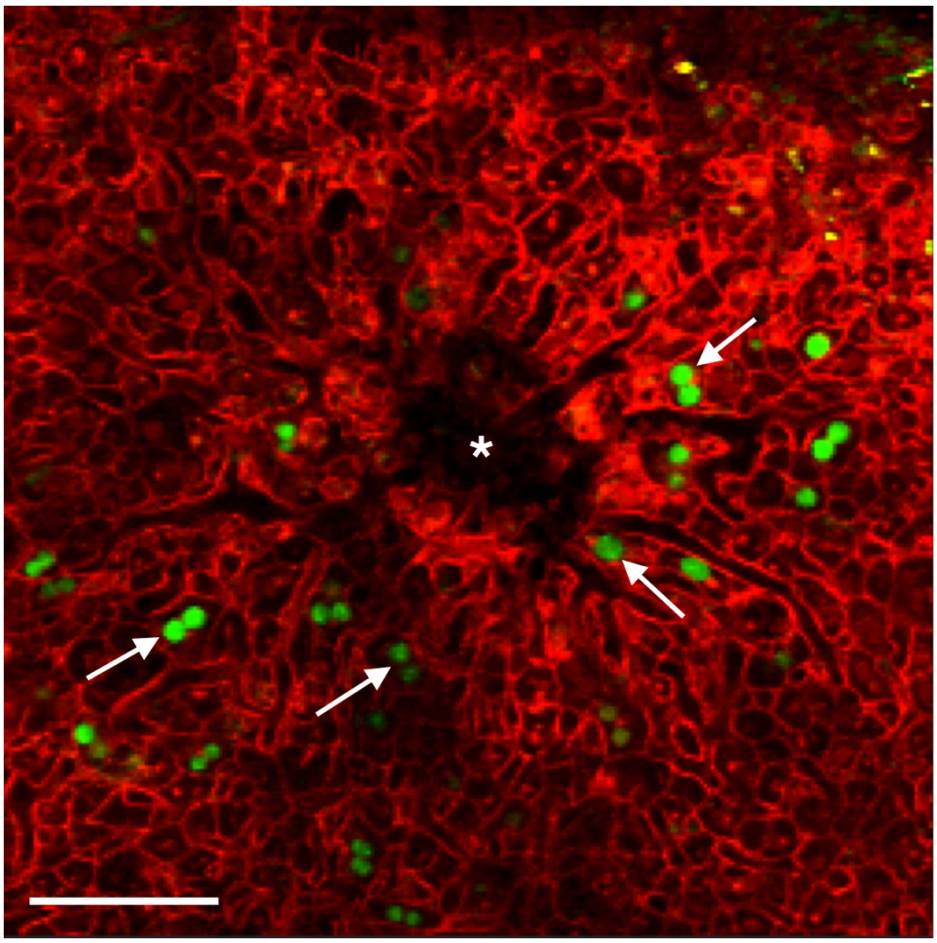

Figure 6 - 5 The Fucci;mTmG reporter mouse allows intravital imaging of hepatocyte injury and cell cycle state following acetaminophen-induced liver injury.
Co-expression of fluorescent nuclear cell cycle (mCherry, red, G1; mVenus, green, S/G2/M) and cell membrane (tdTomato, red) labels facilitates visualisation of centrilobular injury (white asterisk) with surrounding hepatocyte proliferation (white arrows). Image obtained by intravital multiphoton microscopy at 48 hours after acetaminophen. Scale bar 100μm.

Visualising hepatocyte division in vivo

The concentration of cycling hepatocytes around the centrilobular injury in acetaminophen-induced liver injury lent themselves to an attempt to visualise hepatocyte division in vivo. The University of Edinburgh local regulations for imaging of experimental animals permit a

maximum of six hours of imaging under terminal anaesthesia. As such, AIW implantation was performed and followed by baseline intravital imaging and administration of acetaminophen. A mouse with good quality baseline images was then anaesthetised at 42 hours post acetaminophen to allow imaging to be performed around the time of peak hepatocyte proliferation. An area containing several mVenus-positive nuclei was selected and short stacks through this area were obtained every 10 minutes (Figure 6 - 6).

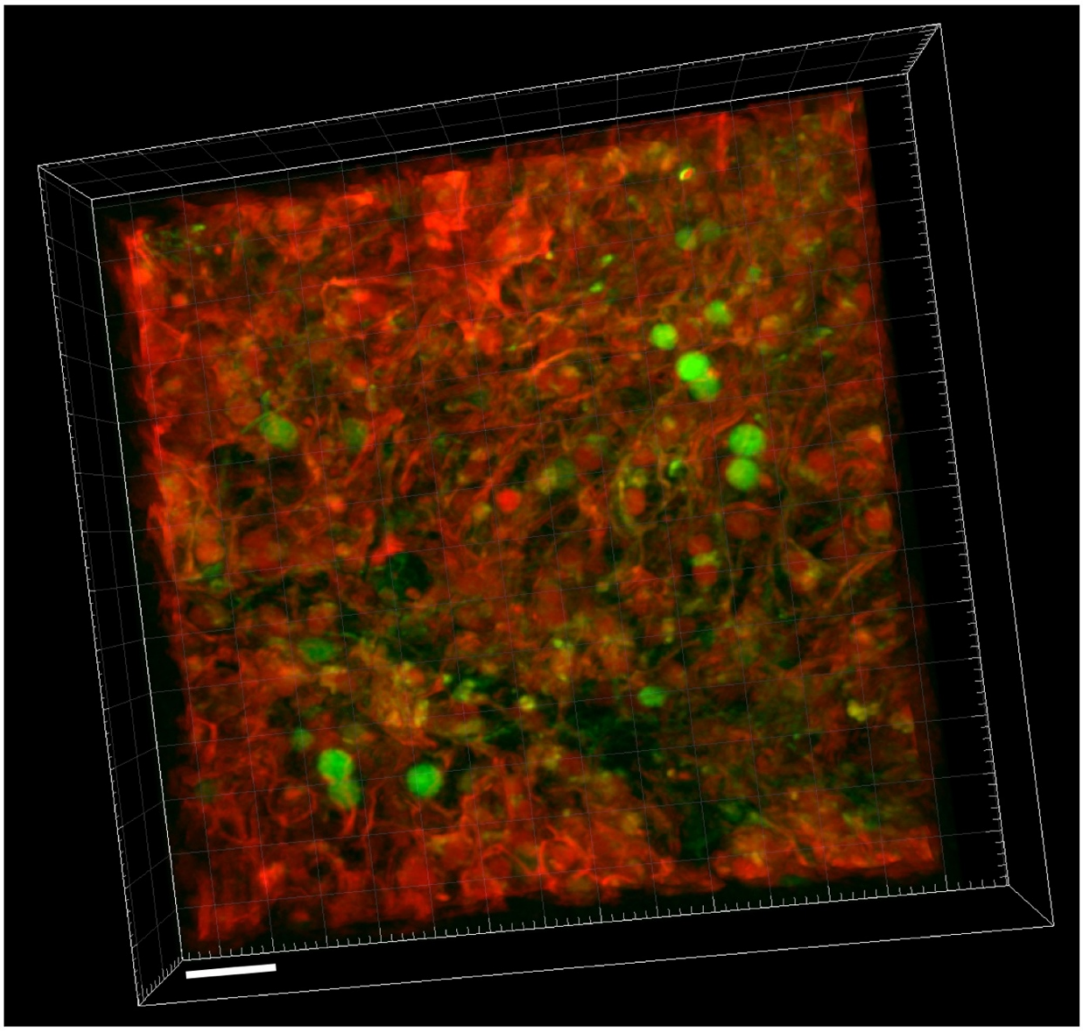

Figure 6 - 6 Timelapse intravital imaging of injured liver tissue with actively cycling hepatocytes. Intravital multiphoton microscopy in a Fucci;mTmG mouse, beginning at 42 hours after administration of acetaminophen. Z-stacks of a 200x200x28μm volume were obtained every 10 minutes. This representative three-dimensional projection shows a swathe of injured hepatocytes with loss of the membrane tdTomato signal (red). Prominent, actively cycling hepatocyte nuclei (mVenus, green, S/G2/M) surround this. mCherry (red) nuclei indicate cells in G1. Scale bar 30μm.

On the image series obtained, it is clearly possible to see the imaged hepatocytes progressing through the cell cycle (Figure 6 - 7). Initially, specks of mVenus fluorescence start to appear in an otherwise mCherry-dominated nucleus (Figure 6 - 7, 0 minutes). The amount of mVenus gradually increases, with a concomitant reduction in the mCherry signal (Figure 6 - 7, 30-100

minutes). Within three hours only mVenus is visible within the nucleus (Figure 6 - 7, 160 minutes). Consistently, it was also noted that hepatocytes containing mVenus-positive nuclei progressed to a stage in which speckled mVenus fluorescence was visible throughout the cell cytoplasm (Figure 6 - 8, 70 minutes). This likely fits with breakdown of the nuclear membrane in preparation for cytokinesis. However, although this is a feature which could be useful to identify cells close to cytokinesis, it also results in the loss of the fluorescent signal, hampering further visualisation (Figure 6 - 8, 100 minutes).

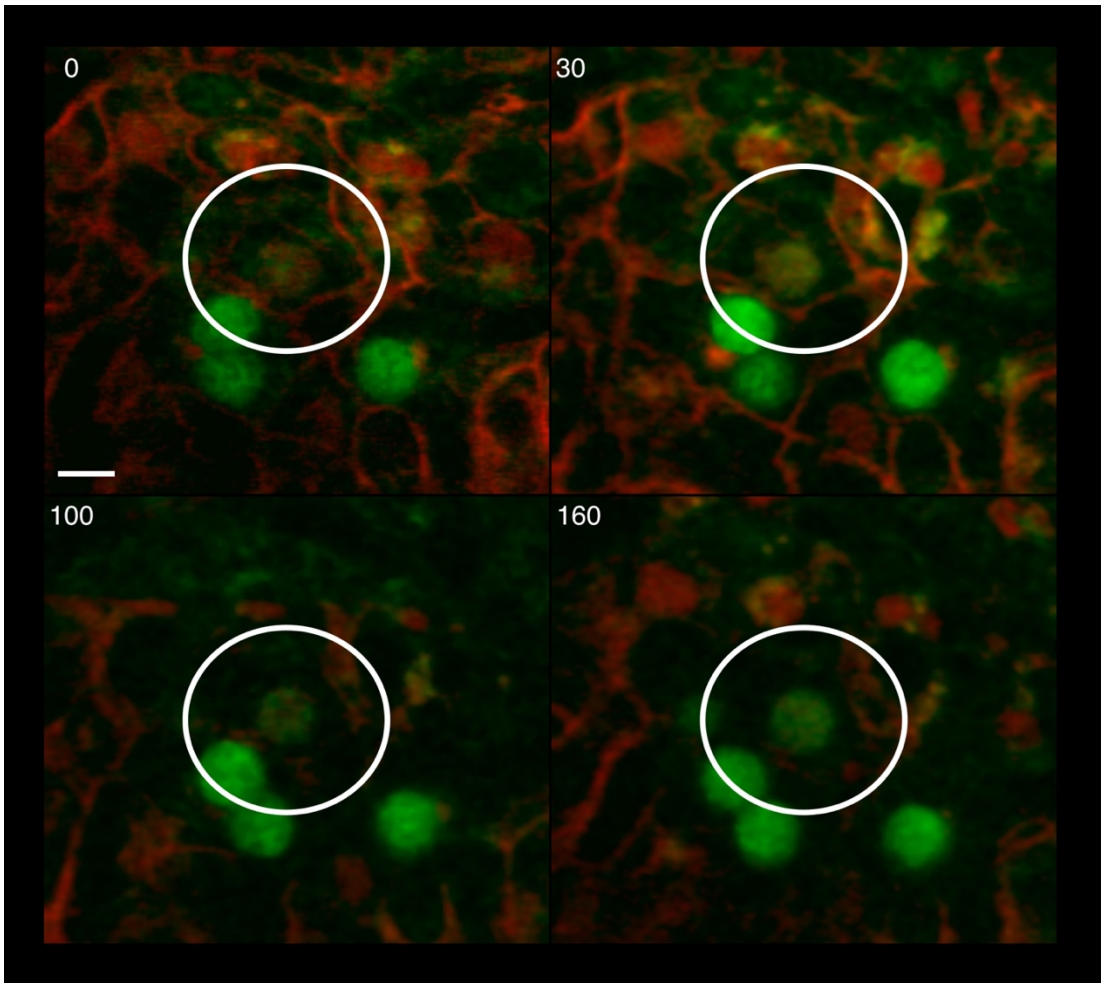

Figure 6 - 7 Intravital imaging of cycling hepatocytes following acetaminophen-induced liver injury.
Selected time points (number indicates time in minutes from the start of the series) from images obtained by intravital multiphoton microscopy in a Fucci;mTmG mouse, 42 hours after acetaminophen administration. White circles identify the same hepatocyte progressing through the cell cycle. Nuclear labels comprise mCherry (red, G1) and/or mVenus (green, S/G2/M); cell membranes are labelled by TdTomato (red). Scale bar 10μm.

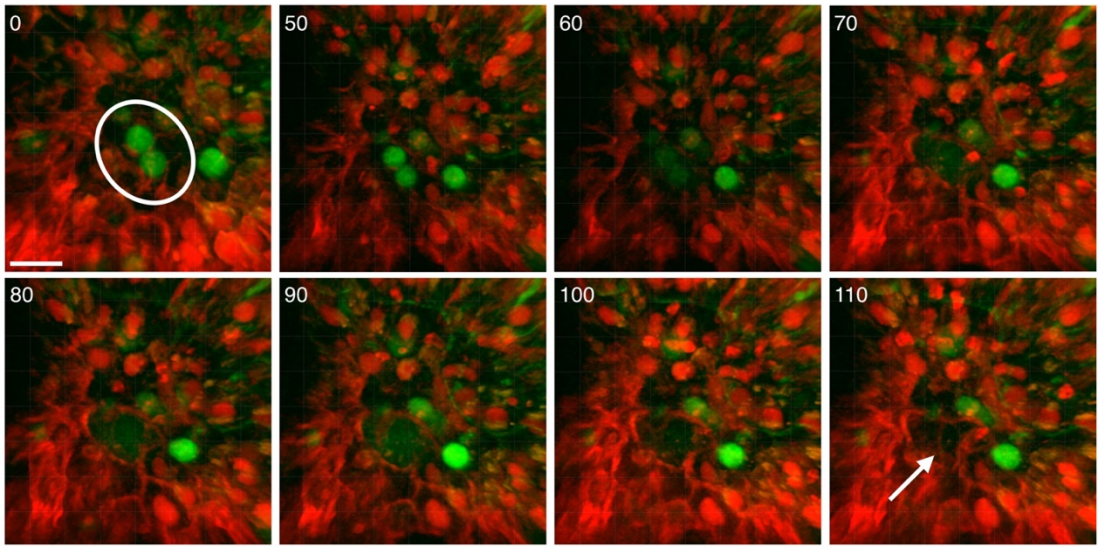

Figure 6 - 8 Disappearance of the Fucci nuclear label towards completion of the cell cycle. Selected time points (number indicates time in minutes from the start of the series) from images obtained by intravital multiphoton microscopy in a Fucci;mTmG mouse, 42 hours after acetaminophen administration. White circle identifies a binucleate hepatocyte progressing through the cell cycle. The mVenus nuclear signal fades before dispersing throughout the cytoplasm and subsequently disappearing. The white arrow highlights a linear structure, fluorescing in the red channel, which could be consistent with the early formation of cell membrane as the cell prepares to divide. Nuclear labels comprise mCherry (red, G1) and/or mVenus (green, S/G2/M); cell membranes are labelled by TdTomato (red). Scale bar 20μm.

To attempt to address the loss of the nuclear signal at the point of cytokinesis and cell division, the experimental protocol outlined above was repeated with the addition of a further nuclear label, the nucleic acid stain Hoechst, administered at the start of the terminal imaging session. This was effective in co-labelling both mCherry- and mVenus-positive hepatocytes (Figure 6 - 9). The Hoechst signal did remain detectable after progression of mVenus-positive nuclei to the point of dispersion of the fluorescent reporter protein into the cytoplasm (Figure 6 - 9, 150 minutes). Unfortunately, over the time course of imaging in this experiment, no hepatocyte was observed to progress beyond this stage, so it is unknown whether the Hoechst signal will remain detectable throughout cytokinesis.

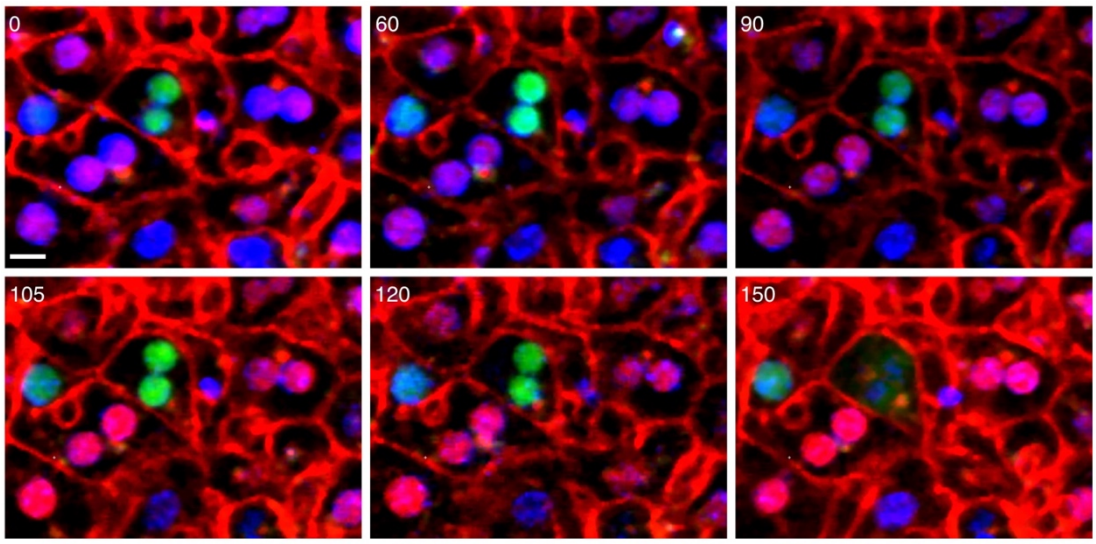

Figure 6 - 9 Combining the Fucci cell cycle reporter with the nucleic acid dye Hoechst.
Selected time points (number indicates time in minutes from the start of the series) from images obtained by intravital multiphoton microscopy in a Fucci;mTmG mouse, 41 hours after acetaminophen administration. mVenus-positive nuclei are visible in a binucleate hepatocyte. The Hoechst label remains detectable even after the mVenus signal fades. Nuclear labels comprise Hoechst (blue), mCherry (red, G1) and/or mVenus (green, S/G2/M); cell membranes are labelled by TdTomato (red). Scale bar 10μm.

Imaging the sinusoidal vasculature following partial hepatectomy

Using the *Cdh5-Cre* to label LSECs

Imaging of the sinusoidal vasculature was achieved by using the inducible *Cdh5-Cre* to drive fluorescent reporter expression in LSECs, either eGFP (in mice carrying the mTmG allele) or Ai14. Each fluorescent reporter offers its own potential advantages. The use of the mTmG allele maintains constitutive express of membranous tdTomato in all other cell types, and therefore offers the benefit of being able to visualise hepatocyte morphology in addition to LSECs (Figure 6 - 10). Conversely, the cytosolic expression of the Ai14 reporter protein gives strong and extremely well-defined reporting of the LSEC (Figure 6 - 11). The Ai14 reporter can also be combined easily with additional labelling strategies, such as the PBAG constitutive reporter allele utilised to label HSCs (see below).

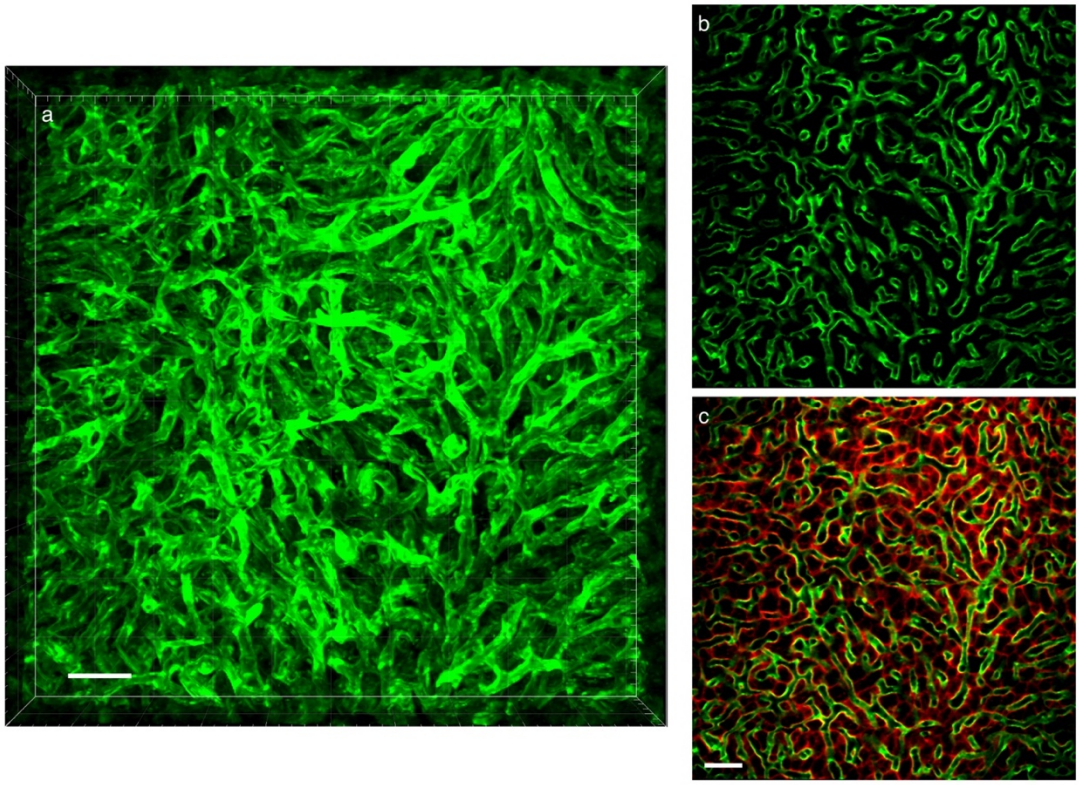

Figure 6 - 10 Labelling the sinusoidal vasculature using the *Cdh5-Cre*;mTmG mouse.
Following tamoxifen administration, widespread membranous eGFP expression (green) is visible in LSECs, allowing three-dimensional reconstruction of the sinusoidal vasculature (a). Images obtained by intravital multiphoton microscopy. In addition to eGFP labelling of LSECs (b), constitutive expression of membranous tdTomato (red) in non-recombined cells allows visualisation of hepatocytes (c). Scale bars 50μm.

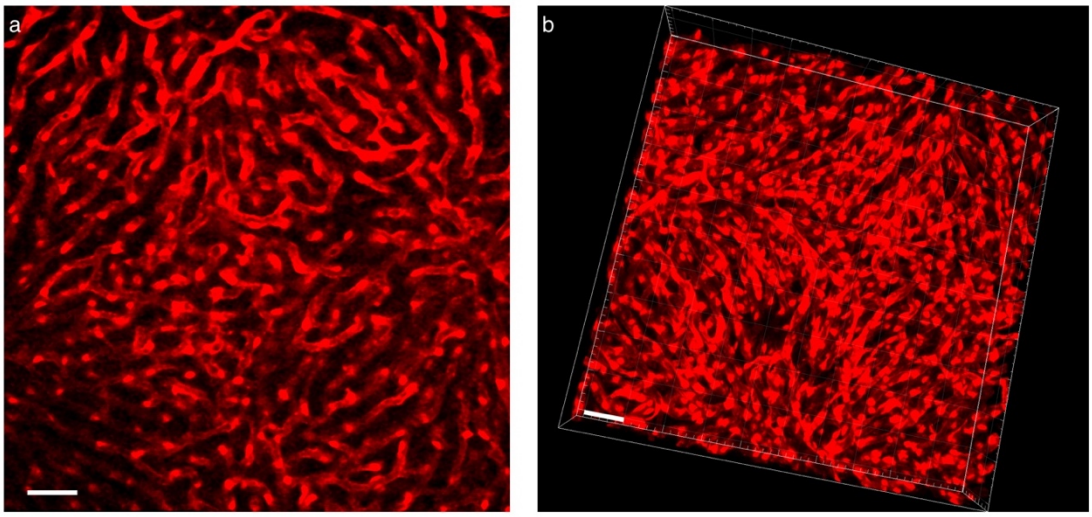

Figure 6 - 11 Labelling the sinusoidal vasculature using the *Cdh5-Cre*;Ai14 mouse.
Following tamoxifen administration, widespread cytosolic Ai14 expression (red) is visible in LSECs (a), allowing three-dimensional reconstruction of the sinusoidal vasculature. Images obtained by intravital multiphoton microscopy. Scale bars 50μm.

Reconstruction and analysis of the sinusoidal vasculature network

During initial optimisation of multiphoton microscopy of the *Cdh5-Cre*;Ai14 mouse, partial hepatectomy was performed and livers harvested at 24, 48 and 72 hours for imaging. Image

review suggested that the vascular network might become less dense between 48 and 72 hours post partial hepatectomy (Figure 6 - 12). This would be consistent with hepatocyte expansion, either in size or number, prior to a later wave of LSEC proliferation. However, this was purely a subjective interpretation with one mouse per time point. Therefore, in a subsequent experiment, AIW implantation, with or without partial hepatectomy, was performed in *Cdh5-Cre*;Ai14 mice, with intravital imaging at 24, 48 and 72 hours post partial hepatectomy. Livers were also imaged in a dish immediately after harvest at 96 hours.

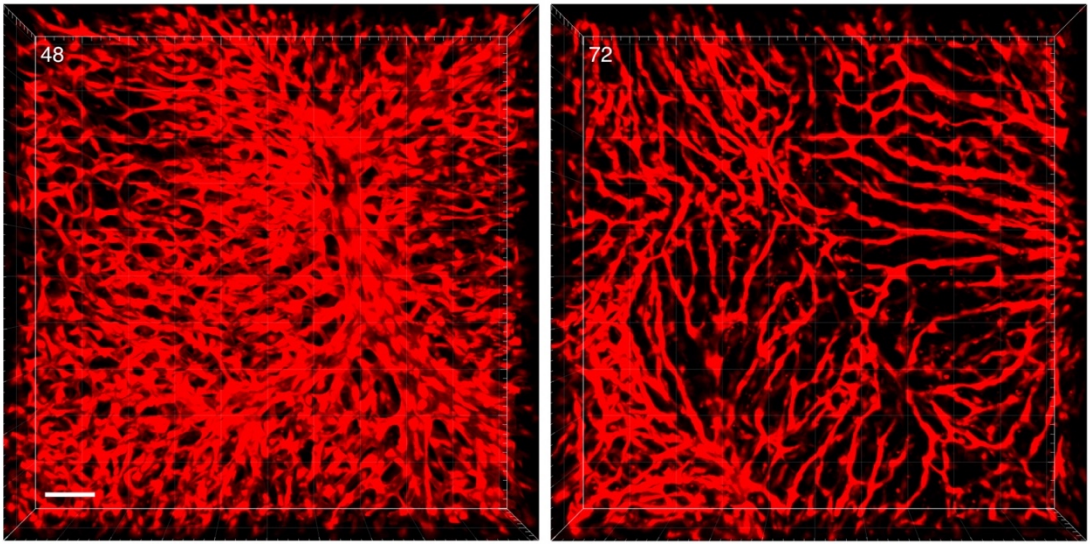

Figure 6 - 12 Multiphoton microscopy of freshly harvested, whole liver from *Cdh5-Cre*;Ai14 mice following partial hepatectomy.
Three-dimensional projection of the sinusoidal vasculature at 48 (left) and 72 (right) hours following partial hepatectomy. Scale bar 50μm.

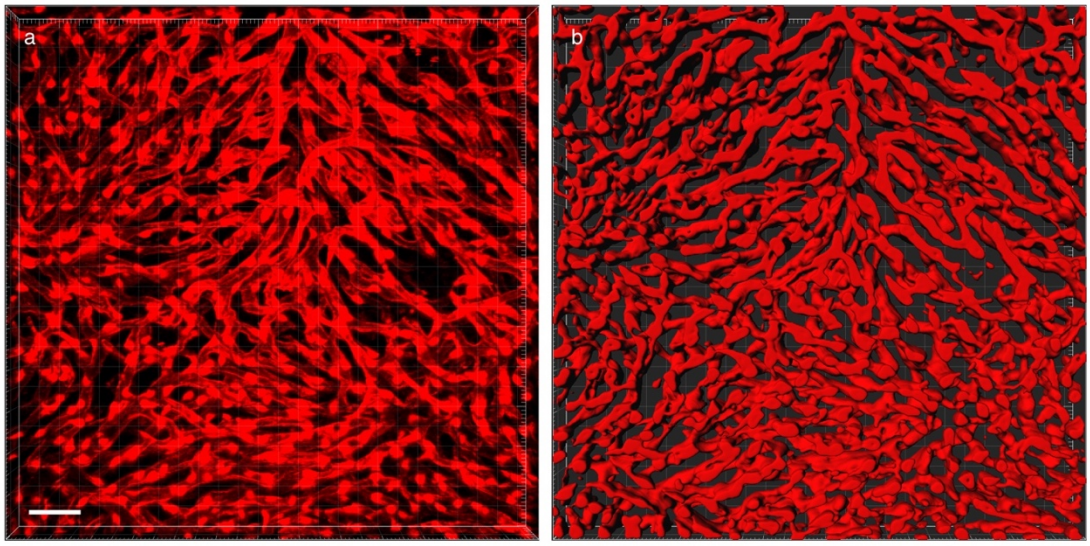

Figure 6 - 13 Intravital imaging of *Cdh5-Cre*;Ai14 mice allows three-dimensional reconstruction of the sinusoidal vasculature.
a) Representative z-stack projection obtained at 24 hours after AIW implantation. b) Three-dimensional surface reconstruction of the image shown in (a). Scale bar 50μm.

Post-imaging reconstruction of the sinusoidal vasculature in three dimensions from z-stacks obtained by intravital microscopy is feasible in *Cdh5-Cre*;Ai14 mice (Figure 6 - 13). This was achieved using Imaris software, as detailed in Chapter Two. However, few useful metrics are currently obtainable following such reconstruction, namely the surface area and volume of the reconstructed structure. This failed to demonstrate any marked difference between mice in which partial hepatectomy had been performed and AIW-only controls (Figure 6 - 14). It is possible that increased numbers would detect a significant reduction in the mean percentage vascular volume or vascular surface area in the early post-partial hepatectomy phase; however, calculation of additional metrics would also be more informative. What the current data does demonstrate is the repeatability of the measurement between imaging sessions in control mice. The relatively low value obtained for mouse 80 at 48 hours may be due to the fact that 13% (by volume) of the reconstructed z-stack at this time point did not contain liver tissue. An attempt was made to reflect this (by adjusting the measured values for the actual volume of liver contained within the image), however, this may still have led to a falsely low value at this time point. The drop in calculated vascular volumes at 96 hours, the time point at which multiphoton microscopy was performed on excised liver in a dish, illustrates the benefit and importance of intravital image acquisition in comparison to ex vivo analysis. It also suggests that this type of vascular reconstruction and volume analysis could be used as a surrogate indicator of sinusoidal perfusion.

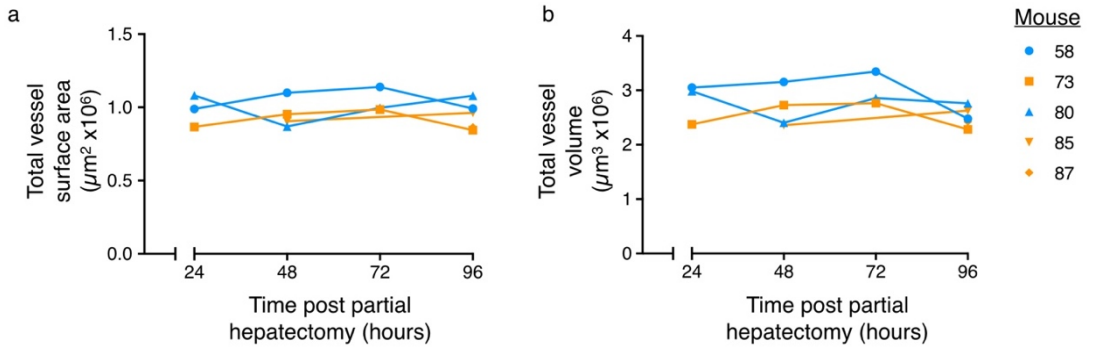

Figure 6 - 14 Intravital imaging of *Cdh5-Cre*;Ai14 mice allows sequential analysis of the sinusoidal vascular network following partial hepatectomy.
Sinusoidal vasculature surface area (a) and volume (b) in uninjured (blue) and post partial hepatectomy (orange) mice calculated from images obtained during intravital multiphoton microscopy. Analysable images were not obtained at all time points for all mice. Images at the 96-hour time point were obtained immediately following harvest. Values obtained for mouse 80 at 48 hours were divided by 0.87 to account for the absence of liver tissue in 13% of the z-stack volume.

An alternative tool for vascular network analysis has been described, called Angiotool.[169] This identifies vessels within an image and computes a range of parameters, including the area occupied, number of junctions, branching index, vessel length and lacunarity.

Unfortunately, the analysis is currently only possible on two-dimensional images. Therefore, maximal intensity projections of the three central slices (4μm total depth) from the z-stacks used for the three-dimensional analysis described above were produced. Following optimisation of the detection parameters, the tool appeared able to identify accurately the sinusoidal vascular network (Figure 6 - 15a,b) Analysis of vascular area gave similar results to the vascular volumes previously calculated with the three-dimensional analysis (Figure 6 - 15c). Both total vessel length and the total number of junctions per image appeared to be consistently lower in mice that underwent partial hepatectomy when compared to control mice (Figure 6 - 15d,e). This would fit with a relative reduction in the number of sinusoids contained within the imaging area, which may occur as a result of proliferation peaking earlier in hepatocytes than in LSECs. However, increased sample sizes are necessary to confirm this.

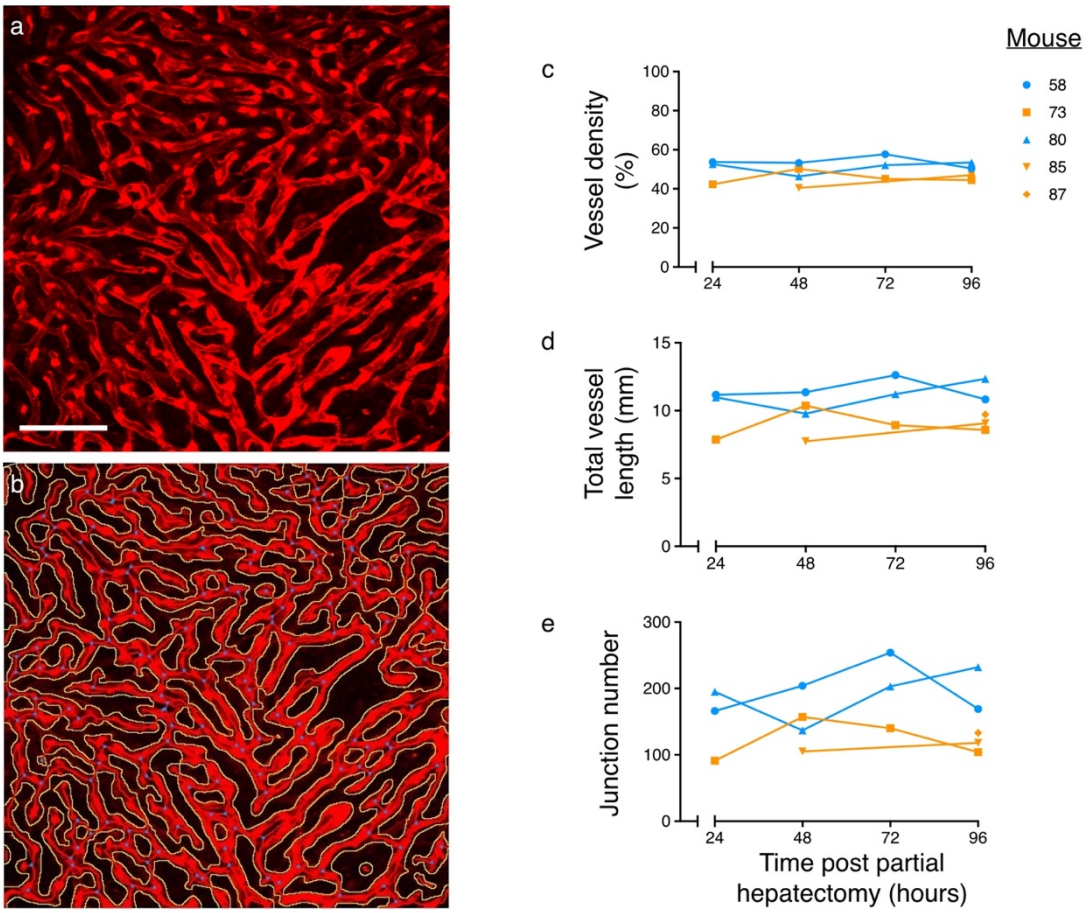

Figure 6 - 15 Two-dimensional analysis using Angiotool of the sinusoidal vascular network following partial hepatectomy.
Maximal intensity projections (a) were produced from three sequential slices (4μm depth) and analysed in Angiotool.[169] The software detects both vasculature (yellow outline) and branch points (blue dots) (b). This was used to calculate vessel density (c), total vessel length (d), and junction number (e) following intravital multiphoton microscopy in uninjured (blue) and post-partial hepatectomy (orange) mice. Analysable images were not obtained at all time points for all mice. Images at the 96-hour time point were obtained immediately following harvest. Vessel length and junction number values obtained for mouse 80 at 48 hours were divided by 0.84 to account for the absence of liver tissue in 16% of the image area. Scale bar 100μm.

Use of the confetti reporter can facilitate the study of angiogenesis following injury

The inducible nature of the *Cdh5-Cre* driver provides the opportunity for it to be employed in fate-mapping studies. Typically, tamoxifen is administered to induce Cre-mediated recombination over a defined time period prior to the induction of injury or, in developmental models, the time point of interest. The location of labelled cells and any change in labelled fraction can be used to test a hypothesis that the labelled population expand or migrate.

In the partial hepatectomy model of liver regeneration, it is known that sinusoidal angiogenesis occurs after the majority of hepatocytes have proliferated.[180] However, the exact mechanism through which the sinusoidal architecture is restored following injury remains unclear. Do sinusoids simply elongate to accommodate the division of hepatocytes in the

remnant lobe? Or does sprouting occur to create new sinusoids and in this manner maintain hepatocyte-sinusoidal contact? In either case, do all LSECs have equal proliferative potential or are a limited number of specialised LSECs (potentially in defined anatomic locations) responsible for the vascular proliferation that occurs as a necessary part of liver regeneration?

Although recombination can be induced in *Cdh5-Cre*;Ai14 or *Cdh5-Cre*;mTmG mice to study hepatic sinusoidal structure as described above, they are unable to detect expansion of a subpopulation of LSECs. However, the Confetti reporter has previously been used to examine clonal expansion of progenitor cells in the liver.[229] This is a multi-colour reporter allele in which Cre-mediated recombination leads to permanent, heritable expression of one of four fluorescent proteins in a stochastic manner. Therefore, mice carrying either the *Cdh5-Cre* or Confetti allele were interbred to generate the *Cdh5-Cre*;Confetti line.

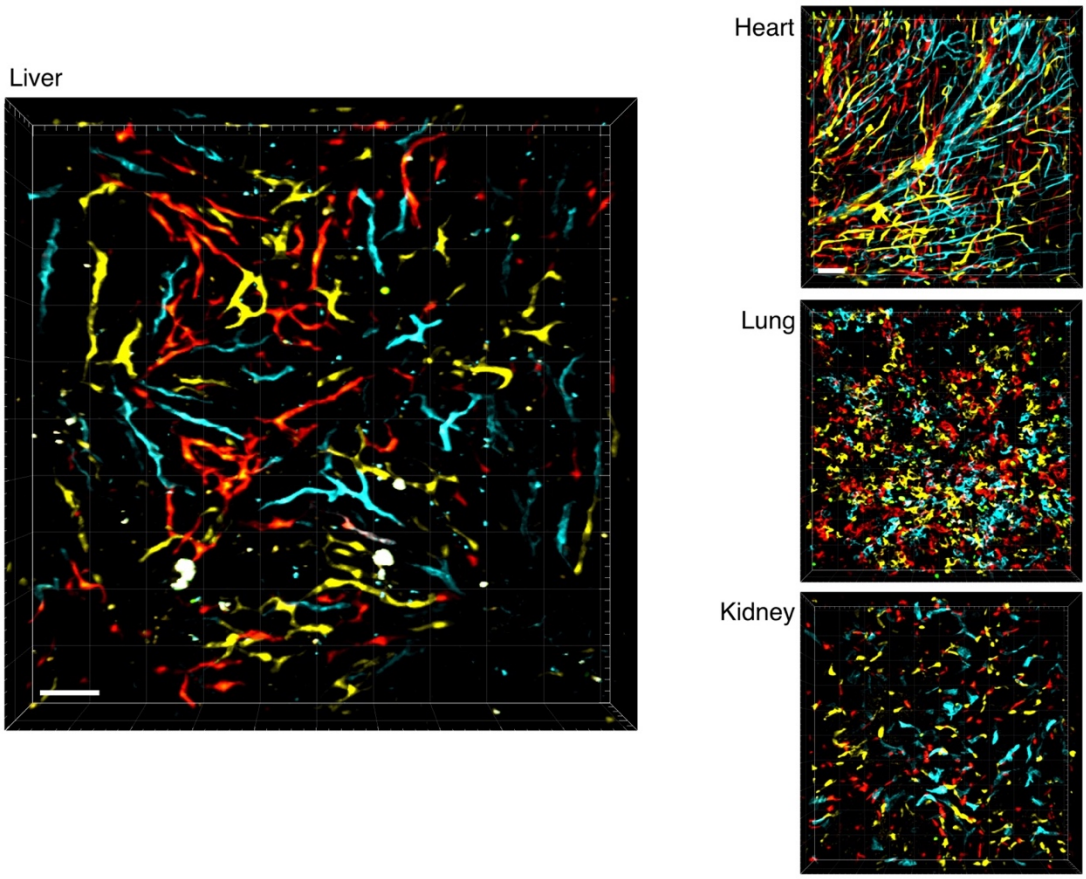

Figure 6 - 16 Multi-colour fluorophore expression in the vasculature of the *Cdh5-Cre*;Confetti mouse.
Tamoxifen administration leads to widespread recombination in the vasculature of liver (a), heart (b), lung (c), and kidney (d). Stochastic expression of either mCerulean, yellow, red or green fluorescent protein occurs in each endothelial cell in which recombination occurs. Three-dimensional projections of images obtained from multiphoton microscopy of freshly harvested whole organs are shown. Scale bars 50μm.

Administration of tamoxifen to *Cdh5-Cre*;Confetti mice according to the standard schedule revealed widespread labelling of the LSEC population (Figure 6 - 16). Approximately equal numbers of LSECs expressed the mCerulean, yellow or red fluorescent proteins, with less frequent expression of GFP. Similar findings were also observed in the vasculature of heart, lung and kidney (Figure 6 - 16). As expected, a reduced tamoxifen dosing schedule resulted in decreased recombination (Figure 6 - 17). This sparse labelling is ideally suited to detect clonal expansion of a subset of LSECs during angiogenesis after liver injury. Hence, the *Cdh5-Cre*;Confetti mouse is a useful tool with which to study the mechanics of sinusoidal regeneration following liver injury.

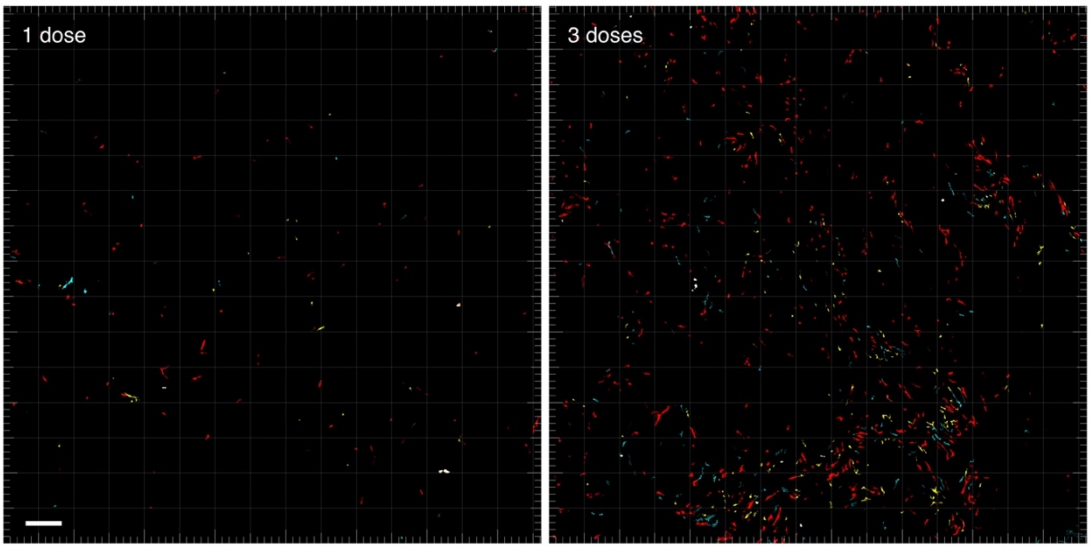

Figure 6 - 17 Tamoxifen dose reduction decreases the number of labelled LSECs in the livers of *Cdh5-Cre*;Confetti mice.
Tiled images obtained from multiphoton microscopy of freshly harvested whole liver are shown. Scale bar 200μm.

Imaging sinusoidal blood flow in the liver

Imaging and measuring blood flow in any tissue can only be performed in a living subject. AIW implantation facilitates blood flow analysis in the liver, in situ. Specifically, it also allows assessment of flow in individual sinusoids, which provides the opportunity to investigate the impact of localised changes in blood flow on the surrounding parenchyma, even where regional or whole organ haemodynamics remain under homeostatic control.

Techniques to allow measurement of red blood cell velocity in a single sinusoid

It is possible to use CARS to visualise red blood cells and this was the first approach that was pursued in attempting to visualise and measure sinusoidal blood flow.[168] The technique involves orientating the multiphoton scan direction to match the direction of flow in the vessel of interest. Pixel dwell time is then adjusted to try to match the speed at which the red blood

cells are flowing through the sinusoid. This then allows calculation of red blood cell velocity. When successful, the sight of red blood cells streaming through the sinusoid is visually impressive (Figure 6 - 18). However, the challenges in obtaining a consistent CARS signal to a reasonable depth and with the necessary resolution have already been alluded to. Also, it can be difficult to differentiate the smears created by individual red blood cells. Therefore, an alternative fluorescent labelling approach was explored. Red blood cells were harvested from a donor mouse of the same line and labelled fluorescently. These were then injected into the recipient mouse, after AIW implantation and prior to intravital imaging. The method for calculating red blood cell velocity has previously been described,[170] and is explained in detail in Chapter Two. Scan direction and speed are adjusted in a similar manner to that described above for CARS imaging of blood flow. This results in a fluorescent streak when a labelled donor red blood cell flows through the vessel under study (Figure 6 - 19a). Resolving the length of a smear, made by a single object of known size, against the elapsed time between scanning its first and last pixel, allows the calculation of an individual blood cell's velocity as it travels through the sinusoid. Measuring multiple smears in a single sinusoid over a period of time allows estimation of red blood cell velocity for that specific location.

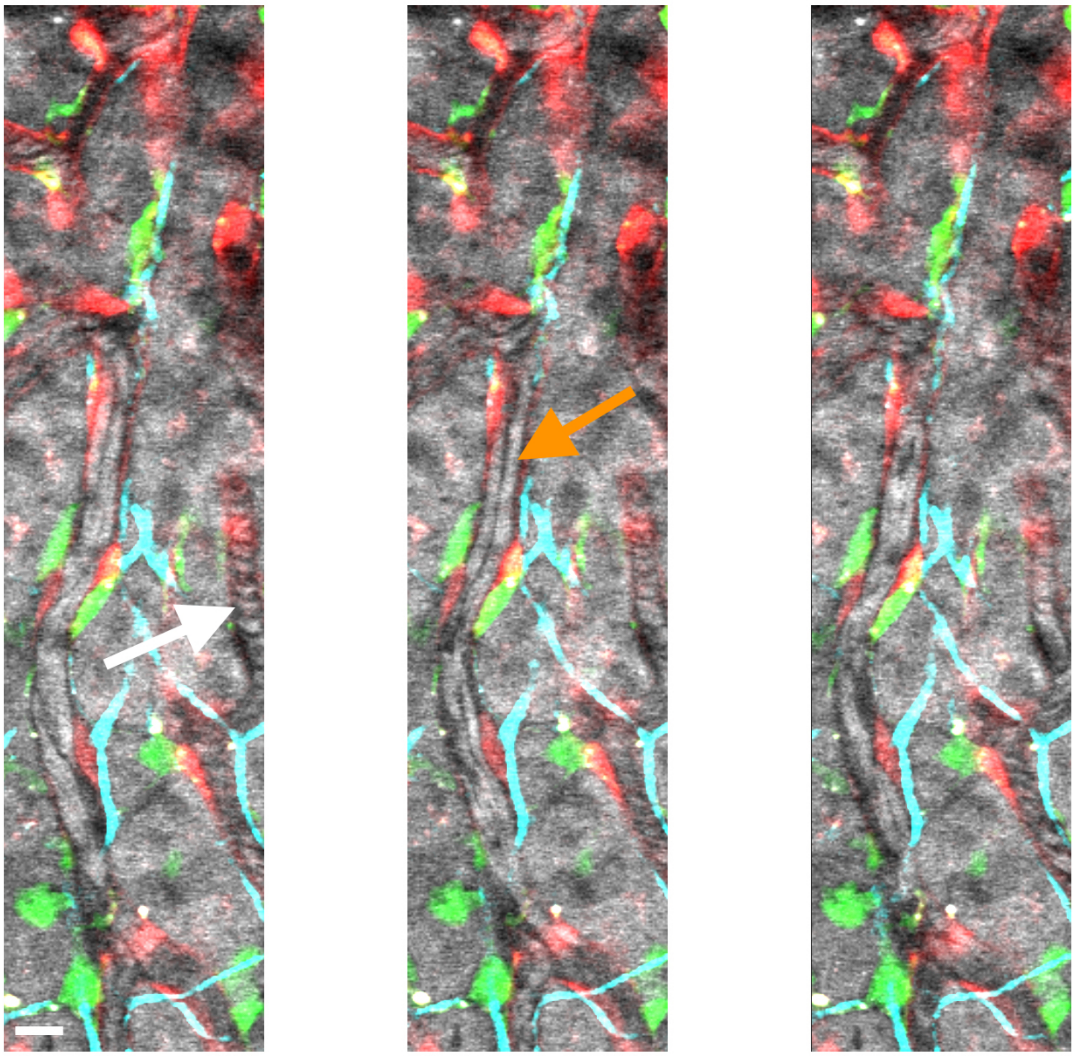

Figure 6 - 18 CARS imaging allows label-free, intravital visualisation of red blood cells in the hepatic sinusoid.
Sequential scans (scan duration 0.85s) obtained by intravital multiphoton microscopy in a *Cdh5-Cre*;PBAG;Ai14 mouse show individual red blood cells stacked in the right-hand sinusoid (white arrow). In the left-hand sinusoid, scan speed is matched to red blood cell velocity, resulting in smears as the red blood cells pass down the sinusoid (orange arrow). LSECs (red), HSCs (green) and collagen (cyan) are also shown. Scale bar 10μm.

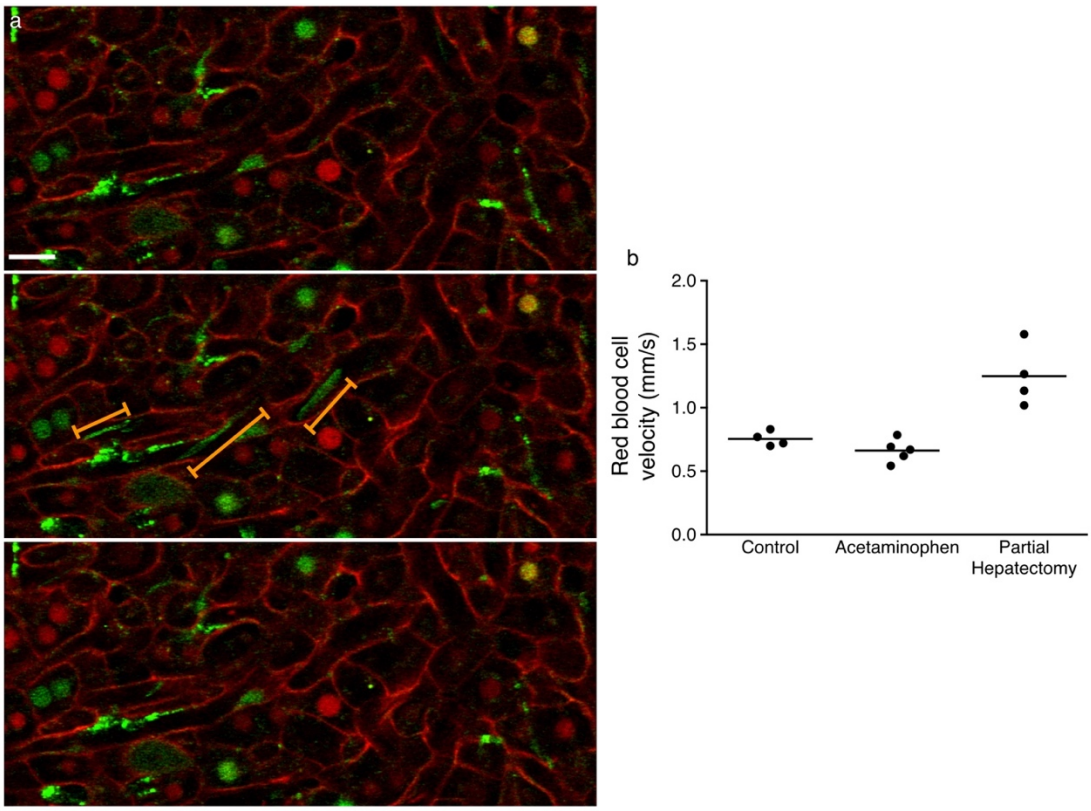

Figure 6 - 19 Labelled red blood cells permit measurement of red blood cell velocity in the hepatic sinusoid.
a) Sequential scans obtained by intravital multiphoton microscopy in a Fucci;mTmG mouse. In the centre image, three green smears (orange bars) are visible, created by labelled, donor red blood cells as they pass through the sinusoids. None are visible in the preceding (top) or subsequent (bottom) image. b) Mean red blood cell velocity in the hepatic sinusoids of control mice, and 24 hours after acetaminophen administration or partial hepatectomy. Scale bar 20μm.

Measurement of sinusoidal red blood cell velocity is possible in uninjured and injured liver

Following AIW implantation and injection of labelled red blood cells, timelapse images of sinusoidal blood flow were recorded in uninjured livers and at 24 hours following acetaminophen administration. Images were also obtained in a separate cohort of mice following partial hepatectomy and AIW implantation. Mean sinusoidal red blood cell velocity was similar in uninjured liver and following acetaminophen (Figure 6 - 19b).[§] However, increased red blood cell velocity was observed in mice that received partial hepatectomy. The increase in velocity observed following partial hepatectomy is likely the result of a similar volume of blood perfusing through a reduced number of sinusoids. Overall, the calculated values were consistent between mice within the same cohort, suggesting that this is a valid and useful technique for assessment of red blood cell velocity at the level of the sinusoid.

[§] Data analysis performed by K. Conroy.

Using label-free imaging to track hepatic lipid following partial hepatectomy

As well as detecting signal from fluorescent reporter proteins, the multiphoton system also provides the ability to generate 'label-free' images. The CARS modality generates an image of the tissue through differences in the vibrational properties of its constituent molecules. Lipid creates a particularly strong CARS signal and therefore intravital multiphoton microscopy is ideally suited to study the dynamic changes in parenchymal lipid content that can occur during liver injury. There is a marked accumulation of lipid within hepatocytes in the immediate aftermath of partial hepatectomy. The effect of this accumulation on, or its relationship to, subsequent hepatocyte proliferation remains unclear.

Parenchymal lipid was imaged using CARS following partial hepatectomy and AIW implantation in two independent cohorts of mice. Z-stacks were reconstructed into three-dimensional volumes and the percentage of lipid within the parenchymal volume was calculated (Figure 6 - 20a,b). This revealed that parenchymal lipid peaks at 48 hours post partial hepatectomy, but returns to baseline by 96 hours (Figure 6 - 20c,d). Interestingly, experimental mouse 151 had a similar parenchymal lipid profile to that of the uninjured control, despite partial hepatectomy being performed. Retrospective review revealed that this mouse had the lowest proportion of liver tissue excised at the time of partial hepatectomy (2.0% vs 2.2% (ID165), 3.1% (ID152)), suggesting insufficient injury may have occurred to trigger lipid accumulation.

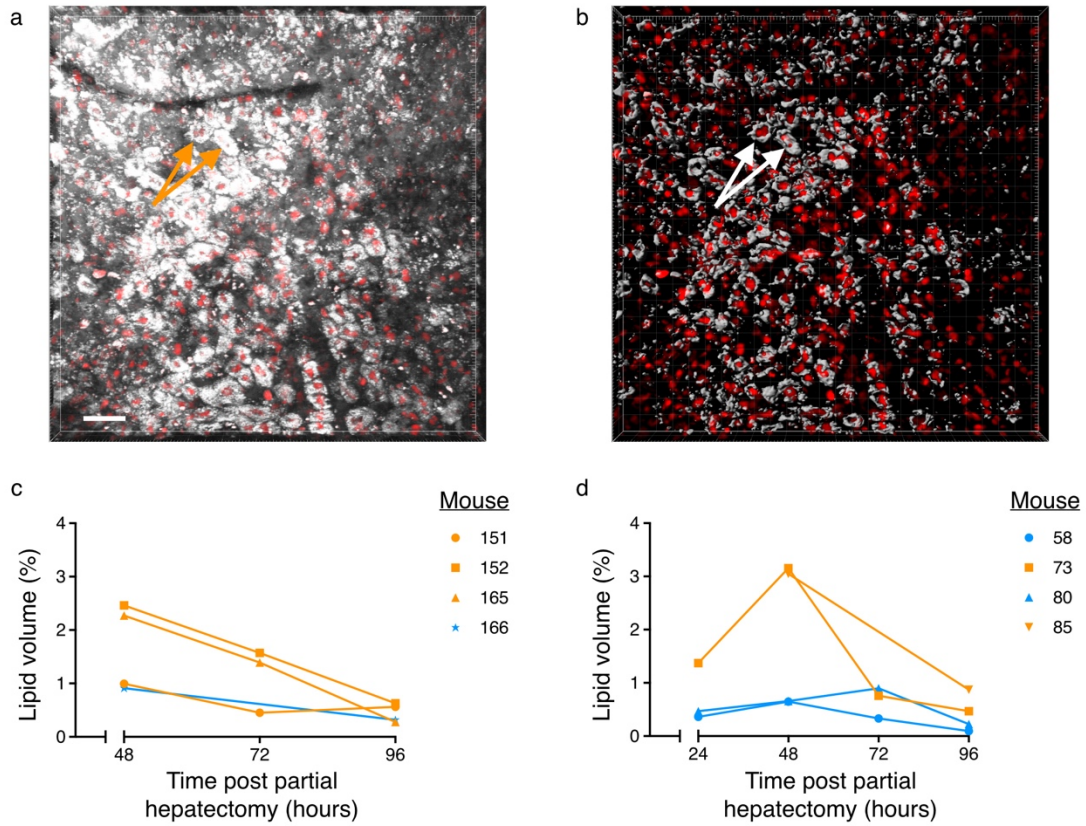

Figure 6 - 20 Analysis of hepatic lipid dynamics following partial hepatectomy, using intravital multiphoton microscopy.
The accumulation of lipid in hepatocytes occurring after partial hepatectomy can be visualised with CARS (a, orange arrows) and reconstructed in three dimensions (b, white arrows). mCherry (red) nuclei are also shown. c,d) Percentage volume of hepatic lipid in control mice (blue) and following partial hepatectomy (orange) in two independent experiments. Scale bar 50μm.

Intravital imaging of non-parenchymal cell populations

Visualising hepatic stellate cells in vivo

Using the PBAG transgenic mouse to label HSCs has previously been described,[29] but this strategy has not been used to image HSCs in vivo. PBAG mice were crossed to the *Chd5-Cre*;Ai14 line to produce triple transgenic reporter mice, with constitutive expression of eGFP in HSCs and inducible expression of Ai14 in LSECs following administration of tamoxifen. Intravital imaging demonstrated well-defined labelling of the hepatic sinusoids, with the close apposition of HSCs in the space of Disse, with their expected filamentous projections (Figure 6 - 21a,b). A noticeably increased density of eGFP-positive cells was noted close to the surface of the liver (Figure 6 - 21c,d,e). To exclude the possibility of this being an experimental artefact due to the presence of the AIW, ex vivo multiphoton microscopy was performed in freshly harvested, uninjured whole liver (Figure 6 - 22). This confirmed the previous observations,

suggesting that either there is an increased number of HSCs peripherally or, more likely, that mesothelial cells in the liver are also labelled in the PBAG mouse.

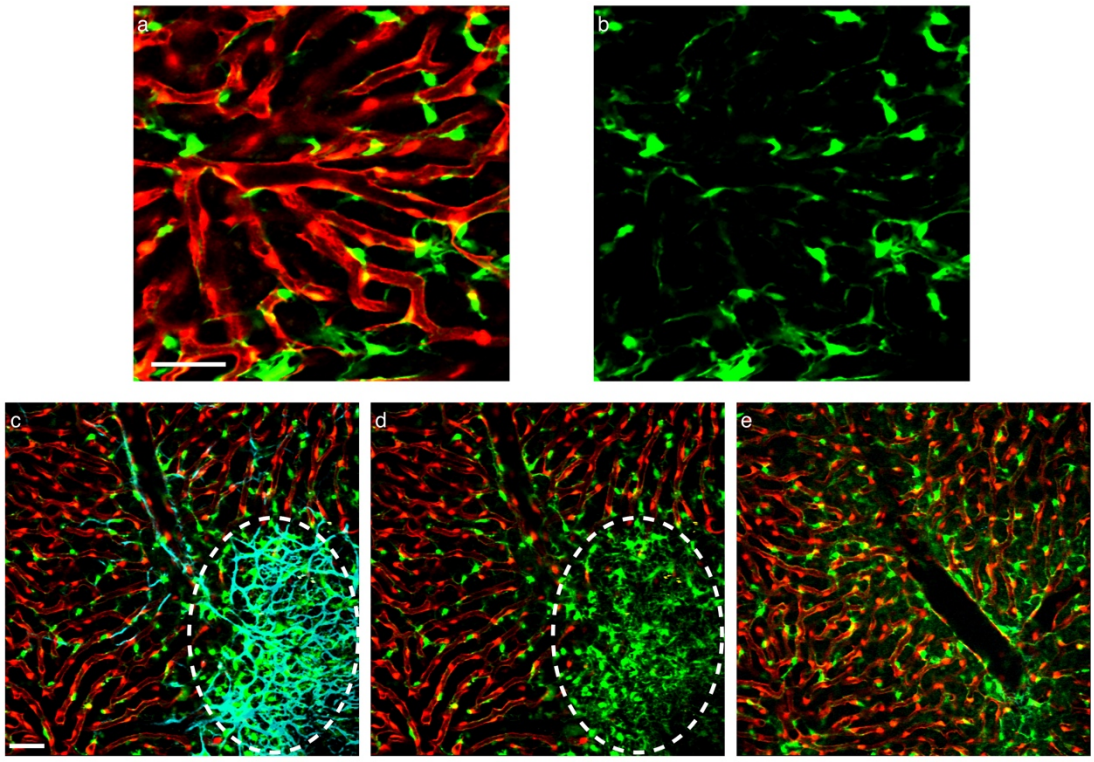

Figure 6 - 21 Visualisation of sinusoidal vasculature and HSCs with intravital multiphoton microscopy.
a) Constitutive labelling of HSCs (green) and tamoxifen-inducible labelling of LSECs (red) in the *Cdh5-Cre*;PBAG;Ai14 mouse. b) The same image as (a), showing only HSCs (green). c,d) The PBAG allele also labels a population of cells (green, contained within the dotted white lines) immediately beneath the collagen-rich liver capsule (shown in cyan in (c)). e) The expected density of HSCs (green) is present at 30μm beneath the capsule. Scale bars 50μm.

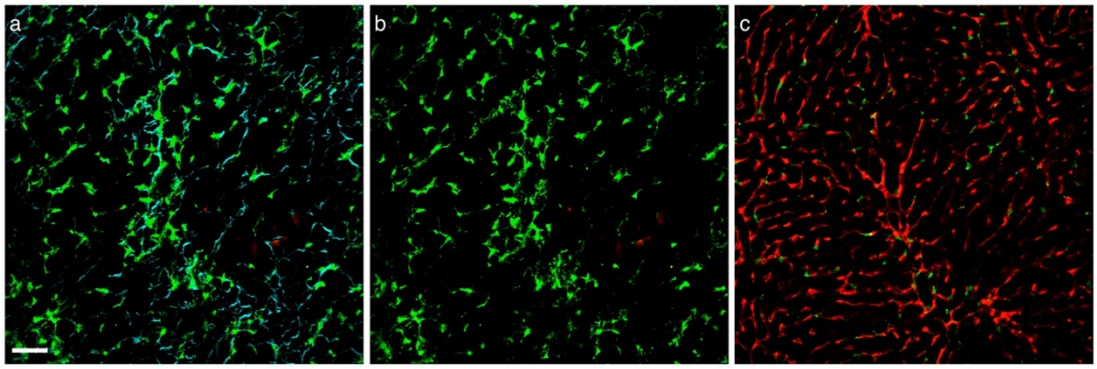

Figure 6 - 22 The PBAG allele labels a population of cells at the liver capsule.
Multiphoton microscopy of freshly harvested, uninjured, whole liver from *Cdh5-Cre*;PBAG;Ai14 mice confirmed the increased density of eGFP-positive cells (green) at the level of the liver capsule, shown in cyan in (a) and removed from the image in (b). c) This density of eGFP-positive cells does not persist at 30μm beneath the surface of the liver (LSECs, red). Scale bar 50μm.

Investigating the possibility of using the MacGreen reporter mouse to label Kupffer cells

Having demonstrated the ability to label hepatocytes, LSECs and HSCs fluorescently for intravital microscopy, a means of visualising Kupffer cells in vivo was also explored. Others have used antibody labelling strategies to label macrophages in the liver for intravital imaging.[143,233] Alternatively, the MacGreen knock-in reporter mouse expresses eGFP in colony-stimulating factor 1 receptor-positive myeloid cells.[163] In liver, reporting location and morphology matches that of F4-80$^+$ macrophages.[163]

MacGreen mice were interbred with mice carrying the mTmG allele to allow assessment of eGFP reporting on a background of membranous tdTomato expression by all cells, thus facilitating visualisation of the hepatic parenchyma. The initial investigations using multiphoton microscopy of the uninjured liver were promising, with a strong eGFP signal in the expected sinusoidal location (Figure 6 - 23a). However, when intravital microscopy was performed in Fucci-MacGreen-mTmG triple transgenic mice following acetaminophen administration, with the aim of tracking the macrophage response to injury and relating this to the hepatic regenerative niche, it became clear that the lack of total specificity of the MacGreen mouse for the macrophage population drastically limits the conclusions that can be drawn using this labelling approach. The size and morphology of many of the eGFP-positive cells flooding the injured liver suggested that neutrophils as well as macrophages were being labelled by the MacGreen allele (Figure 6 - 23b,c). Expression of eGFP has been reported in neutrophils in MacGreen mice.[231] This makes accurate identification of macrophages particularly challenging in the neutrophil-rich inflammatory response that occurs following acetaminophen-induced liver injury. Hence, although the MacGreen allele could be employed to examine the leukocyte response to liver injury in vivo, the inability to distinguish readily between neutrophils and macrophages is a major disadvantage.

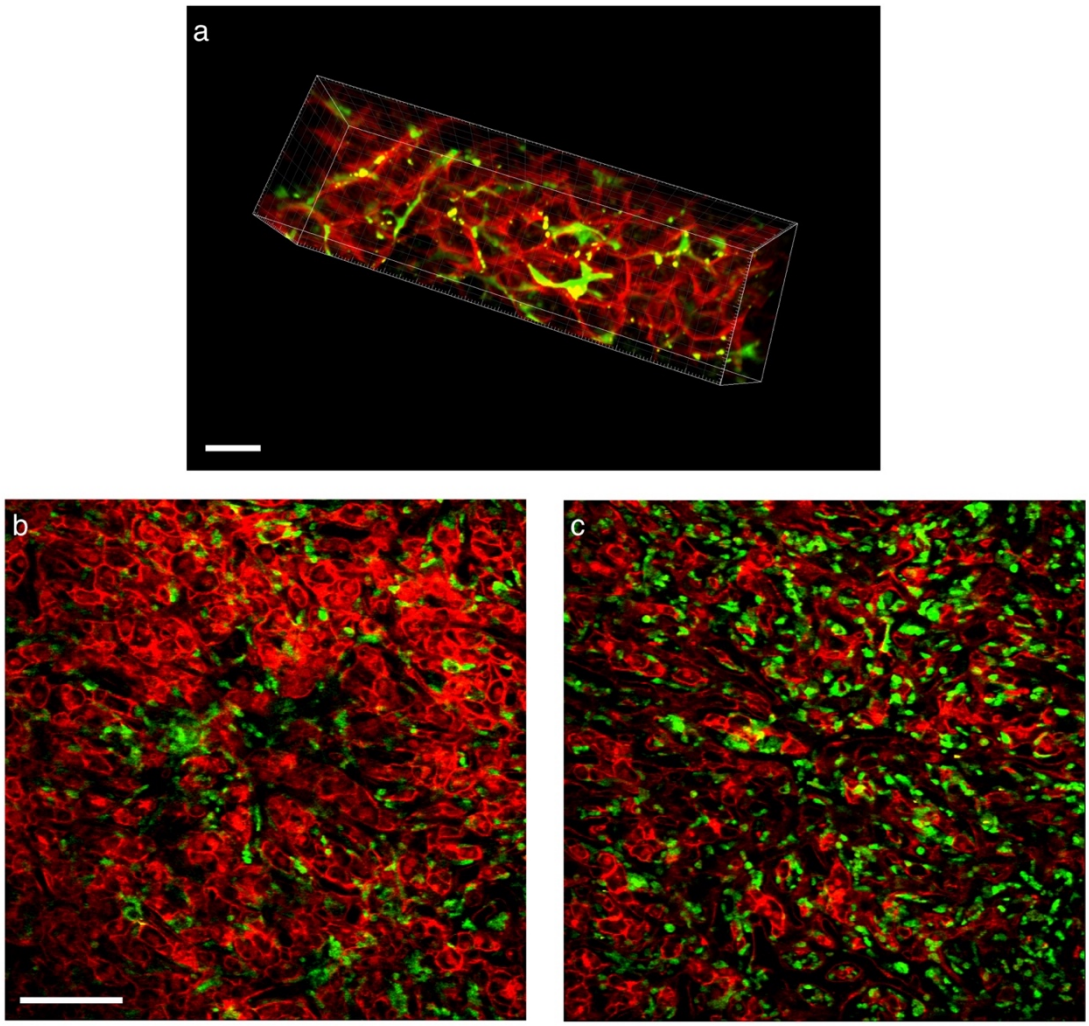

Figure 6 - 23 MacGreen labelling of inflammatory cells in the liver.
a) Three-dimensional projection of images obtained by multiphoton microscopy of freshly harvested, uninjured, whole liver from a MacGreen;mTmG mouse. b,c) Intravital multiphoton microscopy performed 24 hours after acetaminophen administration in a Fucci;MacGreen;mTmG mouse. MacGreen (cytosolic eGFP, green), nuclei (mCherry, red, G1; mVenus, green, S/G2/M) and cell membranes (tdTomato, red). Scale bars 30μm (a) and 100μm (b,c).

Discussion

The principal aim of the body of work described in this chapter was to explore the wide-ranging capabilities of two novel models of AIW implantation, liver injury and repeated intravital multiphoton microscopy, and demonstrate their potential to improve our understanding of multiple facets of liver regeneration. These models are still in their infancy, and certainly present logistical and technical challenges, but the potential rewards for continued perseverance are great. For example, by performing partial hepatectomy and AIW implantation in a single mouse, it is possible to image sinusoidal vasculature in three dimensions, examine the cellular and nuclear morphology of cycling hepatocytes in the

regenerative niche, measure blood flow in multiple individual sinusoids, and track lipid metabolism. All in the living animal. All at multiple time points. In fact, the greatest challenge is probably that of designing a streamlined and efficient workflow to cope with the wealth of data that can be produced.

Using the Fucci reporter allele to identify the hepatic regenerative niche

Transgenic mice expressing nuclear Fucci2a reporter proteins are an extremely useful tool as they enable in vivo visualisation of cycling hepatocytes and the regenerative niche. Nuclei progressing through the S phase of the cell cycle and beyond are easily identifiable through the dominance of the mVenus reporter protein. Although an attempt at hepatocyte-specific Fucci2a expression did not result in highly efficient recombination, the distinctive morphology of the hepatocyte and its large nucleus make hepatocyte nuclei easy to identify following germline Cre-mediated recombination of the R26Fucci2aR allele, which in theory leads to constitutive reporter protein expression in all cells. This germline labelling strategy also offers the fortuitous benefit of visualising cell cycling in other cell types within the liver, although the utility of this remains to be confirmed.

The ability to watch individual hepatocytes in vivo as they progress through the cell cycle allows examination of whether there are particular hepatocyte features, or an anatomic localisation, that predispose a particular hepatocyte to have a regenerative advantage over another. There are a large number of bi-nucleate hepatocytes in the liver and it would be interesting to examine how the cell cycle, and subsequent division, progresses in this subset of cells.

The major disadvantage of the Fucci system is the loss of nuclear labelling immediately prior to cytokinesis, which prevents confirmation of cell division using this system alone. This can potentially be surmounted through the use of an additional nucleic acid label, such as Hoechst. In the study reported above, Hoechst was administered topically to the surface of the liver. Although nuclear labelling was achieved with reasonable efficacy, intravenous administration would likely result in more consistent labelling throughout the parenchyma. In addition, the long-term effects of most nucleic acid dyes are unknown, so at present these labels are only administered in terminal imaging procedures. An easily detectable nucleic acid label that does not interfere with the process of mitosis, and is therefore safe to use in longer-term studies would be preferable. This might also solve another technical challenge posed by the use of Hoechst in the current multiphoton setup. Due to the nature of their respective

excitation spectra, it was not possible to acquire Fucci and Hoechst images simultaneously. Sequential scans are feasible, if somewhat inconvenient. They also increase the potential for tissue movement, reducing the final image resolution, and add to the post-acquisition workload because of the need to pair individual scans.

An additional challenge to the feasibility of intravital imaging of hepatocyte division during liver regeneration is a temporal one. Although coordinated entry into the cell cycle occurs following partial hepatectomy, hepatocytes are not the fastest of cells to complete the cell cycle. Indeed, there can be considerable variation in the time taken to progress from S-phase to mitosis. Extrapolating from data reported by Matsuo et al., hepatocyte mitosis following partial hepatectomy appears to occur 4-12 hours after S-phase.[120] Given that local regulations limit the extent of intravital imaging to a maximum of six hours, further consideration may need to be given as to how best to maximise the extent of hepatocyte proliferation that can be imaged. The mVenus reporter predominates from early S-phase right through to M-phase, so if an individual nucleus appears mVenus-positive at the start of an imaging session, it is difficult to know whether this cell is in early S-phase or close to cytokinesis. One clue may lie in the observation that the mVenus signal disperses into the cytoplasm in a proportion of imaged cells. If this does indeed signify the breakdown of the nuclear membrane in preparation for imminent cytokinesis, then a shift in focus onto hepatocytes exhibiting this feature might well assist in optimising the visualisation of hepatocyte division in vivo.

Reconstructing the sinusoidal vasculature from *Cdh5-Cre*-labelled LSECs

As previously demonstrated in Chapter Three, the *Cdh5-Cre* provides a highly efficient way to drive recombination in LSECs. Combination with either the Ai14 or mTmG fluorescent reporter alleles, and tamoxifen induction, results in clear labelling of the entire liver vasculature. Intravital multiphoton microscopy then allows three-dimensional imaging of the sinusoids in their native, perfused state. Repeated imaging of the same mouse, at baseline and throughout the time course of regeneration, offers an excellent means through which to study how sinusoidal structure adapts during regeneration.

Although the currently available image analysis tools can assist in generating visually striking reconstructions of the complex branching structure of the hepatic sinusoids, their ability to analyse such networks remains limited. The Imaris package produces excellent reconstructions of the sinusoidal network in three dimensions, as shown above. However, its

filamentous analysis tools are optimised for neural networks and so do not cope well with the tubular nature of the sinusoids. This limits its analysis to more simplistic, global measures, such as total vascular volume. Conversely, the Angiotool software is able to assess a range of parameters in vascular networks, including vessel length, degree of branching and lacunarity.[169] However, at present this analysis can only be performed on two-dimensional images.

The ability to link sinusoidal analysis with the hepatic regenerative niche is offered by the combination of *Cdh5-Cre*, mTmG and R26Fucci2aR alleles in the same mouse. Whilst this provides the opportunity to home in on sinusoids contouring cycling hepatocytes, it again poses its own challenges. Practically, mVenus and eGFP have overlapping emission spectra, so accurate vascular reconstruction for analysis would require prior masking of all mVenus-positive nuclear signal. This is certainly feasible, particularly given the different shape of the spherical nucleus and the linear LSEC. However, an alternative would be to make use of another LSEC reporter protein, with different excitation or emission spectra. Injectable dyes have also been used to label the hepatic vasculature,[233] but their administration would add an additional layer of procedural complexity, and adequate signal may not endure repeated imaging over a number of days. Philosophically, there remains the question of how to define whether or not a particular sinusoid, or part thereof, contributes to the regenerative niche. This might prove easier in acetaminophen-induced liver injury, with its distinct centrilobular focus. However, it would still be necessary to produce objective criteria on which to make any distinction, and confirm the cell cycle status of hepatocytes surrounding the sinusoid on all sides.

The inducible nature of the *Cdh5-Cre* allows the exciting possibility of teasing apart how sinusoidal angiogenesis occurs during liver regeneration. Titration of tamoxifen induction to achieve sufficient, but sparse, labelling of LSECs with the stochastic, multi-colour Confetti reporter should enable assessment of whether all LSECs have equal proliferative potential or if instead there are a subset of 'progenitor' LSECs, in a restricted anatomical niche. A similar approach could also be applied to other cell populations in the liver.

Measuring hepatic blood flow at the level of the sinusoid

Both label-free imaging of red blood cells with CARS and fluorescent staining of donor red blood cells were explored as a means of assessing sinusoidal blood flow. Although a CARS-based technique has the advantage of initial simplicity, the variability in the quality of signal

hampered repeatable analysis at depth. Red blood cell velocity in the hepatic sinusoid can be calculated following administration of labelled red blood cells and adapting the measurement technique previously utilised to measure blood flow in tumours of the brain.[170] Further optimisation to the donor protocol is required. Current labelling efficiency is relatively poor, with only around half of the donor red blood cells exhibiting positive staining when imaged prior to injection into recipient mice. It also appears that, although labelled cells can be detected in the sinusoids at least seven days after injection, donor red blood cells may have a decreased lifespan in the circulation or be more prone to sequestration within the liver and subsequent macrophage phagocytosis. These factors, combined with the obvious dilutional effect that occurs when 100μL of labelled cells in suspension are injected into the entire circulating blood volume, mean that timelapse imaging of individual sinusoids must be performed over 10-15 minutes to produce sufficient events for quantification. This therefore limits the number of sinusoids in which red blood cell velocity can be assessed during each recovery imaging session. We plan to improve donor red blood cell labelling efficiency through use of mice carrying the miR-144/451^{eGFP} allele, in which all red blood cells are labelled with eGFP.[234]

Analysis of pilot data revealed that sinusoidal red blood cell velocity appears to increase after partial hepatectomy but not acetaminophen-induced liver injury. The values obtained are of the same order of magnitude as those reported in a previous study comparing sinusoidal red blood cell velocities of uninjured rats and those in which partial portal branch ligation had been performed.[235] However, velocities a factor of ten slower were reported in two much older studies of sinusoidal red blood cell velocities in rats and mice.[236,237] Clearly, these preliminary findings need further interrogation. However, they are not overly surprising at a global level, given that after two-thirds partial hepatectomy it is reasonable to assume that the same volume of blood is forced to pass through one-third of the original volume of parenchyma. Conversely, despite the marked tissue injury which occurs following acetaminophen, the total volume of liver tissue remains the same. Direct comparison of the sinusoidal flow between the two models is challenging but could shed light on the role that changes in sinusoidal blood flow play in driving the hepatocyte regenerative response. What will also be interesting to examine is how sinusoidal blood flow varies within the hepatic lobule, particularly between areas of greater and lesser injury, and how differences in red blood cell velocity relate to hepatocyte proliferation. As with analysis of the sinusoidal vasculature itself, making the distinction between injured and uninjured, or more or less

regenerative, areas of liver should ideally be objective. This may require use of a more localised model of injury, such as focal thermal injury,[238] but would still benefit from the advantages offered by AIW implantation and intravital multiphoton microscopy throughout the time course of regeneration.

As well as consideration of the injury model, the potential effects of anaesthesia on blood flow should not be neglected. Despite the ability of isoflurane to produce dose-dependent vasodilation and hypotension systemically, in the hepatic sinusoid it appears to cause sinusoidal narrowing, although the effects on blood flow are offset by increased red cell velocity.[239] The use of anaesthesia during intravital microscopy is not optional. Isoflurane is currently the agent of choice because of its overall safety profile and the ability to titrate its administration readily to the lowest effective dose. Fortunately, the non-invasive and non-stimulatory nature of multiphoton microscopy via an AIW means that extremely low inspired fractions of isoflurane can be administered. Imaging at multiple time points also means that each mouse is able to act as its own experimental control, with relative changes in sinusoidal flow more important than the absolute values.

The method used to calculate red blood cell velocity, as a surrogate measure of sinusoidal blood flow, is validated but relatively simplistic. Post-acquisition modelling of sinusoidal blood flow, taking into account sinusoidal morphology as well as red blood cell velocity, may provide additional information, such as estimation of shear forces at the sinusoidal wall.[240] Such parameters may play a greater role than red blood cell velocity alone in the regenerative process.

Intravital imaging of hepatic metabolism

The primary function of the liver is metabolism. As such, real-time imaging of metabolic processes during liver injury and regeneration, using intravital microscopy, allows assessment of hepatic health and functional capacity at a cellular level. The CARS images and subsequent analysis presented above demonstrate the feasibility of imaging hepatic lipid, following partial hepatectomy, in vivo and in three dimensions. Indeed the consistency between mice at each time point is striking and bodes well for future studies. Not only does multiphoton microscopy permit the three-dimensional imaging of lipid stores, at multiple time points during regeneration, it negates possible issues with post harvest processing artefact.

It may be purely coincidental that parenchymal lipid peaks at the time of peak hepatocyte proliferation following partial hepatectomy, but this is an observation that merits further consideration. It is certainly feasible to relate hepatocyte lipid stores to cell cycle status, by acquiring CARS images following partial hepatectomy in Fucci reporter mice. The only practical inconvenience under the current setup is that a manual adjustment to the mirror cubes is required between acquiring Fucci and CARS signals. Sequential acquisition and post-imaging reconstruction is still possible.

More precise, molecular assessment of liver metabolism has also been reported, although not yet applied to liver regeneration per se.[154] Most commonly, this utilises the intrinsic, but variable, fluorescent properties of molecules such as NADH (nicotinamide adenine dinucleotide hydride), NADPH (nicotinamide adenine dinucleotide phosphate) and FAD (flavin adenine dinucleotide). The degree of fluorescence of these molecules alters with redox state and therefore its measurement allows assessment of cellular metabolism. An additional microscopy technique, fluorescence lifetime imaging (FLIM), can be performed using multiphoton microscopy. This technique creates an image from the lifetime of an emitted signal, rather than its intensity. In the context of liver metabolism, it allows distinction between the protein-bound, mitochondrial NADH/NADPH, involved in the production of ATP via aerobic respiration, and the free, cytosolic NADH/NADPH, that contributes to anaerobic glycolysis.

Intravital microscopy of hepatic stellate cells

The PBAG reporter mouse provides an excellent means through which to observe HSCs during liver injury and regeneration. This is most informative when combined with one or more additional fluorescent labels since it allows the interaction of HSCs with other cell types in the liver to be clearly observed. The *Cdh5-Cre*;PBAG;Ai14 mouse allows examination of the interaction between HSCs and LSECs, whilst combining PBAG and non-recombined mTmG would permit HSCs and hepatocytes to be imaged simultaneously. The incorporation of the Fucci reporter allele, in addition to PBAG and mTmG, permits assessment of HSCs in relation to cycling hepatocytes. Unlike the challenges of defining whether a sinusoid is within the regenerative niche, it would be relatively simple to measure HSC distance from the nearest cycling hepatocyte, even in three dimensions.

Whilst HSCs are well-known to be a central mediator of hepatic fibrosis, as the principal collagen-producing cells in the liver,[241,242] their role in liver regeneration is less clear. The

PBAG reporter facilitates the study of their behaviour following partial hepatectomy or acetaminophen-induced liver injury. Although the PBAG reporter is primarily useful as a means to identify HSCs, its strong cytoplasmic eGFP expression could be used to detect the morphological changes that typically accompany activation. Similarly, the retinoic acid droplets present in quiescent HSCs are auto-fluorescent and can be imaged using multiphoton microscopy.[142,147] As HSCs activate to a myofibroblast phenotype, they have been reported to lose vitamin A,[243] so the degree of auto-fluorescence could potentially be used to assess HSC activation status in vivo.

The explanation for the increased PBAG-positive cells observed peripherally, at the level of the liver capsule, is unconfirmed. An obvious biological explanation for increased numbers of peripheral HSCs is not immediately apparent, but should not be ruled out. Mesothelial cells, which form a layer of squamous epithelium on the surface of the liver, have been suggested as a source of HSCs in a mouse model of liver fibrosis.[244] Mesothelial cell expression of PDGFRβ has not been widely reported, although they have been shown to express other HSC markers, including PDGFRα.[245] The current literature has focused on the potential of mesothelial cells to act as mesenchymal progenitors during development and after liver injury.[245] Whether the increased number of PBAG-positive cells observed near the surface of the liver does indeed represent mesothelial cells, with potential to differentiate into HSCs and trickle centrally into the liver parenchyma, would need to be confirmed through assessment of further mesothelial cell marker expression and ideally a fate-mapping experimental approach. Given that the increased number of superficial PBAG-labelled cells was also present on imaging of freshly harvested, uninjured, whole liver, this might suggest that mesothelial cells act as a source of HSCs during homeostasis as well as following injury.

Intravital microscopy of inflammatory cell populations in liver injury and regeneration

The role of inflammatory cells in the response to liver injury is a dynamic process which is ideally suited to study with intravital microscopy techniques. Most, if not all, intravital microscopy studies of inflammatory cell populations in liver injury have thus far been performed following externalisation of the liver.[213,233,238,246] This obviously limits the study to a single imaging session per mouse, with a resultant focus on the immediate inflammatory response to injury. Imaging of hepatic inflammatory cell populations via the AIW permits

their study at multiple stages during both the initial inflammatory response and subsequent regenerative phase.

The MacGreen reporter allele was examined as a potential fluorescent labelling strategy for macrophages. However, intravital microscopy following acetaminophen-induced liver injury suggested frequent labelling of neutrophils in addition to macrophages. Expression of eGFP in both neutrophil and dendritic cell populations has been reported in MacGreen reporter mice, in which eGFP expression is driven by the promoter for the colony-stimulating factor 1 receptor.[230,231] This lack of specificity clearly limits the utility of such a strategy to target macrophages alone. A LysM-Cre has also been used to drive highly efficient recombination in macrophages, but suffers from the same drawback of concomitant neutrophil targeting.[247]

At present, antibody labelling strategies may be the most specific means through which to label macrophages and macrophage subpopulations in vivo.[143] Looking beyond the challenges of transgenic targeting of the entire macrophage population, labelling restricted macrophage subpopulations would offer greater clarity as to their differing roles. In particular, the ability to target Kupffer cells, the resident macrophage within the liver, would greatly assist in expanding our knowledge of their functions in liver injury and repair. Recently, *Clec4f* has been identified as a Kupffer cell-specific gene.[181] A mouse containing a *Clec4f-Cre* construct has been generated, and the first publications using this targeting strategy are eagerly anticipated.

Using AIW and multiphoton microscopy to visualise liver regeneration with subcellular resolution

Whilst the combination of AIW insertion and multiphoton microscopy revolutionises our ability to study liver regeneration in situ, it is not without its own challenges and limitations. For example, the current multiphoton setup, with two laser lines and four detectors, limits the breadth of simultaneous multi-fluorophore image acquisition to below that of many confocal microscopy systems. The multiphoton system was optimised for CARS imaging when built and, as a result, does not perform particularly well at the lower and upper extremes of wavelengths detectable with light microscopy. A further limitation is the fact that most transgenic fluorescent reporter and intravital labelling systems have traditionally focused on proteins with emission spectra in the red and green regions of the visible light spectrum. The simultaneous detection of nuclear mCherry and cell membrane tdTomato is relatively easy to

differentiate with the human eye, but resolving these signals for automated image analysis and quantification is challenging.

Further improvement is also possible in several aspects of the image acquisition process, the result of which will be more consistent, biologically-relevant, analysable images. At present, the two biggest limitations to repeatable, high-quality image acquisition are loss of contact between liver and coverslip, and tissue movement during imaging. The former is reduced by improved surgical technique, and optimising AIW design and coverslip preparation, as described in Chapter Five. The latter is reduced by improved stabilisation of the AIW during imaging, also discussed previously, and better titration of anaesthetic depth. Improved anaesthetic monitoring, with measurement of heart rate, pulse oximetry and temperature, not only facilitates maintenance of the lightest possible plane of general anaesthesia, but also maximises consistency between experimental animals and imaging sessions. Together these improvements should result in images that are of sufficient quality for analysis. However, should further post-acquisition processing be required, it is possible to correct movement artefact, both between and within images.[149,150,248]

The underlying principles of the multiphoton technique, with image generation on a per-voxel basis, do place a limit on the rate at which images can be acquired with acceptable resolution. Whilst more than adequate for imaging the architecture of the liver as a whole, and most of the dynamic processes such as cell cycling, it is not able to track fast-moving objects, such as red blood cells in the sinusoids. Matching scan speed to red blood cell velocity offers a workaround to facilitate estimation of velocity. Additionally, high-speed video imaging of blood flow in the superficial sinusoids that are visible via epifluorescence microscopy, available as part of the current multiphoton setup, could offer complementary information.

The varied opportunities offered by the wide range of transgenic reporter alleles are described in detail above. So too is the potential for CARS imaging of parenchymal morphology, red blood cells, and hepatic lipid. However, the second label-free imaging capability provided by multiphoton microscopy, that of SHG, was not explored to its full potential. SHG can be used to detect collagen and is therefore ideally suited to imaging the capsule of the liver and the extracellular matrix. Although extracellular matrix changes do occur during acute liver injury and subsequent regeneration, little or no signal was detected within the liver parenchyma within the first three to seven days following partial hepatectomy or acetaminophen administration. As such, utilisation of this modality is best suited to study of the behaviour of the liver capsule itself or for intravital microscopy of models of liver

disease which generate a more marked fibrotic response, such as bile duct ligation or chronic carbon tetrachloride administration. Intravital imaging of chronic liver disease via an AIW could be extremely informative, but would require demonstration of the feasibility of long-term maintenance of mice with AIWs and the ability to achieve consistently usable images over an extended period. Alternatively, it should be possible to develop a model of late implantation of the AIW, after the onset of chronic liver injury. Even without deposition of significant parenchymal collagen, visualisation of the liver capsule using SHG serves as a useful reference point both for image acquisition and during subsequent analysis.

Although AIW implantation itself is minimally invasive, and does not appear to have major effects on liver injury and subsequent hepatocyte proliferation (see Chapter Five and the work of Alexandra Thompson[214]), the presence of cyanoacrylate adhesive, a titanium implant, and a glass coverslip (albeit with a biologically inert coating) may have local effects at the liver capsule and parenchyma immediately underlying it. Careful handling of the liver during AIW implantation and subsequent changing of the coverslip is required to minimise any superficial trauma and biofilm accumulation. Uninjured controls at every imaging time point are also essential to be able to determine confidently whether the observed findings are a result of the model of liver injury or simply the presence of the AIW alone.

A disadvantage of the experimental model of partial hepatectomy and AIW implantation is the inability to obtain baseline images prior to liver injury. Within the current setup, there is also an enforced delay of twenty-fours between surgery and imaging, on welfare grounds and because of the need to transfer experimental animals to the imaging facility. These issues could be surmounted, at least in part, by situating imaging facilities within the animal units themselves, allowing surgery and imaging to be performed under the same general anaesthetic.

Studying liver regeneration using intravital multiphoton microscopy, in combination with a wide range of cellular, structural and dynamic labels, is an exciting technique with huge potential. However, it results initially in primarily descriptive data, following the time course of injury and subsequent regeneration and making comparisons between time points or the uninjured state. Whilst this alone may suggest novel therapeutic targets or interventions, the true benefit will come from formulating and testing the hypotheses that result from these observations. These same experimental models are also ideally suited to examine the effects of targeted genetic depletion or administration of exogenous substances on the dynamics of liver regeneration, in real time and at high resolution. However, the

volume of data that such studies generate and the importance of efficient, high-fidelity image analysis workflows must not be under-estimated. Appropriate systems must be in place to reap the maximum benefit from these experimental models.

Summary

The ability to combine intravital multiphoton microscopy with two different mouse models of liver injury and regeneration, and multiple combinations of fluorescent reporter alleles, provides extraordinary capacity to study multiple facets of the regenerative process, often simultaneously. Key benefits include the ability to image the same animal repeatedly during the time course of liver regeneration, at subcellular resolution. This permits evaluation of dynamic processes, including cellular metabolism and sinusoidal blood flow. Combinations of cellular labels facilitate visualisation of cellular interactions during regeneration. Fluorescent labelling of cell cycle stage offers the opportunity to study the microenvironment around proliferating hepatocytes. This will allow us to both deepen and expand our understanding of how the injured liver coordinates the regenerative response. Having identified novel mechanisms and potential therapeutic targets, these intravital systems provide an ideal means through which to demonstrate how targeted intervention can promote liver regeneration.

Chapter 7 – Reflections and future work

Introduction

The ultimate goal of the body of work described in this thesis was to improve our understanding of, and ability to study, the process of liver regeneration. Progress in this field is essential because of the huge global burden of liver disease and the lack of effective therapies, other than liver transplantation, for both acute and chronic liver failure. The concept of encouraging the sick liver to heal itself is an attractive one, given the extraordinary regenerative potential of the healthy organ. Our current inability to intervene effectively in this regard is frustrating and renders even more stark the bleak irony that this remarkable organ fails completely when we need it most.

The role of αv integrins in liver regeneration was explored because of recent evidence that they promote the development of liver fibrosis.[29] In chronic liver disease the development of collagen-rich scar tissue goes hand in hand with the loss of functional capacity. As such, potential therapies that can reduce or reverse fibrosis whilst simultaneously promoting hepatocyte proliferation and restoration of functional liver mass are particularly attractive. The vast majority of studies examining αv integrins show that their primary role is to activate latent TGFβ. In the context of liver fibrosis, TGFβ is a major pro-fibrotic cytokine, so it is reassuring that depleting or inhibiting HSC αv integrins has been demonstrated to lead to a reduction in fibrosis through a decrease in the amount of active TGFβ.[29] There is also a historical body of literature demonstrating the growth-inhibitory effect of TGFβ on epithelial cells, including hepatocytes. Therefore, it is eminently feasible that αv integrin-mediated activation of TGFβ could regulate hepatocyte proliferation following liver injury. This might also explain, at least in part, why the restoration of functional capacity fails in the TGFβ-rich environment of the end-stage liver.

Alongside attempts to improve our understanding of the molecular regulation of hepatocyte proliferation and liver regeneration, it is important that the field takes advantage of technological advances that offer the potential for new insight into liver regeneration. Multiphoton microscopy is arguably the best technology currently available to study the regenerative process at a subcellular level because it facilitates intravital imaging and offers additional imaging modalities not available using standard confocal techniques. Liver regeneration is a process ideally suited to intravital study. It is a dynamic process, requiring

multicellular coordination, that in rodent models completes over a concise period of time. Thus, there is the potential to reap great scientific benefit by studying how the liver regenerates in three dimensions, in the living animal, from start to finish. Equally, intravital imaging of liver regeneration does present its own challenges. Principally, these comprise achieving induction of sufficient liver injury to kick-start the regenerative process in conjunction with obtaining artefact-free access to the in situ regenerating liver, in a manner which does not significantly impact either the welfare of the experimental animal or the regenerative response under study.

Integrin αvβ8 in liver regeneration

Depletion of integrin αvβ8 on hepatocytes leads to increased hepatocyte proliferation and accelerated liver regeneration in the mouse partial hepatectomy model of liver regeneration. This appears to be primarily an autocrine effect, since targeted depletion of HSC integrin αvβ8 did not lead to the same phenotype. LSECs do not appear to express integrin αvβ8, at least in the uninjured liver. Kupffer cell expression of integrin αvβ8 was not examined in this body of work and, although they too may not express this particular integrin,[43] it would be preferable to confirm this.

Unfortunately, the same positive effect on hepatocyte proliferation of hepatocyte integrin αvβ8 depletion was not seen at 48 hours after acetaminophen-induced liver injury, nor when a β8 integrin subunit blocking antibody was administered to wild-type mice at the time of partial hepatectomy. Possible reasons for the failure to recapitulate the previously observed positive effects on liver regeneration are discussed in detail in Chapter Three. Whilst these findings could be seen as disappointing, they do not necessarily sound the death knell for integrin αvβ8 as a potential therapeutic target to promote liver regeneration. However, an improved understanding of the precise circumstances in which targeting integrin αvβ8 can promote liver regeneration is required before this integrin can be confidently put forward as a viable therapeutic target.

It is reassuring that human hepatocytes appear to express integrin αvβ8 in both health and disease. One option for further study would be to examine the effects on proliferation of inhibiting integrin αvβ8 in human hepatocytes. Clearly this would need to be performed in vitro in the first instance. Primary human hepatocytes may be challenging to obtain and

maintain in culture, so human hepatocyte cell lines might need to be utilised. This would bring its own set of caveats to any findings.

An alternative would be to continue to assess the pro-regenerative effect of hepatocyte integrin αvβ8 depletion or inhibition in animal models. Acute carbon tetrachloride injury is a relatively straightforward model of liver injury and regeneration that could be examined. A more challenging, but potentially more informative and translationally relevant, model would allow examination of hepatocyte proliferation in the context of liver fibrosis. Chronic carbon tetrachloride or thioacetamide administration are both commonly used to study liver fibrosis. Alone, their use may not result in sufficient stimulation of hepatocyte proliferation to enable detection of a pro-regenerative phenotype following integrin αvβ8 depletion or inhibition. However, an additional stimulus, such as partial hepatectomy or a one-off increased dose of carbon tetrachloride, could be employed after fibrosis has been established, to promote an adequate regenerative response. Such models have been previously reported.[249] Were an intervention such as integrin αvβ8 inhibition shown to be both anti-fibrotic and pro-regenerative, there would certainly be keen interest in attempting to develop it into a therapy for chronic liver disease.

The αv integrins share a common feature, the RGD binding domain, which allows them to activate latent TGFβ. However, as we gradually piece together the subtleties that distinguish individual members of the αv integrin family, it is apparent that the different αv integrins are not interchangeable. The combination of their molecular structure, and cellular and temporal expression patterns, results in members of the αv integrin family having distinct, and potentially unique, functions. It would be intellectually interesting to examine whether hepatocyte depletion of other αv integrins in isolation also results in a pro-regenerative phenotype. However, the time and cost of such an enterprise, particularly if one were to characterise the entire time course of regeneration following partial hepatectomy in each case, prevented this from being undertaken in the present body of work. To investigate the pro-regenerative potential of integrin αvβ8 on other hepatic cell types, assessment of hepatocyte proliferation at a single time point was performed. This is justifiable, since if any effect on regeneration were to occur, one would expect it to be most evident around the time of peak hepatocyte proliferation in this model. However, it should be borne in mind that such an approach takes only a single snapshot of the regenerative process, and differential effects at both earlier and later time points could occur. This emphasises the need for, and benefit of,

experimental systems in which multiple time points during liver regeneration can be assessed in the same experimental animal.

Mechanistic studies of hepatocyte integrin αvβ8

Uncovering and validating a phenotype forms only half of a scientific story; it is always preferable to be able to confirm the explanation for an observed effect. In the case of integrin αvβ8 regulating hepatocyte proliferation, there was an obvious mechanistic candidate: the TGFβ signalling pathway. Given that multiple studies have shown the primary role of integrin αvβ8 to be activation of latent TGFβ, and active TGFβ is well-documented as a repressor of hepatocyte proliferation, it seemed but a small matter to demonstrate that integrin αvβ8 on hepatocytes was performing its expected function. To misquote Shakespeare: the course of true science never did run smooth.

The mRNA expression time course for hepatic integrin αvβ8 matches precisely what might be expected of a cell surface molecule with a homeostatic role in the regulation of proliferation. Immediately following partial hepatectomy, with the liver suddenly bereft of sufficient hepatocytes, expression of *Itgb8* reduces, potentially releasing a tonic brake on hepatocyte proliferation. Subsequently, not only does *Itgb8* expression return to normal, but in the later phase of liver regeneration it increases 10-fold, suggesting it may have a role in terminating the regenerative response as the liver approaches its pre-injury mass.

Unfortunately, despite multiple attempts, it was not possible to demonstrate hepatocyte activation of TGFβ in vitro. This raises more questions than it provides conclusive answers. Could this be simply a technical or operator error with the performance of the assays themselves? The reporter cell system was certainly responsive when active TGFβ was supplied, but TGFβ activation by an HSC cell line was not detected, discordant to what might have been expected. Do hepatocytes not activate sufficient TGFβ for detection? Whilst this is always possible, the assays themselves do appear to be reasonably sensitive, capable of detecting levels of active TGFβ as low as 1pg/mL. Is it possible to accept, at least in part, the 'null' hypothesis and conclude that hepatocyte integrin αvβ8 does not promote hepatocyte proliferation and liver regeneration through activation of TGFβ? Or could it be that, whilst hepatocyte integrin αvβ8 is capable of activating TGFβ, hepatocytes themselves are even better at binding it? Certainly, the proposed mechanism requires that the TGFβ that is activated by hepatocyte integrin αvβ8, binds and signals directly, in an autocrine manner.

These challenges with detecting changes in amounts of active TGFβ in the environs of the hepatocyte led to the attempts to demonstrate alterations in hepatocyte TGFβ signalling. Again, this proved taxing. Canonical TGFβ signalling does occur in hepatocytes following partial hepatectomy, as demonstrated by the detection of nuclear pSMAD3. Unsurprisingly, however, this is not a highly active pathway, particularly around the time of peak hepatocyte proliferation. As such, demonstrating a reduction in signalling, when the baseline is already low, is not easy. This likely also explains why the effects of integrin αvβ8 inhibition on TGFβ-responsive genes, as assessed in the custom qPCR array, were predominantly small. The inhibition of tonically active TGFβ signalling, in uninjured primary hepatocytes, would not be expected to result in mirror-image changes of the same magnitude that occur when exogenous active TGFβ is provided to hepatocytes.

On a more positive note, the finding that inhibition of hepatocyte integrin αvβ8 leads to increased expression of *Plat*, the gene encoding tPA, does provide a possible mechanism through which liver regeneration might be promoted. Not only is tPA expression responsive to TGFβ, tPA has been demonstrated to activate HGF, one of two direct hepatocyte mitogens. As well as confirming this observation at the protein level, it would be interesting to assess levels of tPA activity in post-partial hepatectomy liver tissue, in both control and *Itgb8*$^{flox/flox}$*;Alb-Cre* mice. It would be expected that the latter mice would show increased levels of active tPA at the same time as, or preceding, increased hepatocyte proliferation.

Developing models to study liver regeneration using intravital microscopy

The benefits of studying liver regeneration through an intravital imaging approach have been repeatedly extolled throughout the preceding chapters. However, in order to undertake such studies it was necessary to develop and validate an appropriate experimental model. Partial hepatectomy in the mouse is a widely-used model of liver regeneration, and the possibility of adapting the standard technique to allow placement of an AIW for subsequent intravital multiphoton microscopy was explored and subsequently validated.

Hepatocyte proliferation does not significantly differ between standard partial hepatectomy and the modified procedure that was developed. Nor was it altered by the presence of the AIW. However, a degree of increased weight loss was seen at the seven-day time point, combined with a reduction in total liver weight. If this is primarily due to the initial

procedure itself, or a reduction in food intake in the post-surgical period, then it should be possible to reduce or even eliminate this difference with improved experience and supportive husbandry measures. Future work could repeat the original validation studies to contribute additional data and assess the effect of increased experience. Nevertheless, the modified partial hepatectomy and AIW implantation technique does appear to drive sufficient hepatocyte proliferation and liver regeneration in the AIW lobe to allow study of the regenerative process.

Improvements in the design of both the AIW and the imaging baseplate were necessary, in order to maximise the success of the two liver regeneration models and obtain high-quality intravital images for analysis. This process provided exposure to the world of product design and engineering, and salient lessons in pursuing such endeavours. Most of all, it highlighted that a thorough understanding of the model and the key features of the product being designed are critical to a successful outcome. Furthermore, with every improvement there may be potentially negative consequences that should be considered in advance. For example, the changes to the external diameter of the AIW and the depth of the central groove were instituted to assist with bringing the liver lobe closer to the coverslip and anchoring the AIW in the imaging baseplate. However, in combination, they make seating the purse string suture within the AIW groove, a critical step in the implantation procedure, more challenging. The earlier modification that moved the coverslip onto a removable inlay facilitates its replacement but compromises contact with the liver surface. It would be interesting to explore the possibility of completely re-designing the AIW. The key features of any new version should be ease of implantation, biological inertia (including of the optical window), and minimising the distance between the liver and the microscope objective. Advances in three-dimensional printing in plastic, and laser-controlled machining, facilitate prototype development and relatively inexpensive production.

Possibly the most interesting finding from the early work optimising the two models of liver injury and AIW implantation was the reduction in acetaminophen-induced liver injury in mice receiving additional periods of general anaesthesia for intravital imaging. Unfortunately, there was not the opportunity to explore this potentially novel phenotype further, but it could be investigated relatively easily. In the first instance, one could simply compare liver injury in mice receiving acetaminophen with or without a prior period of general anaesthesia with isoflurane. Were a reduction in injury confirmed, then as well as dissecting the underlying mechanism, it would be fascinating to see whether a protective

effect could also be translated into a therapeutic one. Isoflurane is used on a daily basis in human medicine, so would be extremely easy to re-purpose.

Intravital multiphoton microscopy of liver regeneration

The development, validation and refinement of two models of AIW implantation and liver injury allow intravital multiphoton microscopy of liver regeneration. The extraordinary breadth of transgenic strategies now readily available to label specific cells or structures in mice, combined with exogenous labelling techniques and the label-free imaging possibilities of multiphoton microscopy, open numerous, exciting avenues for exploration. Indeed, when contemplating the range of opportunities now available, the feeling is akin to that of a child in a toy shop before Christmas. The true challenge lies in determining how to derive the best value from the many possible investigations that could be performed with these techniques. The route to surmounting this lies in defining precise research questions, the answers to which will advance our knowledge of liver regeneration.

The Fucci cell cycle label is an extremely useful tool, as it enables the investigator to focus their attention on individual cells at the most relevant time point. Observing an individual hepatocyte dividing, in situ, may be somewhat indulgent, but could reveal interesting features that invite further study, particularly because of the heterogeneity that hepatocytes display with regard to nucleus number and ploidy. More immediately, the Fucci label offers the ability to distinguish regions of increased hepatocyte proliferation and compare these contemporaneously with less proliferative areas in the same liver.

In addition to observing cycling hepatocytes, fluorescent labelling of cells themselves permits morphological assessment. Integral to the process of regeneration is the preceding injury. Although only touched upon in this body of work, the changes that occur in hepatocytes in response to acetaminophen, ultimately leading to necrosis, would be extremely interesting to characterise in the living mouse, particularly with the option to track the behaviour of inflammatory cell populations simultaneously. Observing the interaction of two or more labelled cell types in their native environment is one of the opportunities offered by intravital microscopy.

Along with the Fucci reporter mouse, the *Cdh5-Cre* allele stands out as a particularly useful genetic tool. For an inducible Cre, the recombination observed following tamoxifen administration is extremely impressive. It permits fluorescent labelling of the entire sinusoidal

network, allowing assessment of the changes that occur in this complex structure during liver injury and regeneration. The ability to obtain three-dimensional images of perfused sinusoids in the living organism could also be used to help construct in silica models of sinusoidal flow. Not only would this potentially reduce experimental animal use in the future, its combination with data on the cell cycle status of surrounding hepatocytes could be used to explore how modulating sinusoidal flow might promote hepatocyte proliferation and liver regeneration.

Until such time as accurate computer models of cell behaviour and blood flow in the liver exist, intravital microscopy is really the only way to study these dynamic processes. Ultimately, liver function is entirely a product of blood flowing through the sinusoid, so understanding the haemodynamic alterations that occur during liver injury and regeneration is critical, in order to uncover ways in which we can promote hepatic function and regeneration following injury. Hepatic metabolism goes hand in hand with sinusoidal perfusion, and this again is another field in which intravital multiphoton microscopy comes into its own. There is no other means to assess the metabolic state and activity of a hepatocyte in its native environment over the time course of liver injury and regeneration. Optimising the multiphoton system that was used in the current work, to be able to perform fluorescence lifetime imaging and obtain information about the metabolic state of individual hepatocytes during liver regeneration would provide extremely useful data and allow real-time assessment of how hepatocyte function responds to injury and therapeutic intervention.

Concluding remarks

These forays into researching liver regeneration hopefully demonstrate the fascinating, exquisitely controlled processes at play in the response to liver injury. It is also apparent that teasing apart the key molecules contributing to the regulation of the regenerative process can be challenging and at times frustrating. Hepatocyte integrin $\alpha v\beta 8$ contributes to the regulation of hepatocyte proliferation, but whether this can be translated into a therapeutic approach which can promote regeneration of a patient's own liver remains to be seen. It also proved difficult to elucidate the precise mechanism through which targeting integrin $\alpha v\beta 8$ produced the pro-regenerative effect. In part, this was due to the need to abstract hepatocytes from their native environment within the regenerating liver, in order to examine potential mechanistic pathways. The development of systems that allow direct observation of liver regeneration, at subcellular resolution, paves the way for studies that assess individual cellular or signalling

responses as they occur in the model organism. In the future, it may even be possible to move beyond experimental animal models, and utilise these systems to examine the cellular intrigues at play in the livers of patients themselves.

Bibliography

1. Schuppan, D. & Kim, Y. O. Evolving therapies for liver fibrosis. *J Clin Invest* **123,** 1887–1901 (2013).
2. Seitz, H. K. & Stickel, F. Risk factors and mechanisms of hepatocarcinogenesis with special emphasis on alcohol and oxidative stress. *Biol. Chem.* **387,** 349–360 (2006).
3. Institute for Health Metrics and Evaluation (IHME). GBD Compare Data Visualization. *Seattle, WA: IHME, University of Washington, 2016* Available at: http://vizhub.healthdata.org/gbd-compare. (Accessed: 13 July 2017)
4. European Association for Study of the Liver. HEPAMAP: Prospects for Liver Disease Research in the EU. *www.easl.eu* (2014). Available at: http://www.easl.eu/medias/EASLimg/News/3f9dd90221ef292_file.pdf. (Accessed: 13 July 2017)
5. Williams, R. *et al.* Addressing liver disease in the UK: a blueprint for attaining excellence in health care and reducing premature mortality from lifestyle issues of excess consumption of alcohol, obesity, and viral hepatitis. *Lancet* **384,** 1953–1997 (2014).
6. Williams, R. *et al.* Implementation of the Lancet Standing Commission on Liver Disease in the UK. *Lancet* **386,** 2098–2111 (2015).
7. NHS Blood and Transplant. Organ Donation and Transplantation Activity Data: England. *https://www.organdonation.nhs.uk/supporting-my-decision/statistics-about-organ-donation* (2017). Available at: https://nhsbtdbe.blob.core.windows.net/umbraco-assets/1664/england_march17.pdf. (Accessed: 14 July 2017)
8. NHS Blood and Transplant. Organ Donation and Transplantation Activity Data: Wales. *https://www.organdonation.nhs.uk/supporting-my-decision/statistics-about-organ-donation* (2017). Available at: https://nhsbtdbe.blob.core.windows.net/umbraco-assets/1518/wales.pdf. (Accessed: 14 July 2017)
9. Blachier, M., Leleu, H., Peck-Radosavljevic, M., Valla, D.-C. & Roudot-Thoraval, F. The burden of liver disease in Europe: a review of available epidemiological data. *J. Hepatol.* **58,** 593–608 (2013).
10. American Liver Foundation. The Liver Lowdown – Liver Disease: the big picture. *http://www.liverfoundation.org/education* Available at: http://www.liverfoundation.org/education/liverlowdown/ll1013/bigpicture. (Accessed: 14 July 2017)
11. Yokoyama, H. O., Wilson, M. E., Tsuboi, K. K. & Stowell, R. E. Regeneration of mouse liver after partial hepatectomy. *Cancer Res.* **13,** 80–85 (1953).
12. Marcos, A. *et al.* Liver regeneration and function in donor and recipient after right lobe adult to adult living donor liver transplantation. *Transplantation* **69,** 1375–1379 (2000).
13. Stanger, B. Z. Cellular homeostasis and repair in the mammalian liver. *Annu. Rev. Physiol.* **77,** 179–200 (2015).
14. Roskams, T. A. *et al.* Nomenclature of the finer branches of the biliary tree: canals, ductules, and ductular reactions in human livers. *Hepatology* **39,** 1739–1745 (2004).
15. Lu, W.-Y. *et al.* Hepatic progenitor cells of biliary origin with liver repopulation capacity. *Nature Cell Biology* **17,** 971–983 (2015).
16. Malato, Y. *et al.* Fate tracing of mature hepatocytes in mouse liver homeostasis and regeneration. *J Clin Invest* **121,** 4850–4860 (2011).

17. Yanger, K. *et al.* Adult hepatocytes are generated by self-duplication rather than stem cell differentiation. *Cell Stem Cell* **15,** 340–349 (2014).
18. Hynes, R. O. Integrins: bidirectional, allosteric signaling machines. *Cell* **110,** 673–687 (2002).
19. Munger, J. S., Harpel, J. G., Giancotti, F. G. & Rifkin, D. B. Interactions between growth factors and integrins: latent forms of transforming growth factor-beta are ligands for the integrin alphavbeta1. *Mol. Biol. Cell* **9,** 2627–2638 (1998).
20. Munger, J. S. *et al.* The integrin alpha v beta 6 binds and activates latent TGF beta 1: a mechanism for regulating pulmonary inflammation and fibrosis. *Cell* **96,** 319–328 (1999).
21. Mu, D. *et al.* The integrin alpha(v)beta8 mediates epithelial homeostasis through MT1-MMP-dependent activation of TGF-beta1. *The Journal of Cell Biology* **157,** 493–507 (2002).
22. Asano, Y. *et al.* Increased expression of integrin alpha(v)beta3 contributes to the establishment of autocrine TGF-beta signaling in scleroderma fibroblasts. *J. Immunol.* **175,** 7708–7718 (2005).
23. Asano, Y. *et al.* Involvement of alphavbeta5 integrin-mediated activation of latent transforming growth factor beta1 in autocrine transforming growth factor beta signaling in systemic sclerosis fibroblasts. *Arthritis Rheum.* **52,** 2897–2905 (2005).
24. Reed, N. I. *et al.* The αvβ1 integrin plays a critical in vivo role in tissue fibrosis. *Sci Transl Med* **7,** 288ra79–288ra79 (2015).
25. Nishimura, S. L. Integrin-mediated transforming growth factor-beta activation, a potential therapeutic target in fibrogenic disorders. *Am J Pathol* **175,** 1362–1370 (2009).
26. Katsumoto, T. R., Violette, S. M. & Sheppard, D. Blocking TGFβ via Inhibition of the αvβ6 Integrin: A Possible Therapy for Systemic Sclerosis Interstitial Lung Disease. *International Journal of Rheumatology* **2011,** 208219–7 (2011).
27. Goodman, S. L. & Picard, M. Integrins as therapeutic targets. *Trends Pharmacol. Sci.* **33,** 405–412 (2012).
28. Shattil, S. J., Kim, C. & Ginsberg, M. H. The final steps of integrin activation: the end game. *Nat. Rev. Mol. Cell Biol.* **11,** 288–300 (2010).
29. Henderson, N. C. *et al.* Targeting of αv integrin identifies a core molecular pathway that regulates fibrosis in several organs. *Nat Med* **19,** 1617–1624 (2013).
30. Margadant, C. & Sonnenberg, A. Integrin-TGF-beta crosstalk in fibrosis, cancer and wound healing. *EMBO Rep.* **11,** 97–105 (2010).
31. Bledzka, K., Smyth, S. S. & Plow, E. F. Integrin αIIbβ3: from discovery to efficacious therapeutic target. *Circ. Res.* **112,** 1189–1200 (2013).
32. Haussinger, D., Reinehr, R. & Schliess, F. The hepatocyte integrin system and cell volume sensing. *Acta Physiol (Oxf)* **187,** 249–255 (2006).
33. Friedman, S. L. Hepatic stellate cells: protean, multifunctional, and enigmatic cells of the liver. *Physiol. Rev.* **88,** 125–172 (2008).
34. Lu, M. *et al.* Integrin alpha8beta1 mediates adhesion to LAP-TGFbeta1. *J Cell Sci* **115,** 4641–4648 (2002).
35. Liu Tsang, V. *et al.* Fabrication of 3D hepatic tissues by additive photopatterning of cellular hydrogels. *FASEB J.* **21,** 790–801 (2007).
36. Patsenker, E. & Stickel, F. Role of integrins in fibrosing liver diseases. *Am. J. Physiol. Gastrointest. Liver Physiol.* **301,** G425–34 (2011).
37. Wang, B. *et al.* Role of αvβ6 integrin in acute biliary fibrosis. *Hepatology* **46,** 1404–1412 (2007).

38. Patsenker, E. *et al.* Inhibition of Integrin αvβ6 on Cholangiocytes Blocks Transforming Growth Factor-β Activation and Retards Biliary Fibrosis Progression. *Gastroenterology* **135,** 660–670 (2008).
39. Peng, Z. W. *et al.* Integrin αvβ6 critically regulates hepatic progenitor cell function and promotes ductular reaction, fibrosis, and tumorigenesis. *Hepatology* **63,** 217–232 (2016).
40. Acharya, M. *et al.* αv Integrin expression by DCs is required for Th17 cell differentiation and development of experimental autoimmune encephalomyelitis in mice. *J Clin Invest* **120,** 4445–4452 (2010).
41. Lacy-Hulbert, A. *et al.* Ulcerative colitis and autoimmunity induced by loss of myeloid alphav integrins. *Proc Natl Acad Sci U S A* **104,** 15823–15828 (2007).
42. Savill, J., Dransfield, I., Hogg, N. & Haslett, C. Vitronectin receptor-mediated phagocytosis of cells undergoing apoptosis. *Nature* **343,** 170–173 (1990).
43. Travis, M. A. *et al.* Loss of integrin alpha(v)beta8 on dendritic cells causes autoimmunity and colitis in mice. *Nature* **449,** 361–365 (2007).
44. Wheeler, M. D., Yamashina, S., Froh, M., Rusyn, I. & Thurman, R. G. Adenoviral gene delivery can inactivate Kupffer cells: role of oxidants in NF-kappaB activation and cytokine production. *J Leukoc Biol* **69,** 622–630 (2001).
45. Iivanainen, E., Kähäri, V. M., Heino, J. & Elenius, K. Endothelial cell–Matrix interactions. *Microscopy Research and Technique* **60,** 13–22 (2003).
46. Rüegg, C. & Mariotti, A. Vascular integrins: pleiotropic adhesion and signaling molecules in vascular homeostasis and angiogenesis. *Cell. Mol. Life Sci.* **60,** 1135–1157 (2003).
47. DeLeve, L. D. Liver sinusoidal endothelial cells and liver regeneration. *J Clin Invest* **123,** 1861–1866 (2013).
48. Singh, B., Fu, C. & Bhattacharya, J. Vascular expression of the alpha(v)beta(3)-integrin in lung and other organs. *Am. J. Physiol. Lung Cell Mol. Physiol.* **278,** L217–26 (2000).
49. Hegenbarth, S. *et al.* Liver sinusoidal endothelial cells are not permissive for adenovirus type 5. *Hum. Gene Ther.* **11,** 481–486 (2000).
50. Niu, J. X. *et al.* The role of adhesion molecules, alpha v beta 3, alpha v beta 5 and their ligands in the tumor cell and endothelial cell adhesion. *Eur. J. Cancer Prev.* **16,** 517–527 (2007).
51. Li, X. *et al.* Proteomics analysis of plasma membrane from liver sinusoidal endothelial cells after partial hepatectomy by an improved two-dimensional electrophoresis. *Molecular and Cellular Biochemistry* **344,** 137–150 (2010).
52. Lalor, P. F., Herbert, J., Bicknell, R. & Adams, D. H. Hepatic sinusoidal endothelium avidly binds platelets in an integrin-dependent manner, leading to platelet and endothelial activation and leukocyte recruitment. *Am. J. Physiol. Gastrointest. Liver Physiol.* **304,** G469–78 (2013).
53. Liu, J. *et al.* High glucose regulates LN expression in human liver sinusoidal endothelial cells through ROS/integrin αvβ3 pathway. *Environmental Toxicology and Pharmacology* **42,** 231–236 (2016).
54. Cambier, S. *et al.* A role for the integrin alphavbeta8 in the negative regulation of epithelial cell growth. *Cancer Res.* **60,** 7084–7093 (2000).
55. Fjellbirkeland, L. *et al.* Integrin alphavbeta8-mediated activation of transforming growth factor-beta inhibits human airway epithelial proliferation in intact bronchial tissue. *Am J Pathol* **163,** 533–542 (2003).
56. Worthington, J. J., Klementowicz, J. E. & Travis, M. A. TGFβ: a sleeping giant

awoken by integrins. *Trends Biochem. Sci.* **36,** 47–54 (2011).
57. Aluwihare, P. *et al.* Mice that lack activity of alphavbeta6- and alphavbeta8-integrins reproduce the abnormalities of Tgfb1- and Tgfb3-null mice. *J Cell Sci* **122,** 227–232 (2009).
58. Yang, Z. *et al.* Absence of integrin-mediated TGFbeta1 activation in vivo recapitulates the phenotype of TGFbeta1-null mice. *The Journal of Cell Biology* **176,** 787–793 (2007).
59. Fenton, T. M. *et al.* Inflammatory cues enhance TGFβ activation by distinct subsets of human intestinal dendritic cells via integrin αvβ8. *Mucosal Immunol* **10,** 624–634 (2017).
60. Reboldi, A. *et al.* IgA production requires B cell interaction with subepithelial dendritic cells in Peyer's patches. *Science* **352,** aaf4822 (2016).
61. Worthington, J. J. *et al.* Integrin αvβ8-Mediated TGF-β Activation by Effector Regulatory T Cells Is Essential for Suppression of T-Cell-Mediated Inflammation. *Immunity* **42,** 903–915 (2015).
62. Arnold, T. D. *et al.* Excessive vascular sprouting underlies cerebral hemorrhage in mice lacking αVβ8-TGFβ signaling in the brain. *Development* **141,** 4489–4499 (2014).
63. Minagawa, S. *et al.* Selective targeting of TGF-β activation to treat fibroinflammatory airway disease. *Sci Transl Med* **6,** 241ra79–241ra79 (2014).
64. Miyazono, K. Positive and negative regulation of TGF-beta signaling. *J Cell Sci* **113,** 1101–1109 (2000).
65. Buscemi, L. *et al.* The Single-Molecule Mechanics of the Latent TGF-β1 Complex. *Current Biology* **21,** 2046–2054 (2011).
66. Shi, M. *et al.* Latent TGF-β structure and activation. *Nature* **474,** 343–349 (2011).
67. Dong, X., Hudson, N. E., Lu, C. & Springer, T. A. Structural determinants of integrin β-subunit specificity for latent TGF-β. *Nat. Struct. Mol. Biol.* **21,** 1091–1096 (2014).
68. Dong, X. *et al.* Force interacts with macromolecular structure in activation of TGF-β. *Nature* **542,** 55–59 (2017).
69. Jenkins, R. G. *et al.* Ligation of protease-activated receptor 1 enhances αvβ6 integrin-dependent TGF-β activation and promotes acute lung injury. *J Clin Invest* **116,** 1606–1614 (2006).
70. Xu, M. Y. *et al.* Lysophosphatidic Acid Induces αvβ6 Integrin-Mediated TGF-β Activation via the LPA2 Receptor and the Small G Protein Gαq. *Am J Pathol* **174,** 1264–1279 (2009).
71. Fabregat, I. *et al.* TGF-β Signaling and Liver Disease. *FEBS J.* **283,** n/a–n/a (2016).
72. Wipff, P.-J. & Hinz, B. Integrins and the activation of latent transforming growth factor beta1 - an intimate relationship. *Eur. J. Cell Biol.* **87,** 601–615 (2008).
73. Massagué, J. TGF-beta signal transduction. *Annu. Rev. Biochem.* **67,** 753–791 (1998).
74. Dropmann, A. *et al.* TGF-β1 and TGF-β2 abundance in liver diseases of mice and men. *Oncotarget* **7,** 19499–19518 (2016).
75. Shull, M. M. *et al.* Targeted disruption of the mouse transforming growth factor-beta 1 gene results in multifocal inflammatory disease. *Nature* **359,** 693–699 (1992).
76. Kulkarni, A. B. *et al.* Transforming growth factor beta 1 null mutation in mice causes excessive inflammatory response and early death. *Proc Natl Acad Sci U S A* **90,** 770–774 (1993).
77. Kaartinen, V. *et al.* Abnormal lung development and cleft palate in mice lacking TGF-beta 3 indicates defects of epithelial-mesenchymal interaction. *Nat Genet* **11,** 415–421 (1995).

78. Proetzel, G. *et al.* Transforming growth factor–β3 is required for secondary palate fusion. *Nat Genet* **11,** 409–414 (1995).
79. Sanford, L. P. *et al.* TGF beta 2 knockout mice have multiple developmental defects that are nonoverlapping with other TGF beta knockout phenotypes. *Development* **124,** 2659–2670 (1997).
80. Munger, J. S. *et al.* Latent transforming growth factor-β: Structural features and mechanisms of activation. *Kidney Int* **51,** 1376–1382 (1997).
81. Jenkins, G. The role of proteases in transforming growth factor-beta activation. *Int. J. Biochem. Cell Biol.* **40,** 1068–1078 (2008).
82. Robertson, I. B. & Rifkin, D. B. Regulation of the Bioavailability of TGF-β and TGF-β-Related Proteins. *Cold Spring Harb Perspect Biol* **8,** a021907 (2016).
83. Massagué, J. TGFβ signalling in context. *Nat. Rev. Mol. Cell Biol.* **13,** 616–630 (2012).
84. Budi, E. H., Duan, D. & Derynck, R. Transforming Growth Factor-β Receptors and Smads: Regulatory Complexity and Functional Versatility. *Trends Cell Biol.* **27,** 658–672 (2017).
85. Zhang, Y. E. Non-Smad Signaling Pathways of the TGF-β Family. *Cold Spring Harb Perspect Biol* **9,** a022129 (2017).
86. Giannelli, G., Mazzocca, A., Fransvea, E., Lahn, M. & Antonaci, S. Inhibiting TGF-β signaling in hepatocellular carcinoma. *Biochim. Biophys. Acta* **1815,** 214–223 (2011).
87. Roberts, A. B. *et al.* Type beta transforming growth factor: a bifunctional regulator of cellular growth. *Proc Natl Acad Sci U S A* **82,** 119–123 (1985).
88. Kanzler, S. *et al.* Hepatocellular expression of a dominant-negative mutant TGF-beta type II receptor accelerates chemically induced hepatocarcinogenesis. *Oncogene* **20,** 5015–5024 (2001).
89. Im, Y. H. *et al.* Heterozygous mice for the transforming growth factor-beta type II receptor gene have increased susceptibility to hepatocellular carcinogenesis. *Cancer Res.* **61,** 6665–6668 (2001).
90. Siegel, P. M. & Massagué, J. Cytostatic and apoptotic actions of TGF-beta in homeostasis and cancer. *Nat. Rev. Cancer* **3,** 807–821 (2003).
91. Ling, H. *et al.* Transforming growth factor β neutralization ameliorates pre-existing hepatic fibrosis and reduces cholangiocarcinoma in thioacetamide-treated rats. *PLoS One* **8,** e54499 (2013).
92. Anzano, M. A. *et al.* Synergistic Interaction of Two Classes of Transforming Growth Factors From Murine Sarcoma Cells. *Cancer Res.* **42,** 4776–4778 (1982).
93. McMahon, J. B., Richards, W. L., del Campo, A. A., Song, M. K. & Thorgeirsson, S. S. Differential effects of transforming growth factor-beta on proliferation of normal and malignant rat liver epithelial cells in culture. *Cancer Res.* **46,** 4665–4671 (1986).
94. Carr, B. I., Hayashi, I., Branum, E. L. & Moses, H. L. Inhibition of DNA synthesis in rat hepatocytes by platelet-derived type beta transforming growth factor. *Cancer Res.* **46,** 2330–2334 (1986).
95. Nakamura, T. *et al.* Inhibitory Effect of Transforming Growth Factor-Beta on DNA Synthesis of Adult Rat Hepatocytes in Primary Culture. *Biochem Biophys Res Commun* **133,** 1042–1050 (1985).
96. Russell, W. E. Transforming growth factor beta (TGF-β) inhibits hepatocyte DNA synthesis independently of EGF binding and egf receptor autophosphorylation. *J. Cell. Physiol.* **135,** 253–261 (1988).
97. Lin, P., Liu, C., Tsao, M.-S. & Grisham, J. W. Inhibition of proliferation of cultured rat liver epithelial cells at specific cell cycle stages by transforming growth factor-β. *Biochem Biophys Res Commun* **143,** 26–30 (1987).

98. Russell, W. E., Coffey, R. J., Ouellette, A. J. & Moses, H. L. Type beta transforming growth factor reversibly inhibits the early proliferative response to partial hepatectomy in the rat. *Proc Natl Acad Sci U S A* **85,** 5126–5130 (1988).
99. Braun, L. *et al.* Transforming growth factor beta mRNA increases during liver regeneration: a possible paracrine mechanism of growth regulation. *Proc Natl Acad Sci U S A* **85,** 1539–1543 (1988).
100. Armendariz-Borunda, J. *et al.* Transforming growth factor beta gene expression is transiently enhanced at a critical stage during liver regeneration after CCl4 treatment. *Lab Invest* **69,** 283–294 (1993).
101. Bissell, D. M., Wang, S. S., Jarnagin, W. R. & Roll, F. J. Cell-specific expression of transforming growth factor-beta in rat liver. Evidence for autocrine regulation of hepatocyte proliferation. *J Clin Invest* **96,** 447–455 (1995).
102. Enami, Y. *et al.* Anti-transforming growth factor-beta1 antibody transiently enhances DNA synthesis during liver regeneration after partial hepatectomy in rats. *J Hepatobiliary Pancreat Surg* **8,** 250–258 (2001).
103. Oe, S. *et al.* Intact signaling by transforming growth factor beta is not required for termination of liver regeneration in mice. *Hepatology* **40,** 1098–1105 (2004).
104. Nakamura, T., Sakata, R., Ueno, T., Sata, M. & Ueno, H. Inhibition of transforming growth factor β prevents progression of liver fibrosis and enhances hepatocyte regeneration in dimethylnitrosamine-treated rats. *Hepatology* **32,** 247–255 (2000).
105. Ichikawa, T. *et al.* Transforming growth factor beta and activin tonically inhibit DNA synthesis in the rat liver. *Hepatology* **34,** 918–925 (2001).
106. Crawford, S. E. *et al.* Thrombospondin-1 Is a Major Activator of TGF-β1 In Vivo. *Cell* **93,** 1159–1170 (1998).
107. Hayashi, H., Sakai, K., Baba, H. & Sakai, T. Thrombospondin-1 is a novel negative regulator of liver regeneration after partial hepatectomy through transforming growth factor-beta1 activation in mice. *Hepatology* **55,** 1562–1573 (2012).
108. Akhurst, R. J. & Hata, A. Targeting the TGFβ signalling pathway in disease. *Nat Rev Drug Discov* **11,** 790–811 (2012).
109. Olinga, P. & Schuppan, D. Precision-cut liver slices: A tool to model the liver ex vivo. *J. Hepatol.* **58,** 1252–1253 (2013).
110. Broutier, L. *et al.* Culture and establishment of self-renewing human and mouse adult liver and pancreas 3D organoids and their genetic manipulation. *Nat Protoc* **11,** 1724–1743 (2016).
111. Mitchell, C. & Willenbring, H. A reproducible and well-tolerated method for 2/3 partial hepatectomy in mice. *Nat Protoc* **3,** 1167–1170 (2008).
112. Miyaoka, Y. *et al.* Hypertrophy and unconventional cell division of hepatocytes underlie liver regeneration. *Curr. Biol.* **22,** 1166–1175 (2012).
113. Hori, T. *et al.* Simple and reproducible hepatectomy in the mouse using the clip technique. *World J. Gastroenterol.* **18,** 2767–2774 (2012).
114. Mossanen, J. C. & Tacke, F. Acetaminophen-induced acute liver injury in mice. *Lab Anim* **49,** 30–36 (2015).
115. Bhushan, B. *et al.* Pro-regenerative signaling after acetaminophen-induced acute liver injury in mice identified using a novel incremental dose model. *Am J Pathol* **184,** 3013–3025 (2014).
116. Fishback, F. C. A morphologic study of regeneration of the liver after partial removal. *Archives of Pathology* **7,** 955–977 (1929).
117. Higgins, G. M. & Anderson, R. M. Experimental pathology of the liver I Restoration of the liver of the white rat following partial surgical removal. *Archives of Pathology*

12, 186–202 (1931).
118. Martins, P. N. A., Theruvath, T. P. & Neuhaus, P. Rodent models of partial hepatectomies. *Liver Int.* **28,** 3–11 (2008).
119. Weglarz, T. C. & Sandgren, E. P. Timing of hepatocyte entry into DNA synthesis after partial hepatectomy is cell autonomous. *Proc Natl Acad Sci U S A* **97,** 12595–12600 (2000).
120. Matsuo, T. *et al.* Control Mechanism of the Circadian Clock for Timing of Cell Division in Vivo. *Science* **302,** 255–259 (2003).
121. Michalopoulos, G. K. & DeFrances, M. C. Liver regeneration. *Science* **276,** 60–66 (1997).
122. Michalopoulos, G. K. Hepatostat: Liver regeneration and normal liver tissue maintenance. *Hepatology* **65,** 1384–1392 (2017).
123. Larson, A. M. *et al.* Acetaminophen-induced acute liver failure: results of a United States multicenter, prospective study. *Hepatology* **42,** 1364–1372 (2005).
124. Nagy, A. Cre recombinase: the universal reagent for genome tailoring. *Genesis* **26,** 99–109 (2000).
125. Branda, C. S. & Dymecki, S. M. Talking about a revolution: The impact of site-specific recombinases on genetic analyses in mice. *Dev. Cell* **6,** 7–28 (2004).
126. Murray, S. A., Eppig, J. T., Smedley, D., Simpson, E. M. & Rosenthal, N. Beyond knockouts: cre resources for conditional mutagenesis. *Mamm. Genome* **23,** 587–599 (2012).
127. Zhu, J. *et al.* beta8 integrins are required for vascular morphogenesis in mouse embryos. *Development* **129,** 2891–2903 (2002).
128. Heffner, C. S. *et al.* Supporting conditional mouse mutagenesis with a comprehensive cre characterization resource. *Nat Commun* **3,** 1218 (2012).
129. Greenhalgh, S. N., Conroy, K. P. & Henderson, N. C. Cre-ativity in the liver: Transgenic approaches to targeting hepatic nonparenchymal cells. *Hepatology* **61,** 2091–2099 (2015).
130. Proctor, J. M., Zang, K., Wang, D., Wang, R. & Reichardt, L. F. Vascular development of the brain requires beta8 integrin expression in the neuroepithelium. *J. Neurosci.* **25,** 9940–9948 (2005).
131. Khan, S. A., Joyce, J. & Tsuda, T. Quantification of active and total transforming growth factor-β levels in serum and solid organ tissues by bioassay. *BMC Res Notes* **5,** 636 (2012).
132. Mazzieri, R., Munger, J. S. & Rifkin, D. B. Measurement of active TGF-beta generated by cultured cells. *Methods Mol. Biol.* **142,** 13–27 (2000).
133. Abe, M. *et al.* An assay for transforming growth factor-beta using cells transfected with a plasminogen activator inhibitor-1 promoter-luciferase construct. *Anal. Biochem.* **216,** 276–284 (1994).
134. Tesseur, I., Zou, K., Berber, E., Zhang, H. & Wyss-Coray, T. Highly sensitive and specific bioassay for measuring bioactive TGF-beta. *BMC Cell Biol.* **7,** 15 (2006).
135. Worthington, J. J., Czajkowska, B. I., Melton, A. C. & Travis, M. A. Intestinal dendritic cells specialize to activate transforming growth factor-β and induce Foxp3+ regulatory T cells via integrin αvβ8. *Gastroenterology* **141,** 1802–1812 (2011).
136. Leppäranta, O. *et al.* Regulation of TGF-β storage and activation in the human idiopathic pulmonary fibrosis lung. *Cell Tissue Res* **348,** 491–503 (2012).
137. Coulouarn, C., Factor, V. M. & Thorgeirsson, S. S. Transforming growth factor-β gene expression signature in mouse hepatocytes predicts clinical outcome in human cancer. *Hepatology* **47,** 2059–2067 (2008).

138. Dunn, K. W. & Ryan, J. C. Using quantitative intravital multiphoton microscopy to dissect hepatic transport in rats. *Methods* (2017). doi:10.1016/j.ymeth.2017.04.015
139. Mossanen, J. C. *et al.* Chemokine (C-C motif) receptor 2–positive monocytes aggravate the early phase of acetaminophen-induced acute liver injury. *Hepatology* **64,** 1667–1682 (2016).
140. Heymann, F. *et al.* Long term intravital multiphoton microscopy imaging of immune cells in healthy and diseased liver using CXCR6.Gfp reporter mice. *J Vis Exp* e52607–e52607 (2015). doi:10.3791/52607
141. Tao, W. *et al.* A practical method for monitoring FRET-based biosensors in living animals using two-photon microscopy. *American Journal of Physiology - Cell Physiology* **309,** C724–C735 (2015).
142. Wang, H. *et al.* Real-time histology in liver disease using multiphoton microscopy with fluorescence lifetime imaging. *Biomed Opt Express* **6,** 780–792 (2015).
143. Marques, P. E. *et al.* Imaging liver biology in vivo using conventional confocal microscopy. *Nat Protoc* **10,** 258–268 (2015).
144. Dombeck, D. A., Khabbaz, A. N., Collman, F., Adelman, T. L. & Tank, D. W. Imaging large-scale neural activity with cellular resolution in awake, mobile mice. *Neuron* **56,** 43–57 (2007).
145. Looney, M. R. *et al.* Stabilized imaging of immune surveillance in the mouse lung. *Nat Meth* **8,** 91–96 (2011).
146. Ritsma, L. *et al.* Surgical implantation of an abdominal imaging window for intravital microscopy. *Nat Protoc* **8,** 583–594 (2013).
147. Liu, Y. *et al.* Visualization of hepatobiliary excretory function by intravital multiphoton microscopy. *J Biomed Opt* **12,** 014014 (2007).
148. Presson, R. G. *et al.* Two-photon imaging within the murine thorax without respiratory and cardiac motion artifact. *Am J Pathol* **179,** 75–82 (2011).
149. Dunn, K. W., Lorenz, K. S., Salama, P. & Delp, E. J. IMART software for correction of motion artifacts in images collected in intravital microscopy. *IntraVital* **3,** e28210 (2014).
150. Lee, S., Vinegoni, C., Sebas, M. & Weissleder, R. Automated motion artifact removal for intravital microscopy, without a priori information. *Sci Rep* **4,** 4507 (2014).
151. Vogten, J. M., Smakman, N., Voest, E. E. & Borel Rinkes, I. H. M. Intravital analysis of microcirculation in the regenerating mouse liver. *J Surg Res* **113,** 264–269 (2003).
152. Le, V.-H. *et al.* Brain tumor delineation enhanced by moxifloxacin-based two-photon/CARS combined microscopy. *Biomed Opt Express* **8,** 2148 (2017).
153. Denk, W., Strickler, J. H. & Webb, W. W. Two-photon laser scanning fluorescence microscopy. *Science* **248,** 73–76 (1990).
154. Wang, H. *et al.* Visualizing liver anatomy, physiology and pharmacology using multiphoton microscopy. *J Biophotonics* **10,** 46–60 (2017).
155. Gailhouste, L. *et al.* Fibrillar collagen scoring by second harmonic microscopy: a new tool in the assessment of liver fibrosis. *J. Hepatol.* **52,** 398–406 (2010).
156. Ritsma, L. *et al.* Intravital microscopy through an abdominal imaging window reveals a pre-micrometastasis stage during liver metastasis. *Sci Transl Med* **4,** 158ra145 (2012).
157. Postic, C. *et al.* Dual roles for glucokinase in glucose homeostasis as determined by liver and pancreatic beta cell-specific gene knock-outs using Cre recombinase. *J. Biol. Chem.* **274,** 305–315 (1999).
158. Foo, S. S. *et al.* Ephrin-B2 controls cell motility and adhesion during blood-vessel-

wall assembly. *Cell* **124,** 161–173 (2006).
159. Wang, Y. *et al.* Ephrin-B2 controls VEGF-induced angiogenesis and lymphangiogenesis. *Nature* **465,** 483–486 (2010).
160. Madisen, L. *et al.* A robust and high-throughput Cre reporting and characterization system for the whole mouse brain. *Nat Neurosci* **13,** 133–140 (2010).
161. Muzumdar, M. D., Tasic, B., Miyamichi, K., Li, L. & Luo, L. A global double-fluorescent Cre reporter mouse. *Genesis* **45,** 593–605 (2007).
162. Snippert, H. J. *et al.* Intestinal crypt homeostasis results from neutral competition between symmetrically dividing Lgr5 stem cells. *Cell* **143,** 134–144 (2010).
163. Sasmono, R. T. *et al.* A macrophage colony-stimulating factor receptor-green fluorescent protein transgene is expressed throughout the mononuclear phagocyte system of the mouse. *Blood* **101,** 1155–1163 (2003).
164. Mort, R. L. *et al.* Fucci2a: a bicistronic cell cycle reporter that allows Cre mediated tissue specific expression in mice. *Cell Cycle* **13,** 2681–2696 (2014).
165. Mitchell, C. & Willenbring, H. Addendum: A reproducible and well-tolerated method for 2/3 partial hepatectomy in mice. *Nat Protoc* **9,** (2014).
166. Xu, L. *et al.* Human hepatic stellate cell lines, LX-1 and LX-2: new tools for analysis of hepatic fibrosis. *Gut* **54,** 142–151 (2005).
167. Schindelin, J. *et al.* Fiji: an open-source platform for biological-image analysis. *Nat Meth* **9,** 676–682 (2012).
168. Lee, M. *et al.* In vivo imaging of the tumor and its associated microenvironment using combined CARS / 2-photon microscopy. *IntraVital* **4,** e1055430 (2015).
169. Zudaire, E., Gambardella, L., Kurcz, C. & Vermeren, S. A computational tool for quantitative analysis of vascular networks. *PLoS One* **6,** e27385 (2011).
170. Kamoun, W. S. *et al.* Simultaneous measurement of RBC velocity, flux, hematocrit and shear rate in vascular networks. *Nat Meth* **7,** 655–660 (2010).
171. Willems, E., Leyns, L. & Vandesompele, J. Standardization of real-time PCR gene expression data from independent biological replicates. *Anal. Biochem.* **379,** 127–129 (2008).
172. Han, C. *et al.* Cytosolic phospholipase A2alpha and peroxisome proliferator-activated receptor gamma signaling pathway counteracts transforming growth factor beta-mediated inhibition of primary and transformed hepatocyte growth. *Hepatology* **52,** 644–655 (2010).
173. Popov, Y. *et al.* Integrin alphavbeta6 is a marker of the progression of biliary and portal liver fibrosis and a novel target for antifibrotic therapies. *J. Hepatol.* **48,** 453–464 (2008).
174. Ding, B.-S. *et al.* Inductive angiocrine signals from sinusoidal endothelium are required for liver regeneration. *Nature* **468,** 310–315 (2010).
175. Ding, B.-S. *et al.* Divergent angiocrine signals from vascular niche balance liver regeneration and fibrosis. *Nature* **505,** 97–102 (2014).
176. Speicher, T. *et al.* Knockdown and knockout of β1-integrin in hepatocytes impairs liver regeneration through inhibition of growth factor signalling. *Nat Commun* **5,** 3862 (2014).
177. Morgan, E. A. *et al.* Dissection of platelet and myeloid cell defects by conditional targeting of the beta3-integrin subunit. *FASEB J.* **24,** 1117–1127 (2010).
178. Beier, J. I. *et al.* Fibrin-mediated integrin signaling plays a critical role in hepatic regeneration after partial hepatectomy in mice. *Ann Hepatol* **15,** 762–772 (2016).
179. Patsenker, E. *et al.* Pharmacological inhibition of integrin alphavbeta3 aggravates experimental liver fibrosis and suppresses hepatic angiogenesis. *Hepatology* **50,**

1501–1511 (2009).
180. Michalopoulos, G. K. Liver regeneration. *J. Cell. Physiol.* **213,** 286–300 (2007).
181. Scott, C. L. *et al.* Bone marrow-derived monocytes give rise to self-renewing and fully differentiated Kupffer cells. *Nat Commun* **7,** 10321 (2016).
182. Michalopoulos, G. K. Liver regeneration after partial hepatectomy: critical analysis of mechanistic dilemmas. *Am J Pathol* **176,** 2–13 (2010).
183. Huang, J. *et al.* Postponing the Hypoglycemic Response to Partial Hepatectomy Delays Mouse Liver Regeneration. *Am J Pathol* **186,** 587–599 (2016).
184. Akerman, P. *et al.* Antibodies to tumor necrosis factor-alpha inhibit liver regeneration after partial hepatectomy. *Am J Physiol* **263,** G579–85 (1992).
185. Nishimura, S. L., Sheppard, D. & Pytela, R. Integrin alpha v beta 8. Interaction with vitronectin and functional divergence of the beta 8 cytoplasmic domain. *J. Biol. Chem.* **269,** 28708–28715 (1994).
186. Venstrom, K. & Reichardt, L. Beta 8 integrins mediate interactions of chick sensory neurons with laminin-1, collagen IV, and fibronectin. *Mol. Biol. Cell* **6,** 419–431 (1995).
187. Pan, C., Kumar, C., Bohl, S., Klingmueller, U. & Mann, M. Comparative proteomic phenotyping of cell lines and primary cells to assess preservation of cell type-specific functions. *Mol. Cell Proteomics* **8,** 443–450 (2009).
188. Ning, W. *et al.* TGF-beta1 stimulates HO-1 via the p38 mitogen-activated protein kinase in A549 pulmonary epithelial cells. *Am. J. Physiol. Lung Cell Mol. Physiol.* **283,** L1094–102 (2002).
189. Mars, W. M., Zarnegar, R. & Michalopoulos, G. K. Activation of hepatocyte growth factor by the plasminogen activators uPA and tPA. *Am J Pathol* **143,** 949–958 (1993).
190. Kuiper, J., Otter, M., Rijken, D. C. & van Berkel, T. J. Characterization of the interaction in vivo of tissue-type plasminogen activator with liver cells. *J. Biol. Chem.* **263,** 18220–18224 (1988).
191. Noguchi, T., Noguchi, M., Masubuchi, H., Seki, T. & Ariga, T. IL-1β Down-Regulates Tissue-Type Plasminogen Activator by Up-Regulating Low-Density Lipoprotein Receptor-Related Protein in AML 12 Cells. *Biochem Biophys Res Commun* **288,** 42–48 (2001).
192. Warshawsky, I., Bu, G. & Schwartz, A. L. 39-kD protein inhibits tissue-type plasminogen activator clearance in vivo. *J Clin Invest* **92,** 937–944 (1993).
193. Hatoff, D. E. & Hardison, W. G. Induced synthesis of alkaline phosphatase by bile acids in rat liver cell culture. *Gastroenterology* **77,** 1062–1067 (1979).
194. Halling Linder, C., Englund, U. H., Narisawa, S., Millán, J. L. & Magnusson, P. Isozyme profile and tissue-origin of alkaline phosphatases in mouse serum. *Bone* **53,** 399–408 (2013).
195. Zhang, Y. E. Non-Smad pathways in TGF-β signaling. *Cell Res* **19,** 128–139 (2009).
196. Araya, J., Cambier, S., Morris, A., Finkbeiner, W. & Nishimura, S. L. Integrin-Mediated Transforming Growth Factor-β Activation Regulates Homeostasis of the Pulmonary Epithelial-Mesenchymal Trophic Unit. *Am J Pathol* **169,** 405–415 (2006).
197. Wang, H., Vohra, B. P. S., Zhang, Y. & Heuckeroth, R. O. Transcriptional profiling after bile duct ligation identifies PAI-1 as a contributor to cholestatic injury in mice. *Hepatology* **42,** 1099–1108 (2005).
198. Wang, H., Zhang, Y. & Heuckeroth, R. O. Tissue-type plasminogen activator deficiency exacerbates cholestatic liver injury in mice. *Hepatology* **45,** 1527–1537 (2007).
199. Kang, L.-I. *et al.* Tissue-type plasminogen activator suppresses activated stellate

cells through low-density lipoprotein receptor-related protein 1. *Lab Invest* **95,** 1117–1129 (2015).
200. Roselli, H. T. *et al.* Liver regeneration is transiently impaired in urokinase-deficient mice. *Am J Physiol* **275,** G1472–9 (1998).
201. Shimizu, M. *et al.* Mechanism of retarded liver regeneration in plasminogen activator-deficient mice: Impaired activation of hepatocyte growth factor after Fas-mediated massive hepatic apoptosis. *Hepatology* **33,** 569–576 (2001).
202. Bezerra, J. A. *et al.* Plasminogen Activators Direct Reorganization of the Liver Lobule after Acute Injury. *Am J Pathol* **158,** 921–929 (2001).
203. Mars, W. M. *et al.* Immediate early detection of urokinase receptor after partial hepatectomy and its implications for initiation of liver regeneration. *Hepatology* **21,** 1695–1701 (1995).
204. Tarui, T., Mazar, A. P., Cines, D. B. & Takada, Y. Urokinase-type plasminogen activator receptor (CD87) is a ligand for integrins and mediates cell-cell interaction. *J. Biol. Chem.* **276,** 3983–3990 (2001).
205. Gellert, G. C., Goldfarb, R. H. & Kitson, R. P. Physical association of uPAR with the alphaV integrin on the surface of human NK cells. *Biochem Biophys Res Commun* **315,** 1025–1032 (2004).
206. Franco, P. *et al.* Activation of urokinase receptor by a novel interaction between the connecting peptide region of urokinase and αvβ5 integrin. *J Cell Sci* **119,** 3424–3434 (2006).
207. Ahn, S. B. *et al.* Characterization of the interaction between heterodimeric αvβ6 integrin and urokinase plasminogen activator receptor (uPAR) using functional proteomics. *J. Proteome Res.* **13,** 5956–5964 (2014).
208. Wilcox-Adelman, S. A., Wilkins-Port, C. E. & McKeown-Longo, P. J. Localization of Urokinase Type Plasminogen Activator to Focal Adhesions Requires Ligation of Vitronectin Integrin Receptors. *Cell Adhesion and Communication* **7,** 477–490 (2000).
209. Hapke, S. *et al.* Integrin alpha(v)beta(3)/vitronectin interaction affects expression of the urokinase system in human ovarian cancer cells. *J. Biol. Chem.* **276,** 26340–26348 (2001).
210. Chen, J., Baskerville, C., Han, Q., Pan, Z. K. & Huang, S. Alpha(v) integrin, p38 mitogen-activated protein kinase, and urokinase plasminogen activator are functionally linked in invasive breast cancer cells. *J. Biol. Chem.* **276,** 47901–47905 (2001).
211. Reyes, S. B. *et al.* αvβ8 integrin interacts with RhoGDI1 to regulate Rac1 and Cdc42 activation and drive glioblastoma cell invasion. *Mol. Biol. Cell* **24,** 474–482 (2013).
212. Zhong, Z. *et al.* Activation of the oxygen-sensing signal cascade prevents mitochondrial injury after mouse liver ischemia-reperfusion. *Am J Physiol Gastrointest Liver Physiol* **295,** G823–G832 (2008).
213. Wehr, A. *et al.* Chemokine Receptor CXCR6-Dependent Hepatic NK T Cell Accumulation Promotes Inflammation and Liver Fibrosis. *J. Immunol.* **190,** 5226–5236 (2013).
214. Thompson, A. I. Investigation of the role of hepatic stellate cells in acute liver failure and hepatocarcinogenesis. (Thesis (PhD), University of Edinburgh, 2016).
215. Greene, A. K. & Puder, M. Partial hepatectomy in the mouse: technique and perioperative management. *J Invest Surg* **16,** 99–102 (2003).
216. Cook, M. J. *The anatomy of the laboratory mouse*. (Academic Press, 1965).
217. Sonner, J. M., Gong, D., Li, J., Eger, E. I., II & Laster, M. J. Mouse Strain Modestly Influences Minimum Alveolar Anesthetic Concentration and Convulsivity of

Inhaled Compounds. *Anesthesia & Analgesia* **89,** 1030 (1999).
218. Inderbitzin, D. *et al.* Regenerative capacity of individual liver lobes in the microsurgical mouse model. *Microsurgery* **26,** 465–469 (2006).
219. Gil, F., Fiserova-Bergerova, V. & Altman, N. H. Hepatic protection from chemical injury by isoflurane. *Anesthesia & Analgesia* **67,** 860–867 (1988).
220. Kon, S., Imai, M. & Inaba, H. Isoflurane attenuates early neutrophil-independent hypoxia-reoxygenation injuries in the reperfused liver in fasted rats. *Anesthesiology* **86,** 128–136 (1997).
221. Kharasch, E. D. & Thummel, K. E. Identification of Cytochrome P450 2E1 as the Predominant Enzyme Catalyzing Human Liver Microsomal Defluorination of Sevoflurane, Isoflurane, and Methoxyflurane. *Anesthesiology* **79,** 795–807 (1993).
222. Hoetzel, A. *et al.* Mechanism of hepatic heme oxygenase-1 induction by isoflurane. *Anesthesiology* **104,** 101–109 (2006).
223. Schmidt, R. *et al.* Heme oxygenase-1 induction by the clinically used anesthetic isoflurane protects rat livers from ischemia/reperfusion injury. *Ann. Surg.* **245,** 931–942 (2007).
224. Lv, X. *et al.* Isoflurane preconditioning at clinically relevant doses induce protective effects of heme oxygenase-1 on hepatic ischemia reperfusion in rats. *BMC Gastroenterol* **11,** 31 (2011).
225. Nakazato, K., Yoshida, Y., Takemori, K., Kobayashi, K. & Sakamoto, A. Expressions of genes encoding drug-metabolizing enzymes are altered after sevoflurane, isoflurane, propofol or dexmedetomidine anesthesia. *Biomed. Res.* **30,** 17–24 (2009).
226. Edmands, S. D., LaDow, E. & Hall, A. C. Microarray analyses of genes regulated by isoflurane anesthesia in vivo: a novel approach to identifying potential preconditioning mechanisms. *Anesthesia & Analgesia* **116,** 589–595 (2013).
227. Yamashita, K., Matsumoto, H., Saito, F. & Takeyoshi, M. Differences in gene expression profiles in liver caused by different types of anesthesia: cases of CO2-O2 and isoflurane. *The Journal of Toxicological Sciences* **40,** 829–836 (2015).
228. Sakai, K. & Miyazaki, J. I. A transgenic mouse line that retains Cre recombinase activity in mature oocytes irrespective of the cre transgene transmission. *Biochem Biophys Res Commun* **237,** 318–324 (1997).
229. Tarlow, B. D., Finegold, M. J. & Grompe, M. Clonal tracing of Sox9+ liver progenitors in mouse oval cell injury. *Hepatology* **60,** 278–289 (2014).
230. MacDonald, K. P. A. *et al.* The colony-stimulating factor 1 receptor is expressed on dendritic cells during differentiation and regulates their expansion. *J. Immunol.* **175,** 1399–1405 (2005).
231. Sasmono, R. T. *et al.* Mouse neutrophilic granulocytes express mRNA encoding the macrophage colony-stimulating factor receptor (CSF-1R) as well as many other macrophage-specific transcripts and can transdifferentiate into macrophages in vitro in response to CSF-1. *J Leukoc Biol* **82,** 111–123 (2007).
232. Bertero, A. & Vallier, L. Fucci2a mouse upgrades live cell cycle imaging. *Cell Cycle* **14,** 948–949 (2015).
233. Wang, J. & Kubes, P. A Reservoir of Mature Cavity Macrophages that Can Rapidly Invade Visceral Organs to Affect Tissue Repair. *Cell* **165,** 668–678 (2016).
234. Rasmussen, K. D. & O'Carroll, D. The miR-144/451eGFP allele, a novel tool for resolving the erythroid potential of hematopoietic precursors. *Blood* **118,** 2988–2992 (2011).
235. Gock, M., Eipel, C., Linnebacher, M., Klar, E. & Vollmar, B. Impact of portal branch ligation on tissue regeneration, microcirculatory response and microarchitecture in

portal blood-deprived and undeprived liver tissue. *Microvasc. Res.* **81,** 274–280 (2011).
236. MacPhee, P. J., Schmidt, E. E., Keown, P. A. & Groom, A. C. Microcirculatory Changes in Livers of Mice Infected with Murine Hepatitis-Virus - Evidence From Microcorrosion Casts and Measurements of Red-Cell Velocity. *Microvasc. Res.* **36,** 140–149 (1988).
237. MacPhee, P. J., Schmidt, E. E. & Groom, A. C. Intermittence of blood flow in liver sinusoids, studied by high-resolution in vivo microscopy. *Am J Physiol* **269,** G692–8 (1995).
238. McDonald, B. *et al.* Intravascular danger signals guide neutrophils to sites of sterile inflammation. *Science* **330,** 362–366 (2010).
239. Grundmann, U., Zissis, A., Bauer, C. & Bauer, M. In vivo effects of halothane, enflurane, and isoflurane on hepatic sinusoidal microcirculation. *Acta Anaesthesiologica Scandinavica* **41,** 760–765 (1997).
240. Bernabeu, M. O. *et al.* Computer simulations reveal complex distribution of haemodynamic forces in a mouse retina model of angiogenesis. *Journal of the Royal Society Interface* **11,** (2014).
241. de Leeuw, A. M., Mccarthy, S. P., Geerts, A. & Knook, D. L. Purified rat liver fat-storing cells in culture divide and contain collagen. *Hepatology* **4,** 392–403 (1984).
242. Friedman, S. L., Roll, F. J., Boyles, J. & Bissell, D. M. Hepatic lipocytes: the principal collagen-producing cells of normal rat liver. *Proc Natl Acad Sci U S A* **82,** 8681–8685 (1985).
243. Friedman, S. L., Wei, S. & Blaner, W. S. Retinol release by activated rat hepatic lipocytes: regulation by Kupffer cell-conditioned medium and PDGF. *Am J Physiol* **264,** G947–52 (1993).
244. Li, Y., Wang, J. & Asahina, K. Mesothelial cells give rise to hepatic stellate cells and myofibroblasts via mesothelial-mesenchymal transition in liver injury. *Proc Natl Acad Sci U S A* **110,** 2324–2329 (2013).
245. Lua, I. & Asahina, K. The Role of Mesothelial Cells in Liver Development, Injury, and Regeneration. *Gut Liver* **10,** 166–176 (2016).
246. Dal-Secco, D. *et al.* A dynamic spectrum of monocytes arising from the in situ reprogramming of CCR2+ monocytes at a site of sterile injury. *J Exp Med* **212,** 447–456 (2015).
247. Clausen, B. E., Burkhardt, C., Reith, W., Renkawitz, R. & Förster, I. Conditional gene targeting in macrophages and granulocytes using LysMcre mice. *Transgenic Res* **8,** 265–277 (1999).
248. Lorenz, K. S., Salama, P., Dunn, K. W. & Delp, E. J. Digital correction of motion artefacts in microscopy image sequences collected from living animals using rigid and nonrigid registration. *J Microsc* **245,** 148–160 (2012).
249. Kuramitsu, K. *et al.* Failure of fibrotic liver regeneration in mice is linked to a severe fibrogenic response driven by hepatic progenitor cell activation. *Am J Pathol* **183,** 182–194 (2013).

Appendices

Appendix 1 – qPCR primer details

Name	Gene symbol	Gene ID	Product Name	Cat #
Beta actin	Actb	11461	Mm_Actb_2_SG QuantiTect Primer Assay	QT01136772
C-met	Met	17295	Mm_Met_1_SG QuantiTect Primer Assay	QT00126616
Glyceraldehyde-3-phosphate dehydrogenase	Gapdh	14433	Mm_Gapdh_3_SG QuantiTect Primer Assay	QT01658692
Hepatocyte growth factor	Hgf	15234	Mm_Hgf_1_SG QuantiTect Primer Assay	QT00158046
Low density lipoprotein receptor-related protein 1	Lrp1	16971	Mm_Lrp1_1_SG QuantiTect Primer Assay	QT00155981
Low density lipoprotein receptor-related protein associated protein 1 (RAP)	Lrpap1	16976	Mm_Lrpap1_1_SG QuantiTect Primer Assay	QT00162197
PAI-1	Serpine1	18787	Mm_Serpine1_1_SG QuantiTect Primer Assay	QT00154756
Plasminogen	Plg	18815	Mm_Plg_1_SG QuantiTect Primer Assay	QT01053332
Plasminogen activator, tissue	Plat	18791	Mm_Plat_1_SG QuantiTect Primer Assay	QT00133630
Plasminogen activator, urokinase	Plau	18792	Mm_Plau_1_SG QuantiTect Primer Assay	QT00103159
Plasminogen activator, urokinase receptor	Plaur	18793	Mm_Plaur_1_SG QuantiTect Primer Assay	QT00102984
			Forward	Reverse
Integrin beta 8	Itgb8	320910	CTG AAG AAA TAC CCC GTG GA	ATG GGG AGG CAT ACA GTC T

Appendix 2 – Gene list for TGFβ signalling qPCR array

Name	Gene Symbol	Gene ID	Reason for Inclusion	Predicted response to β8 integrin inhibition
actin, beta	Actb	11461	Cont	N/A
activin A receptor, type 1	Acvr1	11477	c, Q1	down
activin A receptor, type 1B	Acvr1b	11479	c	down
alpha fetoprotein	Afp	11576	c	up
aldehyde dehydrogenase family 1, subfamily A1	Aldh1a1	11668	c	up
aldolase B, fructose-bisphosphate	Aldob	230163	c	up
Rho GTPase-activating protein 6	Arhgap6	11856	c	up
BCL2-like 14 (apoptosis facilitator)	Bcl2l14	66813	c	up
coiled-coil domain containing 166	Ccdc166	223648	c	down
coiled-coil domain containing 85A	Ccdc85a	216613	c	down
cyclin A2	Ccna2	12428	I	up
cyclin D1	Ccnd1	12443	I	up
cyclin E1	Ccne1	12447	I	up
cyclin-dependent kinase inhibitor 1a (p21)	Cdkn1a	12575	Q2	?down
cyclin dependent kinase inhibitor 1b (p27)	Cdkn1b	12576	Q1, Q2	down
cyclin-dependent kinase inhibitor 2B (p15, inhibits CDK4)	Cdkn2b	12579	Q2	down
cysteine-rich C-terminal 1	Crct1	74175	c	up
CREB binding protein	Crebbp	12914	Q1	?down
connective tissue growth factor	Ctgf	14219	c	down
coxsackievirus and adenovirus receptor	Cxadr	13052	c	up
cytochrome P450, family 2, subfamily c, polypeptide 70	Cyp2c70	226105	c	up
E2F transcription factor 4	E2f4	104394	Q1	down
fibronectin 1	Fn1	14268	Q1	down
furin (paired basic amino acid cleaving enzyme)	Furin	18550	Q1	down
growth arrest and DNA-damage-inducible 45 beta	Gadd45b	17873	c, Q1, Q2	U / none
glyceraldehyde-3-phosphate dehydrogenase	Gapdh	14433	Cont	N/A
GINS complex subunit 2 (Psf2 homolog)	Gins2	272551	c	down
glutamate-ammonia ligase (glutamine synthetase)	Glul	14645	c	down
guanine nucleotide binding protein (G protein), gamma 13	Gng13	64337	c	down
glycerol-3-phosphate dehydrogenase 1 (soluble)	Gpd1	14555	c	up
glutathione S-transferase, alpha 1 (Ya)	Gsta1	14857	c	up

Name	Gene Symbol	Gene ID	Reason for Inclusion	Predicted response to β8 integrin inhibition
hyperpolarization-activated, cyclic nucleotide-gated K+ 2	Hcn2	15166	c	down
hypocretin	Hcrt	15171	c	down
histone cluster 1, H2bn	Hist1h2bn	319187	c	down
HMG box domain containing 4	Hmgxb4	70823	c	down
heme oxygenase 1	Hmox1	15368	Q1	down
inhibitor of DNA binding 2	Id2	15902	c, Q1, Q2	up
insulin-like growth factor binding protein 3	Igfbp3	16009	c, Q2	down
insulin-like growth factor binding protein 4	Igfbp4	16010	c	up
inscuteable homolog (Drosophila)	Insc	233752	c	down
integrin alpha V	Itgav	16410	I	U
integrin beta 8	Itgb8	320910	I	U
IZUMO1 receptor, JUNO	Izumo1r	64931	c	up
jagged 1	Jag1	16449	c	both
Kruppel-Like Factor 10	Klf10	21847	Q1	down
low density lipoprotein receptor	Ldlr	16835	c	up
legumain	Lgmn	19141	c	down
mastermind like 2 (Drosophila)	Maml2	270118	c	down
mitogen-activated protein kinase 14 (p38a)	Mapk14	26416	Q1	down
matrix metallopeptidase 14 (membrane-inserted)	Mmp14	17387	I	U
MOK protein kinase	Mok	26448	c	down
motile sperm domain containing 3	Mospd3	68929	c	down
myelocytomatosis oncogene	Myc	17869	Q1, Q2	up
neuroepithelial cell transforming gene 1	Net1	56349	c	up
nuclear factor of kappa light polypeptide gene enhancer in B cells inhibitor, alpha	Nfkbia	18035	c, Q1	both
platelet derived growth factor, alpha	Pdgfa	18590	c, Q1	down
PDZ and LIM domain 7	Pdlim7	67399	c	down
phosphatidylinositol glycan anchor biosynthesis, class H	Pigh	110417	c	down
plasminogen activator, tissue	Plat	18791	c	up
proteoglycan 4 (megakaryocyte stimulating factor, articular superficial zone protein)	Prg4	96875	c	down
phosphoserine aminotransferase 1	Psat1	107272	c	up
ras homolog family member B	Rhob	11852	c, Q1	down

Name	Gene Symbol	Gene ID	Reason for Inclusion	Predicted response to β8 integrin inhibition
selenium binding protein 1	Selenbp1	20341	c	up
selenoprotein P	Sepp1	20363	c	both
serine incorporator 2	Serinc2	230779	c	down
serine (or cysteine) peptidase inhibitor, clade E, member 1 (PAI1)	Serpine1	18787	c, Q1, Q2	down
SKI-like	Skil	20482	c	both
solute carrier family 26 (sulfate transporter), member 1	Slc26a1	231583	c	up
SMAD family member 2	Smad2	17126	Q2	?down
SMAD family member 3	Smad3	17127	Q1, Q2	?down
SMAD family member 4	Smad4	17128	Q2	?down
SMAD family member 7	Smad7	17131	c, Q2	down
SMAD specific E3 ubiquitin protein ligase 2	Smurf2	66313	c	down
SRY (sex determining region Y)-box 4	Sox4	20677	c, Q1, Q2	both
trans-acting transcription factor 1	Sp1	20683	Q1	?down
small proline-rich protein 1A	Sprr1a	20753	c	up
small proline-rich protein 3	Sprr3	20766	c	up
SPRY domain containing 4	Spryd4	66701	c	down
syntaxin 5A	Stx5a	56389	c	down
sulfotransferase family 1E, member 1	Sult1e1	20860	c	both
tissue factor pathway inhibitor 2	Tfpi2	21789	c	down
transforming growth factor, beta 1	Tgfb1	21803	Q2	U
transforming growth factor, beta 3	Tgfb3	21809	Q2	U
transforming growth factor, beta receptor I	Tgfbr1	21812	c, Q2	both
transforming growth factor, beta receptor II	Tgfbr2	21813	Q1, Q2	U
transmembrane 7 superfamily member 2	Tm7sf2	73166	c	down
thymosin, beta 4, X chromosome	Tmsb4x	19241	c	both
UDP glucuronosyltransferase 1 family, polypeptide A9	Ugt1a9	394434	c	up
unc-5 netrin receptor B	Unc5b	107449	c	down
Genomic DNA control	N/A	N/A	Cont	N/A
Reverse Transcription control	N/A	N/A	Cont	N/A
Positive PCR control	N/A	N/A	Cont	N/A

Notes: c, Coulouarn et al.;[137] Cont, control; down, downregulation; Q1, Qiagen TGFβ signalling targets array (330231, PAMM-235Z); Q2, Qiagen TGFβ-BMP signalling pathway array (330231, PAMM-035Z); I, gene of interest; U, uncertain; up, upregulation

Appendix 3 – FIJI macro to calculate percentage positive DAB staining in multiple images

Prior to running the below macro, the Trainable Weka Segmentation tool in FIJI is trained to identify positive DAB staining. This is achieved by loading a stack of representative images from the experiment in question and indicating areas of positive and negative staining in an iterative manner, until the tool is able to differentiate positive and negative staining with acceptable accuracy. Recommended minimum training features are Gaussian blur and Sobel filter. Additional features can be added, but this can dramatically increase processing time without significant improvement in classification. All other settings are left at their default values. The final classification algorithm is then saved as a .model file.

```
/*
 * DAB staining analysis macro v3 19/08/16
 * Stephen Greenhalgh
 * Input: a working directory containing RGB TIFF images.
 * Input: a WEKA segmentation model file for classifying the above images.
 *
 * Credits:
 * Elements of code from
 * BrdU pos/neg nuclei counter v3 28/8/15 by Stephen Greenhalgh and John Wilson-
Kanamori
 * TrainableWekaMacro v1.1 by Sébastien Tosi (IRB / Barcelona)
 */

//start with a clean slate
run("Close All");
print("\\Clear");

setOption("JFileChooser", true);
//workaround required in Mac OS X 10.11 otherwise dialog boxes do not display correctly

//define current FIJI Trainable Weka Segmentation version
//this part of the code may need to be updated to reflect the current version
WekaVersion = "Trainable Weka Segmentation v3.1.2";
SaveClassification = true;
// this second line may be surplus

// Find all files in the image folder
InputFile = File.openDialog("Select an image file from the folder you wish to analyse");
open(InputFile);

OutputLocation = getDirectory("Select location of output files");
```

```
DialogTitle = "Enter name of results folder";

Dialog.create("Enter name of results folder");
  Dialog.addString("Results folder name: "," ");
  Dialog.show();
  ResultFolderName = Dialog.getString();

SegOutFolder = OutputLocation + ResultFolderName + File.separator;
File.makeDirectory(SegOutFolder);

classifier = File.openDialog("Please select your classifier...");

// Initialize Trainable Weka
run("Trainable Weka Segmentation");
wait(500);

//ensure correct Weka version is entered here
selectWindow("Trainable Weka Segmentation v3.1.2");
call("trainableSegmentation.Weka_Segmentation.loadClassifier", classifier);

//get the input directory
 dir = getDirectory("Choose a Directory ");
//set the batch mode to true
   setBatchMode(true);
//declare and initialise variable count
   count = 0;
//run user-defined function countFiles
   countFiles(dir);
//declare and initialise variable n
   n = 0;
//run user-defined function processFiles
   processFiles(dir);
//print number of file processed in log in window
   print(count+" files processed");

//user-defined countFiles function
   function countFiles(dir) {
//list of items in input directory (files and subfolders)
      list = getFileList(dir);
//start of loop through the list of items
      for (i=0; i<list.length; i++) {
//if item end with / it is a folder
         if (endsWith(list[i], "/"))
//if a folder run the user-defined countFiles functions
            countFiles(""+dir+list[i]);
         else
//else ad +1 to the file count
            count++;
      }
```

```
 }

function processFiles(dir) {
//list of items in input directory (files and subfolders)
    list = getFileList(dir);
//start of loop through the list of items
    for (i=0; i<list.length; i++) {
//if item end with / it is a folder
       if (endsWith(list[i], "/"))
//if a folder run the user-defined processFiles(dir) function
          processFiles(""+dir+list[i]);
       else {
//if a file
          showProgress(n++, count);
//declare the variable path
          path = dir+list[i];
//run the user defined processFile(path) function
          processFile(path);
       }
    }
 }

//user-defined processFile(path) function
 function processFile(path) {
//if the file is a tif file
     if (endsWith(path, ".tif")) {
//open the image
        open(path);
//run wekaSegment function
        wekaSegment(path);

    }
 }
// Main loop over all .tif images in the folder

function wekaSegment(path){
                    selectWindow(WekaVersion);
                    call("trainableSegmentation.Weka_Segmentation.applyClassifier", dir, list[i],
"showResults=true", "storeResults=false", "probabilityMaps=false", "");
                    selectImage("Classification result");
                    saveAs("Tif",SegOutFolder+"Segmented "+list[i]);
          }

//measure positive staining percentage

FileListSeg = getFileList(SegOutFolder);

for(i=0;i<FileListSeg.length;i++){
          getPos(SegOutFolder+FileListSeg[i]);
```

```
}

saveAs("Results", SegOutFolder+"Results.csv");

function getPos(baseimage){
	open(baseimage);
	setAutoThreshold("Default dark");
	run("Threshold...");
	setThreshold (0.51, 1.00);
	run("Set Measurements...", "area standard area_fraction limit display redirect=None
decimal=3");
	run("Measure");
	}
```

Appendix 4 – Imaris surface generation algorithms

Vascular surface algorithm applied to Ai14 channel in *Cdh5-Cre*;Ai14 mice

Enable Region Of Interest = false

Enable Region Growing = false

Enable Tracking = false

[Source Channel]

Source Channel Index = 3

Enable Smooth = true

Surface Grain Size = 1.99 um

Enable Eliminate Background = true

Diameter Of Largest Sphere = 7.45 um

[Threshold]

Enable Automatic Threshold = false

Manual Threshold Value = 47.9868

Active Threshold = true

Enable Automatic Threshold B = false

Manual Threshold Value B = 2240.56

Active Threshold B = true

[Classify Surfaces]

"Number of Voxels" not activated

Lipid surface algorithm

Enable Region Of Interest = false

Enable Region Growing = false

Enable Tracking = false

[Source Channel]

Source Channel Index = 5

Enable Smooth = true

Surface Grain Size = 1.00 um

Enable Eliminate Background = true

Diameter Of Largest Sphere = 5.00 um

[Threshold]

Enable Automatic Threshold = false

Manual Threshold Value = 991.494

Active Threshold = true

Enable Automatic Threshold B = false

Manual Threshold Value B = 3869.72

Active Threshold B = false

[Classify Surfaces]

"Number of Voxels" above 1.00

Appendix 5 – Raw data from TGFβ signalling qPCR array

Gene Symbol	Assay Catalog #	A1a Ct	B1a Ct	A2a Ct	B2a Ct	A3a Ct	B3a Ct	A1a ΔCt*	B1a ΔCt*	A2a ΔCt*	B2a ΔCt*	A3a ΔCt*	B3a ΔCt*	ΔΔCt (A1a-B1a)	ΔΔCt (A2a-B2a)	ΔΔCt (A3a-B3a)	Fold change A1vsB1	Fold change A2vsB2	Fold change A3vsB3
Actb	PPM02945B	17.842318	17.596804	17.138197	17.228771	17.87367	17.723974	-0.1809003	-0.307411	-0.394097	-0.332768	-0.0633823	-0.1499733	0.12651075	-0.061329	0.086591	0.91604428	1.04342652	0.94174541
Actb	PPM02945B	17.912785	17.621145	17.182076	17.28061	17.84212	17.75618	-0.1104333	-0.28307	-0.350218	-0.280929	-0.0949322	-0.1177673	0.17263675	-0.069289	0.022835	0.88721967	1.04919948	0.98429659
Acvr1	PPM03069C	26.61426	26.679857	25.728626	25.786602	26.506798	25.990396	8.59104175	8.775642	8.196332	8.225063	8.56974575	8.11644875	-0.1846002	-0.028731	0.453297	1.13650202	1.02011443	0.73037182
Acvr1b	PPM04453F	26.820168	26.846941	26.830256	26.623377	26.568502	26.629347	8.79694975	8.942726	9.297962	9.061838	8.63144975	8.75539975	-0.1457763	0.236124	-0.12395	1.10632576	0.84902327	1.08971434
Afp	PPM04781A	31.386059	31.512815	30.775682	30.484158	30.784283	30.950384	13.3628408	13.6086	13.243388	12.922619	12.8472308	13.0764368	-0.2457592	0.320769	-0.229206	1.18571662	0.800643	1.17218965
Aldh1a1	PPM04398F	22.276861	21.919699	21.09213	21.212454	21.585415	21.761072	4.25364275	4.015484	3.559836	3.650915	3.64836275	3.88712475	0.23815875	-0.091079	-0.238762	0.84782667	1.06516653	1.17997967
Aldob	PPM33644A	18.50872	18.729216	18.346518	18.305199	17.805918	17.981886	0.48550175	0.825001	0.814224	0.74366	-0.1311343	0.10793875	-0.3394992	0.070564	-0.239073	1.26531733	0.95226565	1.18023406
Arhgap6	PPM35735B	31.00735	31.374062	29.751236	29.707516	31.349905	31.549698	12.9841318	13.469847	12.218942	12.145977	13.4128528	13.6757508	-0.4857152	0.072965	-0.262898	1.40027992	0.95068216	1.19988655
Bcl2l14	PPM35858A	26.882187	26.906425	25.819448	25.919233	28.243296	27.393745	8.85896875	9.00221	8.287154	8.357694	10.3062438	9.51979775	-0.1432412	-0.07054	0.786446	1.10438351	1.05010967	0.57977057
Ccdc166	PPM41871A	29.526426	29.76424	29.212484	28.85697	29.258747	29.290474	11.5032078	11.860025	11.68019	11.295431	11.3216948	11.4165268	-0.3568172	0.384759	-0.094832	1.28059763	0.76590693	1.06794104
Ccdc85a	PPM30390A	40	39.382935	40	40	40	37.85573	21.9767818	21.47872	22.467706	22.438461	22.0629478	19.9817828	0.49806175	0.029245	2.081165	0.70805741	0.97993299	0.2363235
Ccna2	PPM02913D	31.60808	31.000391	31.853643	32.087902	32.511734	31.72244	13.5848618	13.096176	14.321349	14.526363	14.5746818	13.8484928	0.48868575	-0.205014	0.726189	0.71267403	1.15269753	0.60449864
Ccnd1	PPM02903F	28.945053	28.784319	28.40661	28.379827	28.965204	28.692747	10.9218348	10.880104	10.874316	10.818288	11.0281518	10.8187998	0.04173075	0.056028	0.209352	0.97148879	0.96190879	0.86492563
Ccne1	PPM02891B	28.504368	28.731144	27.842157	27.645964	28.443052	28.646692	10.4811498	10.826929	10.309863	10.084425	10.5059998	10.7727448	-0.3457793	0.225438	-0.266745	1.27083722	0.85533531	1.20309036
Cdkn1a	PPM02901B	21.432566	21.435894	21.327282	21.387367	21.226122	21.317947	3.40934775	3.531679	3.794988	3.825828	3.28906975	3.44399975	-0.1223312	-0.03084	-0.15493	1.08849234	1.02160678	1.1133676
Cdkn1b	PPM02909C	24.94188	24.876863	24.953548	24.962255	25.11072	24.820587	6.91866175	6.972648	7.421254	7.400716	7.17366775	6.94663975	-0.0539862	0.020538	0.227028	1.03812938	0.98586499	0.85439316
Cdkn2b	PPM02910F	27.825083	27.524727	26.713888	26.623674	27.440132	27.194107	9.80186475	9.620512	9.181594	9.062135	9.50307975	9.32015975	0.18135275	0.119459	0.18292	0.88187571	0.92053278	0.88091822
Crct1	PPM28367A	28.66607	28.795027	27.52387	27.92757	30.407536	29.895422	10.6428518	10.890812	9.991576	10.366031	12.4704838	12.0214748	-0.2479602	-0.374455	0.449009	1.18752695	1.29634975	0.73254587
Crebbp	PPM04423B	25.19615	25.12441	24.358185	24.290506	24.700544	24.553602	7.17293175	7.220195	6.825891	6.728967	6.76349175	6.67965475	-0.0472633	0.096924	0.083837	1.03330292	0.93502445	0.94354485
Ctgf	PPM03798B	22.733156	21.947495	21.062393	21.373295	22.601614	22.353523	4.70993775	4.04328	3.530099	3.811756	4.66456175	4.47957575	0.66665775	-0.281657	0.184986	0.62996442	1.21559024	0.87965761
Cxadr	PPM03214A	22.692215	22.750254	22.143347	22.124348	22.461493	22.460028	4.66899675	4.846039	4.611053	4.562809	4.52444075	4.58608075	-0.1770423	0.048244	-0.06164	1.13056368	0.96711275	1.04365147
Cyp2c70	PPM05264B	20.464605	20.428995	20.497454	20.45993	20.581541	20.364979	2.44138675	2.52478	2.96516	2.898391	2.64448875	2.49103175	-0.0833933	0.066769	0.153457	1.0595071	0.95477388	0.89909346
E2f4	PPM03464A	24.815771	24.78424	24.129198	24.189398	24.652372	24.659231	6.79255275	6.880025	6.596904	6.627859	6.71531975	6.78528375	-0.0874722	-0.030955	-0.069964	1.06250693	1.02168821	1.04969049
FN1	PPM03786A	19.55322	19.572075	19.732521	19.820036	19.237707	19.2518	1.53000175	1.66786	2.200227	2.258497	1.30065475	1.37785275	-0.1378583	-0.05827	-0.077198	1.1002705	1.04121644	1.05496709
Furin	PPM25284E	22.429638	22.273102	22.629307	22.601954	22.369984	22.432934	4.40641975	4.368887	5.097013	5.040415	4.43293175	4.55898675	0.03753275	0.056598	-0.126055	0.97431977	0.96152882	1.09130548
Gadd45b	PPM03566A	27.77603	26.838776	27.44486	27.487066	27.552494	26.880173	9.75281175	8.934561	9.912566	9.925527	9.61544175	9.00622575	0.81825075	-0.012961	0.609216	0.56712916	1.00902436	0.65555285
Gapdh	PPM02946E	18.15642	18.140291	17.926039	17.89143	17.976809	18.057753	0.13320175	0.236076	0.393745	0.329891	0.03975675	0.18380575	-0.1028742	0.063854	-0.144049	1.07391086	0.95670497	1.10500201
Gapdh	PPM02946E	18.18135	18.25862	17.882864	17.845345	18.05561	17.957882	0.15813175	0.354405	0.35057	0.283806	0.11855775	0.08393475	-0.1962733	0.066764	0.034623	1.14573488	0.95477719	0.97628685
Gins2	PPM36918A	30.960106	31.261673	29.71128	29.682451	30.44438	30.544184	12.9368878	13.357458	12.178986	12.120912	12.5073278	12.6702368	-0.4205702	0.058074	-0.162909	1.3384565	0.96054559	1.11954227
Glul	PPM33322F	22.973644	22.793018	23.120857	22.905321	21.991163	22.191223	4.95042575	4.888803	5.588563	5.343782	4.05411075	4.31727575	0.06162275	0.244781	-0.263165	0.95818574	0.8439439	1.20010863
Gng13	PPM32319A	35.868835	35.65355	40	36.895416	40	39	17.8456168	17.749335	22.467706	19.333877	22.0629478	21.1260528	0.09628175	3.133829	0.936895	0.93544079	0.11392616	0.5223559
Gpd1	PPM03296A	24.303509	23.900223	23.608006	23.763754	24.128826	24.457914	6.28029075	5.996008	6.075712	6.202215	6.19177375	6.58396675	0.28428275	-0.126503	-0.392193	0.82114975	1.09164442	1.31238681
Gsta1	PPM03858C	23.127272	22.99185	21.41156	21.164953	23.127022	22.701763	5.10405375	5.087635	3.879266	3.603414	5.18996975	4.82781575	0.01641875	0.275852	0.362154	0.9886839	0.82596239	0.77800212
Hcn2	PPM06968A	31.497427	31.122591	31.612553	31.507236	31.38889	31.756548	13.4742088	13.218376	14.080259	13.945697	13.4518378	13.8826008	0.25583275	0.134562	-0.430763	0.83750357	0.91094635	1.34794628
Hcrt	PPM04332C	40	40	40	40	40	40	21.9767818	22.095785	22.467706	22.438461	22.0629478	22.1260528	-0.1190032	0.029245	-0.063105	1.0859843	0.97993299	1.04471179
Hist1h2bn	PPM35914A	28.480335	27.935326	28.085526	28.1139	28.449839	28.207642	10.4571168	10.031111	10.553232	10.552361	10.5127868	10.3336948	0.42600575	0.000871	0.179092	0.74431966	0.99939645	0.88325872
Hmgxb4	PPM35920A	27.74279	27.955738	27.596731	27.698483	27.421377	27.197388	9.71957175	10.051523	10.064437	10.136944	9.48432475	9.32344075	-0.3319512	-0.072507	0.160884	1.25871464	1.05154238	0.89447682
Hmox1	PPM04356B	23.30922	23.102213	24.930645	24.275557	23.604513	22.906149	5.28600175	5.197998	7.398351	6.714018	5.66746075	5.03220175	0.08800375	0.684333	0.635259	0.94082366	0.62229346	0.64382522
Id2	PPM04420C	24.180578	24.188683	23.779346	23.796839	24.207907	24.201803	6.15735975	6.284468	6.247052	6.2353	6.27085475	6.32785575	-0.1271082	0.011752	-0.057001	1.09210249	0.99188722	1.04030099
Igfbp3	PPM03820F	30.666779	30.763536	30.866465	30.844038	32.228447	31.588045	12.6435608	12.859321	13.334171	13.282499	14.2913948	13.7140978	-0.2157602	0.051672	0.577297	1.16131573	0.96481751	0.67021831
Igfbp4	PPM06091F	22.997808	22.797195	22.262325	22.304579	22.53614	22.607895	4.97458975	4.89298	4.730031	4.74304	4.59908775	4.73394775	0.08160975	-0.013009	-0.13486	0.94500263	1.00905793	1.09798626
Insc	PPM30079A	29.455454	28.932796	27.911196	27.7935	28.521809	28.658096	11.4322358	11.028581	10.378902	10.231961	10.5847568	10.7841488	0.40365475	0.146941	-0.199392	0.75594085	0.90316344	1.14821436
Itgav	PPM03662D	23.88761	23.892612	23.271608	23.33058	23.984648	23.600006	5.86439175	5.988397	5.739314	5.769041	6.04759575	5.72605875	-0.1240053	-0.029727	0.321537	1.08975608	1.02081894	0.8002169
Itgb8	PPM57652C	40	40	40	40	40	40	21.9767818	22.095785	22.467706	22.438461	22.0629478	22.1260528	-0.1190032	0.029245	-0.063105	1.0859843	0.97993299	1.04471179
Izumo1r	PPM30194A	40	40	40	40	35.745617	40	21.9767818	22.095785	22.467706	22.438461	17.8085648	22.1260528	-0.1190032	0.029245	-4.317488	1.0859843	0.97993299	19.9385418
Jag1	PPM26291A	28.52682	28.44928	27.614372	27.84039	28.538633	28.197586	10.5036018	10.545065	10.082078	10.278851	10.6015808	10.3236388	-0.0414632	-0.196773	0.277942	1.02915712	1.14613183	0.82476671
Klf10	PPM05167F	27.829165	27.710241	27.269703	27.47764	27.28511	27.357964	9.80594675	9.806026	9.737409	9.916101	9.34805775	9.48401675	-7.925E-05	-0.178692	-0.135959	1.00005493	1.13185724	1.09882299
Ldlr	PPM24937F	23.380028	22.72646	22.616562	22.579113	22.947414	22.87681	5.35680975	4.822245	5.084268	5.017574	5.01036175	5.00286275	0.53456475	0.066694	0.007499	0.69036692	0.95482351	0.99481558
Lgmn	PPM04969A	26.218447	25.66206	25.86099	25.503729	25.75739	25.368834	8.19522875	7.757845	8.328696	7.94219	7.82033775	7.49488675	0.43738375	0.386506	0.325451	0.73847258	0.76498003	0.79804887
Maml2	PPM30858A	40	40	38.992683	40	40	40	21.9767818	22.095785	21.460389	22.438461	22.0629478	22.1260528	-0.1190032	-0.978072	-0.063105	1.0859843	1.96983119	1.04471179
Mapk14	PPM03578A	24.55495	24.3978	23.798914	23.873308	24.22219	24.210302	6.53173175	6.493585	6.26662	6.311769	6.28513775	6.33635475	0.03814675	-0.045149	-0.051217	0.9739052	1.03178974	1.0361386
Mmp14	PPM03617D	24.998507	24.816645	24.65643	24.76294	24.830181	24.749243	6.97528875	6.91243	7.124136	7.201401	6.89312875	6.87529575	0.06285875	-0.077265	0.017833	0.95736519	1.05501609	0.98771519
Mok	PPM26986A	31.261187	31.21638	31.247637	30.844923	31.571024	30.64117	13.2379688	13.312165	13.715343	13.283384	13.6339718	12.7672228	-0.0741963	0.431959	0.866749	1.05277435	0.74125457	0.54838119
Mospd3	PPM60265A	28.151642	27.586142	27.701124	27.6772	27.84658	28.17171	10.1284238	9.681927	10.16883	10.115661	9.90952775	10.2977628	0.44649675	0.053169	-0.388235	0.7338226	0.9638169	1.30879124
Myc	PPM02924F	23.377947	23.288643	22.513271	22.47715	23.303755	22.989248	5.35472875	5.384428	4.980977	4.915611	5.36670275	5.11530075	-0.0296993	0.065366	0.251402	1.0207993	0.95570283	0.84007964
Net1	PPM26273A	24.599422	24.575075	23.901218	23.899971	24.423512	24.200922	6.57620375	6.67086	6.368924	6.338432	6.48645975	6.32697475	-0.0946562	0.030492	0.159485	1.06781095	0.97908634	0.89534463
Nfkbia	PPM02943B	24.867443	24.667566	24.697319	24.510294	24.591751	24.363247	6.84422475	6.763351	7.165025	6.948755	6.65469875	6.48929975	0.08087375	0.21627	0.165399	0.94548485	0.86078808	0.89168188
Pdgfa	PPM03103E	26.731844	26.37822	25.98981	26.185804	26.548836	26.28187	8.70862575	8.474005	8.457516	8.624265	8.61178375	8.40792275	0.23462075	-0.166749	0.203861	0.84990839	1.12252611	0.86822387
Pdlim7	PPM36878A	25.667126	25.27757	24.279936	24.498978	25.74086	25.560926	7.64390775	7.373355	6.747642	6.937439	7.80380775	7.68697875	0.27055275	-0.189797	0.116829	0.82900186	1.14060321	0.92221242
Pigh	PPM37289A	28.844654	28.468605	28.140898	28.19784	28.481493	27.920237	10.8214358	10.56439	10.608604	10.636301	10.5444408	10.0462898	0.25704575	-0.027697	0.498151	0.83679971	1.01938357	0.70801361
Plat	PPM03855B	32.358425	33.517677	32.47663	32.528305	32.17893	34.789814	14.3352068	15.613462	14.944336	14.966766	14.2418778	16.9158668	-1.2782553	-0.02243	-2.673989	2.42545473	1.01566878	6.38191326
Prg4	PPM40699E	25.523478	24.963257	24.67124	24.605513	24.244232	23.896757	7.50025975	7.059042	7.138946	7.043974	6.30717975	6.02280975	0.44121775	0.094972	0.28437	0.73651267	0.93629042	0.82110009
Psat1	PPM37722C	24.219477	23.749441	22.341753	22.477346	23.900185	23.722908	6.19625875	5.845226	4.809459	4.915807	5.96313275	5.84896075	0.35103275	-0.106348	0.114172	0.78402266	1.07649976	0.92391242
Rhob	PPM24564C	23.640583	23.447672	23.248474	23.309216	23.430578	23.526743	5.61736475	5.543457	5.71618	5.747677	5.49352575	5.65279575	0.07390775	-0.031497	-0.15927	0.95006113	1.02207212	1.11672194

Gene Symbol	Assay Catalog #	A1a Ct	B1a Ct	A2a Ct	B2a Ct	A3a Ct	B3a Ct	A1a ΔCt*	B1a ΔCt*	A2a ΔCt*	B2a ΔCt*	A3a ΔCt*	B3a ΔCt*	ΔΔCt (A1a-B1a)	ΔΔCt (A2a-B2a)	ΔΔCt (A3a-B3a)	Fold change A1vsB1	Fold change A2vsB2	Fold change A3vsB3
Selenbp1	PPM32861A	19.42977	19.573044	20.360348	20.500061	19.314316	19.247885	1.40655175	1.668829	2.828054	2.938522	1.37726375	1.37393775	-0.2622772	-0.110468	0.003326	1.19937038	1.07957839	0.99769725
Sepp1	PPM06184A	17.608131	17.35229	17.414537	17.349035	17.220375	16.983828	-0.4150872	-0.551925	-0.117757	-0.212504	-0.7166773	-0.8901193	0.13683775	0.094747	0.173442	0.90951053	0.93643645	0.8867246
Selrnc2	PPM29144A	26.922716	26.905617	26.234291	26.504442	26.43645	26.45952	8.8894775	9.001402	8.701997	8.942903	8.4993775	8.5557275	-0.1019042	-0.240906	-0.086175	1.07318906	1.18173455	1.0615197
Serpine1	PPM03093C	21.87007	22.014187	23.208801	23.714806	22.871605	3.846851175	4.109972	5.676507	6.153267	4.9345527	4.4578207	-0.2631203	-0.47676	0.476732	1.200071	1.39161467	0.71860357	
Skl	PPM25818B	25.655312	25.501726	24.671589	24.775364	25.277496	25.33153	7.6320937	7.597511	7.139295	7.213815	7.34044375	7.45756275	0.03458275	-0.07452	-0.117139	0.97631409	1.05301063	1.0845819
Slc26a1	PPM31074A	24.005625	23.869898	23.228659	23.226684	23.533388	23.52394	5.9824067	5.965683	7.581493	7.392301	5.6963365	5.6653575	0.01672375	0.03124	-0.053664	0.98847491	0.97857885	1.0378975
Smad2	PPM04430C	25.55131	25.485708	24.924595	24.905514	25.45477	25.151432	7.5280917	7.581493	7.392301	7.343975	7.51771775	7.27748475	-0.0534012	0.048326	0.240233	1.03770851	0.96705778	0.8466085
Smad3	PPM04461C	26.380142	26.238624	25.253542	25.327702	26.30487	25.99607	8.3669237	8.332409	7.721248	7.766163	8.36781775	8.12212275	0.03451475	-0.044915	0.245695	0.9763601	1.031622	0.8434094
Smad4	PPM04411A	24.062534	23.436523	23.541426	23.499355	23.806223	23.478434	6.0393157	5.532308	6.009132	5.937816	5.86917075	5.60448675	0.50700775	0.071316	0.264684	0.70368041	0.95178942	0.8323810
Smad7	PPM03073F	28.804598	28.533617	27.55368	27.670769	28.131626	28.890429	10.781379	10.629402	10.021386	10.10923	11.1945738	11.0164818	0.15197775	0.093275	0.178092	0.90001581	1.06278075	0.8838711
Smurf2	PPM32943A	24.566761	24.35443	24.002567	23.99434	24.57871	24.27262	6.5435427	6.450215	6.470273	6.432801	6.84165775	6.3867275	0.09332775	0.037472	0.242985	0.93735812	0.9743608	0.8449957
Sox4	PPM04422A	29.839449	29.840164	29.957792	30.283209	30.93073	31.20466	11.816230	11.935949	12.425498	12.72167	12.9936778	13.3307128	-0.1197183	-0.296172	-0.337035	1.08652265	1.22788206	1.2631579
Sp1	PPM04585F	25.146613	25.184519	24.91896	24.794188	24.855143	24.767271	7.1223947	7.280304	7.386666	7.232649	6.91809075	6.8933275	0.01579092	0.154017	0.024767	1.11566914	0.98874454	0.9829793
Sprr1a	PPM40924B	20.242737	19.859833	19.17641	19.31123	20.751148	20.109566	2.2195187	1.955618	1.644116	1.746691	2.81409575	2.23561875	0.26390075	-0.105575	-0.337035	1.08652265	1.22788206	1.2631579
Sprr3	PPM29586A	38.536644	40	40	40	39.861103	40	20.513425	22.095785	22.467706	22.438461	21.9240508	22.1260528	-1.5823593	0.029245	-0.202002	2.99459157	0.97993299	1.1502934
Spry4	PPM27611A	25.58401	25.433311	24.885351	24.856478	25.256119	25.219904	7.5607917	7.529096	7.353057	7.294839	7.31906675	7.34595675	0.03169575	0.058118	-0.02689	0.97826976	0.9605163	1.0188135
Stx5a	PPM04273A	25.354761	25.485693	24.98639	25.089075	24.985023	25.250128	7.3315427	7.581478	7.454096	7.527536	7.04797075	7.37618075	-0.2499353	-0.07344	-0.32821	1.18815374	1.0522264	1.2554572
Sulf1e1	PPM04009B	26.426468	25.89267	26.138163	25.704327	25.123035	24.763145	8.4032497	7.988455	8.605869	8.142788	7.18598275	6.88919775	0.44730975	0.463081	0.236785	0.75012621	0.72543537	0.8140644
Tfpi2	PPM05315B	27.608807	27.453245	27.153912	26.757576	26.900196	26.826105	9.5855887	9.54903	9.621618	9.196037	8.96314375	8.95215775	0.03656875	0.425581	0.010986	0.97497778	0.74453863	0.9924140
Tgfb1	PPM02991B	30.304092	30.539436	29.518473	29.538925	30.300459	30.470268	12.280873	12.635221	11.986179	11.977386	12.3634068	12.5963208	-0.3543472	0.006793	-0.232914	1.27840703	0.99392369	1.1752062
Tgfb3	PPM02993A	32.88391	35.02017	33.48369	25.706928	33.480556	33.79715	14.860691	17.115955	15.951396	14.637119	15.5435038	15.9232028	-2.2552633	1.314277	-0.379699	4.77421405	0.40212697	1.3010703
Tgfbr1	PPM03072C	26.114649	26.102167	25.706928	25.921778	26.103403	26.168882	8.0914307	8.197952	8.174634	8.360239	8.16635075	8.29493475	-0.1065213	-0.185605	-0.128584	1.07662904	1.1372938	1.0932201
Tgfbr2	PPM03599B	24.917507	24.928284	24.621199	24.60858	24.973738	24.746538	6.8942887	7.024069	7.088905	7.047041	7.03686575	6.87259075	-0.1297803	0.041864	0.164095	1.09412703	0.97139906	0.8924882
Tm7sf2	PPM40742A	24.651533	24.61285	24.389742	24.417131	24.550747	24.738455	6.6283147	6.708635	6.857448	6.855592	6.81369475	6.86450775	-0.0803202	0.001856	-0.250813	1.0572527	0.99871435	1.1898774
Tmsb4x	PPM05609A	24.300941	23.88793	23.09981	23.215706	24.581911	24.187325	6.2777225	5.983715	5.566616	5.654167	6.64485875	6.31337775	0.29400775	-0.087551	0.331481	0.81563311	1.06256943	0.7947202
Ugt1a9	PPM72424A	25.677847	25.437508	24.97266	24.813711	24.89165	24.732449	7.6546287	7.533293	7.440366	7.252172	6.95459775	6.85850175	0.12133575	0.186194	0.096096	0.91933607	0.9777037	0.9355612
UncSb	PPM37758A	25.419537	25.383183	24.326456	24.616064	25.716745	25.57529	7.3963187	7.478968	7.794162	7.054525	7.77989275	7.70134275	-0.0826492	-0.260363	0.07835	1.05896085	1.19778004	0.9474102
RTC	PPX63340	22.037874	22.295841	22.23898	22.233929	22.311314	22.30024	4.0146557	4.391626	4.706686	4.67239	4.37426175	4.42629275	-0.3769702	0.034296	-0.052031	1.29861182	0.97650816	1.0367233
PPC	PPX63340	22.203264	22.406956	22.274332	22.314556	22.425844	22.331064	4.1800457	4.502741	4.742038	4.753017	4.48879175	4.45711675	-0.3226952	-0.010979	0.031675	1.25066487	1.00763909	0.9782838
PPC	PPX63339	20.550272	19.026546	20.345005	20.411043	20.578066	20.25292	2.5270537	1.122331	2.812711	2.849504	2.64101375	2.37897275	1.40472275	-0.036793	0.262041	0.37769072	1.02583095	0.8339073
PPC	PPX63339	20.576623	19.177284	20.32782	20.482225	20.362654	20.260862	2.5524047	1.273069	2.795526	2.920686	2.42560175	2.38671475	1.27933575	-0.12516	0.038887	0.41198515	1.09062868	0.9734056
MGDC	PPM65836A	40	40	40	40	40	40	21.976781	22.095785	22.467706	22.438461	22.0629478	22.1260528	-0.1190032	0.029245	-0.063105	1.0859843	0.97993299	1.0447117

Notes: Undetermined samples set to Ct of 40; *ΔCt=Ct(gene of interest) - Ct(arithmetic mean of housekeeping genes); housekeeping genes are Actb and Gapdh; RTC, reverse transcription control; PPC, positive PCR control; MGDC, mouse genomic DNA control

Appendix 6 – HO-1 and tPA immunohistochemistry

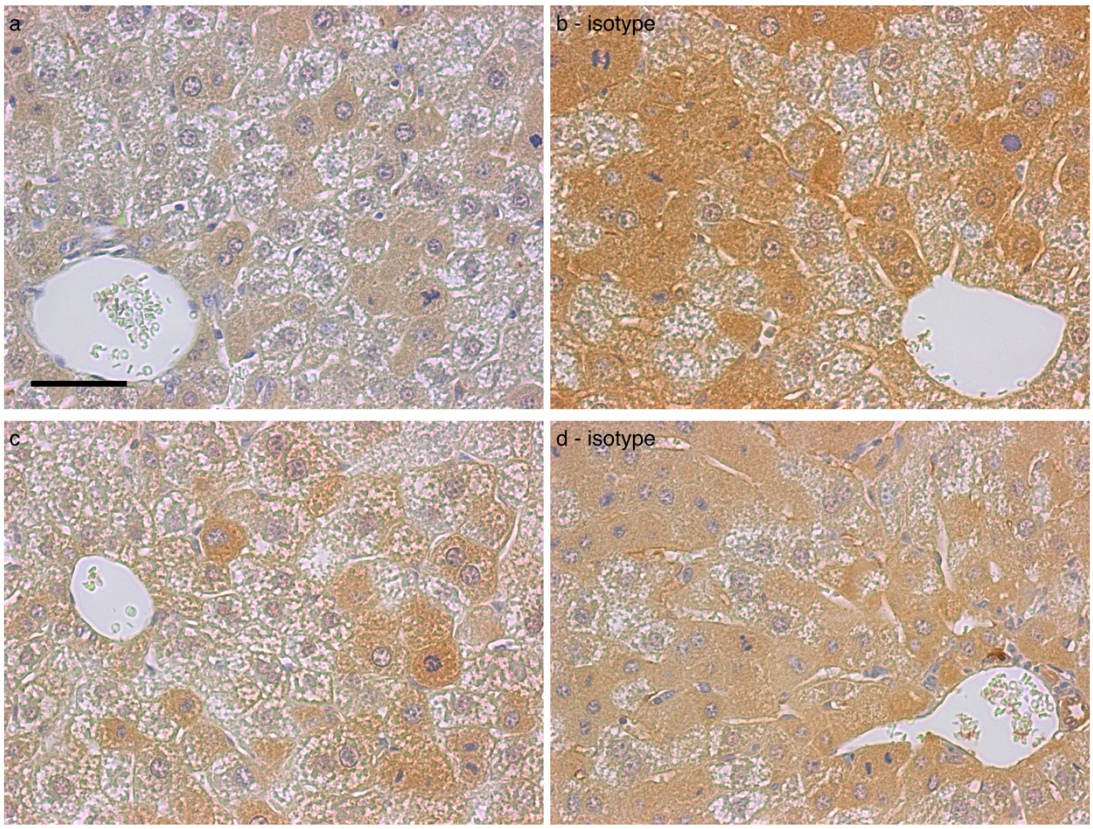

Immunostaining of post-partial hepatectomy liver for HO-1 (a, b – isotype control) and tPA (c, d – isotype control) reveal only non-specific background staining. Scale bar 50μm. Immunostaining protocol as for GR1 (see Chapter Two), with HO-1 antibody (Abcam, 52947, 1:100) and tPA antibody (Abcam, 157469, 1:500). Rabbit IgG isotype control was added at an equivalent concentration (Santa Cruz, SC-2027)